Acceptance Test Specifications and Guidelines for Fiber-Reinforced Polymeric Bridge Decks

Progress Report No. 6

Prepared For

U.S. Department of Transportation
Federal Highway Administration

By

A. Zureick
Georgia Institute of Technology
School of Civil Engineering

October 2001

A. Accomplishments/Significant Findings for the Period May 2001-June 2001

TASK A – Annotated Bibliography

- This draft chapter is under review by the FHWA Panel Members..

TASK B – Material Acceptance Tests & Statistically-Based Analysis

- This task is now complete. A revised copy of this chapter will be prepared and sent to COTR. Two technical papers were also prepared and sent to COTR electronically and via US mail.

TASK C – Acceptance Test Criteria for FRP Bridge Deck/Superstructure Components

- Acceptance test criteria are finalized. A presentation on the subject was present during the August 2001 meeting with AASHTO Technical Committee T21 members. In general positive comments were received and there was no objection to the proposed tests. PI will also seek additional external reviews if approved by the COTR.

TASK D – Quality Control of Structural System Assembly

A draft chapter addressing the quality control of manufactured composite materials for bridge deck components was completed.

TASK E – Draft and Final Specifications and Commentary

Draft of the final specifications and commentary is currently under preparation.

TASK F – Draft and Final Report/TRB Presentation

No activities

TASK G – Coordinate with AASHTO Technical Committee T21

- One meeting with AASHTO TC-21 members was held on August 3, 2001 in Madison, Wisconsin. Another review is proposed for the month of December 2001 in Atlanta, Ga.

GEORGIA INSTITUTE OF TECHNOLOGY — OFFICE OF CONTRACT ADMINISTRATION

RESEARCH REPORT APPROVAL SHEET

Project No. E20-F43

School of Civil and Environmental Engineering
(Lab/School)

I. GENERAL

A. Report Title: Acceptance Test Specifications and Guidelines for Fiber-Reinforced Polymeric Bridge Decks

B. Author(s) and/or Proj. Dir.: Dr. Abdul-Hamid Zureick — Phone No.: 404-894-2294

C. Period Covered: February 16, 2000 - May 15, 2002 — Due Date: Dec. 15, 2001

II. REPORT IDENTIFICATION

A. Deliverable Line No. 9 (from Deliverable Schedule)

Duplicate received rpt 2/7/02

B. Type Report:

- ☐ Monthly ☐ Quarterly ☐ Semi-Annual
- ☐ Annual ☐ Progress ☐ Cost & Performance
- ☐ Contract Mgt. ☐ Final ☒ Other Comprehensive Draft of Final

C. Draft Copy for Sponsor Approval ☐

D. Approval Copy for Distribution:

1. ☐ Send Copy to Sponsor
2. ☐ Send Master to Sponsor
3. ☐ Return Master to PD/PI

III. SECURITY CLASSIFICATION

- ☒ Unclassified ☐ Secret ☐ In Confidence (Specified Industrial Contracts Only)
- ☐ Confidential ☐ Top Secret ☐ Other _____ (Specify)

IV. DATA RESTRICTIONS ☐ Yes ☒ No

Proprietary Data (Confidential Disclosure); Export License; Trade Secret; Copyright or Publishing Restrictions; Patentable Technology. **NOTE: If "Yes", contact OCA LEGAL SERVICES, Ext. 4-4812.**

V. PRINTING/DISTRIBUTION INSTRUCTIONS

A. No. Copies to be Printed/Distributed

Sponsor 2 OCA 2 School/Lab 0 Other 0 Total 4

B. Printing Desired: ☐ One-side only ☐ Two sides

C. Binding Desired: ☐ Staple ☐ Staple & Tape ☐ Spiral Bind ☐ Velobind ☐ Other _____

D. Cover Desired:

- ☐ Standard ☐ Sponsor-Prescribed
- ☒ None ☐ Special Design (VPR/OCA Approval Required) _____
- ☐ White ☐ Other Color (Specify) _____ 18-02-02P03:55 RCVD

E. Approval of Check Copy by School/Lab before binding: ☐ Yes ☐ No If Yes, Phone _____

F. Distributon to be by:

☒ Lab/School ☐ OCA Contracting Support Division

1. If distribution made by lab/school, attach transmittal letter and 2 copies of report for archives. Indicate date mailed: 12/20/01 . (This is the mailing date OCA/CSD will enter into the database).

2. If distribution made by OCA/CSD, the signature of employee handling the report and the mailing date are shown here: Distributed by: _____ Date mailed: _____

VI. APPROVALS

		DATE
A. PD/PI	Dr. Abdul-Hamid Zureick Abdul-Hamid Zureick	
B. Div. Chief/Branch Head		
C. Lab/School Director (Required on Finals)	Dr. Bruce Ellingwood Bruce R. Ellingwood	12/20/01
D. Coordinator Log Entry:		

Printed by an electronic version of OCA Form 09-0593.

19-FEB-2002 JW

E-20-F43
#9
"Duplicate"

TABLE OF CONTENTS

TABLE OF CONTENTS

CHAPTER 1: BIBLIOGRAPHY

1.1 Introduction

In recent years, highway bridge decks constructed from modular Fiber-Reinforced Polymeric (FRP) materials have been the subject of a great deal of research on the part of structural engineering community. The major advantages of these decks are their low weight (less than one-third the weight of a comparable concrete bridge deck), corrosion resistance, good fatigue performance, and potential for rapid field assembly, which greatly reduces the construction cost and traffic disruption.

The design and development of new bridge deck systems made from FRP materials requires a careful integration of the following:

1. In-depth structural engineering studies to develop a preliminary prototype design and to effectively integrate attributes of the anisotropic material properties and manufacturing methodologies with the actual structural and operational requirements for replacing or retrofit upgrading deficient highway bridge decks.

2. Extensive applied materials and structural testing of elements, modules and full size sections of FRP bridge decks (including their connections) to develop and validate the final design that must address every potential aspect of deck behavior over the life of the bridge;

3. Practical considerations pertaining to construction tolerances -- especially straightness of steel and prestressed concrete stringers, weight of modules for handling by construction workers, environmental factors at construction sites, safety, and the ability to make field adjustments to accommodate bridge skews, joints, curbs and the like.

4. The development of a nondestructive evaluation method that must have the degree of accuracy, reliability, and repeatability necessary not only for the quantitative evaluation of the remaining strength but also for the detection and prediction of progressive and catastrophic failure of existing FRP bridge components.

1.2 Objective

The objective of this chapter is to present a comprehensive up-to-date literature review of information related to fiber-reinforced polymeric bridge decks and to provide a synopsis of the information contained in each published reference. This review will update a previously published literature survey article on the subject presented by Zureick et al. (1995) and establish the foundations upon which future materials, components, and quality control acceptance test specifications pertaining to polymeric composite bridge decks will be based. All references surveyed in this report were placed in in an electronic data base that is easy to access, query, and update as additional research is completed.

1.3 Electronic data base

References addressed in this report were stored in the Microsoft ACCESS data base management software running under the Windows environment. This data base program was chosen for its user-friendliness, its straightforward, intuitive and graphical approach to design, its ability to generate printed reports and screen forms, and its compatibility with almost all other commercial data base programs.

The information pertaining to a given reference is stored in five different fields representing the title, author(s), publication, year , and a summary of the publication. In addition, to these five major fields, check-boxes were added to the data base form to act as keywords in this survey. Additional check boxes can be added at any time to reflect other categories not selected in the present data base. Figure 1 shows the data base form along with all different fields and check boxes.

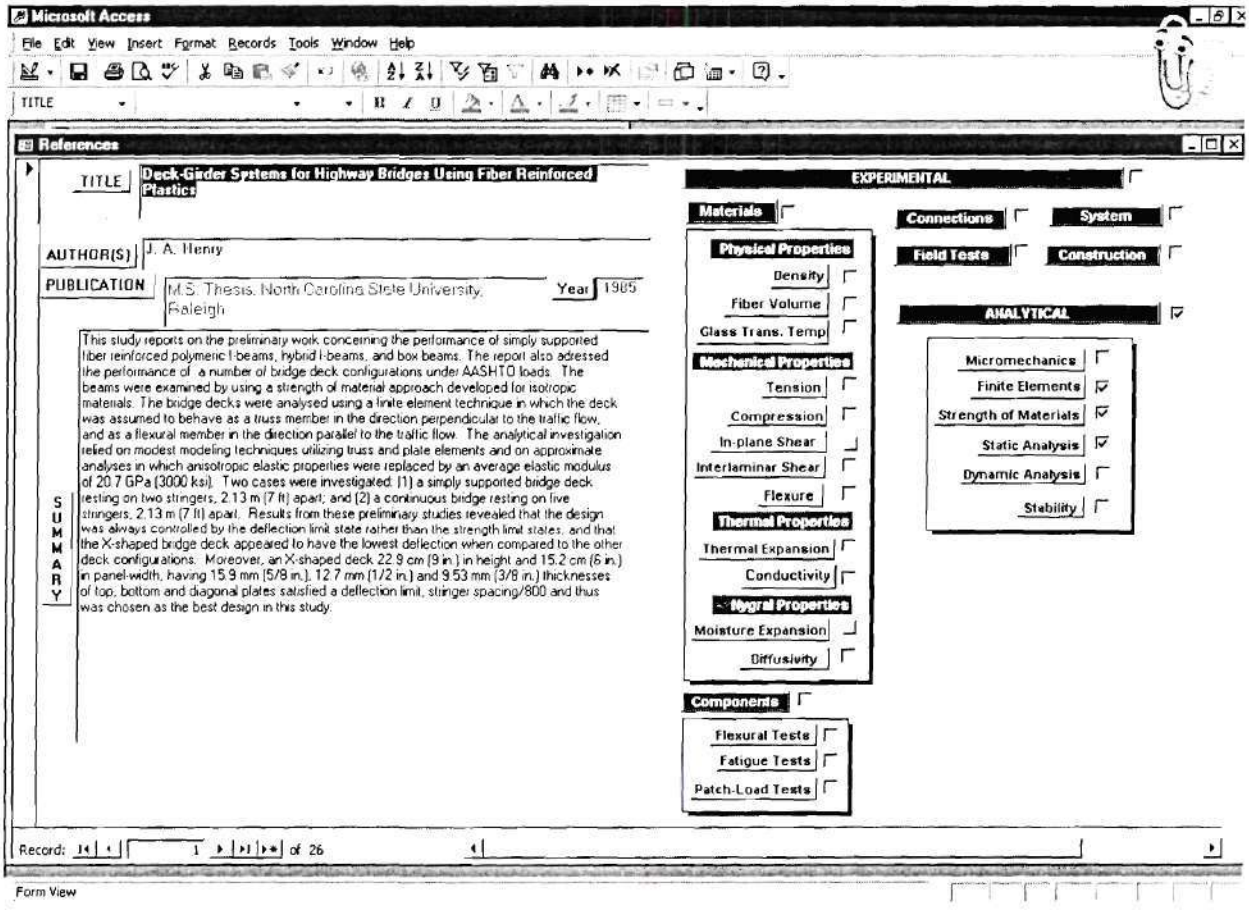

Figure 1. A view of the electronic databse form

1.4 FRP bridge deck design concepts--A historical perspective

Research concerning polymeric composite bridge concepts commenced in the U.S. in the early 1980's under the auspices of both the National Science Foundation and the Federal Highway Administration. The earliest published documents on the subject were by Plecnik and his co-workers (Henry, 1985; Ahmad and Plecnik, 1986; Plecnik and Azar, 1991) who examined analytically the performance of several glass reinforced polymer bridge deck configurations, shown in figure 2, with the general purpose finite element code, SAP IV. The design philosophy behind all of these configurations was that an FRP deck behaves as a truss member in the direction perpendicular to the support girders, and as a flexural member in the direction parallel to the support girders. The analytical investigation relied on modest modeling techniques utilizing truss and plate elements and on approximate analyses in which anisotropic elastic properties were ignored and replaced by an average elastic modulus of 20.7 GPa (3000 ksi). Two cases were initially investigated: 1) a simply supported bridge deck resting on two stringers, 2.13 m (7 ft) apart; and 2) a continuous bridge deck resting on five stringers, 2.13 m (7 ft) apart.

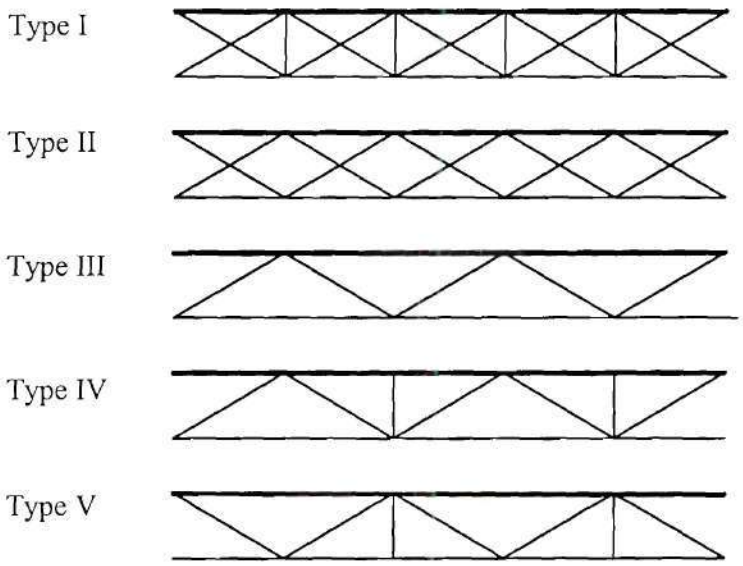

Figure 2. FRP dridge deck cross section types considered by Plecnik and co-workers

Results from these preliminary studies revealed that the design was always controlled by the deflection limit state rather than the strength limit states, and that the X-shaped bridge deck, Type II in Figure 2, appeared to have the lowest deflection when compared to the other deck configurations. Moreover, an X-shaped deck 22.9 cm (9 in) in height and 15.2 cm (6 in) in panel-width, having 15.9-mm (5/8-in), 12.7-mm (1/2-in) and 9.53-mm (3/8-in) thicknesses of top, bottom and diagonal plates satisfied a deflection limit, *stringer spacing/800,* set by the authors and thus was chosen as the best design in the study.

This X-shaped bridge deck design concept was later fabricated (figure 3) using a combination of filament winding and hand lay-up processes in order to determine the static and fatigue behavior experimentally. Filament wound E-glass/Vinylester diamond and triangular shapes having [27/-27/0/90/27/-27/90/0/27/-27] laminate stacking sequences were first bonded together. Unidirectional tapes were then added manually. A description of the assembly technique is described in the reference by Plecnik and Azar (1991).

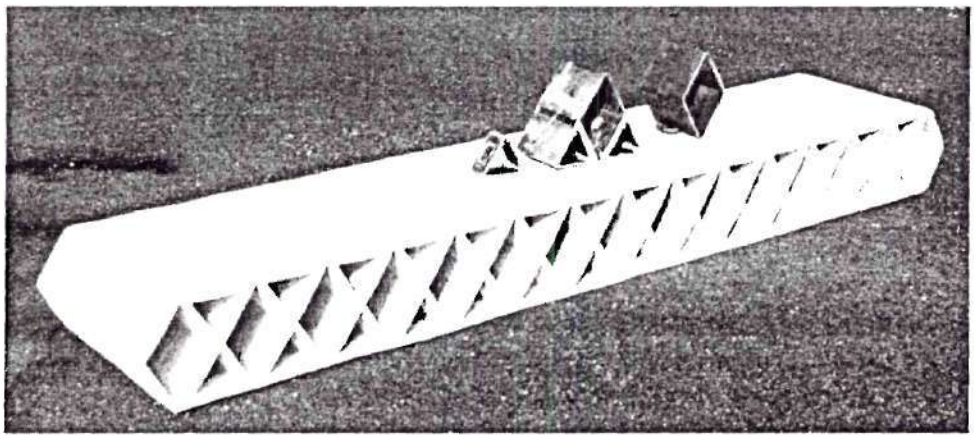

Figure 3. X-Shaped bridge deck by Plecnik and co-workers

Zureick and Shih (1991) conducted finite element analyses on the continuous X-shaped deck subjected to the same boundary and loading conditions as proposed by Henry (1985) and Ahmad and Plecnik (1989). In Zureick and Shih's analyses values of the anisotropic properties were calculated from the laminate theory. Results have shown that when the cells are oriented parallel to the support girders (also in the direction of the traffic flow), the maximum deflection was only 11 percent higher than that reported by Henry (1985) and Ahmad and plecnik (1989). Values of the stress components were, in general, lower than 29 MPa (4.2 ksi). Furthermore, analyses were conducted on the FRP deck in which the cells were oriented perpendicularly to the support girders, the results of which showed a reduction of 30 percent in the deflection and 23 percent in the maximum stress over the case in which cells were oriented parallel to the traffic flow.

Guided by the work of Plecnik, Zureick (1988) commenced an experimental and analytical program aimed toward assessing the strength and serviceability of fiber-reinforced polymeric composite bridge decks for use in new construction and also in the rehabilitation of aging bridges. The analytical portion of this study involved the examination of various multi-cell bridge deck configurations shown Figure 4 and the establishment of general guidelines pertaining not only to the range but also to the optimal values of the cell width as well as the thicknesses of different parts of the bridge deck. In virtually all cases examined, it was found, for example, that as the cell width increases over approximately 8 inches, the weight of the FRP deck increases at the rate shown in Figure 5. It was also found that the triangular truss configuration (Figure 4c) was the most structurally efficient shape that can be manufactured economically. Furthermore it was recommended that

- Neither buckling nor any form of failure in the web (vertical or inclined) of a multicellar deck occur under a 75 kip patch load distributed over a contact area measuring 10 in. x 20 in.

- The minimum plate thickness of any part of the cross section not be less than 1/4 in.

The optimum practical reinforcing scheme depends in general upon the support conditions and the selected manufacturing method. For one application (Brown and Zureick 1998, 1999), the deck was designed to be constructed from top and bottom plates bonded to the triangulated multi-cell trusses, as shown in Figure 13. Design requirements for bridge loads and loading configurations were adopted from the AASHTO Standard Specifications for Highway Bridges (AASHTO 1994) in one case and from both the Trilateral Design and Test Code for Military Bridging (Army 1966) and the Circular of Requirements for New construction Sealift Ships (Navy 1992) in another case. Two simply supported deck panels each of which measuring 10 ft x 18 ft were fabricated and constructed at a site on Interstate 81 near Roanoke, Virginia. The site is an exacavated section of pavement adjacent to "weigh-in-motion" scales. Traffic consists of approximately 15,000 tractor-trailers per day, moving at approximately 60 km/hour. The deck is instrumented with fiber optic strain measurement devices built -in at critical locations of the deck structure. Figure 6 shows the Georgia Tech V-shaped bridge deck during the construction.

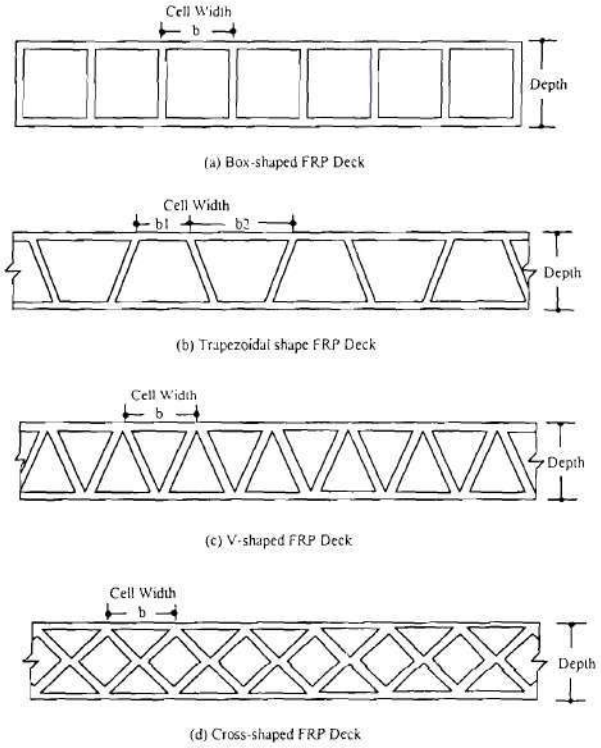

Figure 4. Multi-cell type bridge decks (Zureick, 1988)

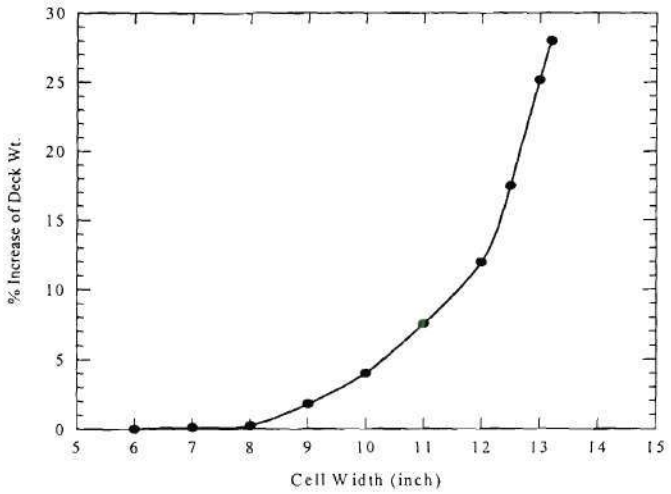

Figure 5. Cell width vs. weight increase (Zureick,1992)

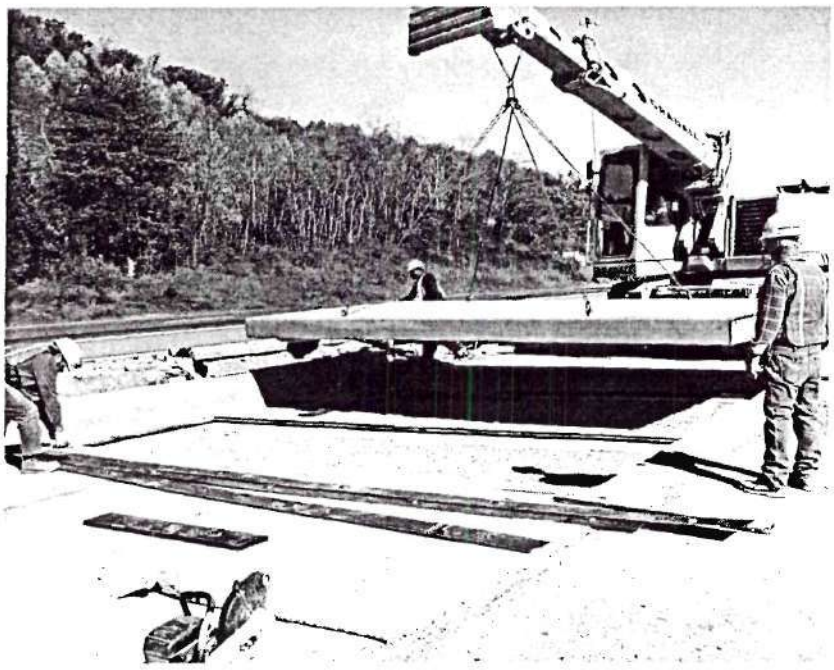

Figure 6. Construction of the V-shaped polymeric bridge deck in Troutville, VA

At West Virginia University, extensive work on FRP bridge deck systems began by studying analytically and experimentally FRP bridge superstructures consisting of bridge decks and stringers (GangaRao and Sotiropoulos,1991). Two concepts whose cross sections are shown in Figure 7 and Figure 8 were examined. The first concept consisted of five parts: two exterior stringers as channels; an interior I-section stringer made from two back-to-back connected channels; and two solid composite plates placed on the top and bottom of the box section. The fiber direction of the solid plates was perpendicular to that of the stringers to provide better transverse load distribution. The second concept used a cellular section as a substitute for the top plate of the first specimen in order to improve the bending stiffness. These two concepts were fabricated and tested with simple supports under various loading conditions.

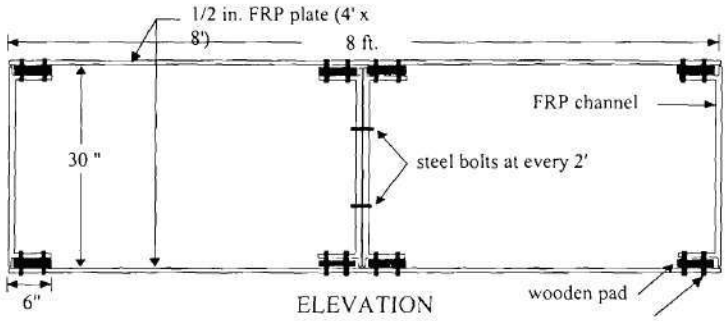

Figure 7. Cross Section of First Tested Specimen by GangaRao and Sotiropoulos

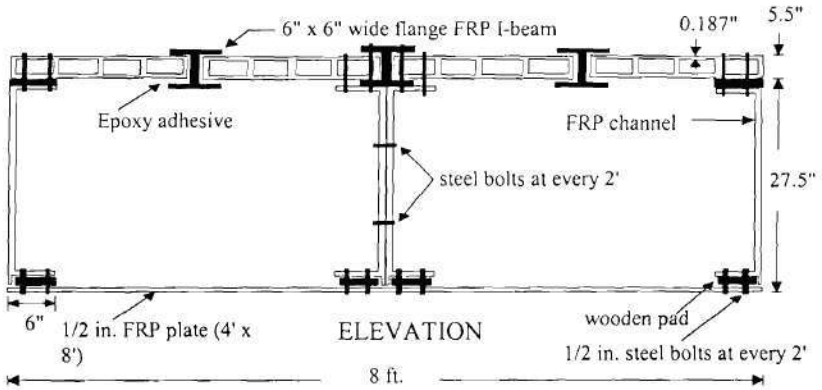

Figure 8. Cross Section of Second Tested Specimen by GangaRao and Sotiropoulos

Efforts by researchers at West Virginia University during the 1990's has resulted in the development of a fiber-reinforced polymeric bridge deck fabricated by the pultrusion process. The bridge deck has the cross section shown in Figure 9 and made by bonding hexagonal tubes with half-depth trapezoidal elements. Composite bridge decks adopting the West Virginia University design concept were fabricated and installed first at two bridge sites in West Virginia; the Wick Wire Run bridge located off Route 119 in Taylor Conty, West Virginia, and the the 20-ft

span all composite bridge (Laurel Lick Bridge) located on county Road 26/6 in Lewis County West Virginia (Figure 10). A description of the development that led to the construction of the aformentioned bridges along with other applications is given by GangaRao et al. (1999).

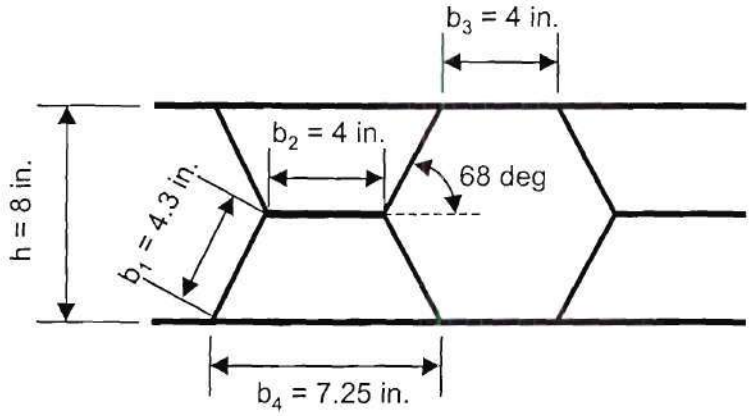

Figure 9. Cross-section of WVU FRP bridge deck (GangaRao et al., 1999)

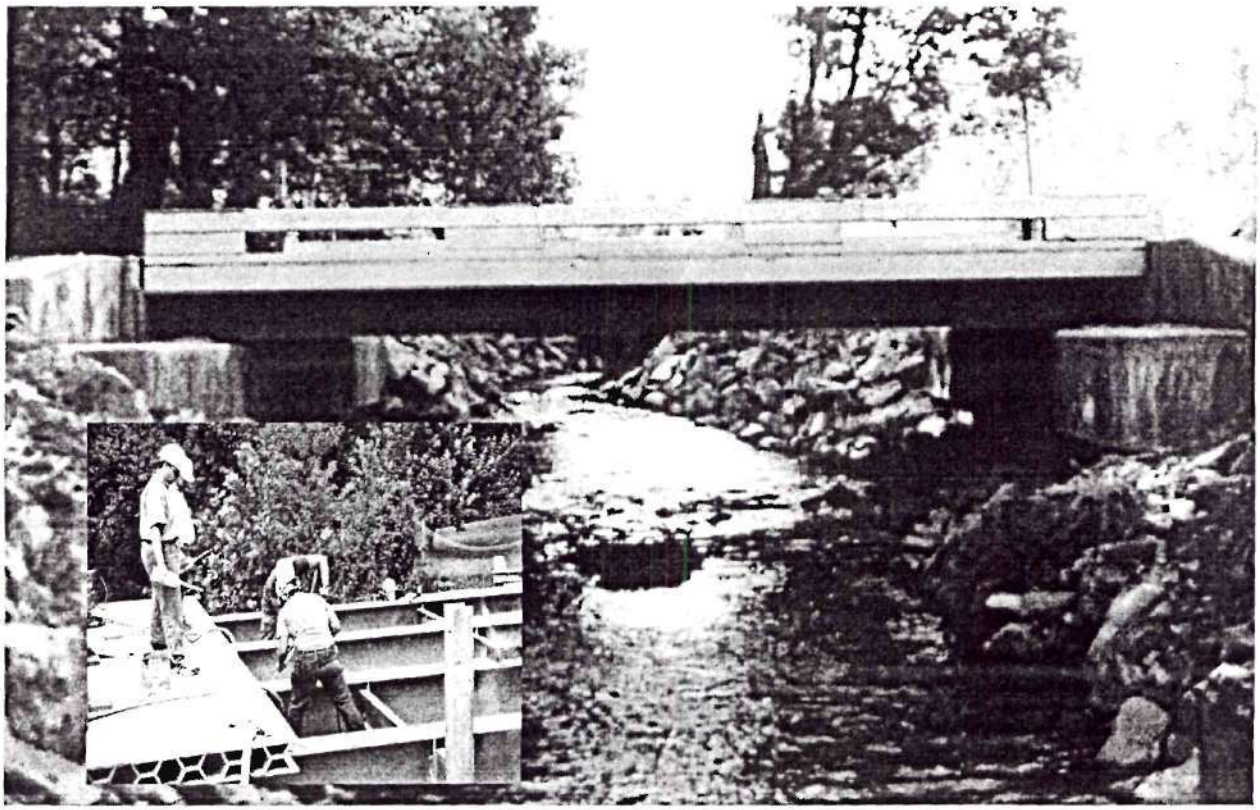

Figure 10. View of the all-composite Laurel Lick Bridge

Bakeri (1989) and Bakeri and Sunder (1990) used balanced symmetrical lamina having a stacking sequence of $[0/60/-60]_s$ and $[0/45/-45/90]_s$ to investigate analytically the feasibility of a number of FRP bridge decks (Bakri, 1989; Bakri and Sunder 1990). They concluded that the hybrid concept, shown in figure 11, composed of glass fiber-reinforced polymer, carbon fiber-reinforced polymer and light weight concrete resulted in a bridge deck system having a deflection less than s/800, where s represents the stringer spacing. Their concept assumed a perfect bond between the concrete and the polymer composite, which was not addressed in their work.

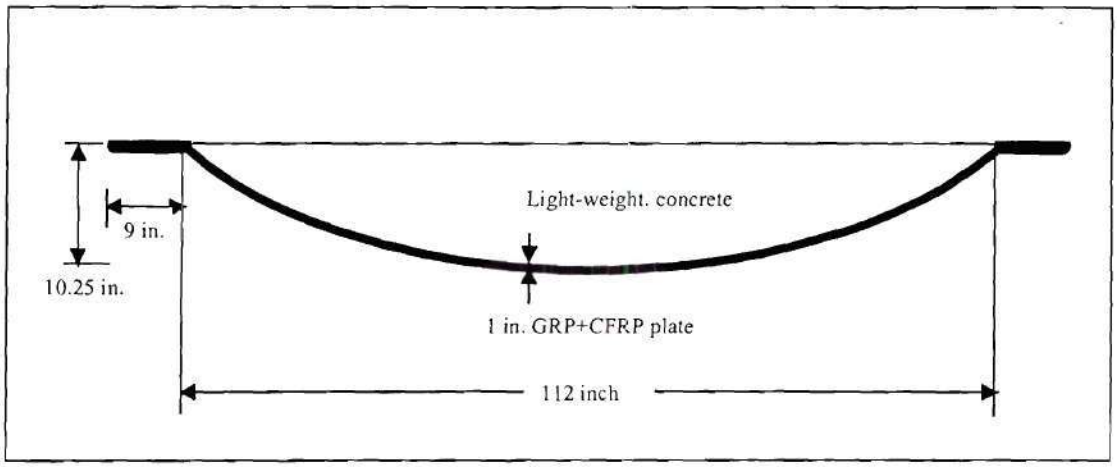

Figure 11. Hybrid FRP bridge deck studied by Bakeri and Bakeri & Sunder

In addition, an analytical study conducted at the University of Virginia (McGhee, 1990; McGhee *et al.*, 1991) presented results of the least-weight design of four cross-section types of FRP bridge decks subjected to 1989 AASHTO loading. These bridge deck concepts were adopted from the studies of Henry (1985) and Ahmad and Plecnik (1989) and consisted of types I, II, and III, as well as a slightly modified version of type IV, of Figure 2. The mathematical optimization problem was formulated such that the objective function was represented by the weight of the bridge deck while the behavioral constraints included ultimate strength, local buckling and s/800 deflection limit states. Linear elastic finite element analysis in which orthotropic plane stress elements combined with space frame members was used to simulate the cellular deck. The study concluded that the type III cross section could efficiently provide fabrication savings and result in an FRP deck weighing approximately 20 lb./ft^2 of deck surface.

During the late 1990's, several bridge deck concepts were referenced briefly in a limited number of technical and trade publications. Some of these concepts were clearly guided by the invistigations reviewed earlier while others differed substantially. It is unfortunate that the technical backgound to the development of such concepts have not been documented properly in the literature. Therefore, we only provide a list of these concepts:

- The Martin Marietta Composites, Inc. pultruded bridge deck (DuraSpan^{TM}), whose cross sectional shape is a slight modification to Type IV and Type V of plecnik's original concepts.

- Honeycomb FRP bridge decks manufactured by Hardcore Composites.

- Fiber-reinforced foam core sandwich panels (TYCOR^{TM}) consisting of a foam core reinforced with 3-dimensional multi-axial performs and glass fiber reinforced skins at the top and bottom of the panel. This concept is not intended for spans that exceed 3 ft.

- Fiber-reinforced polymeric honeycomb sandwich panels manufactured by Kansas Structural Composites, Inc. (Figure 12)

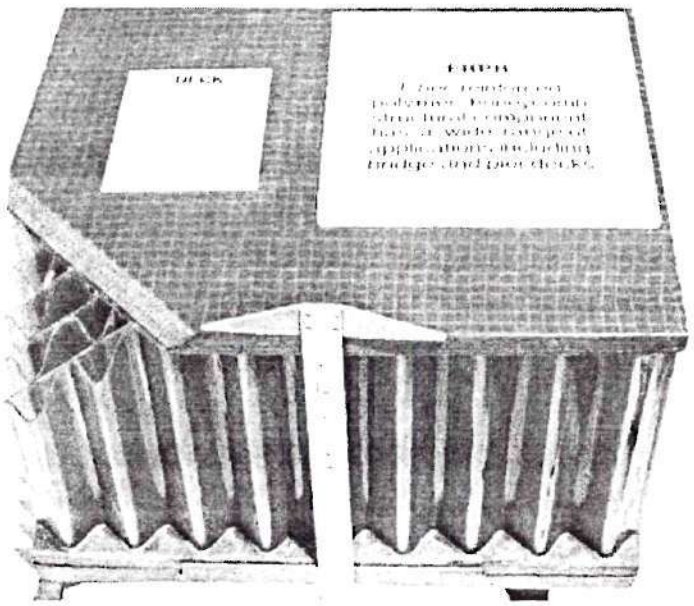

Figure 12. Fiber-reinforced polymeric honeycomb snadwich panel (Courtesy of KSC)

1.5 EXperimental Evaluations of FRP bridge deck concepts

Laboratory and field tests were performed on some but not all of the fiber-reinforced polymeric bridge deck concepts mentioned earlier in the previous section. Hereafter, a review of the level of experimental activities associated with the evaluation of the material and structural properties of FRP deck concepts encountered in the literature is presented. This review is limited to investigations that were documented in the form of technical reports and papers.

1.5.1. MATERIAL CHARACTERIZATION

The experimental characterization of the properties of the composite materials used for a bridge deck applications plays a significant role not only in the analysis and design of the structural system but also in the assessment of the quality control of the manufactured system during the fabrication process.

There are a limited number of bridge deck studies that have documented data bases associated with material characterizations. One of these studies was carried out at the Georgia Institute of Technology (Zureick and Acosta 1999) in conjuction with the development of a lightweight modular deck for application to the landing shipquay/causeway and mobile offshore base. Testing at the coupon level was a continuous process to ensure that there was an acceptable variation limit in the material properties of the fabricated components. Tests were conducted on coupons excised from the top and bottom plates as well as the triangles, comprising the FRP deck section, as shown in Figure 13, to determine the relevant physical properties (density, fiber volume, and glass transition temperature) and the mechanical properties (tension, compression, in-plane shear, and flexure) associated with the x-, y-, and 45° directions shown on the figure. The top and bottom plates that were fabricated by the semi-automated hand lay-up technique had an average fiber volume of 35%. The average fiber volume attained during the fabrication of the pultruded triangles was 47%. An important finding resulted from the coupon testing program was that the mechanical properties of the pultruded triangles could be improved by post cure at 140°C. Presumably the matrix was not fully reacted as it left the die and post cure maximize the resin performance.

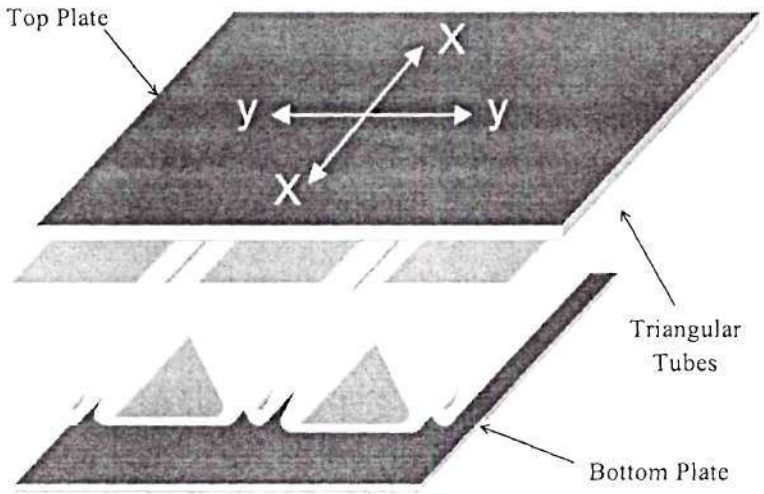

Figure 13. Bridge deck elements

In connection with the development of the West Virginia University hexgonal shaped bridge deck (Vedam 1997), coupon tension and bending tests were conducted to examine the properties of various plate elements comprising the hexagonal and double-trapezoid components manufactured by the Vacuum Assisted Resin Transfer Molding (VARTM) process. The reinforcement in these components were in the form of rovings, stiched fabrics, choped strand mats, and continuous filament mats. In a later study (Shekar 2000) coupon tension, flexual, and short-beam tests were conducted on composite materials reinforced with stitched fabrics and fabricated by both the pultrusion process and the Seeman Composite Resin Infusion Molding Process (SCRIIMP) to examine the effects of various fiber architecture and fabrication processes on the

properties and modes of failure. It was found by Shekar (2000) that the stiffness and strength values of coupons fabricated by the the SCRIMP were approximately 50% of those of the pultruded coupons. Such a reduction was attributed to the lack of resin obseption, improper wet-out, and low-curing temperature of the SCRIMP.

1.5.2. COMPONENT TESTING

The objective of component testing is to evaluate various strength and serviceability limit states that the structure may reach during the actual use conditions. These tests can be static or dynamic.

The earliest of these tests condcuted on FRP bridge decks were performed by Azar (1989) who examined the performance of the X-shaped deck developed by plecnik under static and fatigue loading conditions. Three different types of components, one diamond combined with two triangular sections, two diamonds combined with four triangular sections, and three diamonds combined with six triangular sections, were studied. Practically all specimens experienced debonding at the unidirectional tapes/filament wound section interface, due to fatigue loading. These series of tests were followed by static and fatigue testing of simply supported deck panels, 2.12 m (7 ft) wide and 0.45 m (1.5 ft) long , constructed from 15 diamonds and 28 triangular sections (Plecnik and Azar, 1991). Acoustic emission sensors, strain gages and deflection gages were deployed to monitor the deck's response. Tests indicated that when the deck specimen was fatigued at a load ranging from 9.45 kN (2.1 kips) to 37.8 kN (8.5 kips) for 2 million cycles, a negligible loss of stiffness (approximately 2 percent) was observed. When the specimen was subjected to an additional 2 million cycles, the loss of stiffness was about 34 percent. In the higher load range, when the deck specimen was fatigued at a load range from 13.9 kN (3.1 kips) to 55.6 kN (12.5 kips), the loss in stiffness was approximately 5 percent. In both cases, the behavior of the deck during the loading and unloading stages was linear and elastic. From the extensive testing conducted by Plecnik and his co-workers, it was evident that damage under fatigue loadings consisted primarily of delamination initiation caused by inadequate or defective interface bonding between laminated panels or between adjacent layers of different fiber orientations within a laminate. Local buckling of thin delaminated layers under compressive service loads results in a severe opening action along the front of delamination crack and this may cause catastrophic delamination growth.

Mongi (1991) tested a multicellular deck system having the dimensions 142"x 48.25" x 5.5" under three different loading conditions; a midspan concentric load, midspan eccentric load,and midspan line load. The measured deflections compared very well with those computed from engineering type beam analysis as well as finite element analyses.

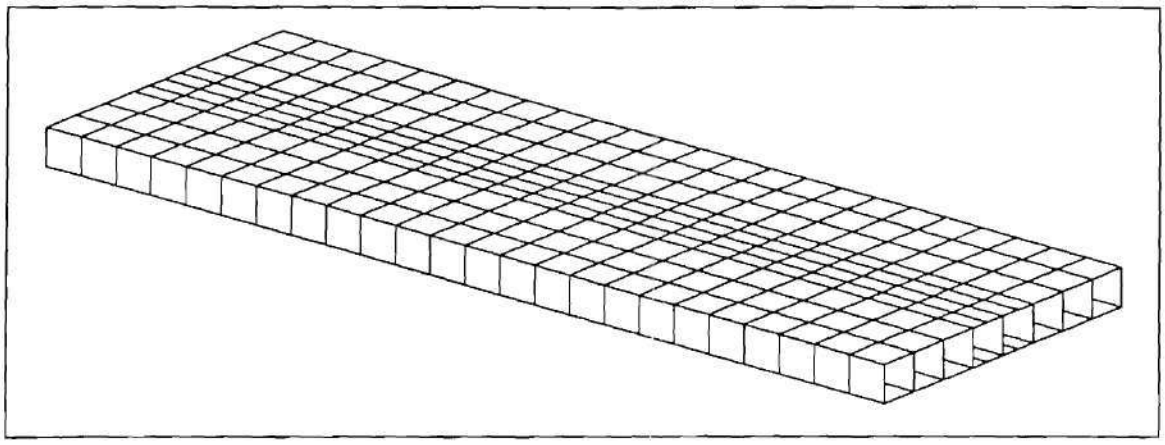

Figure 14. Multicellular deck system tested by Mongi (1991)

Lopez-Anido et al. (1998) presented the results of static and fatigue tests conducted on bridge deck components fabricated by the vacuum assisted resin transfer molding (VARTM) process. The strength and stiffness properties the deck elements reported to have been obtained experimentally at two different laboratories were not presented in the paper. Flexural tests conducted on fabricated components having a width of 45 inches and a length of 120 inches were conducted under two types of loading conditions: 1) a transverse line load of a width of 11.5 inches; and 2) rectangular patch load applied on area measuring 10 in x 20 in, as shown in Figure 15. The panels were instrumented with strain gauges and linear variable displacement transducers. The deflections under both the patch load and the line load were reported in a graphical form in which the span to deflection ratio is presented as a function of span to deck depth values. Finite element analyses of the experiments in which the deck component was subjected to a patch load showed that the deflection-load ratios at three different locations were very close to those measured experimentally. They also reported the results from a 2,000,000 cycle fatigue testing at a frequency of 3 Hz with the load ranging from 2000 lbs to 50,000 lbs. It was concluded that stiffness of the deck component did not degrade as a result of the fatigue testing.

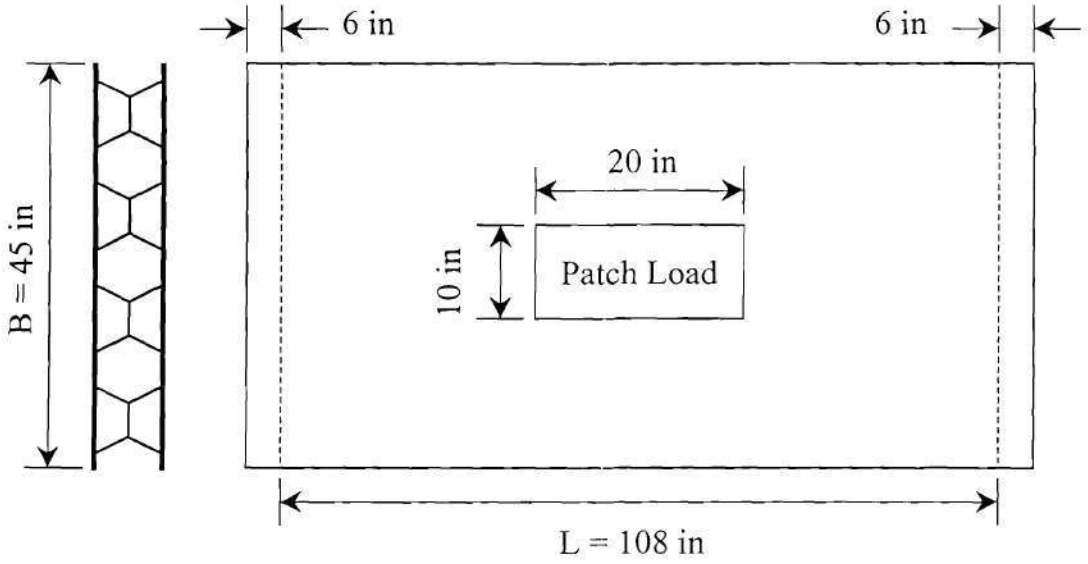

Figure 15. Component Test by Lopez-Anido et al. (1998)

At the Georgia Institute of Technology, structural components during the fabrication and also during the assembly were tested for quality control purposes and for establishing the strength and deflection limit states of various elements of the bridge deck. Three and four-point bending tests were performed on both laid up and pultruded triangular sections. A gravity load simulator (shown in Figure 16) was used as a loading fixuture so that measurements of vertical, horizontal, and rotational displacements of the triangles during loading were properly obtained. Rotation and out-of-plane distortion is an indication of material and dimensional non-uniformity. The braided/pultruded triangles showed significantly less lateral displacement and rotation than the laid up version.

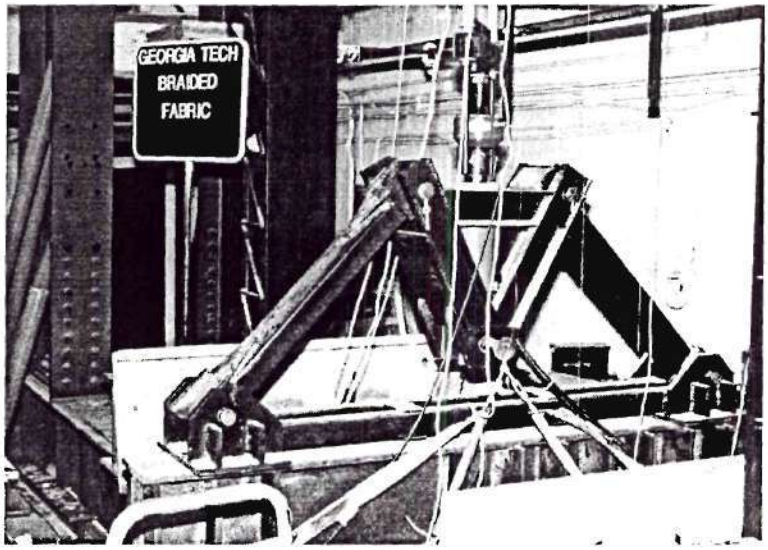

Figure 16. Gravity load simulator

A schematic of the three-point flexural test set-up of a triangular beam reinforced with 3D braided fabric is shown in Figure 15. The load-deflection and load-torsional rotation characteristics are shown in Figures 17 and 18, respectively. A five-cell assembly bridge deck component spanning 2.87 m was tested to failure. Figure 19 presents the load-deflection curve and shows the maximum load of 425 kN at which tensile failure of the bottom plate occurred.

Finally, 3 m by 3 m deck panels were tested in flexure under midspan line loading condition and also under a simulated wheel load whose dimensions were 20 in x 13 in. Under the effect of a simulated wheel load, the deck panel was able to resist a total load of 143 kips without failure. At this maximum load, the maximum tensile strain in the bottom plate was less than 0.3% , with a deflection of less than 17.8 mm.

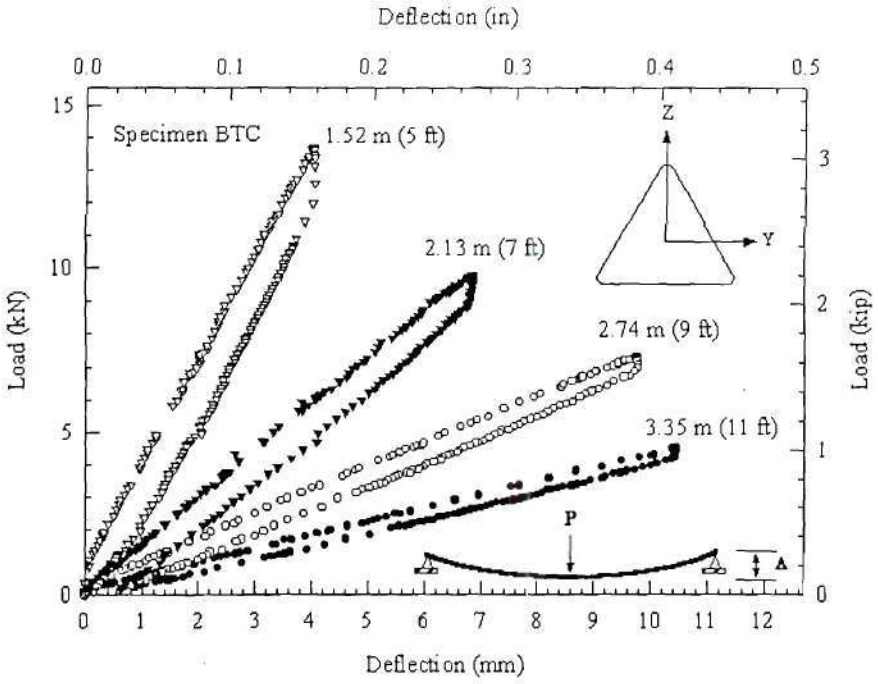

Figure 17. Load-deflection curves of a triangular beam with different spans

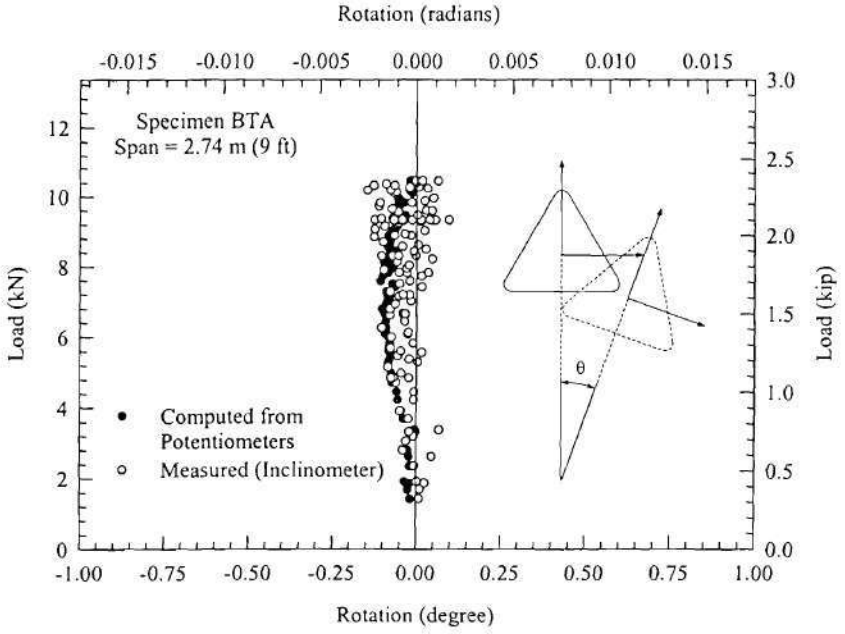

Figure 18. Load-rotation response of a triangular beam

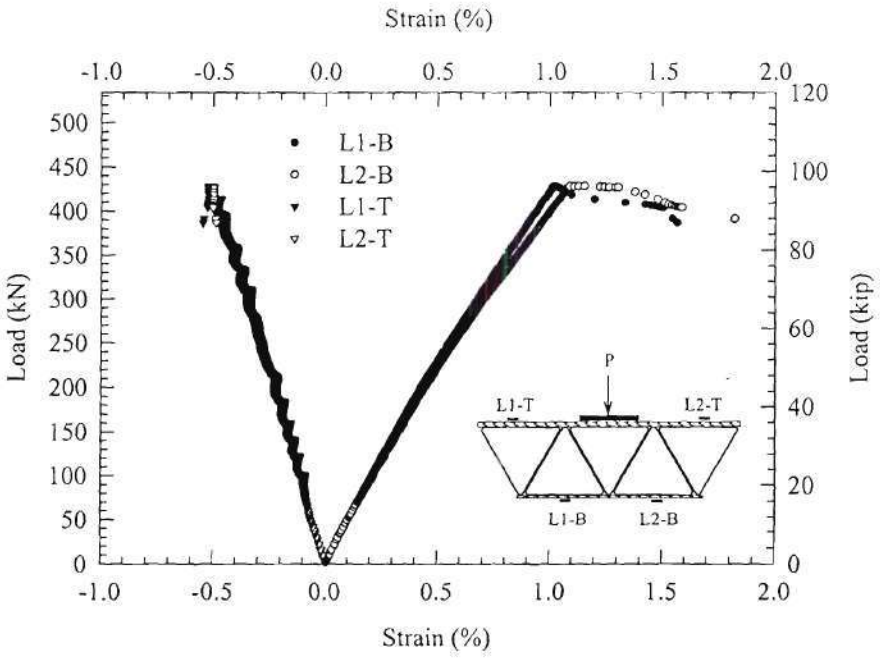

Figure 19. Load-deflection curves for a deck component

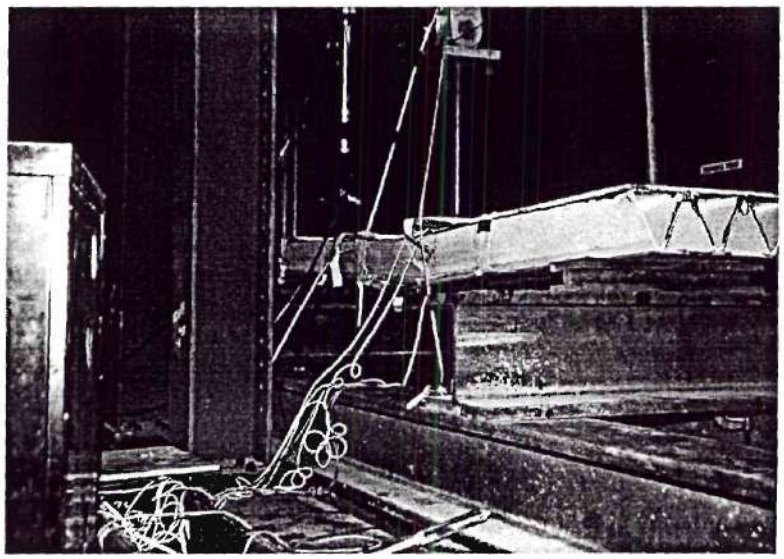

Figure 20. Failure of the 5-cell assembly under a single patch load

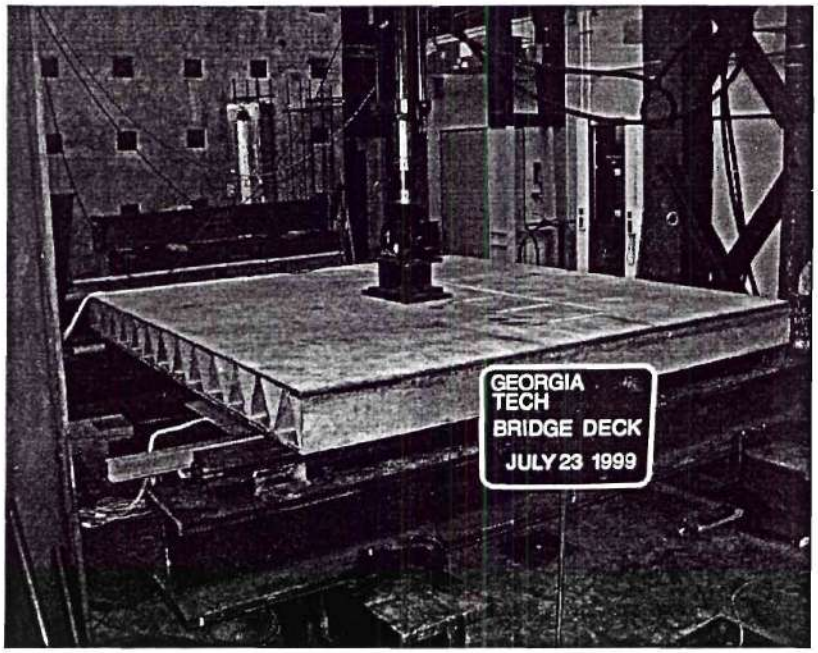

Figure 21. Testing of a 3m x 3m deck panel

At the Univesrsity of California San Diego, Karbhari et al. (1997) presented the results of experiments conducted on the bridge deck components shown in Figure 22. The length of these components was reported as 14 ft. They were placed on two high-strength concrete abutments spaced 8 ft. center-to center and tested with a load applied at the middle between the abutments. The load-deflection curves of each tested component were presented. It was shown that the stiffness of each tested polymer composite component was between two values representing the stiffness of an ucracked and cracked steel-reinforced concrete deck panel having almost the same dimensions as those made of polymer composites. Details regarding tests set-up, measured dimensions of each deck components, instrumentation plans, and material properties were not reported.

Finally, following concepts examined analytically and experimentally by Zureick (1989) and Mongi (1991), Hayes et al. (2000) evaluated the static and fatigue performance of an E-glass/polyester pultruded deck made by bonding square tubes with top and bottom plates under a simulated wheel load measuring 20 in x 12 in. The assembled component, 4-ft-wide, 14-ft-long, and 4.75-in-deep, was placed on W16x40 steel beam supports spaced 4 ft apart. Three different tests were conducted. In the first test, when the middle section was loaded to a maximum value of 25 kips, the deflection reached 0.15 in., which was equivalent to the unsupported span divided by 270. In the second test, one of the end deck panel was first subjected to a number of static load cycles prior to loading to failure at approximately 83 kips. In the third and final test, the other end panel was subjected to 3,000,000 cycles of loading between 2.5 kips and 25 kips at a frequency of 2 to 3 Hz. This fatigued panel was then tested to failure and showed a strength

almost equal to that of the unfatigued section. It was noted, however, that at the service load of 20.8 kips the defelction of the fatigued panel was approximately 14% higher than that of the unfatigued panel.

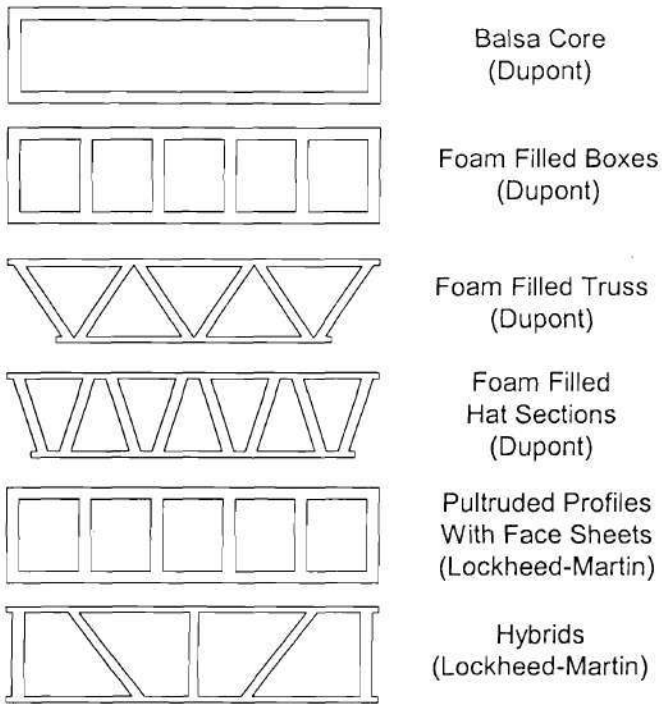

Figure 22. Bridge deck components tested by Karbhari et al. (1997)

1.5.3. CONNECTION TESTING

An analytical and experimental investigation related to connecting the bridge deck to supporting girders was conducted by Sampaga (1991), who showed that a promising approach to this type of connection was to place solid core inserts at the bottom of the diamond shape section and then bolt the deck to the supporting girders. He warned, however, that the use of access holes from the deck top could be detrimental as a result of fatigue loads in adverse environments, and proposed three designs, all of which eliminated the need to drill holes in the top deck surface. This deck-to-girder connection study was complemented by another analytical and experimental investigation aimed at developing the connection of deck-to-deck panels using 610 mm (24 in) long filament wound diamond-shaped wood inserts (Ali-kahn, 1991). It should be pointed out that the analytical results obtained from the above investigations underestimated the stress and deflection values measured experimentally.

1.5.4. FIELD TESTING

A limited number of field tests on polymeric composite bridge decks have been conducted and showed that there was very little composite action between the bridge decks and the support girders. Details of these investigations will be published in a separate report by Ganga-Rao (200x) However, presented briefly herein are only published field studies concerning the computation of the impact as well as the load distribution factors to the supporting girders.

Load distribition factors: GangaRao et al. (1999) reported that the load distribution factors determined experimentally on Wickwire Run bridge ranged from 0.15 to 0.35. These distrubution factors were found to be close to those computed from a simplified orthotropic plate theory using an assumption that the degree of composite action between the deck and the supporting girders was 50%. Reising et al. (2001) described the field tests conducted on three types of prefabricated fiber-reinforced polymeric bridge decks and one type of concrete bridge deck reinforced with polymer composite bars. These bridge decks were installed on bridges located on route 49 in Dayton, Ohio. Computed load distribution factors from experiemental data obtained from the Ohio bridge resulted in values ranging from approximately 0.2 to 0.75. Such values were lower than those computed from the current AASHTO Standard Specifications for Highway Bridges. All of the above conclusions were in line with the results of the anlytical study preconducted by Zureick and Shih (1994) who showed that the wheel load distribution factors of cellular FRP bridge decks supported by steel or Type II prestressed concrete girders were less than those computed by the AASHTO Standard Specifications for Highway Bridges.

Impact factor: In the study reported by Reising et al. (2001) it was concluded that for bridges having FRP decks, the values of the impact factor did not exceed the limit of 0.3 specified in the AASHTO Standard Specifications for Highway Bridges.

1.6 Summary

Based on the references reviewed in this chapter, the following conclusions are made:

1- Despite the limited number of available bridge deck composite materials data bases, there exists information sufficient to recommend guidelines pertaining acceptable consistent material property test methods and a uniform data reporting procedure to be followed by composite bridge deck manufacturers.

2- The majority of the bridge deck material property data found in the literature were concerned with the determination of physical (density, fiber volume fraction, glass transition temperature) and mechanical (tension, compression, shear) properties. Very little attention has been given to both thermal (thermal expansions and conductivities) and hygral (moisture expansion).

3- properties. wepolymer composite bridge deck for use by engineers and public agencies d establish recommendations pertaining the appropriate material property test methods and to examine such information statistically allow the defenitions of test methodsthe development of a methodology recommendations pertaining the determination of the probability distribution and

the characteristic design values of the properties. These databases have been assembled from tested coupons associated with accumulatedOne of the databases was generated under an FHWA study related to development of a lightweight modular deck for application to the landing shipquay/causeway and mobile offshore base.

used to propose examine Composite material property databases related to composite materials used for bridge deck applications are very limited.

Most research and development programs associated with polymeric composite bridge decks For virtually all cases in which polymeric composite bridge decks were investigated experimentally, flexural tests were among the most

CHAPTER 1: TEST METHOD AND DATA ANALYSIS

1.1 INTRODUCTION

The increased use of composite materials in bridge deck applications has focused the attention on the need for establishing an experimental data base for composite design engineers. In order to establish such a data base, standard test methods, failure criteria, and a data base of material properties need be identified, developed, and agreed upon by the bridge engineering community.

At present there is a scarcity of information concerning not only the material properties of composites but also the test methods that need to be adopted for reliable characterization of such properties. There is not a consistent basis for testing and reporting test data for use by structural engineers. Manufacturers report their data in many different forms, often without sufficient information to know exactly how the data were obtained. In addition, different test methods may be employed. For composites to be used in bridge applications, consistent test methods, analysis techniques, and reporting formats are needed to evaluate their reliability.

This chapter reviews various test methods available for characterizing composite materials and recommends the most suitable test method for each desired property. In addition, proposed is a specific explicit method for conducting consistent, statistically-valid analysis for reporting composite mechanical property data. Such a method accounts for the uncertainties arising from the parameters being determined from a finite population.

1.2 PROPERTY CHARACTERIZATION TEST METHODS

The analysis, design, or material qualification methods pertaining to polymeric composite bridge structures require an understanding of the response of the mechanical, thermal and hygral properties of the material under a variety of mechanical loading and environmental conditions. These properties can be classified into four categories:

1) Physical Properties: density, fiber volume fraction, and the glass transition temperature,
2) Mechanical Properties: tension, compression, and shear,
3) Thermal Properties: thermal expansion, and
4) Hygral Properties: diffusivity and moisture expansion coefficients.

Standard test methods to properly characterize the aformentioned properties have been developed in the past within the context of aerospace structures with most emphasis being placed on the mechanical properties. Descriptions of these test methods with commentaries on their applicabilities to composite materials having thicknesses and fiber architecture similar to those intended for bridge structures are hereafter described.

1.2.1. PHYSICAL PROPERTY TESTS

1.2.1.1. Density

The density of composite materials can be determined according to ASTM D792 Standard Test Methods for Density and Specific Gravity (Relative Density) of Plastics by Displacement. In such a standard, small samples representative of the element for which the data are required are cut to any size and shape of a volume not less than $1 cm^3 (0.06 in^3)$. The density measurement is determined by evaluating the difference between the weight of a sample in air and in air-free, distilled, or demineralized water as follows:

$$\rho_c = SG \cdot \gamma_w \tag{1}$$

where

$$SG = \frac{W_a}{W_a - W_w} \tag{2}$$

in the above equations

ρ_c = Density of the composite

SG = Specific gravity of the water at the water measured temperature during the experiment.

W_a = Weight of the sample in air.

W_w = Weight of the sample in water

1.2.1.2. Fiber Volume Fraction

The fiber contents of fiber-reinforced polymeric composites are determined according to either the ASTM D3171 Standard Test Method for Fiber Content of Resin-Matrix Composites by Matrix Digestion or the ASTM D2584 Standard Test Method for Ignition Loss of Cured Reinforced Resins. In the ASTM D3171 standard, weighed samples of the composite are immersed in a hot digestion medium to dissolve the resin portion. The digested samples are then filtered, washed, dried, and weighed again. The fiber content by weight can then be computed and converted to a volume percent provided that the densities of both the composite and the fibers are known. In the ASTM D2584 standard a weighed composite sample placed in a crucible is ignited and allowed to burn until ash and carbon remain. The residue is reduced further to an ash by heating in furnace at 565° C, cooled in a desicator, and weighed again so that fiber content by weiegt can be computed and converted to a volume percent. It should also be noted that the ASTM D2584 is most suitable for composites reinforced with glass fibers only. In addition, neither the ASTM D2584 nor ASTM D3171 standard accounts for the presence of fillers in the resin matrix, which is very common in commercially available polymeric composite bridge decks. This issue was addressed by Ye et al. (1995) who proposed a simple approach to supplement the

ASTM D2584 Standard. Such a proposal has not yet been adopted in the ASTM D2585 Standard. Since most commercially available composite bridge decks are manufactured with resin matrices containing fillers in the form of Kaolin clay, calcium carbonate, or alumina trihydrate with reinforcements in the form of unidirectional roving and randomly oriented short or long fiber mats, it is recommended that the approach of Ye et al. for separating the fillers be followed. Prior experience associated with the development of a triangulated polymer composite bridge deck (Zureick and Acosta 1998) showed that sulfiric acid- hydrogene poroxide mixture (Procedure B of ASTM D3171) was found unsuccessful in breaking up vinylester/E-glass based composite samples. Digestion in nitric acid was found to work after a very long digestion time. Because dilution of the concentrated nitric acid caused precipitation of vinylester particles, an acetone rinse worked much better. After several drying cycles in an oven at 110 ^{o}C, a constant weight was attained from which the fiber content could be estimated.

When the weight of the composite constitents are determined experimentally by any appropriate method, the following equations are hereafter developed for the determination of the fiber, resin, fillers, and void content of a composite sample consisting of both roving and mats or fabric as shown in Figure 1.

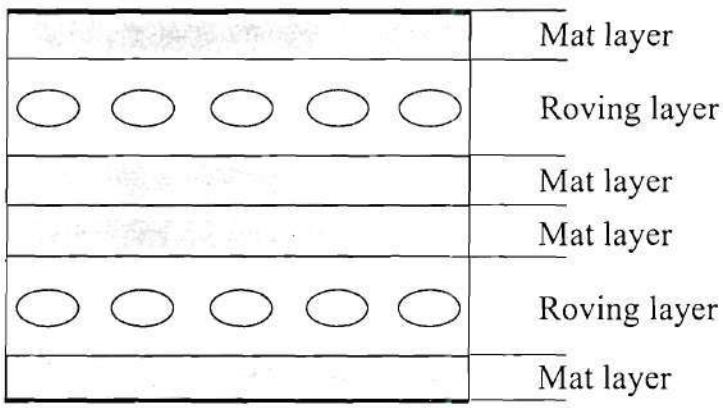

Figure 1. A composite sample reinforced with roving and mats

For such a case, the total weight of a composite sample, W_c, can be expressed mathematically in the form:

$$W_c = W_f + W_m \tag{3}$$

Where W_f and W_m are the weight of fibers and the matrix, respectively.
For the case of reinforcing fibers in the form of roving and randomly oriented filament mats, the above equations can be expressed further in the form:

$$W_f = W_{f/roving} + W_{f/mat} \tag{4}$$

$$W_m = W_{m/roving} + W_{m/mat} \tag{5}$$

where $W_{f/roving}$ and $W_{f/mat}$ are the weight of roving fibers and the weight of mat fibers, respectively. $W_{m/roving}$ and $W_{m/mat}$ are the weights of the matrices in the roving layers and the mat layers, respectively.

Since the matrix of the composites consists of resin, filler and voids, the total weight of the matrix is expressed as

$$W_m = W_r + W_{\text{filler}} \tag{6}$$

where W_r and W_{filler} are the weight of the resin and fillers, respectively.

Computation of Weight Fractions:The weight fractions of the fibers, w_f, and matrix, w_m, satisfy the equation:

$$w_f + w_m = 1 \tag{7}$$

where

$$w_f = \frac{W_f}{W_c} \tag{8}$$

$$w_m = \frac{W_m}{W_c} \tag{9}$$

The fiber weight fraction w_f can now be written in the form

$$w_f = w_{f/roving} + w_{f/mat} \tag{10}$$

where

$$w_{f/roving} = \frac{W_{f/roving}}{W_c} \tag{11}$$

$$w_{f/mat} = \frac{W_{f/mat}}{W_c} \tag{12}$$

The weight fraction of the matrix can also be expressed in terms of two parts:

$$w_m = w_r + w_{\text{filler}} \tag{13}$$

and

$$w_r = \frac{W_r}{W_c}$$
$$w_{\text{filler}} = \frac{W_{\text{filler}}}{W_c} \tag{14}$$

where w_r and w_{filler} are the weight fractions of the resin and the filler, respectively.

It is noted that when the method of ignition loss is used, a percent of the amount of filler will be lost after burning-out. Thus, the estimated weight of fillers in terms of that after the burn-out procedure can be obtained as follows from:

$$W_{\text{filler}} = W^*_{\text{filler}} \times (1 + \delta) \tag{15}$$

where W^*_{filler} is the weight of filler after burn-out process and δ is the percentage of weight loss of fillers (δ=14% for kaolin clay; δ=34.6% for alumina trihydrate, Ye et al., 1995).

Computation of Volume Fractions: The total volume of the composite sample, V_c, can be expressed as follows:

$$V_c = V_f + V_m + V_{\text{void}/p} \tag{16}$$

where V_f, V_m and $V_{\text{void}/p}$ are total volumes of fibers, matrix and voids resulted from the pultrusion process. V_f can be obtained using the weight and the density of the fibers. Similarly, V_f and V_m can be divided as follows:

$$V_f = V_{f/roving} + V_{f/mat}$$
$$V_m = V_{m/roving} + V_{m/mat} \tag{17}$$

where $V_{f/roving}$ and $V_{f/mat}$ are volumes of fibers in the roving layers and in the mat (CSM) layers, respectively. $V_{m/roving}$ and $V_{m/mat}$ are volumes of the matrix in the roving layers and in the mat layers, respectively.

The volume of the matrix can also be expressed as follows:

$$V_m = V_r + V_{\text{filler}} + V_{\text{void}/m} \tag{18}$$

where V_r, V_{filler} and $V_{\text{void}/m}$ are the volumes of resin, filler and voids contained in the matrix (resin+filler mixture). The total void content in the pultruded composites, V_{void} can be written as

$$V_{\text{void}} = V_{\text{void}/m} + V_{\text{void}/p} \tag{19}$$

Dividing Equation (16) by V_c, the following relation is obtained.

$$v_f + v_m + v_{\text{void}/p} = 1 \tag{20}$$

and

$$\begin{aligned} v_f &= \frac{V_f}{V_c} \\ v_m &= \frac{V_m}{V_c} \\ v_{\text{void}/p} &= \frac{V_{\text{void}/p}}{V_c} \end{aligned} \tag{21}$$

where v_f is the volume fraction of the total fiber content, and v_m is the total volume fraction of the matrix. $v_{\text{void}/p}$ is the volume fraction of the void contents that resulted from the fabrication process.

The volume fractions of the matrix can also be written as

$$v_m = v_r + v_{\text{filler}} + \frac{V_{\text{void}/m}}{V_c} \tag{22}$$

and

$$\begin{aligned} v_r &= \frac{V_r}{V_c} \\ v_{\text{filler}} &= \frac{V_{\text{filler}}}{V_c} \end{aligned} \tag{23}$$

where v_r and v_{filler} are the volume fractions of the resin and filler. The volume fraction of voids in the composites, v_{filler}, can be expressed as

$$v_{\text{void}} = v_{\text{void}/p} + \frac{V_{\text{void}/m}}{V_c} \tag{24}$$

With the volume fractions of the roving fibers, the mat fibers and the matrix, the following relations can be employed for computing the volume fractions of the roving layers, v_{roving} and volume fraction of the mat layers, v_{mat}.

$$v_{roving} = \frac{V_{f/roving} + V_{m/roving}}{V_c}$$
$$v_{mat} = \frac{V_{f/mat} + V_{m/mat}}{V_c} \quad (25)$$

and the following condition must be satisfied.

$$v_{roving} + v_{mat} = 1 \quad (26)$$

1.2.1.3. Glass Transition Temperature

Temperature is of particular importance. Defining the operating temperature range requires, of course, a proper examination of the climatological data for the location in which the structure is to be built. The data can be statistically analysed for trends and variations (see as an example Von Storch and Zwiers ,1999) so that high and low temperature values can be estimated for a region and time interval, which have a specified annual probability of being within the admissible range. Temperature records in the United States are readily available through the National Climatic Data Center (NCDC). The AASHTO bridge design specifications (AASTO 19xx) adopts five low temperature zones in connection with the design of bridge bearings. As a first approximation, we will define the operating temperatures by the range bounded by the all-time daily temperature maximum and minimum recorded in a given location from the observed climate. Figures 2 and 3 show these extreme values for each state individually (Source NCDC)

To appropriately select the polymeric composite most suitable for bridge deck applications, the designer will rely upon the dimensional stability, strength and stiffness properties of the materials for which the main determinant is their glass transition temperature, T_g . The glass transition temperature is defined as the approximate temperature value or temperature range at which the matrix changes from a glassy to a rubbery state. Above T_g , the composite softens and looses its mechanical properties as illustrated in Figure 4. In addition, it is to be noted that T_g decreases as the moisture content in the composite increases. The glass transition temperature can be estimated in accordance with D3418-99 Standard Test Method for Transition Temperatures of Polymers by Differential Scanning Calorimetry. Laboratory measurements of the air temperature inside one of the tringular cells of one polymeric composite bridge were on the average 17°C (° F) higher than the ambient air temperature. Analytical studies (Suchinda 2000) showed that the material surface temperature in an FRP bridge deck could easily be as high as 30°C (° F) when the deck is covered with a material having absorptivity of 0.5. Thus, it is recommended that glass transition temperature of the resin of fabricated composites intended for use in bridge components be at least 30°C (86° F) above the record highest temperature shown in Figure 2.

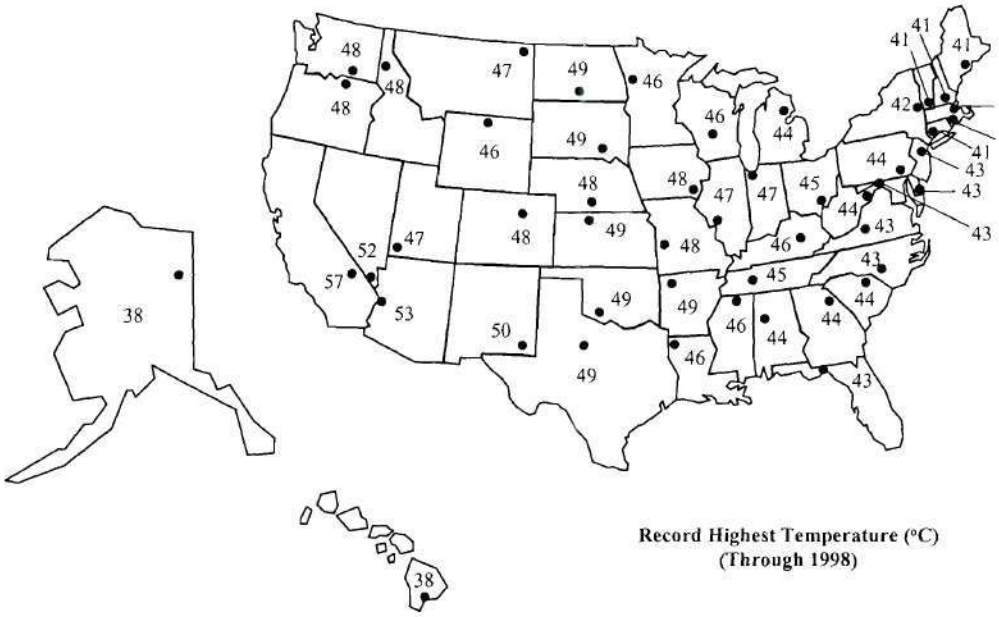

Figure 2. Record Highest Temperature (^{0}C) by States (Source: NCDC)

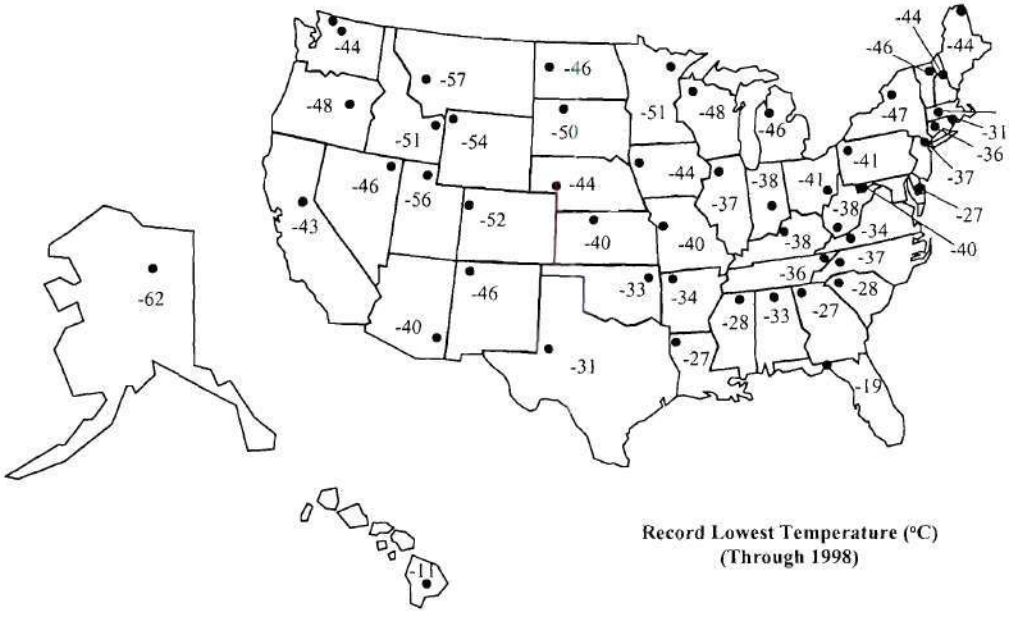

Figure 3. Record Lowest Temperature (^{0}C) by States (Source: NCDC)

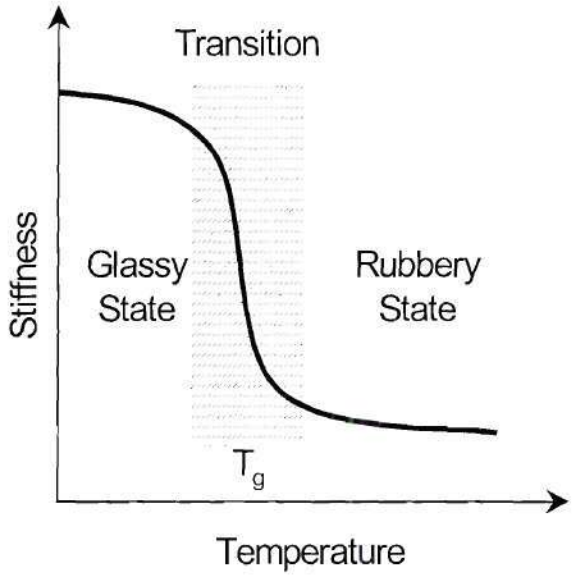

Figure 4. Above the glass transition temperature, T_g , the composite softens

1.2.2. MECHANICAL PROPERTIES

1.2.2.1. Tensile Properties

At the present time, there are two ASTM tensile test methods used by the composite industry: the D638 Test Method for Tensile Properties of Plastics and the D 3039/D 3039M Test Method for Tensile Properties of Polymer Matrix Composite Materials. The D638 Standard is not applicable to composites reinforced with oriented fibers, which is the likely case for bridge decks. In addition, the ASTM D638 Standard adopts a dumbbell-shaped coupon that requires careful machining for the formation of an external notch, and subsequently cutting some of the continuous fibers. The stress concentration due to the presence of an external notch aggravated by the damage due to cutting the longitudinal fibers significantly influences the failure mode in a dumbbell-shaped coupon under tension. Such a failure was found experimentally to occur prematurely almost always at the notch prior to reaching the true ultimate strength of the materials as shown in Figure 5. .

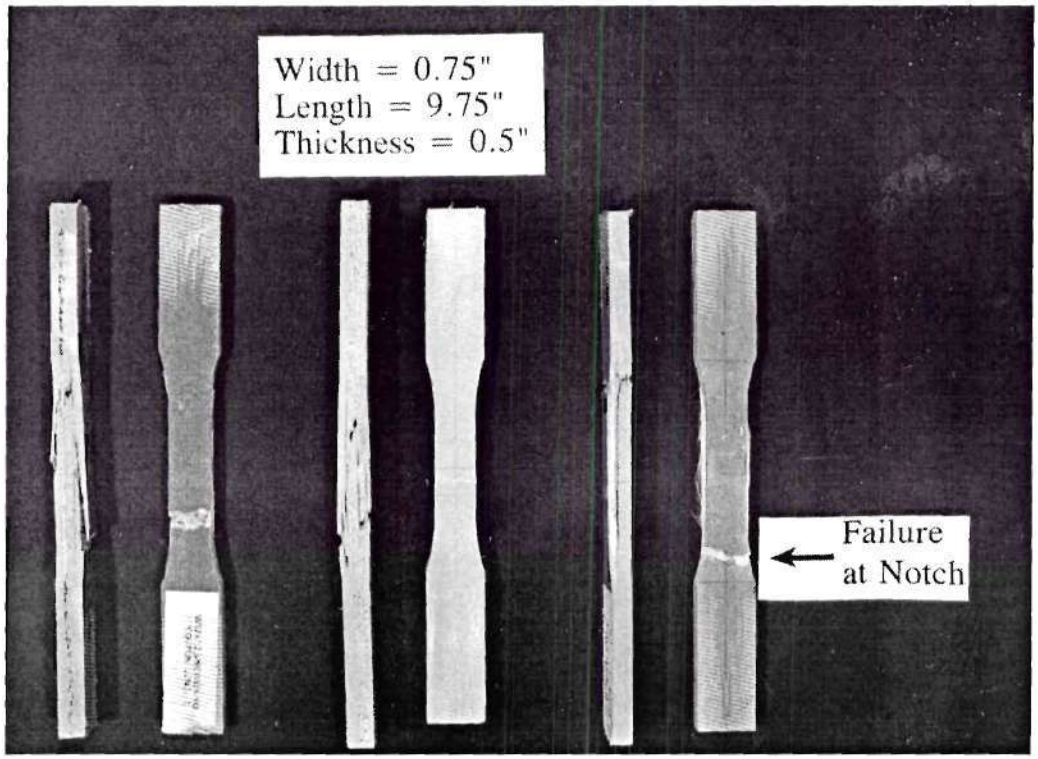

Figure 5. Failure of tested Dumbbell-shaped tensile coupons at the notch radii

The ASTM D3039 Standard uses prismatic coupons but requires tabs to be machined and bonded to the end of the coupon. Tabs protects the coupon ends from damage resulting from the testing machine grip pressure but produces stress concentration that promotes failure near the grip. Researchers (Turvey, 1992 , Wang and Zureick 1994; Zureick and Scott 1997) found that for thick composites (thickness greater than 2 mm or 1/16 in) the use of tabs was unecessary. The tensile property results for thick tensile tabbed coupons are similar to those without tabs.

1.2.2.2. Compressive Properties

The determination of the compressive properties of composites have been the subject of numerous investigations during the past 40 years. Two ASTM Standards are available: ASTM D 695 Test Method for Compressive Properties of Rigid Plastics or the ASTM D 3410 /D3410M Test Method for Compressive Properties of Polymer Matrix Composite Materials. The D 695 Standard does not require the use of strain gages and allows the width of the test coupon to vary. The coupons in the ASTM D 695 Standard require precision machining to obtain the dogbone shape and often fail either by crushing at the ends or at the end grip as a result of high stress concentration at the radii. The coupons in the ASTM D3410 Standard are prismatic but requires end tabs that also produce stress concentration. Experience with testing thick composites in compression have showed that the use of prismatic coupons without end tabs consitutes acceptable tests as long as the out-of-plane bending resulting from the test does not exceed the recommended

value in the ASTM D3410 Standard. Failure of a compression coupon without tabs is shown in Figure 6. It is to be noted that the ASTM D30 Committee is presently in the process of approving a new standard for a compression test in which no coupon tabs are required. This effort should be completed by the end of year 2001.

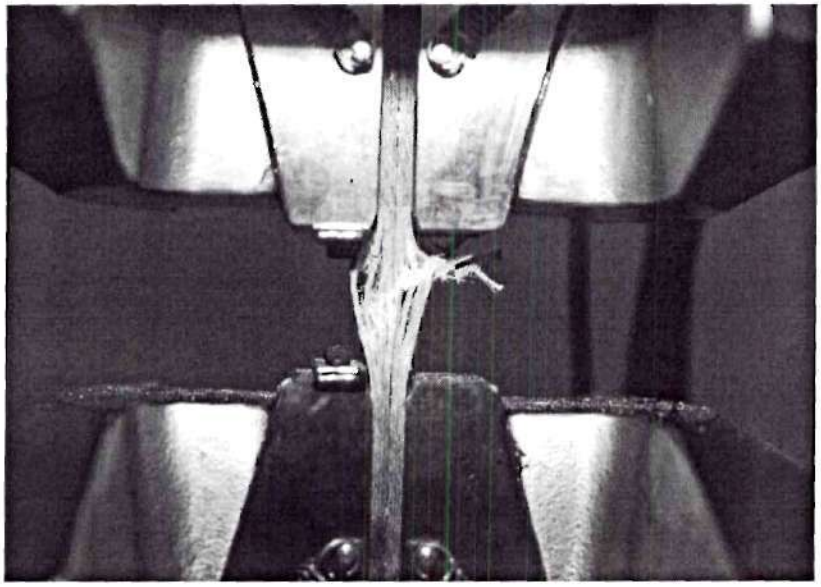

Figure 6. Failure of a compression coupon without end tabs

1.2.2.3. Shear Properties

Shear behavior has always been a foremost consideration in the utilization of fibrous composite materials as structural components. Indeed, shear tractions are inherent at the interfaces of the different materials; fibers and matrix, due to their different mechanical properties. Early experimental research used photoelastic procedures with built-up models, and with models of normal scale containing individual fibers or small numbers of fibers (Berghaus and Aderholdt, 1975; Jenkins, 1969; Maclaughlin, 1968; Schuster, 1964). These studies showed the presence of high stresses in the matrix, adjacent to the fibers, and of high shear stresses in the interlaminar region between fiber layers.

Thus, it is not surprising that special attention is given to shear testing of structural composites as shear force under service conditions might produce very high states of stress and structural failure. Different methods and methodologies of shear testing of composites have been developed over the past 20 years. Some of these test methods were adopted by the ASTM in the forms of :

- Standard test methods (D5379/D5379M-98 Standard Test Method for Shear Properties of Composite Materials by the V-Notched Beam Method , D3846-94 Standard Test Method for In-Plane Shear Strength of Reinforced Plastics, and D2344/D2344M-00e1 Standard Test Method for Short-Beam Strength of Polymer Matrix Composite Materials and Their Laminates),

- Standard guides(D4255/D4255M-83(1994)e1 Standard Guide for Testing In-plane Shear Properties of Composite Laminates), and

- Standard practice for testing (D3518/D3518M-94e1 Standard Practice for In-Plane Shear Response of Polymer Matrix Composite Materials by Tensile Test of a +/- 45° Laminate).

A detailed review and evaluation of previously developed shear property test methods was presented by Chaterjee et al. (1993). Lee and Munroe (1986) evaluated all available shear property test methods by a decision analysis technique based on criteria representing the cost of specimen fabrication, cost of testing, data producibility, and the accuracy of the experimental results and concluded that the Iosipescue test method, which was refined to become the ASTM D5379 Standard, and the +/- 45° off-axis tensile test, known now as the ASTM D3518/D3518M-94e1 Standard Practice, were top choices. These two test methods are described hereafter in more detail.

The ASTM D 3518 Standard Practice: The ±45° off-axis tensile test was suggested by Petit (1969). This method can be used to determine shear modulus and strength of composite materials having symmetric cross ply lay-up such as $[0/90]_{ns}$ laminates. A uniaxial tensile load is applied to a ±45° symmetric laminate specimen with the loading configurations as recommended by ASTM standard D 3518. The in-plane shear strength and shear modulus of the $[\pm 45]_{ns}$ laminate can be found using a conventional tensile testing machine with axial and transverse strain gage alignment. The schematic representation of the coupon and loading configurations are shown in Figure 7. This test method has the limitation that it can be used only for $[\pm 45]_{ns}$ or $[0/90]_{ns}$ laminates. Instead of a state of pure shear, a very complex stress state exists in the laminate specimen. Longitudinal normal stress and transverse normal stress are a function of the applied axial stress and of the shear stress induced in each lamina ply. The longitudinal normal stress, σ_{11}, transverse normal stress, σ_{22}, and in-plane shear stress, τ_{12}, can be expressed by

$$\sigma_{11} = \frac{1}{2}\sigma_x \pm \tau_{xy} \tag{27}$$

$$\sigma_{22} = \frac{1}{2}\sigma_x \mp \tau_{xy} \tag{28}$$

$$\tau_{12} = \frac{1}{2}\sigma_x \tag{29}$$

where σ_x is load P divided by the cross area (see Figure 7) and τ_{xy} is shear stress induced in each lamina ply.

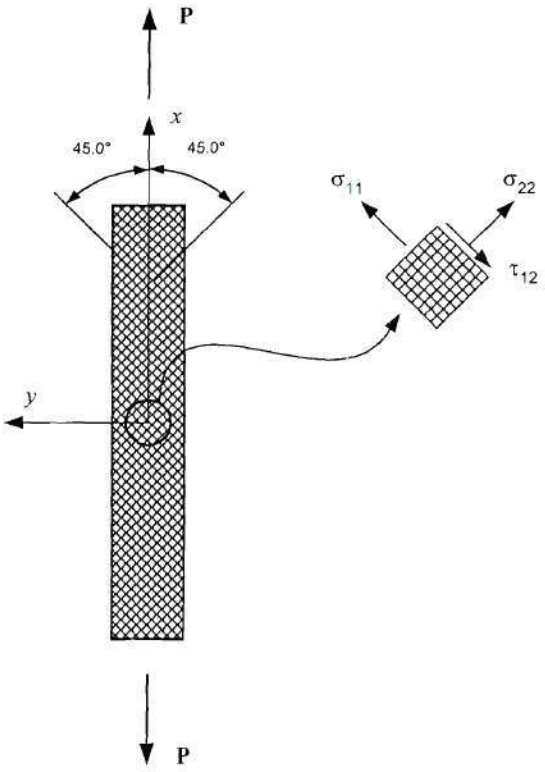

Figure 7. Configuration of the ±45° off-axis tensile test

The +45° ply uses the positive value in eq. (27) and the negative value in eqs. (28), respectively. The -45° ply uses the negative value in eq. (27) and the positive value in eqs. (28), respectively. The in-plane shear modulus, G_{12} can be obtained by following equation.

$$G_{12} = \frac{\sigma_x}{2(\varepsilon_y - \varepsilon_x)} \tag{1-1}$$

where ε_x and ε_y are magnitude of extensional strains in x- and y- directions, respectively.

The ASTM D 5379 Standard: The v-notched beam test method was first introduced by Iosipescu (1967) for determining the shear strength and shear modulus for isotropic materials. The Iosipescu shear test examines the strain in the plane of a prismatic beam that has near "pure" shear state region at its center. It has been modified and used for testing composite materials (Barnes, et al., 1987; Adams & Walrath, 1987a; Lee & Munro, 1990; Odom, et al., 1994). The ASTM D5379 Standard uses a shear test fixture (also known as Wyoming fixture and test

method; Adams and Walrath, 1987b) and v-notched beam specimen as shown schematically in Figure 8. This fixture consists of two identical halves that contain the specimen and provide the load. One is fixed on the base of the fixture; the other is designed to move along a sliding post parallel to loading direction. A photo of the Wyoming shear fixture is shown in Figure 9.

The loading mechanism of the ASTM 5379 Standard produces shear force and bending moment identical to those obtained from simple four-point loading case shown in Figure 10. It is shown that a region of constant shear, with zero moment, is produced at the center of the beam. The cross-sectional area of the beam is also reduced at this location through the use of 90° notches on the top and on the bottom of the beam. The notches permit non-zero shear stresses at the upper and lower boundaries. They also produce a smaller cross-section for increased stress magnitude and a consistent specimen shear failure zone. The uniformity of the shear stress is a function of the relative depth of the notches (Iosipescu, 1963).

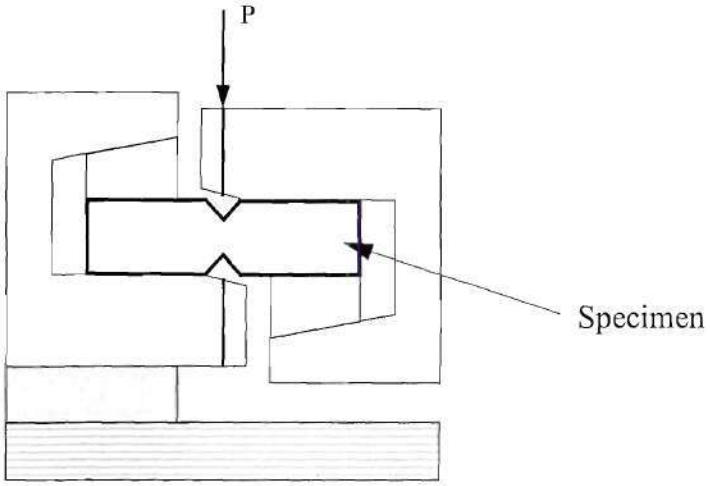

Figure 8. ASTM D 5379 shear test fixture and specimen

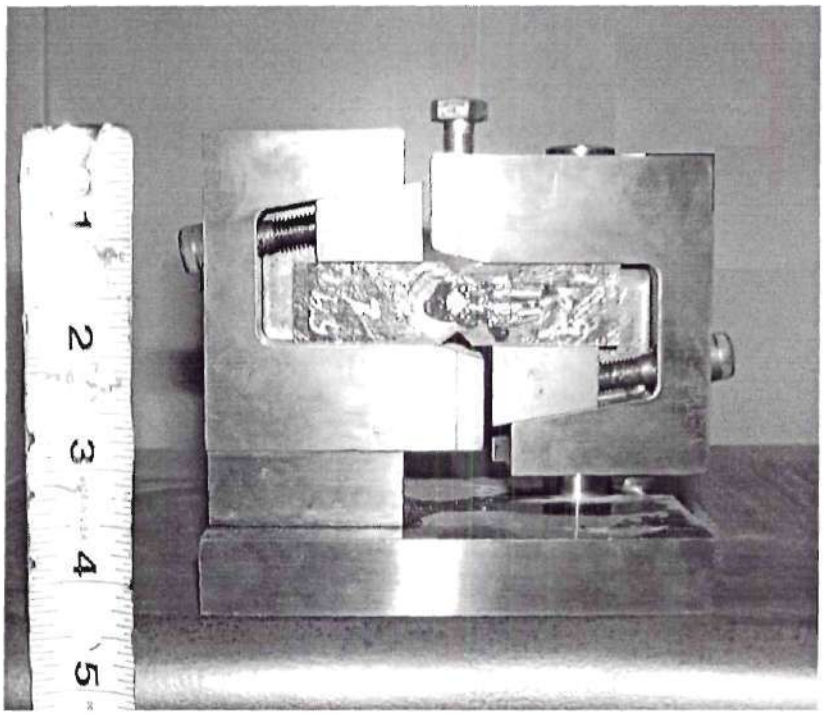

Figure 9. Wyoming (ASTM D 5379) shear test fixture with a coupon

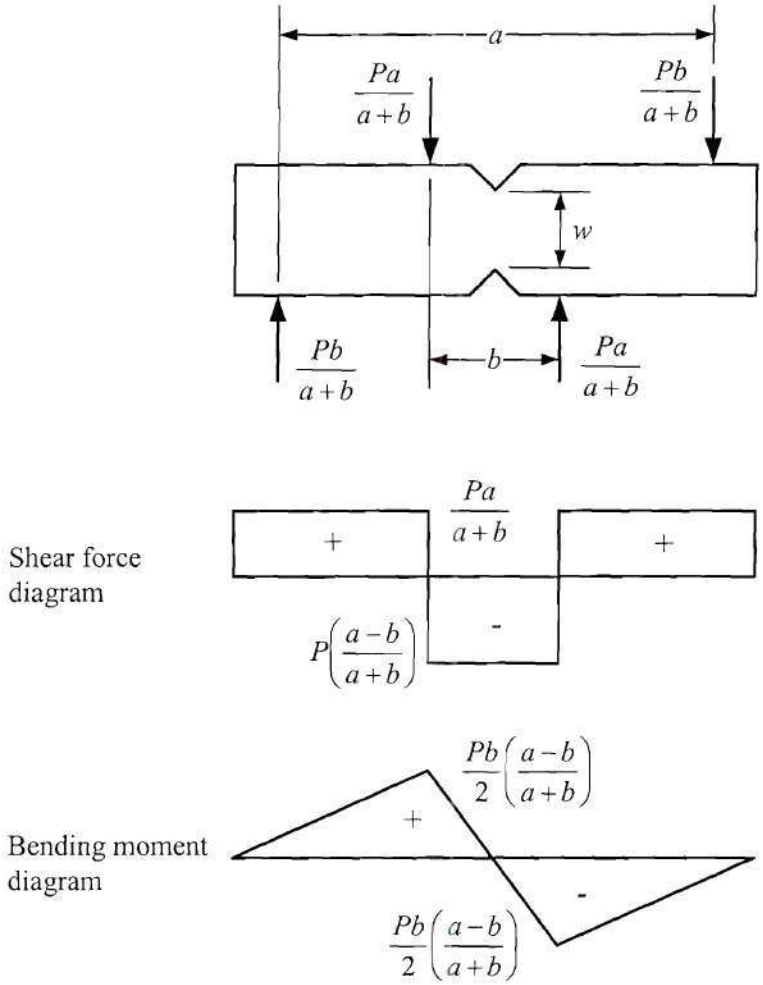

Figure 10. Shear and moment diagram for four point bending V-notched beam test

Under a 1993 study sponsored by the Federal Highway Administration, Zureick et al. (1997) developed a new test method and fixure for the determination of the in-plane and out-of-plane properties of composites used in highway structures. This test method was based upon the ASTM D5379 Standard that required many modifications to better represent the materials used in bridge applications. The developed shear property test adopts a specimen whose basic geometry and loading system are shown in Figure 11. The overall length of the specimen is 20.3 cm (8.0 in.) and the height is 3.81 cm (1.5 in.). The outside loads, P_e, are 15.2 cm (6.0 in.) and the inside loads, P_i, are 5.08 cm (2.0 in.) apart. Loading pads of 2.54 cm (1.0 in.) locally distribute the applied forces. This specimen and loading system are very similar to those devised by Iosipescu (1967) for producing a region of essentially pure shear in the central notch region. The shear and moment diagrams resulting from the new fixture are shown in Figure 12.

To produce a more expeditious test procedure, a four-point-loading fixture was developed to utilize the self-aligning feature of the tensile mode of test machine operation. Such tensile configuration is similar to that used by Slepetz, Zagaeski, and Novello (1978). For the new fixture, freely rotating bearing blocks are used at all four load points on the specimen. Pre-alignment pins are used to assure rapid specimen insertion and alignment. They are removed for testing. Adjustable horizontal stabilizers are used to permit testing interchangeability using specimens with different thicknesses. This fixture is less tedious to use than the compression loaded fixture, which required careful specimen insertion and alignment and placement of load distribution tabs. This new test fixture is shown schematically in Figure 13. A photo of the fixture is shown in Figure 14. A complete set of drawings for fabricating the fixture is presented in the Appendix.

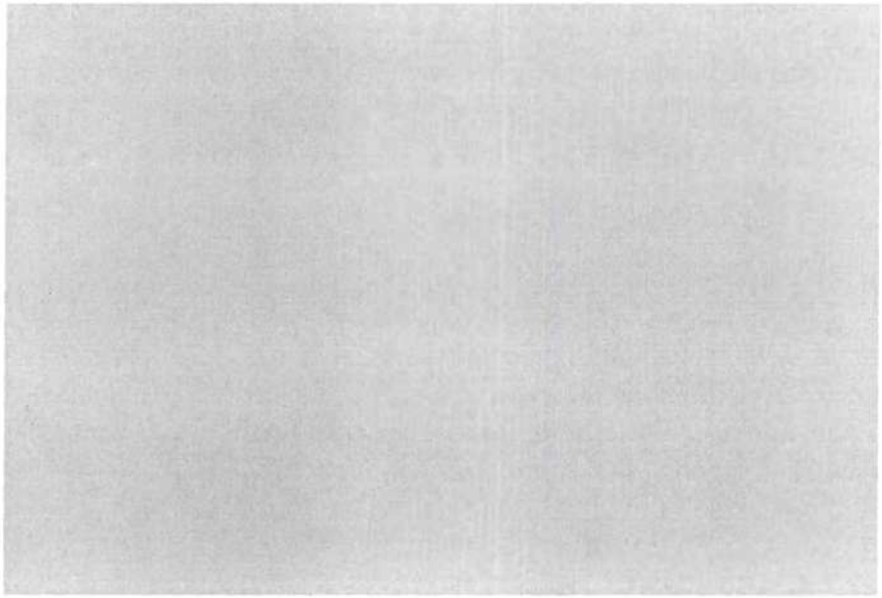

Figure 11. Shear specimen loading system

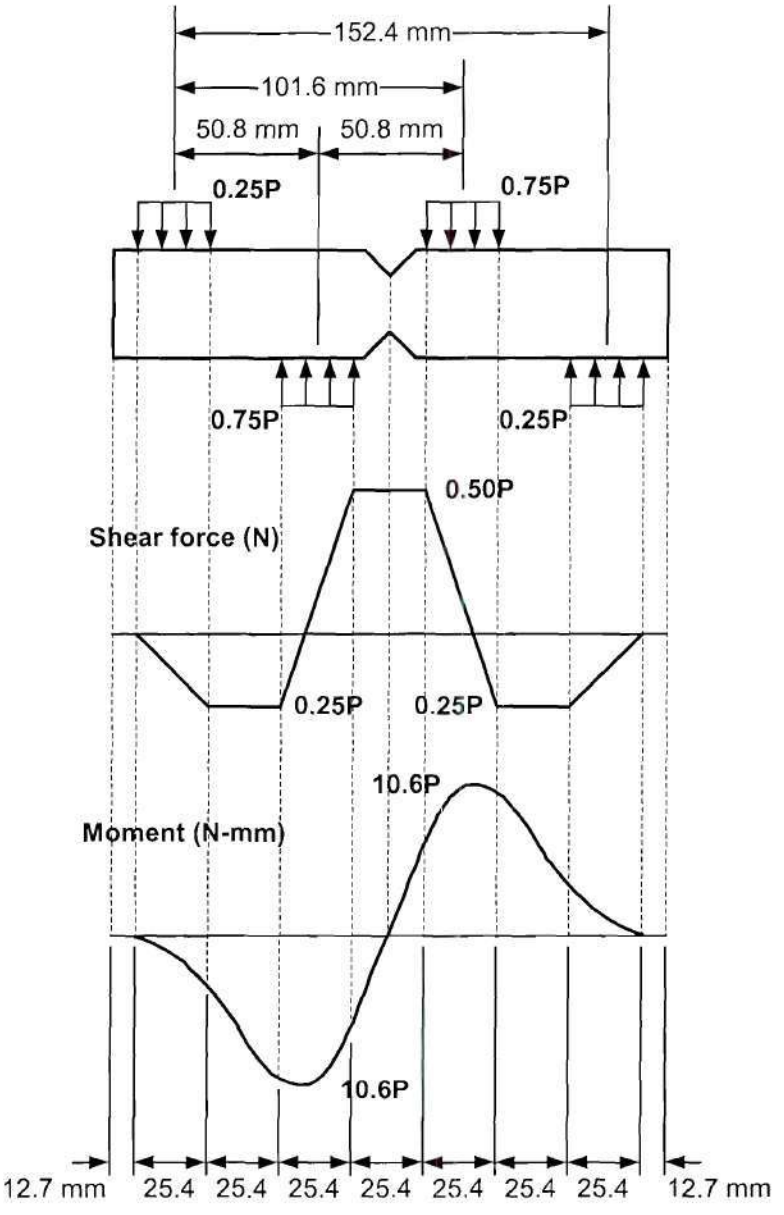

Figure 12. Shear coupon dimensions and moment diagram for the present shear test with applied load, *P* (N)

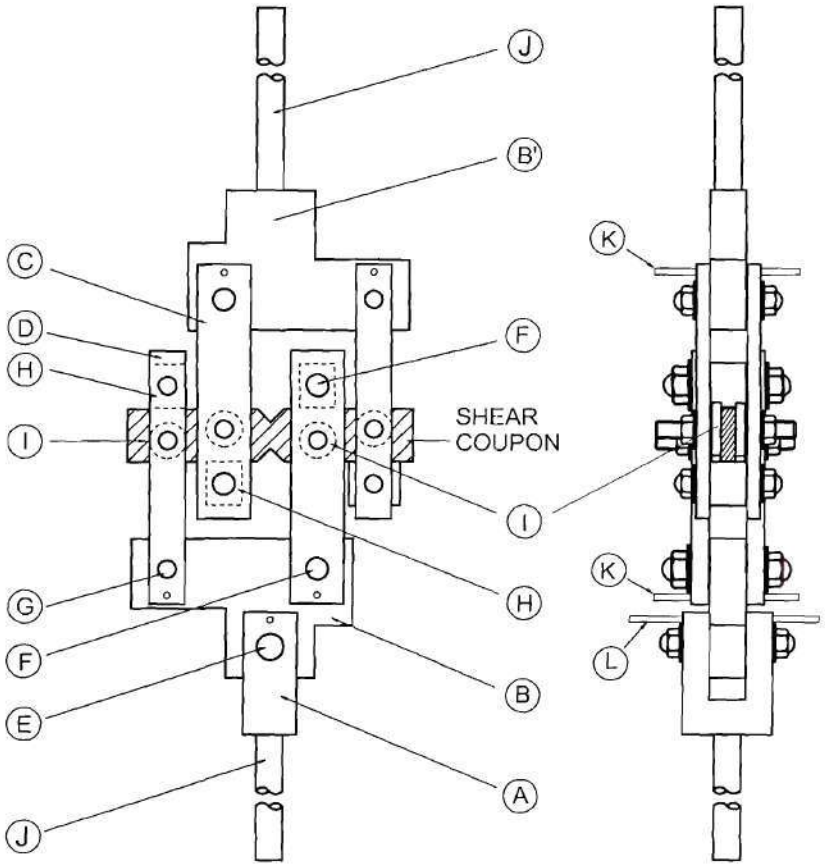

Part	Name	Utility
A	Main load Adaptor	Moment-free connection between main load shaft and l block
B, B'	Load Blocks	Load dividers
C	Large load bar	Tensile link
D	Small load bar	Tensile link
E, F, G	Pins	Moment-free connections
H	Bearing block	Applying a load to a specimen through the contacted su face between the bearing block and a specimen

Figure 13. Alignment and connections of the present shear test fixture

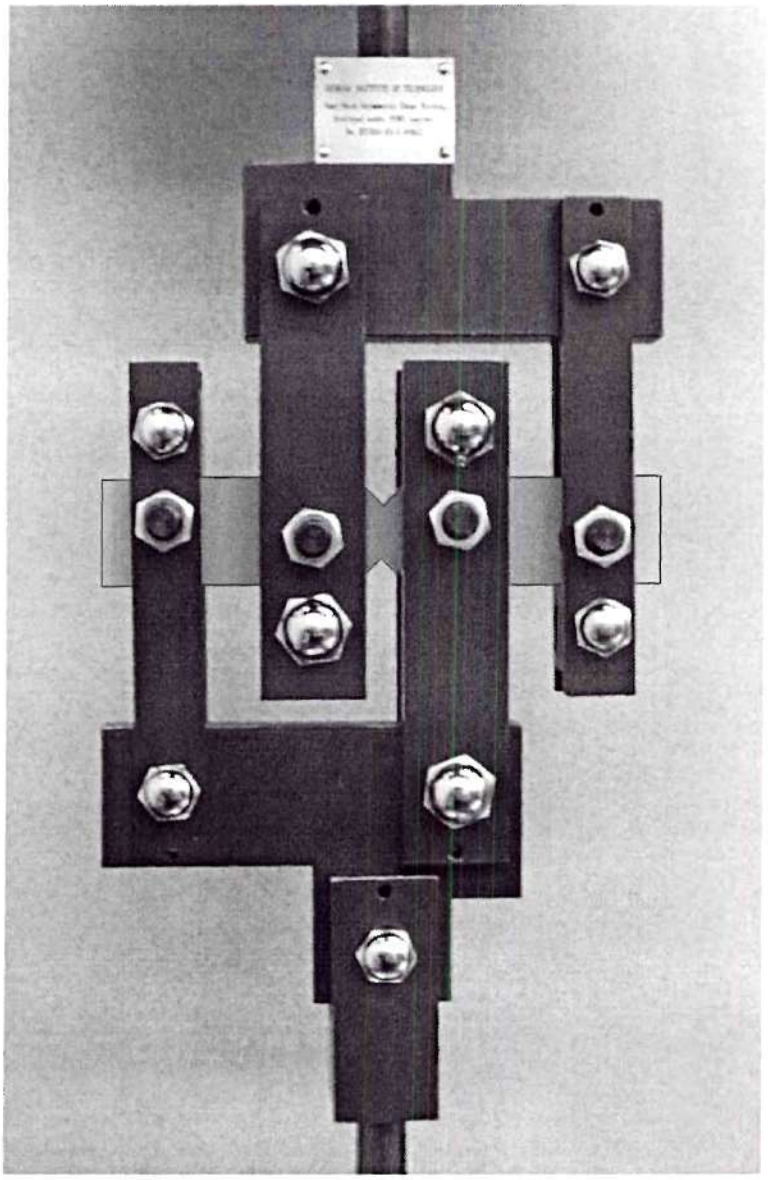

Figure 14. New shear fixure developed for FHWA (Zureick et al. 1997)

For polymeric composite materials, it is well known that the shear stress-strain relationship is nonlinear. ASTM D 5369 Standard recommends that the shear modulus be determined from the slope of the line connecting the 0.1% and 0.6% strain points in the stress-strain curve. A linear regression between the 0.1% and 0.6% strain points is a better approach. This is because one

would like to avoid incosistent results for cases in which any of the two strain readings (at 0.1% and 0.6%) are recorded incorrectly. Comparisons between the Wyoming shear fixture and the one developed for FHWA were made by comparing the longitudinal strain percent obtained from tests conducted in each fixture. Results are shown in Figure 15. This index is defined by the following equation:

$$\begin{aligned} \text{Longitudinal Strain Percent} &= \frac{\varepsilon_x}{\gamma_{xy}} \times 100(\%) \\ &= \frac{|\varepsilon_{0^\circ}|}{|\varepsilon_{-45^\circ}| + |\varepsilon_{+45^\circ}|} \times 100(\%) \end{aligned} \tag{30}$$

where the longitudinal strain percent was obtained at $\gamma_{xy} = 0.6\%$. In a pure shear strain field, the longitudinal strain measurement ε_{0° of the v-notched specimen should be zero at the center. Practically, the value of $|\varepsilon_{0^\circ}|$ will not be zero. A recommended requirement for a valid shear test is that the longitudinal strain percent is less than or equal to 5%.

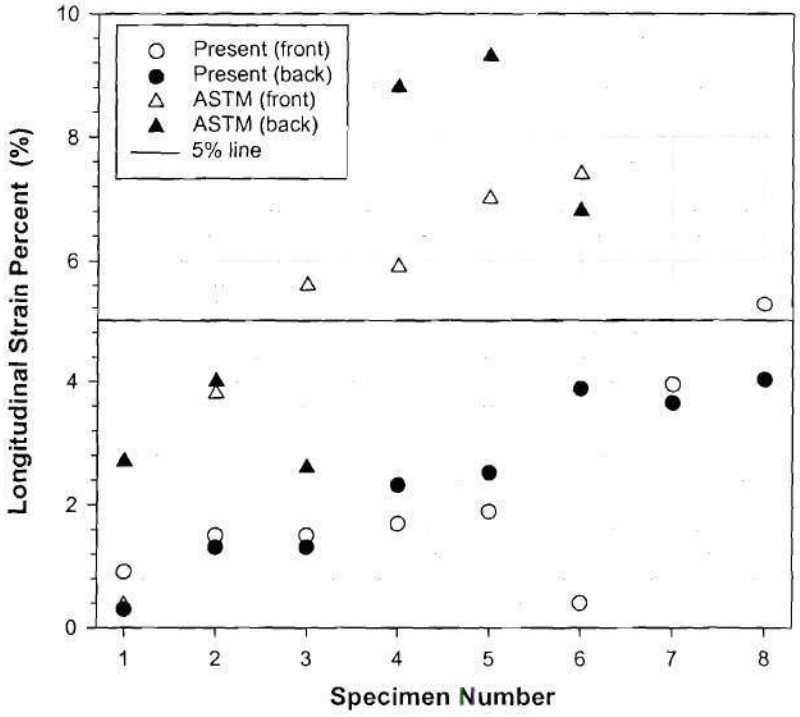

Figure 15. Comparison of longitudinal strain percent measured from specimens tested with the Wyoming shear fixture and the newly developed shear fixture

1.2.3. THERMAL PROPERTIES

Three ASTM Standard tests methods are available for the determiniation of the coefficients of thermal expansion of polymeric composites. These are:

1- ASTM D 696 Standard Test Method for Coefficient of Linear Thermal Expansion of Plastic Between -30° C and 30° C,
2- ASTM E228 Test Method for Linear Thermal Expansion of Solid Materials with Vitreous Silica Dilatometer, and
3-ASTM E 831 Test Method for Linear Thermal Expansion of Solid materials by Thermimechanical Analysis,

The ASTM D696 Standard is an approximate method for measuring the thermal expansion of plastic materials. It is applicable in the temperature range of -30° C and 30° C and shall not be used on materials having a coefficient of expansion smaller than $1x10^{-6}/^{o}$ C. The ASTM E 228 covers the determination of the linear thermal expansion of rigid solid materials over the temperature range of -180 to 900°C using vitreous silica push-rod or tube dilatometers. The ASTM E 831 uses thermomechanical analysis techniques and is applicable to the temperature range from -120°C to 600°C. The E228 Standard is more precise than either the ASTM D696 or the ASTM E831 Standards.

1.2.4. HYGRAL PROPERTIES

The moisture absorption characteristic (moisture diffusivity coefficient and the moisture equilibrium content) of composites used in bridge decks can be determined in accordance with ASTM D5229 Standard Test Method for Moisture Absorption Properties and Equilibrium Conditioning of Polymer Matrix Composite Materials. This Standard is directly applicable to flat panels as well as coupons intended to be conditioned for use in other test methods.

1.3 Statistical Analysis of mechanical property data

1.3.1. SPECIMEN LOCATION

Material properties are obtained from coupons cut from full-size specimens. An important aspect of the testing is the location from which the coupons are obtained. To examine variations in longitudinal tensile strength both along and throughout a composite section, Wang and Zureick (1994) tested specimens from a 254 x 254 mm I-shaped pultruded section as shown in Figure 16. The member had an isophthalic polyester matrix with E-glass rovings and non-woven mats with the lay-up shown in Figure 2.

The member was divided into six groups along the length. In each group, 18 coupons were obtained, three from each of the four flanges, and six from the web, Figure 3. Thus, the total number of specimens was 108, with each measuring 25.4 mm in width, 9.5 mm in thickness, and 254 mm in length. These coupons were tested in tension at a loading rate of 2.5 mm/

minute. The coupons were tested without tabs, with twelve failing due to stress concentrations from the grips. Those failing in the grips were not used in the statistical analysis. In order to maintain a balanced statistical design, the twelve missing data points (six from the flanges and six from the webs) were estimated. The data for each flange or web half was treated as a separate randomized block, and the missing value was chosen which had a zero residual. When there was more than one missing value, an iterative process was performed to converge to the estimates. For each estimated value, one degree of freedom in the statistical analysis was lost.

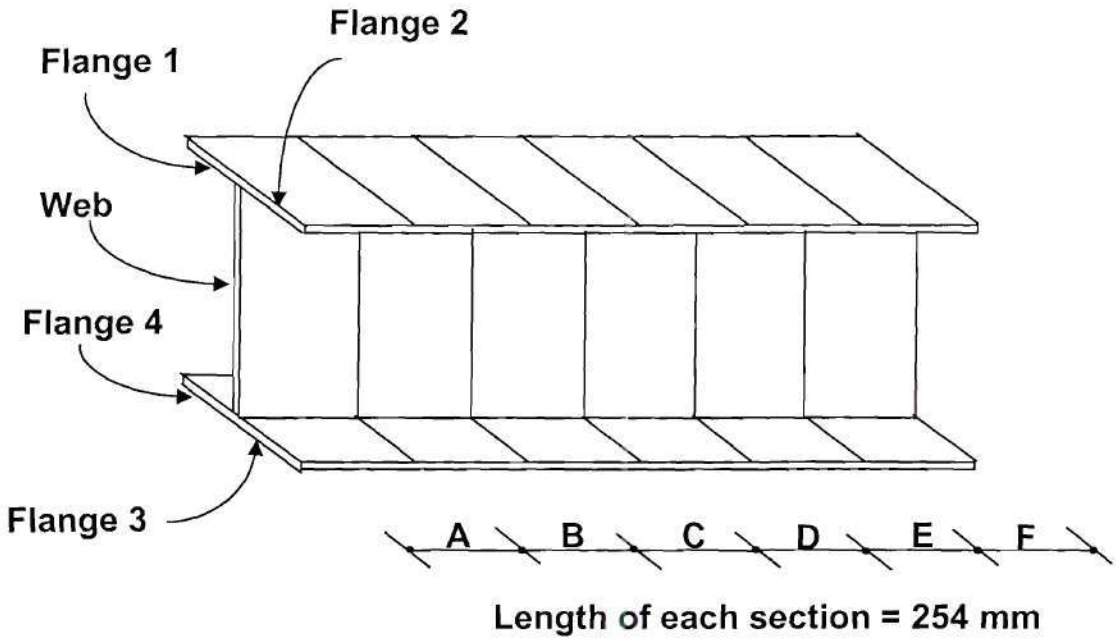

Figure 16. Polymer composite structural shape used for material property tests

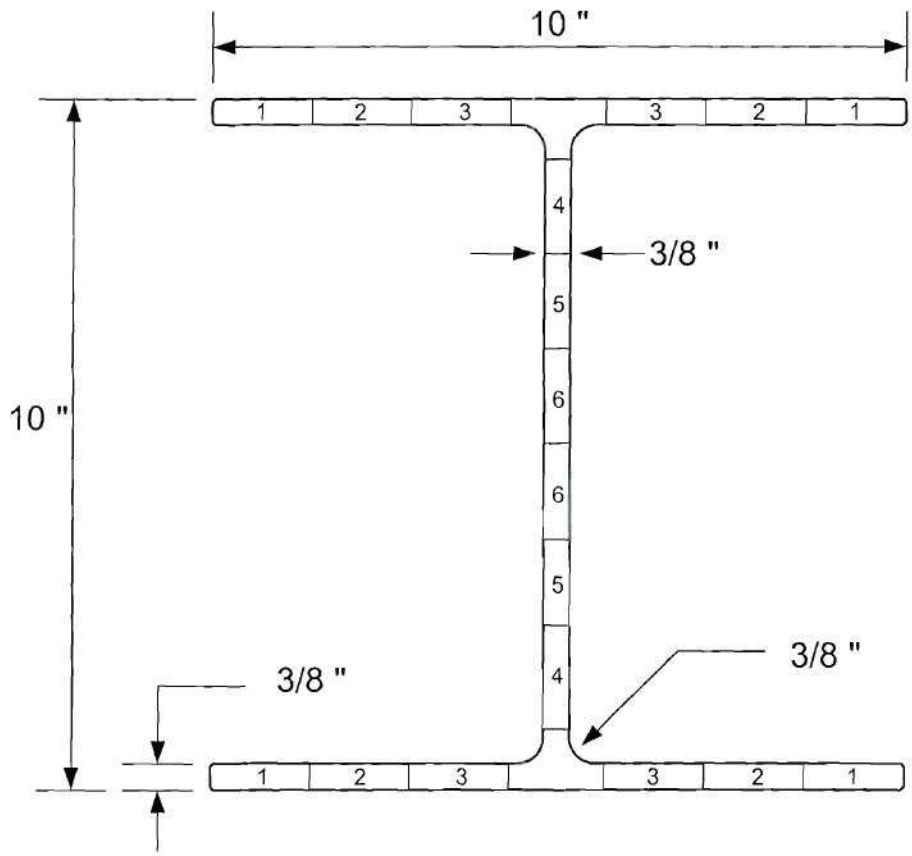

Figure 17. Coupon locations

An analysis of variance was conducted to test seven hypotheses concerning the variation in strength. The hypotheses, and the results of the statistical testing are shown in Table 0. A two-sided 95% confidence level was used for all tests. The first three hypotheses were tested using a three-way analysis of variance with the treatments being the location along the length (group A, B, ... , F), the section (flange 1, ..., 4), and the coupon (1, 2, 3). A similar three-way analysis of variance test was also performed for the web. A paired t-test was performed to compare the difference in average strength between the flanges and the web due to the differing number of samples. All null hypotheses, with the null hypothesis being that the compared strengths were the same, could not be rejected except for the strength varying across the flange and the strength varying in the web from the centroid to the flange junction.

A Duncan's Multiple Range test was performed to further investigate the difference of strength within the flange. It was determined that coupon 3 (part of the flange near the web juncture, see Figure 17) is not significantly different from coupon 2, but coupons 2 and 3 are both significantly different from coupon 1. The results further show that the strength increased from flange tip to web junction, with coupon 3 having the highest strength. The differences in the

strength across the flange were also investigated by determining correlation coefficients between the locations, with the results shown in Table 0. It is interesting that all the correlation coefficients between different locations are negative. However, the null hypothesis that the correlation coefficient is 0.0 cannot be rejected at the 5% level (only an absolute value of the correlation coefficient of greater than 0.42 would have caused rejection of the null hypothesis).

Table 0: Hypothesis, test statistics, and results for location effects on coupon strength

Null Hypothesis, H_O	Alternate Hypothesis H_A	Test Statistic	Critical Statistic (95% confidence level)	Accept or Reject H_O
Average strength of all the flanges is the same (Flange 1 = Flange 2 = Flange 3 = Flange 4)	Average strength of any pair of flanges is different	2.11	2.78	Accept
Average strength of all the flanges per group is the same along the beam (Flanges A = Flanges B = ,..., = Flanges F)	Average strength of flanges varies along the length	0.35	2.39	Accept
Average strength within the flanges is the same (Coupon 1 = Coupon 2 = Coupon 3)	Average strength varies from tip of flange to web junction	3.98	3.17	Reject
Average strength of top half and bottom half of the web is the same	Average strength of top half and bottom half of web is different	2.38	4.32	Accept
Average strength of the web per group is the same along the beam (Flanges A = Flanges B = ,..., = Flanges F)	Average strength of web varies along the length	0.28	2.68	Accept
Average strength within the web does not vary from the centroid to the flange-web junction (Coupon 4 = Coupon 5 = Coupon 6)	Average strength varies from centroid to flange-web junction	6.14	3.47	Reject
Average strength of the flanges is the same as the average strength of the webs	Average strength of the flanges is different from the average strength of the webs	0.32	2.03	Accept

Table 0: Correlation coefficients between strength values

Specimen Location	Flange Location		
	Location 1	Location 2	Location 3
Location 1	1.00	-0.22	-0.26
Location 2	-0.22	1.00	-0.17
Location 3	-0.26	-0.17	1.00
	Web Location		
	Location 4	Location 5	Location 6
Location 4	1.00	0.10	0.09
Location 5	0.10	1.00	-0.57
Location 6	-0.09	-0.57	1.00

The differences in the web were also investigated using Duncan's Multiple Range test. It was concluded that coupon 5 was significantly different from coupons 4 or 6, but coupons 4 and 6 were not significantly different. Coupon 5 (the middle section of both the top and bottom half of the web) had the greatest strength. An examination of the correlation coefficients between the locations indicates a rather large negative correlation between location 5 and 6. However, again the null hypothesis that the correlation coefficient is 0.0 cannot be rejected at the 5% level (critical absolute value of the correlation coefficient for the web is 0.63; this is higher than the flanges due to the smaller statistical degrees of freedom).

The variances in the web were much larger than those in the flanges, with the coefficient of variation of the strength of all flange coupons being 8.9%, and the coefficient of variation of the web strength for all coupons being 22.1%. The top of the web had a much larger coefficient of variation than the bottom half, 27.4% versus 15.4%. We do not have any explanation for why there would be such a large difference between the top and bottom half of the web, and it may just be an anomaly of the chosen pultruded member.

In conclusion, coupons for material property determination need to be obtained from throughout the cross-section of the specimen if such a section is reinforced with the same fiber architecture. Coupons from just one strip or location in the cross-section may not be representative of the entire cross-section.

It is suggested that the number of coupons from each part of the cross-section of the member be in proportion to the ratio of the area of the part of the cross-section to the entire area of the cross-section. In other words, if the flanges in I-shape cross section comprise 70% of the cross-sec-

tional area, 70% of the coupons should come from the flanges. These coupons should be taken from different parts of the flange, and not all from the same location within the flange. It is also concluded that the samples obtained from different locations in the cross-section can be considered to be independent samples. Although only the longitudinal tensile strength was examined, it is assumed that similar trends would hold for other properties.

1.3.2. SPECIMEN WIDTH FOR TENSION AND COMPRESSION TESTS

For structural applications, composites are often considered to be homogenous. This is similar to concrete, which on a micro scale is not homogenous, but on a macro, or civil engineering infrastructure scale, is homogenous. Thus, an appropriate material test specimen size needs to be established. The size needs to be large enough to be representative of the member properties, but small enough to facilitate testing.

The effect of specimen width on the strength was obtained by using a W305 x 305 mm I-shaped section with 12.7 mm thick flanges and webs. Specimens 305 mm in length were obtained both from the flanges and the webs. The specimens were tested without tabs in tension at a loading rate of 2.5 mm/minute. A summary of the test results is given in Table 0.

The null hypothesis that the mean values for the different specimen widths were the same was checked using the U-test. The U-test is distribution-free, is nearly statistically efficient as the t-test, can handle different sample sizes, and is robust against different variances (Sachs, 1984). The results of the U-test are given in Table 0 where the test statistic is given, and the critical U-statistic at the 5% level is shown in parentheses. If the test statistic is greater than the critical value, the null hypothesis cannot be rejected at the 5% level. For all pairwise comparisons of different test widths, the null hypothesis that the mean values are the same cannot be rejected at the 5% significance level. Thus, specimen width does not affect the mean value.

Table 0: Results from Testing of Specimens with Different Widths

Specimen Width (mm)	Number of Samples	Mean Strength (MPa)	Coefficient of Variation (%)
12.7	34	239	19.8
19.0	27	228	14.5
25.4	22	234	10.6
31.8	36	237	8.7
38.1	33	241	7.7
44.4	25	238	6.3
50.8	24	239	6.0
57.2	23	238	5.1

Table 0: U-Statistics for Different Specimen Widths

Specimen Width mm	U-Statistic (Critical statistic given in parentheses)						
	19.0 mm	25.4 mm	31.8 mm	38.1 mm	44.4 mm	50.8 mm	57.2 mm
12.7	413 (324)	367 (257)	602 (445)	521 (405)	398 (297)	380 (284)	365 (270)
19.0		259 (199)	405 (345)	321 (314)	260 (230)	244 (220)	246 (210)
25.4			376 (274)	298 (249)	253 (183)	223 (175)	242 (167)
31.8				512 (431)	416 (316)	392 (302)	390 (288)
38.1					361 (288)	362 (275)	328 (262)
44.4						288 (202)	277 (192)
50.8							260 (184)

A plot of the coefficient of variation of the strength versus specimen width is shown in Figure 18. A regression relationship can be developed between the coefficient of variation of the tensile strength and the specimen width as (r^2=0.99)

$$COV = \frac{200}{W^{0.9}} \tag{31}$$

in which COV is the coefficient of variation in percent, and W is the width of the specimen in mm. This regression line is also shown in Figure 18. Clearly the specimen width affects the variance of the strength. Thus, a standard width needs to be chosen for probabilistic code calibration purposes. For practical applications we propose the use of the following simplified version of Equation (31):

$$COV = \frac{300}{W} \tag{32}$$

Both Equation (31) and Equation (32) yield almost the same numerical results for specimen widths between 12.7 mm and 101.6 mm.

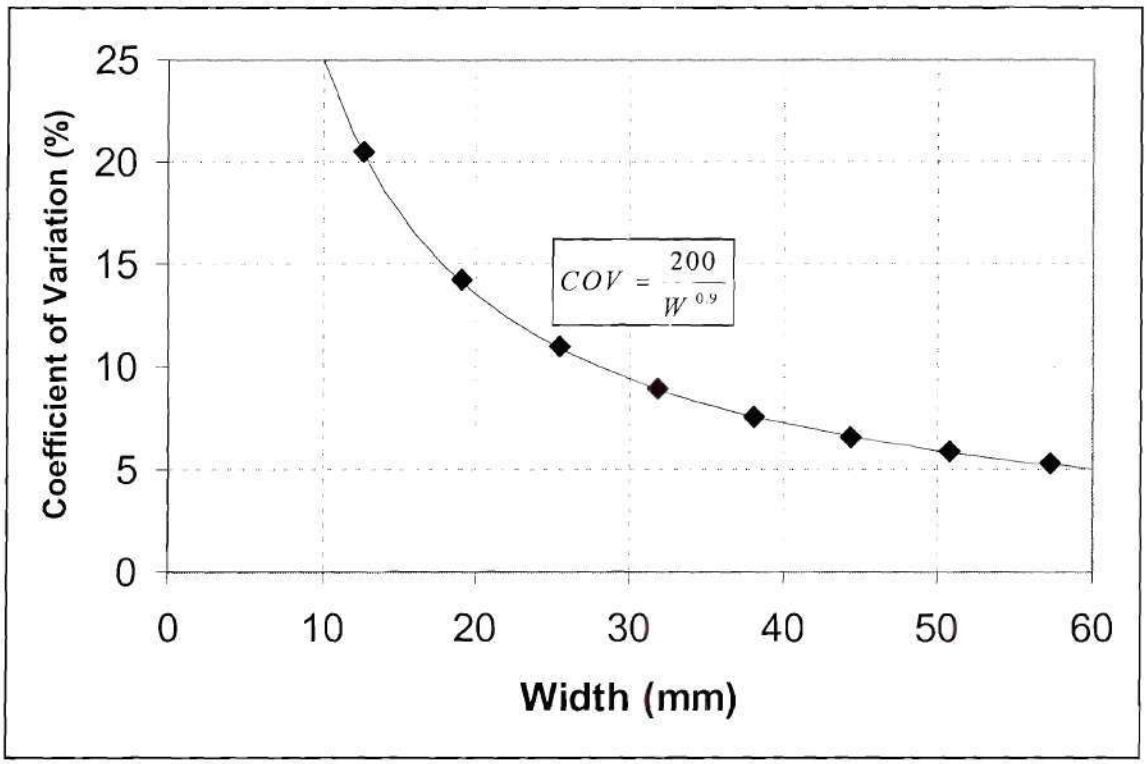

Figure 18. Tensile strength coefficient of variation vs. coupon width

For development of a probabilistic based code, we recommend that a 25 mm width for specimen size. There are several reasons for this recommendation. ASTM D3039 recommends a width of 25 mm for 90E unidirectional fibers, balanced and symmetric fibers, and random-discontinuous fibers. A width of 15 mm is recommended in the ASTM D3039 for 0E unidirectional fibers. For consistency and based on the significantly larger coefficient of variation obtained for specimens with less than 25 mm width, we recommend a width of 25 mm for the 0E unidirectional fibers case. The 25 mm specimen width is consistent with other related ASTM specifications. ASTM D5083, which is a test method for tensile testing of reinforced thermosetting plastics, gives a preferred testing width of 25 mm. ASTM D579, which is a test for greige woven glass fibers, uses a 25 mm specimen width.

Another reason for choosing a 25 mm width is that the reduction in variation for widths greater than 25 mm will have little impact on reliability calculations. The reliability will be approximately indirectly proportional to the coefficient of variation of the safety margin, which is the load minus the resistance. Loads, except for dead loads, have coefficients of variation larger than 25%. The coefficient of variation of the safety margin is the square-root-of-the-sum-of-the-squares of the coefficient of variation of the load and resistance. Thus, further reductions in the coefficient of variation from that for the 25 mm specimen width (10%), will not signifi-

cantly reduce the coefficient of variation of the safety margin, and hence affect the reliability of the system.

In conclusion, we recommend that a 25 mm width be adopted as the standard for the testing of pultruded shapes for civil engineering applications. The 25 mm width provides a balance between a width large enough to be representative of the member, but small enough to facilitate testing.

Should a width other than 25 mm be used for testing, the coefficient of variation should be adjusted to that for the standard width of 25 mm. Equation (31) indicates that the coefficient of variation is inversely proportional to the width raised to the 0.9 power. Based on this, Equation 2 is developed for adjusting the coefficient of variation.

$$COV_{25} = \left(\frac{W}{25}\right)^{0.9} COV_W \tag{33}$$

in which COV_{25} is the adjusted coefficient of variation and COV_W is the coefficient of variation at the tested width.

If Equation (32) is preferred over Equation (31), then the adjusted coefficient of variation COV_{25} becomes:

$$COV_{25} = \left(\frac{W}{25}\right) COV_W \tag{34}$$

1.3.3. PROBABILITY DISTRIBUTION

The distribution chosen to represent the data will have a large effect on the calculated reliability. Assuming two different distributions can result in computed probability of failures that vary by over an order of magnitude. For a constant reliability, different chosen distributions would result in required design capacities that could vary by as much as 50%. The reason for this is the difference in the lower tail behavior of the different cumulative distribution functions, which has become known as the tail-sensitivity problem in structural reliability (Ditlevsen, 1981). The lower tails of the normal, lognormal, and Weibull distribution are shown in Figure 19 for a random variable with a unit mean and a coefficient of variation of 10 percent. Note that for a given value, there is a large difference in the cumulative distribution function for the three distributions.

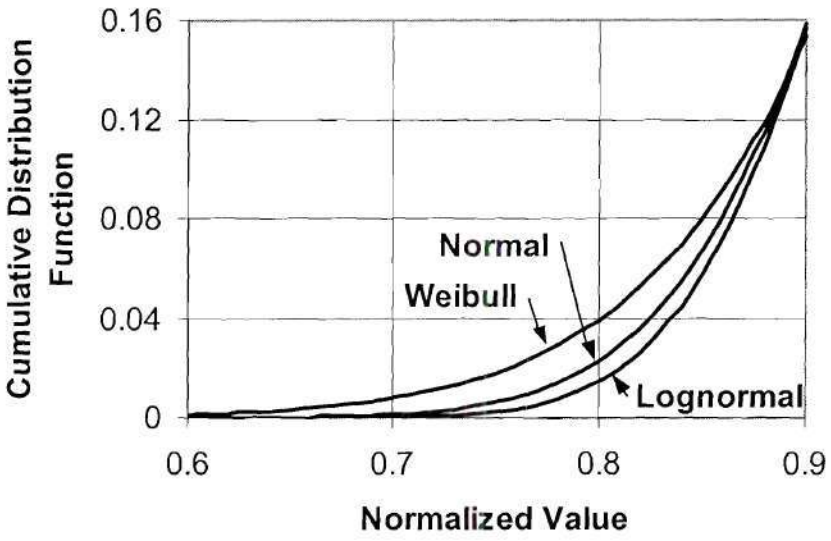

Figure 19. Lower Tail Cumulative Distribution Functions

There have been several approaches to the distribution problem. One approach has been to prescribe a distribution. The steel industry did this by assuming a lognormal distribution for steel material properties (e.g., Elllingwood et al., 1980; AISC, 1993, Commentary section A5). The concrete industry has used the normal distribution to characterize concrete material properties (Ellingwood et al., 1980). The use of the normal distribution was based on a German study (Mirza et al., 1979). The wood industry in the recent development of their load and resistance factor code prescribed a two parameter Weibull distribution (Gromala et al, 1990). The determination of the probability distribution was identified as an area of confusion in the development of the wood LRFD code (Murphy, 1988). The wood industry states that choosing a distribution function "Unfortunately ... does not address the confusion (and inequity) which arises when different material groups choose different distributional assumptions." (Gromala et al., 1990). The wood industry was able to calibrate the LRFD code to the existing allowable stress design code, and the years of experience with wood structures. Unfortunately, there is no established design code for FRP structures, and there is not the years of experience with FRP materials. Thus, the choice of the distribution function is more critical.

An alternate approach to the distribution problem is to prescribe an order of examining probability distributions. The Military Handbook (Mil-HDBK, 1997) takes this approach for FRP composites, where the two parameter Weibull is examined first. If this distribution cannot be rejected, it is chosen and no further distribution is examined. If the Weibull is rejected, then other distributions (lognormal and normal) are examined.

The AASHTO LRFD specifications were developed by using a probability distribution for member resistances such as moment in a composite steel girder. The member resistance was

assumed to follow a lognormal distribution (Nowak, 1995). Monte Carlo simulation was used to develop the statistics for the member resistances using statistics for the individual material property random variables, such as concrete strength and steel yield strength. Random variables for concrete material properties were assumed to follow a normal distribution, and random variables for steel material properties were assumed to follow a lognormal distribution (Tabsh and Nowak, 1991; Nowak et al., 1994). Thus, implicitly, the AASHTO LRFD specification is based on the same probability distributions for material properties that were used for the development of probabilistic based building codes.

In this study we examined three different probability distribution functions. These are the normal, lognormal and Weibull that are described mathematically along with their statistics in Table 0. Typically, the two parameter Weibull distribution is used, although the three parameter Weibull distribution is more robust and can provide a better characterization of the data. However, the determination of the parameters for the three parameter Weibull distribution is difficult, and different methods result in different estimates of the parameters (Zanakis, 1979). Thus, only the two parameter Weibull distribution will be considered.

Various methods exist for determining the goodness of fit of different probability distributions to a set of data. Most of these methods work primarily with the central portion of the data, while civil engineering applications are most affected by the performance of the tails of the distribution. Probability distributions that are essentially similar in the central regions of the data can have vastly different behavior in the tail regions. The Anderson-Darling test was used to examine the data, since the Anderson-Darling test statistic is sensitive to discrepancies in the tail regions (Mil-HDBK, 1997).

The Anderson-Darling statistic, AD, is computed for each material property data set from the following equation:

$$AD = \sum_{i=1}^{n} \left[\frac{(1-2i)}{n} \{ \ln(F_i) + \ln(1 - F_{n+1-i}) \} \right] - n \tag{35}$$

In the above equation, F_i denotes the cumulative distribution function values of the sample data for the distribution being considered, e.g., normal, lognormal, or Weibull. The observed significance level (OSL) of each data set, which is a measure of the goodness-of-fit of a distribution under consideration is calculated as follows:

Table 0: Probability Distributions

	Normal	Lognormal	Weibull
Variable	$-\infty < x < \infty$	$0 < x < \infty$	$0 < x < \infty$
Probability density function $f(x)$	$\frac{1}{\sigma\sqrt{2\pi}}\exp\left[\frac{-(x-\mu)^2}{2\cdot\sigma^2}\right]$	$\frac{1}{x\sigma_L\sqrt{2\pi}}\exp\left[\frac{-(\ln x-\mu_L)^2}{2\cdot\sigma_L^2}\right]$	$\frac{\beta}{\alpha}\left(\frac{x}{\alpha}\right)^{\beta-1}\exp\left[-\left(\frac{x}{\alpha}\right)^{\beta}\right]$
Sample mean $\bar{X}$	$\frac{1}{n}\sum_{i=1}^{n} x_i$	$\exp\left(\hat{\mu}_L+\frac{\hat{\sigma}_L^2}{2}\right)$	$\hat{\alpha}\cdot\Gamma\left(1+\frac{1}{\hat{\beta}}\right)$
Sample standard deviation S	$\sqrt{\frac{1}{n-1}\sum_{i=1}^{n}(x_i-\bar{x})^2}$	$\exp\left(\hat{\mu}_L+\frac{\hat{\sigma}_L^2}{2}\right)\sqrt{\exp\left(\hat{\sigma}_L^2\right)-1}$	$\hat{\alpha}\cdot\sqrt{\Gamma\left(1+\frac{2}{\hat{\beta}}\right)-\Gamma^2\left(1+\frac{1}{\hat{\beta}}\right)}$
Coefficient of variation	$\frac{S}{\bar{X}}$		

Note:

1) $\hat{\mu}_L$ and $\hat{\sigma}_L$ are estimated by $\hat{\mu_L} = \frac{1}{n}\sum_{i=1}^{n}\ln(x_i)$ and $\hat{\sigma_L} = \sqrt{\frac{1}{n-1}\sum_{i=1}^{n}[\ln(x_i)-\hat{\mu}_L]^2}$.

2) $\hat{\alpha}$ and $\hat{\beta}$ are estimated by the Maximum-Likelihood Estimate (MLE) method, (Dodson, 1994).

For the normal and lognormal distributions,

$$OSL = 1/\{1+\exp[-0.48+0.78\ln(AD^*)+4.58AD^*]\} \tag{36}$$

where

$$AD^* = \left[1+\frac{4}{n}-\frac{25}{n^2}\right]AD \tag{37}$$

and for the Weibull distribution,

$$OSL = 1/\{1 + \exp[-0.1 + 1.24\ln(AD^*) + 4.548AD^*]\} \tag{38}$$

where

$$AD^* = \left[1 + \frac{0.2}{\sqrt{n}}\right]AD \tag{39}$$

The OSL is the probability of obtaining a value of the test statistic at least as large as that obtained from the data if the hypothesis that the data are actually from the distribution being tested is true. Typically, a 5 percent significance level is used, so that the null hypothesis is only rejected if the OSL is less than 0.05.

The material property data from coupons obtained as part of a structural member study sponsored by FHWA (Zureick and Scott, 1997) were analyzed with respect to the appropriate probability distribution. Coupons were obtained from both I-shaped and box sections. These specimens are labelled as VG specimens. Also shown is data from coupons obtained as part of beam-column tests (Kang, 2001), which are labeled as K specimens. The observed significance levels (OSL) for the three different distributions for different data sets are shown in Table 0. The lower confidence limit values of both the moduli and strengths are presented graphically in Figures 20 and 21.

With respect to strength, neither the normal nor the lognormal distribution can be rejected for any of the twelve data sets. In eight out of the twelve cases, the lognormal is the preferred distribution. For stiffness, none of the three distributions is appropriate in three out of twelve cases. The Weibull distribution is acceptable for all of the remaining nine data sets. The lognormal distribution is the most preferred distribution, being preferred in six cases.

We are proposing that the two parameter Weibull distribution be used to describe the material properties, both strength and stiffness, for FRP materials. Although Table 0 indicates the lognormal distribution may be a better choice, the Weibull distribution has been the most commonly used distribution for composites (King, 1986) and is the preferred distribution in the Military Handbook (Mil-HDBK-17, 1997) in the sense that if Weibull distribution cannot be rejected, it is used to describe the data. The Weibull distribution is "conservative" in that it generally results in lower computed reliabilities than either the normal or lognormal distribution, as indicated by the lower tail behavior in Figure 19. The two parameter Weibull cumulative distribution function is given by:

$$F_x = 1 - e^{-\left(\frac{x}{\alpha}\right)^k} \tag{40}$$

in which k is the shape parameter, and " is the scale parameter. There are various methods of determining the parameters of the Weibull distribution, including maximum likelihood estimators and linear regression. With linear regression, the data has to be ranked, and there are various ranking methods, including mid-point, mean, and median. To provide consistency, it is recommended that the Weibull parameters be determined using maximum likelihood estimators. The shape parameter is determined by numerically solving the following equation,

$$\frac{n}{k} + \sum_{i=1}^{n} \ln x_i - \frac{n}{\sum_{i=1}^{n} x_i^k} \sum_{1}^{n} x_i^k \ln x_i \tag{41}$$

in which n is the number of data points. The scale parameter is then determined from:

$$\alpha = \left(\frac{\sum_{i=1}^{n} x_i^k}{n} \right)^{\frac{1}{k}} \tag{42}$$

In conclusion, we are proposing that the two parameter Weibull distribution be prescribed for all strength and stiffness properties of FRP composite materials. The parameters are to be determined using maximum likelihood estimators. Although other probability distributions may better fit a given data set, prescribing the Weibull distribution provides consistency in statistical analysis and reliability calculations. The prescription of the Weibull distribution has proved quite workable in the wood industry, and should also with FRP composites.

Table 0: Observed Significance Level of Anderson-Darling Statistic for Weibull, Normal, and Lognormal Distribution. Values of OSL >0.05 (for which the distribution cannot be rejected) are in bold. Greatest value of OSL for each data set is underlined.

Property	N	Observed Significance Level (OSL)		
		Weibull	Normal	Lognormal
Longitudinal Tensile Strength				
VG1-6	30	0.009	0.113	0.195
VG 7-12	30	0.302	0.198	0.120
VG 13-18	24	0.136	0.142	0.147
VG 19-24	24	0.008	0.142	0.260
K	30	0.699	0.757	0.684
Longitudinal Compressive Strength				
VG1-6	30	0.001	0.064	0.154
VG 7-12	30	0.213	0.576	0.662
VG 13-18	24	0.088	0.106	0.117
VG 19-24	24	0.469	0.542	0.467
K	30	0.214	0.147	0.106
Shear Strength VG 19-24	24	0.517	0.204	0.103
K	18	0.073	0.195	0.275
Longitudinal Tensile Modulus				
VG1-6	30	0.179	0.500	0.517
VG 7-12	30	0.022	0.001	0.000
VG 13-18	24	0.010	0.012	0.012
VG 19-24	24	0.171	0.519	0.546
K	30	0.180	0.372	0.379
Longitudinal Compressive Modulus				
VG1-6	30	0.154	0.333	0.361
VG 7-12	30	0.053	0.006	0.002
VG 13-18	24	0.010	0.012	0.015
VG 19-24	23	0.299	0.199	0.174
K	30	0.504	0.587	0.563
Shear Modulus, VG 19-24	24	0.065	0.297	0.350
K	18	0.116	0.320	0.473

Table 0: Modulus Statistics

		E_L^t GPa (ksi)	E_L^c GPa (ksi)	G_{LT} GPa (ksi)	E_L^b GPa (ksi)
Sample Size		30	30	18	30
Normal	$\bar{X}$	23.8 (3,445)	23.8 (3,456)	2.7 (396)	21.8 (3,161)
	S	1.5 (218)	1.0 (140)	0.3 (41)	2.3 (337)
	COV	6.3%	4.0%	10.4%	10.7%
	$X_{p=0.05}$	21.3 (3,088)	22.3 (3,227)	2.3 (329)	18.0 (2,608)
	$X_{p=0.10}$	21.8 (3,166)	22.6 (3,278)	2.4 (344)	18.8 (2,730)
	$LX_{p=0.05}$	20.4 (2,961)	21.7 (3,146)	2.0 (295)	16.6 (2,413)
	$LX_{p=0.10}$	21.1 (3,058)	22.1 (3,208)	2.2 (315)	17.7 (2,562)
Log-normal	$\hat{\mu}_L$	3.166 (8.143)	3.170 (8.147)	1.00 (5.98)	3.076 (8.053)
	$\hat{\sigma}_L$	0.064 (0.064)	0.041 (0.041)	0.10 (0.10)	0.108 (0.108)
	$\bar{X}$	23.8 (3,446)	23.8 (3,456)	2.7 (396)	21.8 (3,162)
	S	1.5 (221)	1.0 (142)	0.3 (41)	2.4 (342)
	COV	6.4%	4.1%	10.3%	10.8%
	$X_{p=0.05}$	21.4 (3,097)	22.3 (3,228)	2.3 (333)	18.2 (2,633)
	$X_{p=0.10}$	21.8 (3,169)	22.6 (3,276)	2.4 (346)	18.9 (2,737)
	$LX_{p=0.05}$	20.6 (2,984)	21.7 (3,153)	2.1 (306)	17.1 (2,473)
	$LX_{p=0.10}$	21.2 (3,070)	22.1 (3,210)	2.2 (322)	17.9 (2,594)
Weibull	$\hat{\alpha}$	24.45 (3546)	24.29 (3523)	2.86 (415)	22.83 (3311)
	$\hat{\beta}$	17.8 (17.8)	27.3 (27.3)	10.3 (10.3)	10.6 (10.6)
	$\bar{X}$	23.7 (3,441)	23.8 (3,453)	2.7 (395)	21.8 (3,157)
	S	1.6 (238)	1.1 (158)	0.3 (46)	2.5 (360)
	COV	6.9%	4.6%	11.7%	11.4%
	$X_{p=0.05}$	20.7 (3,001)	21.8 (3,160)	2.1 (311)	17.2 (2,500)
	$X_{p=0.10}$	21.5 (3,125)	22.4 (3,244)	2.3 (333)	18.5 (2,676)
	$LX_{p=0.05}$	19.4 (2,819)	20.9 (3,034)	1.8 (260)	15.5 (2,250)
	$LX_{p=0.10}$	20.5 (2,967)	21.6 (3,136)	2.0 (293)	16.9 (2,453)

Table 0: Strength Statistics

		F_L^t MPa (ksi)	F_L^c MPa (ksi)	F_V MPa (ksi)	F_L^b MPa (ksi)
Sample Size		30	30	18	30
Normal	$\bar{X}$	373.0 (54.1)	379.2 (55.0)	73.1 (10.6)	493.0 (71.5)
	S	25.5 (3.7)	46.2 (6.7)	6.9 (1.0)	45.5 (6.6)
	COV	6.8%	12.2%	9.4%	9.2%
	$X_{p=0.05}$	331.2 (48.0)	303.5 (44.0)	61.8 (9.0)	418.4 (60.7)
	$X_{p=0.10}$	340.4 (49.4)	320.1 (46.4)	64.3 (9.3)	434.7 (63.1)
	$LX_{p=0.05}$	316.4 (45.9)	276.7 (40.1)	56.2 (8.1)	392.0 (56.8)
	$LX_{p=0.10}$	327.7 (47.5)	297.1 (43.1)	59.5 (8.6)	412.1 (59.8)
Log-normal	$\hat{\mu}_L$	5.919 (3.988)	5.931 (4.001)	4.29 (2.36)	6.196 (4.265)
	$\hat{\sigma}_L$	0.070 (0.070)	0.123 (0.123)	0.1 (0.1)	0.093 (0.093)
	$\bar{X}$	372.9 (54.1)	379.7 (55.1)	73.0 (10.6)	492.8 (71.5)
	S	26.1 (3.8)	46.9 (6.8)	7.0 (1.0)	45.9 (6.7)
	COV	7.0%	12.3%	9.6%	9.3%
	$X_{p=0.05}$	331.6 (48.1)	308.0 (44.7)	62.1 (9.0)	421.3 (61.1)
	$X_{p=0.10}$	340.1 (49.3)	321.9 (46.7)	64.3 (9.3)	435.6 (63.2)
	$LX_{p=0.05}$	318.4 (46.2)	286.8 (41.6)	57.4 (8.3)	399.1 (57.9)
	$LX_{p=0.10}$	328.5 (47.6)	302.8 (43.9)	60.1 (8.7)	415.9 (60.3)
Weibull	$\hat{\alpha}$	384.5 (55.76)	399.7 (57.97)	76.2 (11.05)	513.5 (74.48)
	$\hat{\beta}$	16.67 (16.67)	9.23 (9.23)	11.23 (11.23)	12.0 (12.0)
	$\bar{X}$	372.3 (54.0)	379.2 (55.0)	73.1 (10.6)	492.3 (71.4)
	S	27.6 (4.0)	49.0 (7.1)	7.6 (1.1)	49.6 (7.2)
	COV	7.4%	12.9%	10.4%	10.1%
	$X_{p=0.05}$	321.7 (46.7)	289.7 (42.0)	58.5 (8.5)	400.9 (58.1)
	$X_{p=0.10}$	335.9 (48.7)	313.2 (45.4)	62.4 (9.0)	425.7 (61.7)
	$LX_{p=0.05}$	300.9 (43.6)	256.8 (37.2)	49.8 (7.2)	365.4 (53.0)
	$LX_{p=0.10}$	317.8 (46.1)	283.4 (41.1)	55.4 (8.0)	394.2 (57.2)

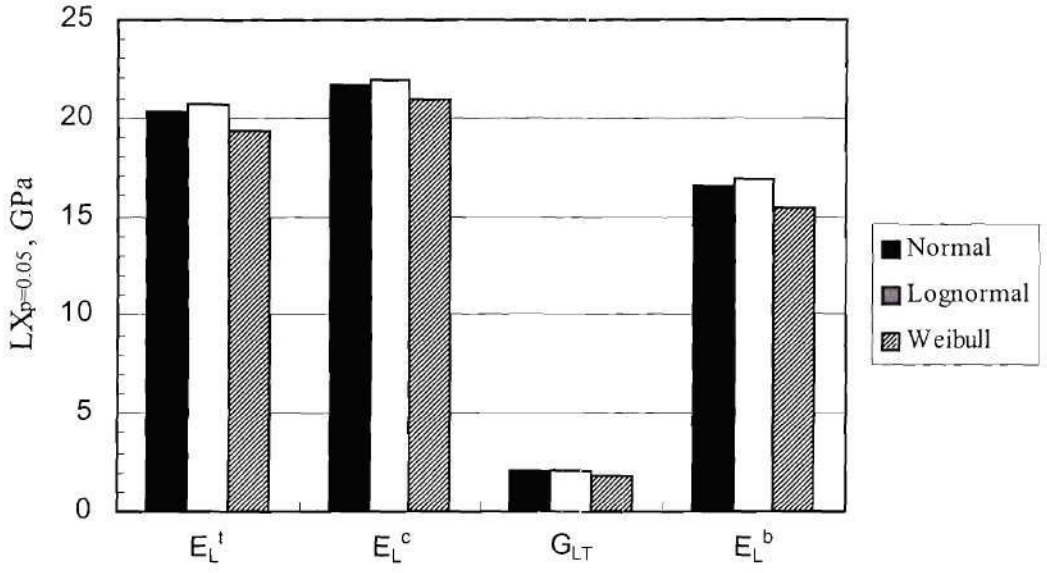

(a) 5 Percentile, $X_{p=0.05}$

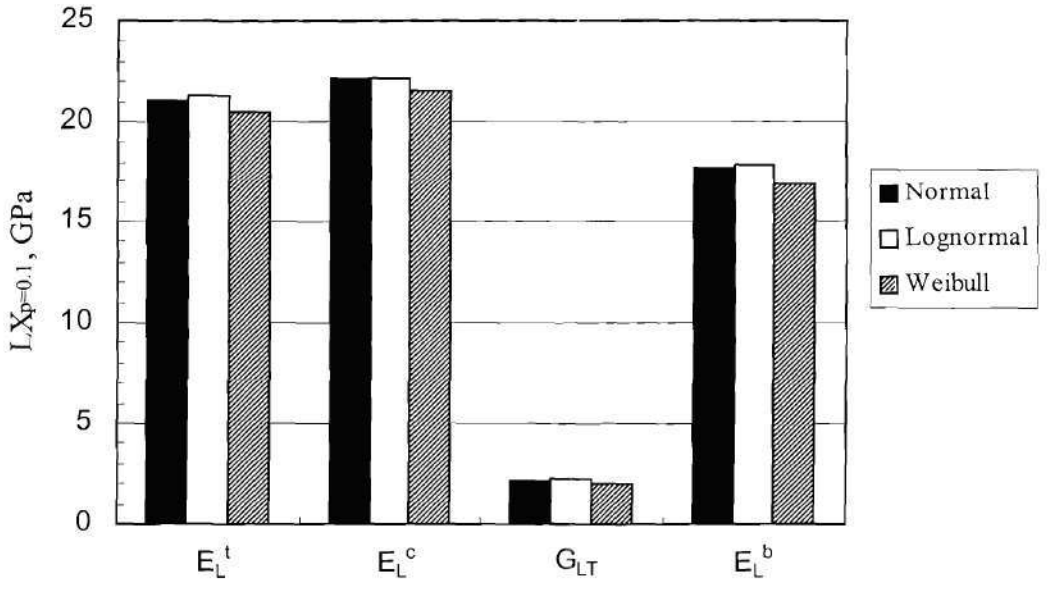

(b) 10 Percentile, $X_{p=0.1}$

Figure 20. Lower Confidence Limit of Moduli

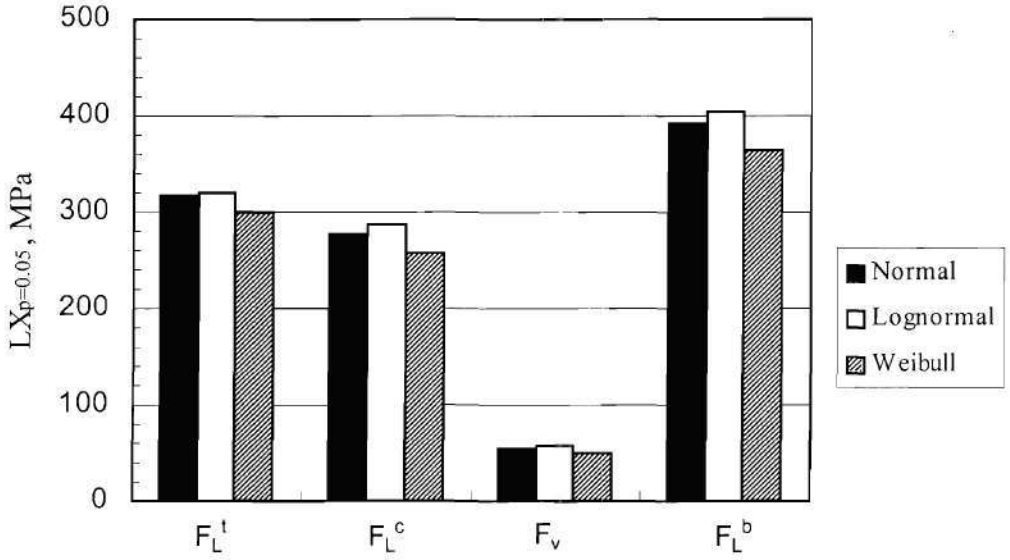

(a) 5 Percentile, $X_{p=0.05}$

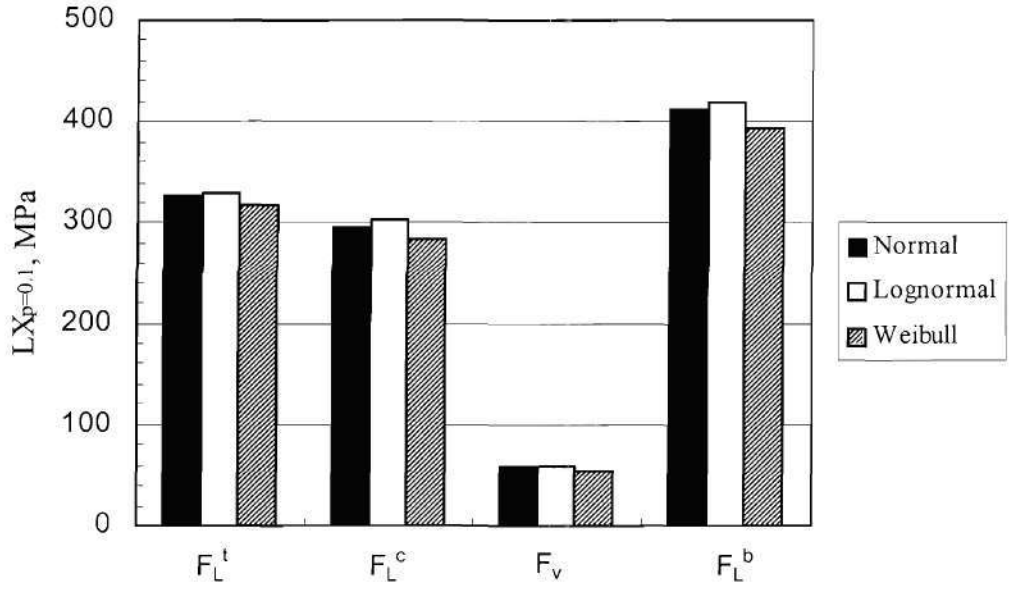

(b) 10 Percentile, $X_{p=0.1}$

Figure 21. Lower Confidence Limit of Strengths

1.4 Proposed Approach for design property data reporting

Nominal properties are typically used for design, as opposed to mean or median properties. In aerospace composites design, either the A-basis value or the B-basis value is often used. The A-basis value is the 95% lower tolerance bound for the upper 99% of a specified population, while the B-basis value is the 95% lower tolerance bound for the upper 90% of a specified population. The nominal design property is in fact arbitrary as it is further adjusted by a resistance factor in the actual design process. Thus, if the A-basis value is chosen for nominal design property, the resistance factor would be higher than if the B-basis value for chosen for the nominal design property. Zureick and Steffen (2000) used the 95% lower confidence level on the upper 95% of a specified population.

Since the nominal design property is arbitrary, any value could be chosen. However, a nominal design property should be chosen such that the resulting resistance factors are similar to those used for other materials. It is important that engineers have a proper feel for the design, and widely varying resistance factors between materials could cause the erroneous conclusion to be reached that some materials are more reliable than others. We feel that the A-basis value would result in too high of resistance factors (sometimes greater than 1.0), while the B-basis value would result in resistance factors generally lower than those used for other materials. Preliminary work (McNutt, 1998) suggests that using the 5% value (95% of the specified population is above this value) for the nominal design property will result in resistance factors similar to those for other materials. The 5% value is also what is used in many civil engineering applications (Ellingwood, 2000). The value of the nominal design property, x_{nom} is obtained as:

$$x_{nom} = (-\ln(1-p))^{\frac{1}{k}} \tag{43}$$

in which p is the desired percentile. For the 5% value, this equation reduces to:

$$x_{nom} = \alpha(0.0513)^{\frac{1}{k}} \tag{44}$$

Statistical Uncertainty

The nominal design value does not account for statistical uncertainty. Statistical uncertainty arises from the parameters being determined from less than an infinite population. The most common method used to account for statistical uncertainty is the use of confidence intervals. Bain and Engelhardt (1991) present a method for determining the confidence interval for a p-percentile value from the Weibull distribution. The confidence interval is a function of a derived distribution that only depends on the desired probability percentile, p, the confidence level desired, and the number of samples. The method is attractive in the sense that once p and the confidence level are chosen, the confidence interval is only a function of the number of data points. However, the derived distribution is obtained through Monte Carlo simulation (Thoman et al., 1970). Thus, the method requires tables that are not readily available, and in many cases

interpolation is required. Linear interpolation can be suspect in cases where one has to interpolate outside the range of tables which can occur when obtaining the 95th percent lower confidence limit for the 5th percentile value.
Another method presented by Dodson (1994) is suggested for calculating the confidence intervals. This method is an approximate method that assumes normality of the sampling distribution, but avoids the use of tables and is based on maximum likelihood estimators. The method should not be used for values of k<2, but this will rarely, if ever, be the case with composite properties as this would imply a coefficient of variation > 52%. The following paragraphs outline the method to determine the confidence interval or bound on a p-percentile value from the Weibull distribution.

A local information matrix is determined, which is the negatives of the second partial derivatives of the log-likelihood equation, L. The matrix and equations used to calculate each of the terms are:

$$F = \begin{bmatrix} F_{11} & F_{12} \\ F_{21} & F_{22} \end{bmatrix} \tag{45}$$

$$F_{11} = -\frac{\partial^2 L}{\partial \alpha^2} = -\sum_{i=1}^{n} \left[\frac{k}{\alpha^2} - \left(\frac{x_i}{\alpha}\right)^k \left(\frac{k}{\alpha^2}\right)(k+1) \right] \tag{46}$$

$$F_{22} = -\frac{\partial^2 L}{\partial k^2} = -\sum_{i=1}^{n} \left[\left(\frac{-1}{k^2}\right) - \left(\frac{x_i}{\alpha}\right)^k \left(\ln\left(\frac{x_i}{\alpha}\right)\right)^2 \right] \tag{47}$$

$$F_{12} = F_{21} = -\frac{\partial^2 L}{\partial \alpha \partial k} = -\sum_{i=1}^{n} \left[\left(\frac{-1}{\alpha}\right) + \left(\frac{x_i}{\alpha}\right)^k \left(\frac{1}{\alpha}\right) \left(k \ln\left(\frac{x_i}{\alpha}\right) + 1\right) \right] \tag{48}$$

The local information matrix is inverted, which gives the variance and covariance of the parameters k and α :.

$$F^{-1} = \begin{bmatrix} var(\alpha) & cov(\alpha, k)) \\ cov(\alpha, k)) & var(\alpha) \end{bmatrix} \tag{49}$$

For a given percentile, p, the following is calculated. For a 5% value, p=0.05.

$$u = \ln[-\ln(1-p)] \tag{50}$$

$$y = \ln\left(\alpha + \frac{u}{k}\right) \tag{51}$$

$$var(y) = \frac{var(\alpha)}{\alpha^2} + \frac{u^2 var(k)}{k^4} - \frac{2ucov(\alpha, k)}{k^2\alpha} \tag{52}$$

$$y_l = y - \Phi(\gamma)\sqrt{var(y)} \tag{53}$$

in which $\Phi(\gamma)$ is the standard normal cumulative distribution function and γ is the percent confidence level on the p-percentile value. For $\gamma = 0.95$, $\Phi(\gamma) = 1.645$. The 100th γ confidence level on the p-percentile value, (x_p) is obtained as:

$$(x_p)_\gamma = e^{y_l} \tag{54}$$

As an illustration of the difference between the 5-percentile value, and the 95th percent confidence level on the 5-percentile value, the results for the data sets considered in Table 0 are given in Table 0. The values are given in a nondimensional ratio of the value to the mean value of the data set. Also given in Table 9 is the coefficient of variation of the data set. Both the mean value and the coefficient of variation are obtained from the maximum likelihood estimates of the shape and scale parameter, Table 5.

From Table 9, it is observed that the 95th confidence level of the 5-percentile value obtained using Dodson's method is slightly higher than that obtained using Bain and Engelhardt's tables. However, the difference is rather small, only 3.4%. Due to the fact that Dodson's method does not involve the use of tables developed from Monte Carlo simulation, and the associated problems with simulation and interpolation, we recommend that the 95th confidence level be obtained using Dodson's method.

Table 0: Ratio of 5-percentile value and 95th percent confidence on 5-percentile value to mean value

Property	COV	Ratio of value to mean value Property COV		
		5-percentile value	95th confidence level of 5-percentile value using Bain and Engelhardt (1991)	95th confidence level of 5-percentile value using Dodson (1994)
Longitudinal Tensile Strength				
VG1-6	0.093	0.829	0.760	0.780
VG 7-12	0.135	0.755	0.664	0.685
VG 13-18	0.109	0.801	0.704	0.735
VG 19-24	0.098	0.821	0.732	0.764
K	0.074	0.864	0.807	0.821
Longitudinal Compressive Strength	0.095	0.825	0.756	0.776
VG1-6	0.105	0.807	0.732	0.752
VG 7-12	0.124	0.774	0.667	0.702
VG 13-18	0.117	0.787	0.684	0.719
VG 19-24	0.129	0.766	0.678	0.699
K				
Shear Strength				
VG 19-24	0.068	0.875	0.809	0.830
K	0.108	0.803	0.683	0.729
Longitudinal Tensile Modulus				
VG1-6	0.066	0.859	0.801	0.816
VG 7-12	0.096	0.854	0.794	0.805
VG 13-18	0.116	0.785	0.682	0.713
VG 19-24	0.046	0.900	0.846	0.865
K	0.063	0.872	0.819	0.832
Longitudinal Compressive Modulus	0.054	0.886	0.837	0.850
VG1-6	0.087	0.854	0.794	0.806
VG 7-12	0.132	0.749	0.633	0.669
VG 13-18	0.040	0.926	0.884	0.897
VG 19-24	0.040	0.915	0.878	0.888
K				

Table 0: Ratio of 5-percentile value and 95th percent confidence on 5-percentile value to mean value

Shear Modulus				
VG 19-24	0.113	0.763	0.652	0.691
K	0.104	0.786	0.659	0.708

1.4.1. EXTENSION TO LRFD FORMAT

There is no direct method to account for statistical uncertainty in a Load and Resistance Factor (LRFD) design format. Two methods that have been used for other materials are discussed in the following. There appears to be no advantage of one method over the other.

The first method is to use confidence levels on the nominal design value. This method implicity shifts the probability density function of the resistance, while keeping the variability the same. This is the method used in the wood industry. A data confidence factor is used in obtaining the nominal design property, where the data confidence factor is a number less than 1.0. A table is given for obtaining the data confidence factor based on the sample size and the coefficient of variation (ASTM 5457). The data confidence factor is the ratio of the specified percentile with 75% confidence to the estimate with 50% confidence using binominal confidence bounds. A minimum number sample size of 30 is required in the wood industry, and values of the data confidence factor for a coefficient of variation of 0.10 are used when the actual coefficient of variation is less than 0.10. Values of the wood industry data confidence factor are given in Table 10 for test data reported in Table 6 with 30 samples. Also reported in Table 10 is the ratio of the 95th confidence level on the 5-percentile value to the expected 5-percentile value, which would be analagous to the wood industry's data confidence factor. Even though the confidence levels are different (75th for wood, 95th used herein), the values are quite similar. Thus, using the 95th confidence value for the 5-percentile value in FRP composite design would be very similar to using the data confidence value from ASTM D5457. However, the 95th confidence level can be calculated with interpolation from a table, and can be used with coefficients of variation less than 0.10.

Table 0: Data confidence factors

Property	COV	Data confidence factor	Ratio of 95th confidence level to expected value
Longitudinal Tensile Strength			
VG1-6	0.093	0.95	0.94
VG 7-12	0.135	0.93	0.91
K	0.074	0.95	0.95

Table 0: Data confidence factors

Longitudinal Compressive Strength			
VG1-6	0.095	0.95	0.94
VG 7-12	0.105	0.95	0.93
K	0.129	0.93	0.91
Longitudinal Tensile Modulus			
VG1-6	0.066	0.95	0.95
VG 7-12	0.096	0.95	0.94
K	0.063	0.95	0.95
Longitudinal Compressive Modulus			
VG1-6	0.054	0.95	0.96
VG 7-12	0.087	0.95	0.94
K	0.040	0.95	0.97

Another approach to statistical uncertainty was taken by the cold-formed steel industry. The cold-formed steel specification (AISI, 1996) uses a correction factor to account for statistical uncertainty which is simply a function of sample size. The correction factor is a number greater than 1.0 that is multiplied by the coefficient of variation to obtain a new value of the material property coefficient of variation to be used in reliability calculations. The correction factor, C_p, is obtained as:

$$C_p = \frac{\left(1 + \frac{1}{n}\right)(n-1)}{n-3} \tag{55}$$

This equation can be regarded as a first-order approximation for the effects of sample uncertainty (Tsai, 1992). It is based on the variance of the standard Student t distribution with degree of freedom n-1 for simple sampling and the uncertainty in the sample mean. Although directly not applicable to a Weibull variable, the method is quite simple, and meets the spirit of first-order reliability methods, which were used to develop load and resistance factors. This method is different than the first method in that it does not shift the probability density function, but rather increases the level of uncertainty to account for statistical uncertainty. There is no direct means of comparing Equation 23 with confidence levels. At the present, we recommend the use of confidence levels, but include this method for completeness, and perhaps future consideration.

The cold-formed steel specification (AISI, 1996) allows Equation 23 to be used for sample sizes as small as 4, and gives a value for C_p of 5.7 for a sample size of 3. It is felt that a sample size of 3 or 4 is too small, and a larger minimum sample size needs to be specified for mechanical material properties of FRP composite structures. This is because of variations in material properties throughout the cross-section, as discussed in an earlier section. The wood industry requires a minimum sample size of 30 (ASTM D5457), and states that extreme care must be taken during sampling to ensure a representative sample for sample sizes less than 60. Given the established variation in properties through the cross-section, and the necessity to

obtain samples from all parts of the cross-sectional elements, it is felt that a minimum sample size of 30 is necessary to obtain a representative sample for FRP structures.

In summary, we are proposing that a minimum of 30 samples be tested to determine mechanical material properties. The nominal design value would be reported as the 95th confidence level of the 5% value

1.5 CONCLUSIONS

There is the need for consistency and uniformity in the material property testing and statistical reporting of FRP composite materials. Both standard coupon testing methods and statistical analysis methods have been developed and reported in this paper. The results are summarized in the following paragraphs both for material testing and statistical analysis.

Material Property Testing: Coupons for material mechanical property testing need to be obtained from all parts of the cross-section of the member. Tensile and compressive properties are determined using straight specimens with unbonded tabs. 25 mm is the preferred width to be used for tension and compression specimens. If another width is used, the coefficient of variation should be adjusted to specimen width according to Equation 34. The shear properties are recommended to be obtained from tests developed for FHWA. Such a test recognizes the size effects associated with composite materials used in bridge applications. The physical, thermal, and hygral properties can be determined in accordance with the current ASTM Standards. Table 0 summarizes the properties to be reported along with the recommended needed number of samples for each propertu value.

Statistical Analysis: A minimum of 30 coupon samples needs to be tested for the material mechanical property. A Weibull distribution is prescribed for the material properties, and the parameters of the Weibull distribution are determined using maximum likelihood estimators. A 5% value is determined and used as the nominal design property. Statistical uncertainty is accounted for by using a 95th confidence level on the 5-percentile value. The method presented in this report using Equations 45 to 54 is recommended for calculating the property values.

Table 0: Material Properties

		Property	Symbol	Unit SI	Unit Imperial	ASTM	Number of Test
Physical		Density	ρ	g/cm^3	$(lb)/in^3$	D792	6
		Glass Transition Temperature	T_g	^0C	^0F	D3418	6
		Fiber Volume Fraction	v_f	-	-	D3171,D2584	6
Mechanical	Tension	Longitudinal Modulus	E_L^t	GPa	ksi	D3039	30
		Ultimate Longitudinal Strength	F_L^t	MPa	ksi		
		Ultimate Longitudinal Strain	ε_{uL}^t	%	%		
		Major Poisson's Ratio	ν_L^t	-	-		
		Transverse Modulus	E_T^t	GPa	ksi		
		Ultimate Transverse Strength	F_T^t	MPa	ksi		
		Ultimate Transverse Strain	ε_{uT}^t	%	%		
		Minor Poisson's Ratio	ν_T^t	-	-		
	Compression	Longitudinal Modulus	E_L^c	GPa	ksi	D3410	30
		Ultimate Longitudinal Strength	F_L^c	MPa	ksi		
		Ultimate Longitudinal Strain	ε_{uL}^c	%	%		
		Major Poisson's Ratio	ν_{LT}^c	-	-		
		Transverse Modulus	E_T^c	GPa	ksi		
		Transverse Strength	F_T^c	MPa	ksi		
		Ultimate Transverse Strain	ε_{uT}^c	%	%		
		Minor Poisson's Ratio	ν_{TL}^c	-	-		
	In-Plane Shear	Shear Modulus (Longitudinal)	G_{LT}	GPa	ksi	Modified D5379	30
		Ultimate Shear Strength (Longitudinal)	τ_L^u	MPa	ksi		
		Ultimate Shear Strain (Longitudinal)	γ_L^u	%	%		
		Shear Modulus (Transverse)	G_{TL}	GPa	ksi		
		Ultimate Shear Strength (Transverse)	τ_T^u	MPa	ksi		
		Ultimate Shear Strain (Transverse)	γ_T^u	%	%		
Thermal		Longitudinal Thermal Expansion Coefficient	α_L	$1/^0C$	$1/^0F$		
		Transverse Thermal Expansion Coefficient	α_T	$1/^0C$	$1/^0F$		

Table 0: Material Properties

			Unit			
Hygral	Moisture Diffusivity Coefficient	D	cm^2/sec	in^2/sec		
	Moisture Equilibrium Content	Mm	%	%		

REFERENCES

AISC (1993). *Load and Resistance Factor Design Specification for Steel Buildings.* American Institute of Steel Construction, Chicago, IL.

AISI (1996). *Specification for the Design of Cold-Formed Steel Structural Members.* American Iron and Steel Institute, Washington, DC.

ASTM D579-97 (1997). *Standard Specification for Greige Woven Glass Fibers.*

ASTM D3039-95a (19956). *Standard Test Method for Tensile Properties of Polymer Matrix Composite Materials.*

ASTM D5083-96 (1996). *Standard Test Method for Tensile Properties of Reinforced Thermo-setting Plastics using Straight-Sided Specimens.*

ASTM D5457-93 (1993*). Standard Specification for Computing the Reference Resistance of Wood-Based Materials and Structural Connections for Load and Resistance Factor Design.*

Bain, L.J., and Engelhardt, M. (1991). *Statistical Analysis of Reliability and Life-Testing Models: Theory and Methods*. 2nd edition, Marcel Dekker, New York, NY.

Chaterjee, S., Adams, D., and Oplinger, D. W. (1993). *Test Methods for composites-A status report volume III: Shear test methods*, DOT/FAA/CT-93/17, Springfield, Virginia.

Ditlevsen, O. *Uncertainty Modeling with Applications to Multidimensional Civil Engineering Systems.* McGraw-Hill, New York, NY.

Dodson, B. (1994). *Weibull Analysis*. ASQ Quality Press, Milwaukee, Wisconsin.

Ellingwood, B.R. (2000). *Load and Resistance Factor Design (LRFD) for Structures using Fiber-Reinforced Polymer (FRP) Composites.* NIST GCR 00-793, National Institute of Standards and Technology.

Elllingwood, B., Galambos, T.V., MacGregor, J.G., and Cornell, C.A. (1980). *Development of a Probability Based Load Criterion for American National Standard A58.* NBS Special Publication 577, National Bureau of Standards.

Gromala, D.S., Sharp, D.J., Pollock, D.G., and Goodman, J.R. (1990). "Load and resistance factor design for wood: the new U.S. wood design specification." *International Timber Engineering Conference*, Tokyo, Japan, 311-318.

Iosipescu, N., (1967). "*New Accurate Procedure for single Shear Testing of Metals*", J. of Mat., 2(3), 537-566.

Kang, J.O. (2001). *Behavior and Design of Pultruded Fiber Reinforced Polymeric Members and Beam-columns under Sustained Loads.* Ph.D. Dissertation, Georgia Tech University.

King, R.L. (1986). "Statistical methods for determining design allowable properties for advanced composite materials." *15th Reinforced Plastics Congress*, British Plastics Federation, Nottingham, England, 79-85.

Lee, S. and Munro, M., (

McNutt, J.A. (1998). *Reliability analysis of FRP composite columns.* Master's thesis, The University of Tennessee.

Mil-HDBK-17 (1997). "Polymer matrix composites." *Department of Defense.*

Mirza, S.A., Hatzinikolas, M., and MacGregor, J.G. (1979). "Statistical descriptions of strength of concrete." *Journal of the Structural Division*, ASCE, 105(ST6), 1021-1037.

Mottram, J.T. (1991). "Structural properties of a pultruded E-glass fibre-reinforced polymeric I-beam." *Composite Structures*, 6.

Murhpy, J.F., ed. (1988). Load and Resistance Factor Design for Engineered Wood Construction – A pre-Standard Report. American Society of Civil Engineers, New York, New York.

Nowak, AS. (1995). "Calibration of LRFD bridge code." Journal of Structural Engineering, AWE, 121(8), 1245-1251.

Nowak, AS., Yamani, AS., and Tabsh, SW. (1994). "Probabilistic models for resistance of concrete bridge girders." ACI Structural journal, 91(3), 269-276.

Sachs, L. (1984). *Applied Statistics, A Handbook in Techniques,* 2nd edition, Springer-Verlag, New York.

Slepetz, J. M., Zagaeski, T. F., and Novello, R. F. (1978). "In-Plane Shear Test for Composite Materials", Report No. AMMRC TR 78-30, Army Materials and Mechanics Research Center, Watertown, MA.

Tabsh, SW. and Nowak, A.S. (1991). "Reliability of highway girder bridges." Journal of Structural Engineering, ASCE, 117(8), 2372-2388.

Thoman, D.R., Bain, L.J., and Antle, C.E. (1970). "Maximum likelihood estimation, exact confidence intervals for reliability, and tolerance limits in the Weibull distribution." *Technometrics*, 12(2), 363-371.

Tsai, M. (1992). *Reliability Models of Load Testing*. Ph.D. Dissertation, University of Illinois at Urbana-Champaign, IL.

Wang, Y., and Zureick, A-H. (1994). "Characterization of the longitudinal tensile behavior of pultruded I-shape structural members using coupon specimens." *Composite Structures,* 29, 463-472.

Zanakis, S.H. (1979). "A simulation study of some simple estimators for the three-parameter Weibull distribution." *Journal of Statistical Computing and Simulation, 9, 101-116.*

Zureick, A. and Scott, D. (1997). "Short-term behavior and design of fiber-reinforced polymeric slender members under axial compression." *Journal of Composites for Construction.* 1(4), 140-149.

Zureick, A., Berghaus, D., Park, J., and Cho, B. (1997). "Shear Properties of Pultruded Composite Materials," SEM 97-2, School of Civil & Environmental Engineering, Georgia Institute of Technology.

Zureick, A. and Steffen, R. (2000). "Behavior and Design of Concentrically Loaded Pultruded Angle Struts," Journal of Structural Engineering, ASCE, Vol. 126, No. 3, pp. 406-416.

CHAPTER 2: ACCEPTANCE TEST CRITERIA FOR FRP BRIDGE DECK COMPONENTS

2.1 Introduction

This chapter presents recommendations for coupons and component-level testing protocols intended for use by state engineers and inspectors as a basis for evaluating both the quality control and the certification of manufactured polymeric composite bridge decks. Descriptions of each test protocol and the acceptance criteria associated with it are included.

2.2 Proposed Test Methods at the component level

2.2.1. FLEXURAL TESTS

Flexural test methods are proposed for obtaining the one dimensional flexural property data (flexural strength, strain, and stiffness) that can be used for evaluating the quality control, structural analysis, and design of polymeric composite bridge decks. Such properties are usually influenced by the bridge deck material and geometry, reinforcement architecture, test component preparation, specimen conditioning, environment of testing including temperature and humidity, and speed of loading. The width of the test component should not be less than four times its depth, nor greater than one half the span length.

Bridge decks are designed under the action of both dead loading and a vehicular live loading consisting of a combination of the design truck or design tandem, and a design lane load as specified in the AASHTO Design Specifications (AASHTO 1994). Standard quality control tests must be easy to configure and interpret. Such tests do not have to reproduce the complex three-dimensional state of stress of an actual bridge deck in order to evaluate its properties and quality.

The proposed tests are carried out by monotonically loading to failure the test component under one of two possible loading conditions: (1) a single mid-span line load uniformly distributed across the entire width of the specimen as shown in Figure 22 or (2) two equal, uniformly distributed line loads across the entire width of the specimen (Fig. 2) where the load is loacted at a disstance from their reaction equal to one third of the span. For special purposes other distances may be specified. The load, mid-span deflection, and strains are recorded throughout the duration of the flexural test.

One of the objectives of two-equal uniform line loading condition is to subject the portion of the specimen between load points to a uniform bending moment, free of shear, and with comparatively small loads along the load lines.

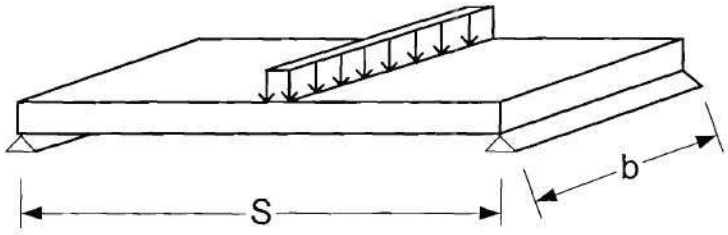

Figure 22. FRP bridge deck component under uniform line load

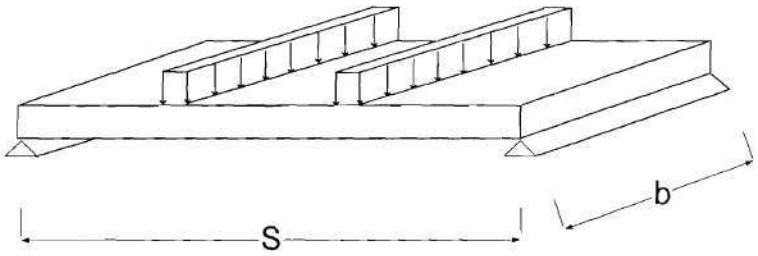

Figure 23. FRP bridge deck component under two uniform line loads

2.2.1.1. Test Set-up

The test component is mounted in testing machine on metal bearing plate supports extending over the entire width to prevent damage to the specimen at the point of contact between specimen and reaction support. The bearing plates shall be supported by either a single roller sandwiched between bearing plates, multiple rollers under a fixed knife edge reaction, or a rocker type-knife edge reaction so that lengthening of the bottom fibers and rotation of the specimen about the reaction due to deflection are unrestricted. It is important that provisions be made at the reactions to ensure equal and even distribution of forces across the entire width of the specimen. Full contact shall be maintained between support bearings and the specimen surface.

The load can be applied through one of the two following options:

1. Bearing blocks across the full width component. These bearing blocks must have sufficient thickness to eliminate high-stress concentrations at places of contact between the test component and the bearing blocks. The blocks also should have a radius of curvature and be allowed

to rotate about an axis perpendicular to the span length when the load is applied. Rotatable bearings or shims should be used to ensure full contact between the test component and the loading blocks. In the case of flexure under two line load configuration, metal bearing plates and rollers shall be used in conjunction with one load bearing block to permit load deflection without restraint. The size of these plates and rollers may vary with the size and shape of the specimen.

2. Water-filled blader across the full width of the test component. This loading mechanism almost always ensure the full contact between the test component and the loading mechanism.

The load should applied at a near constant strain rate. If strain control is not available on the testing machine, this may be approximated by repeated monitoring and adjusting of the rate of load application to maintain a nearly constant strain rate, as measured by strain transducer response versus time. The strain rate should be selected so as to produce failure within 1 to 20 minutes from the beginning of load application. If the ultimate strain of the material cannot be reasonably estimated, initial trials can be carried out with standard speeds until the ultimate strain of the material and the compliance of the system are known, and the strain rate can be adjusted.

2.2.1.2. Instrumentation

Devices shall be provided by which the deflection of the bottom surface of the specimen at the center of the span is measured with respect to either the reaction or between cross sections free of shear deflections. For strength purposes, strain shall be measured by a strain transducer as long as the attachment of this device does not cause damage to the specimen surface. Resistance gages of 350 ohms or higher are preferred to reduce heating effects on low-conductivity materials.

2.2.1.3. Calculations

The apparent flexural stiffness of the specimen shall be calculated with the following equations:

For single mid span loading: $D_a = \frac{PS^3}{48\Delta}$

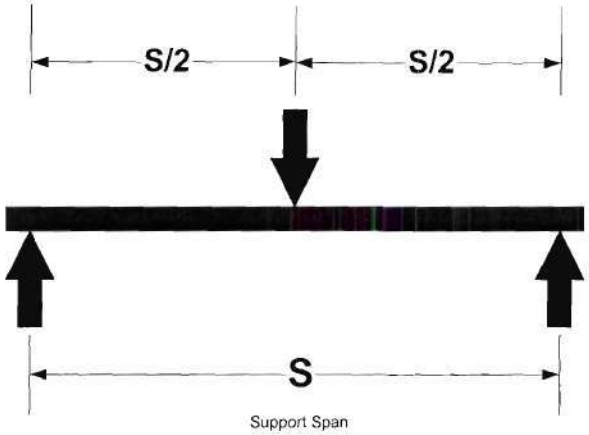

Figure 24. Mid span loading condition

For two-load configuration: $D_a = \frac{Pa}{24\Delta}(3S^2 - a^2)$

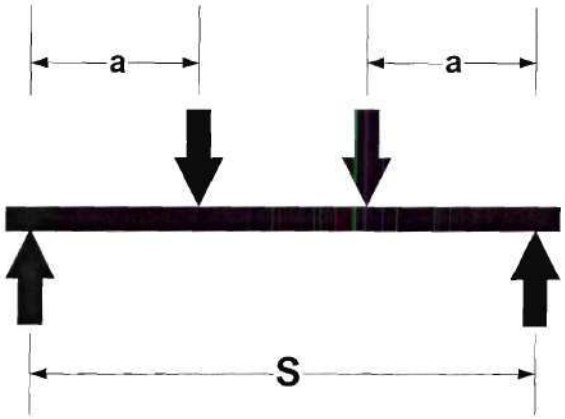

where:

D_a = apparent flexural stiffness, kip-in^2 (N-mm^2),
P = load at observed deflection, kip (N),
a = distance between load and nearest support, in (mm)
Δ = deflection at mid span, in (mm)

2.2.1.4. Acceptance criteria

To establish acceptance criteria associated with the flexural test on polymeric composite bridge decks, it is useful to know what are the strength and deflection characteristics of currently in-use bridge decks when tested under the same span and loading configuration proposed in Section 2.2.1.1. For simplicity, we will adopt details from reinforced concrete bridge decks designed by the Georgia Department of Transportation in accordance with AASHTO Bridge Design Specifications for deck design spans ranging from 3.5 ft to 12 ft. Computations will be performed on reinforced concrete panels having a width of b and a span of S and loaded with a single uniformly distributed line loading at mid-span as shown in Figure 25. A general cross section is shown in Figure 26, for which dimensions and amount of steel reinforcement are given in Table 0. In all computations to follow it is assumed that normal concrete weight (W_c=150 pcf) with a compressive strength of f_c' = 3,500 psi is used. The modulus of elasticity of concrete E_c can be computed according to Section 5.4.2.4 of the AASHTO, LRFD Bridge Design Specifications (1994) from $E_c = 57000\sqrt{f_c'}$. The yield strength and modulus of elasticity of the steel are assumed to be f_y = 60,000 psi and E_s = 29,000 ksi, respectively.

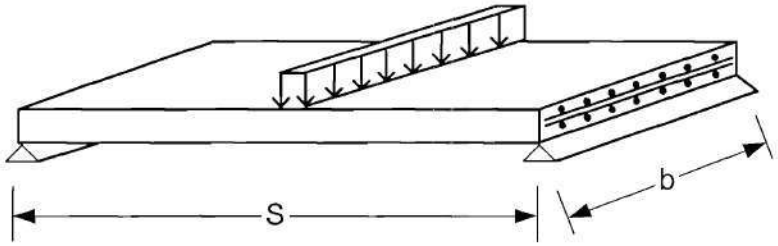

Figure 25. Loading on bridge deck

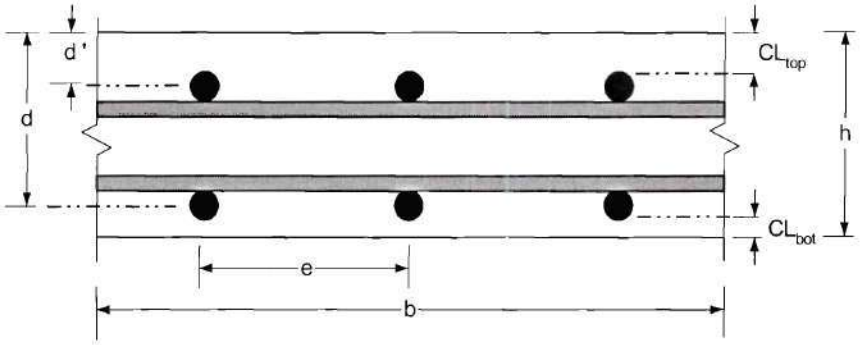

Figure 26. Cross-section of a reinforced concrete bridge deck

where

h : Bridge deck thickness,
d: Distance from extreme compression fiber to centroid of bottom steel,
d': Distance from extreme compression fiber to centroid of top steel,
b: Width of bridge deck,
e: Spacing of main reinforcement,
CL_{top}: Clear cover at the top,
CL_{bot}: Clear cover at the bottom.

Table 0: Typical GDOT details of reinforced concrete bridge decks. (CL_{top} = 2.75 in)

S (ft)	h (in)	Main Reinforcement	As (in^2/ft)	d' (in)	d (in)
3.5	6.875	# 5 @ 8.250	0.451	3.0625	5.5625
4.0	7.000	# 5 @ 7.750	0.480	3.0625	5.6875
4.5	7.250	# 5 @ 7.500	0.496	3.0625	5.9375
5.0	7.375	# 5 @ 7.125	0.522	3.0625	6.0625
5.5	7.625	# 5 @ 7.000	0.531	3.0625	6.3125
6.0	7.750	# 5 @ 6.625	0.562	3.0625	6.4375
6.5	8.000	# 5 @ 6.500	0.572	3.0625	6.6875
7.0	8.125	# 5 @ 6.250	0.595	3.0625	6.8125
7.5	8.250	# 5 @ 6.000	0.620	3.0625	6.9375
8.0	8.500	# 5 @ 5.875	0.633	3.0625	7.1875
8.5	8.625	# 5 @ 5.625	0.661	3.0625	7.3125
9.0	8.750	# 5 @ 5.375	0.692	3.0625	7.4375
9.5	9.000	# 5 @ 5.375	0.692	3.0625	7.6875
10.0	9.125	# 5 @ 5.125	0.726	3.0625	7.8125
10.5	9.250	# 5 @ 5.000	0.744	3.0625	7.9375
11.0	9.500	# 6 @ 6.875	0.768	3.1250	8.1250
11.5	9.625	# 6 @ 6.625	0.797	3.1250	8.2500
12.0	9.875	# 6 @ 6.625	0.797	3.1250	8.5000
$A_s = \frac{b}{e} A_{bar}$	A_s = Area per unit width of top or bottom reinforcing bar A_{bar} = Area of one main reinforcing bar				

Load-deflection characterization: The stiffness and strength for all bridge deck spans given in Table 4 were calculated at different loading stages representing the bridge deck prior to concrete's first cracking and after the concrete's first cracking but before the onset of tension steel yielding, and at ultimate in the following manner:

The bridge deck flexural moments at concrete first crack, M_{cr}, at the onset of tension steel yielding, M_y, and at ultimate, M_u, can be computed from:

$$M_{cr} = \frac{f_r I_g}{y_t} \tag{56}$$

$$M_y = \frac{2}{3} F_{cc} c_y + F_s'(c_y - d') + F_s(d - c_y) \tag{57}$$

$$M_u = F_{cc}\left(1 - \frac{\beta_1}{2}\right) c_u + F_s'(c_u - d') + F_s(d - c_u) \tag{58}$$

where:

f_r = modulus of rupture of concrete = $7.5\sqrt{f_c'}psi$,

I_g = moment of inertia of the gross concrete section about the centroidal axis, neglecting the reinforcement,

y_t = distance from the centroidal axis of the cross section, neglecting steel, to the extreme fiber in tension.

F_{cc} = total compressive force carried by concrete,

F_s' = total force carried by compression steel.

F_s = total force carried by tension steel.

c_y = distance from the neutral axis to center of concrete compressive force and is computed from

$$\frac{b c_y^{\,2}}{2(d - c_y)} \varepsilon_s E_c + \frac{(c_y - d')}{(d - c_y)} \varepsilon_s E_s A'_s - f_y A_s = 0 \tag{59}$$

c_u is computed from

$$0.85f_c'\beta_1 c_u b + \frac{(c_u - d')}{c_u}\varepsilon_t E_s A'_s - f_y A_s = 0 \tag{60}$$

The parameters b, d, d', ε_s, are shown in Figure 27, f_y is the yield strength of steel, and E_c, E_s are the moduli of concrete and steel, respectively. The parameter c in the figure represents c_y for the case of tension steel first yielding and c_u when the moment is computed at ultimate. f_c' is the compressive strength of concrete, β_1 is the ratio of the depth of rectangular stress block to "c" (0.85 for $f_c' \leq 4000\,psi$ concrete), and ε_t is the strain at the top concrete surface as shown in Figure 27.

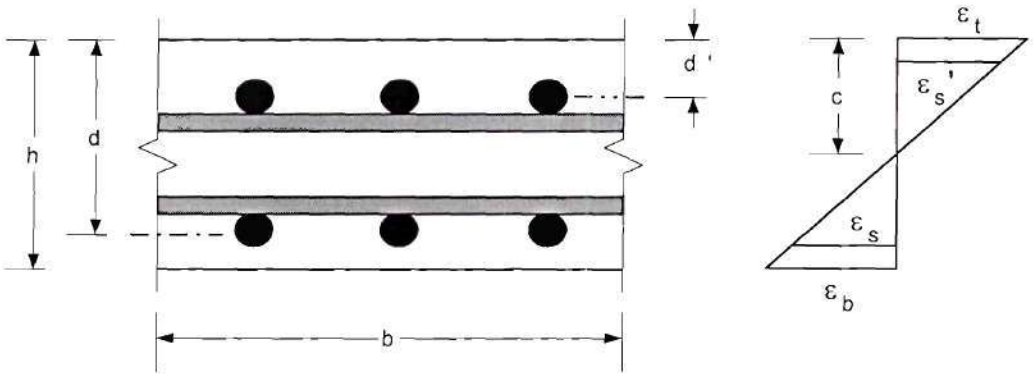

Figure 27. Strain diagram of the cross-section

The load, P_i, corresponding to a computed moment, M_i, can simply be obtained from the following equation:

$$P_i = \frac{4M_i}{L} \tag{61}$$

The deflection of the panel at any load smaller than the yield load, P_y, can be estimated from:

$$\Delta = \frac{PS^3}{48E_c I_e} \tag{62}$$

where $I_e = I_g$ for $P \le P_{cr}$ and $I_e = \left(\frac{M_{cr}}{M_a}\right)^3 I_g + \left[1 - \left(\frac{M_{cr}}{M_a}\right)^3\right] I_{cr}$ for $P_{cr} \le P \le P_y$. In these equations:

I_e = Effective moment of inertia.

M_a = Moment in the bridge deck at a stage for which deflection is being computed.

M_{cr}, f_r, and I_g have been defined previously.

The computed load-deflection curves up to the yielding load are presented graphically in Figure 28.

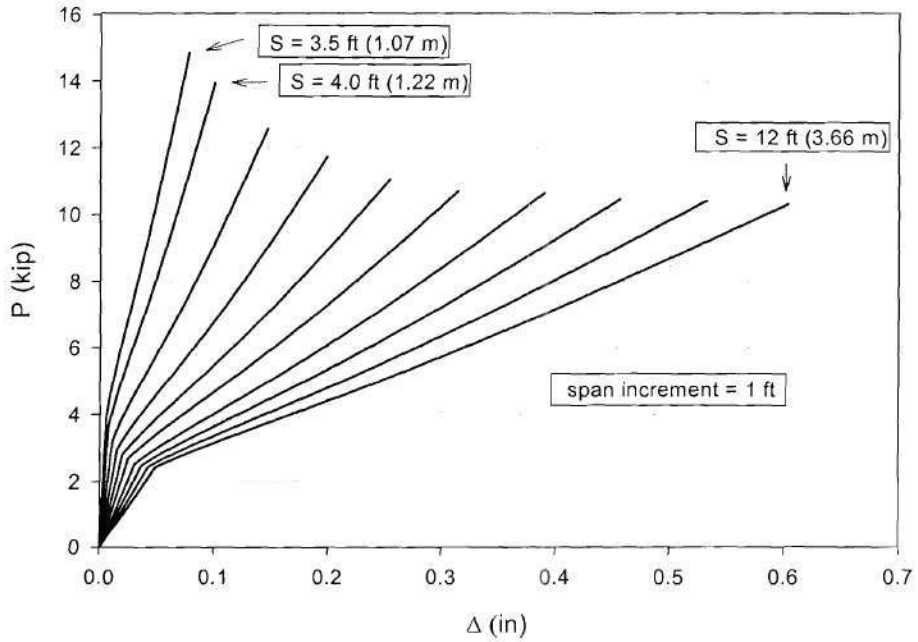

Figure 28. Computed P-Δ curves for reinforced concrete bridge decks (CL_{top}=2.75 in)

The deflection at ultimate was computed from the moment-curvature curves and the load-deflection relationship between the yielding load and the ultimate load was approximated as linear. A typical assumed load-deflection curve is shown in Figure 29. Values of P_{cr}, Δ_{cr},P_y,Δ_y , S/Δ_y, P_u, Δ_u, and S/Δ_u are listed in Table 0. The ultimate load versus the bridge deck span is presented in Figure 30.

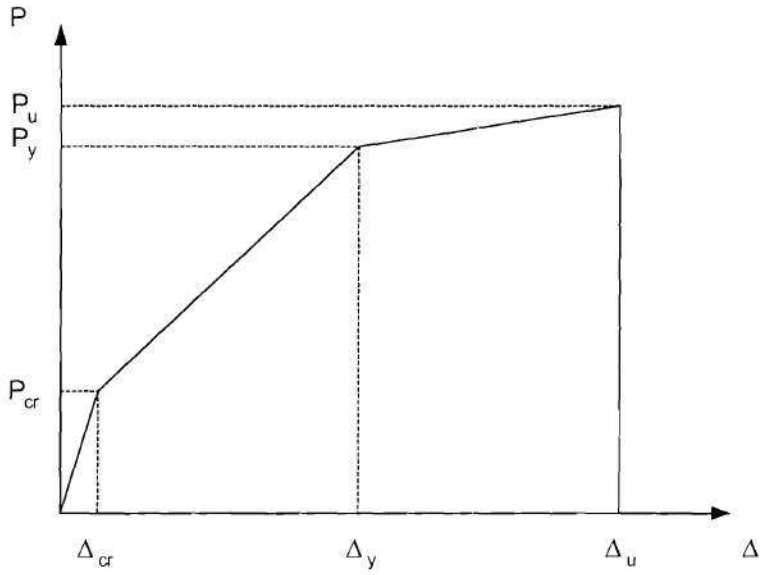

Figure 29. Assumed Load-deflection curve of a reinforced concrete bridge deck panel

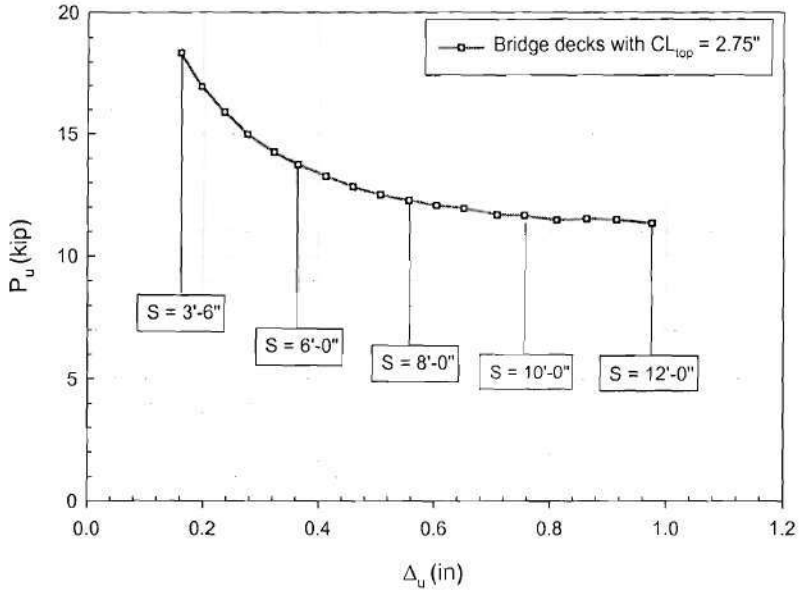

Figure 30. Load-deflection values at ultimate

Table 0: Strength and deflection results for three limit states (CL_{top} = 2.75 in)

S (ft)	P_{cr}^{RC} (kips)	Δ_{cr}^{RC} (in)	P_{y}^{RC} (kips)	Δ_{y}^{RC} (in)	S/Δ_{y}^{RC}	P_{u}^{RC} (kips)	Δ_{u}^{RC} (in)	S/Δ_{u}^{RC}
3.5	4.00	0.0059	15	0.0774	542	18	0.1603	262
4.0	3.62	0.0076	14	0.1002	479	17	0.1960	245
4.5	3.46	0.0092	13	0.1205	448	16	0.2356	229
5.0	3.22	0.0112	13	0.1468	409	15	0.2758	218
5.5	3.13	0.0131	12	0.1684	392	14	0.3212	205
6.0	2.96	0.0154	12	0.1990	362	14	0.3630	198
6.5	2.91	0.0175	11	0.2225	351	13	0.4110	190
7.0	2.79	0.0199	11	0.2543	330	13	0.4579	183
7.5	2.68	0.0225	11	0.2884	312	13	0.5053	178
8.0	2.67	0.0249	11	0.3144	305	12	0.5552	173
8.5	2.59	0.0277	11	0.3517	290	12	0.6029	169
9.0	2.52	0.0306	11	0.3907	276	12	0.6502	166
9.5	2.52	0.0331	10	0.4156	274	12	0.7080	161
10.0	2.46	0.0362	10	0.4567	263	12	0.7550	159
10.5	2.41	0.0394	10	0.4961	254	12	0.8106	155
11.0	2.43	0.0421	10	0.5324	248	12	0.8622	153
11.5	2.38	0.0454	10	0.5766	239	12	0.9138	151
12.0	2.40	0.0482	10	0.6036	239	12	0.9743	148

SERVICE LOAD-DEFLECTION CALCULATIONS

To estimate the deflection at the service load level, the AASHTO Section 3.24.3.1, "Case A-Main Reinforcement Perpendicular to Traffic" is used to first calculate the total moment:

$$M_T = M_D + (1 + I)M_L \tag{63}$$

where M_D and M_L are the dead load and the live load moment, respectively, and I is an impact factor defined in AASHTO section 3.8.2 as:

$$I = \frac{50}{S + 125} \leq 0.3 \tag{64}$$

M_D and M_L can be calculated from:

$$M_D = \frac{w_d S^2}{8} \tag{65}$$

$$M_L = \frac{P(S+2)}{32} \tag{66}$$

for simple spans, where:
w_d: Dead load per unit length of slab,
S: Effective span in feet (as defined in AASHTO 3.24.1),
P: Load on one rear wheel of an AASHTO truck (P = 16 kips for an AASHTO HS20 loading).

Then,

$$M_T = \frac{(\gamma_{conc} h) b S^2}{8} + (1+I)\frac{P_{20}(S+2)}{32} \tag{67}$$

The equivalent uniform line load which produces the same total moment can be calculated from:

$$M_T = \frac{(qb)S}{4} = \frac{P_d S}{4} \tag{68}$$

where P_d is the service load. Equation 67 was also evaluated by considering the contribution of asphalt (1.5-2.0 in) but was found to make a maximum moment difference of 4%. The service load P_d is shown on the general load-deflection curve in Figure 31.

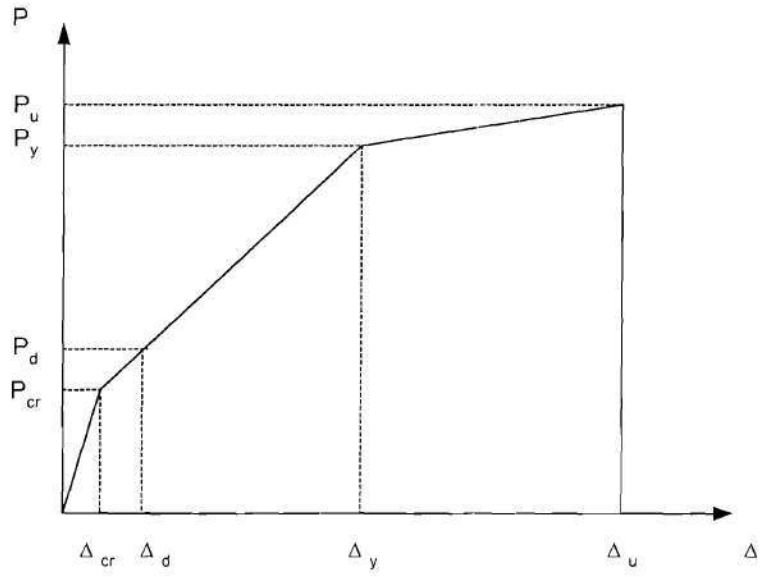

Figure 31. Load-deflection curve of a reinforced concrete bridge deck panel

Flexural toughness: Toughness is the energy absorption capability, determined from the area under the load-deflection curve up to a specified deflection. For the load-deflection curve approximated by trilinear segments as shown in 31, the flexural toughness computed at four deflection levels, Δ_{cr}, Δ_d, Δ_y, and Δ_u can be computed from the following equations:

$$E_{cr} = \frac{1}{2} P_{cr} \Delta_{cr} \tag{69}$$

$$E_d = \frac{1}{2} P_{cr} \Delta_{cr} + \frac{1}{2} (P_{cr} + P_d)(\Delta_d - \Delta_{cr}) \tag{70}$$

$$E_y = \frac{1}{2} P_{cr} \Delta_{cr} + \frac{1}{2} (P_{cr} + P_y)(\Delta_y - \Delta_{cr}) \tag{71}$$

$$E_u = \frac{1}{2} P_{cr} \Delta_{cr} + \frac{1}{2} (P_{cr} + P_y)(\Delta_y - \Delta_{cr}) + \frac{1}{2} (P_y + P_u)(\Delta_u - \Delta_y) \tag{72}$$

Results from the above equations are given in Table 0 and shown graphically in Figure 32.

Table 0: Computed flexural toughness for reinforced concrete bridge decks for different spans (CL_{top} = 2.75 in)

S (ft)	E_{cr} (kip.in)	E_d (kip.in)	E_y (kip.in)	E_u (kip.in)
3.5	0.012	0.016	0.686	2.063
4.0	0.014	0.026	0.827	2.306
4.5	0.016	0.033	0.939	2.611
5.0	0.018	0.047	1.088	2.867
5.5	0.020	0.056	1.192	3.194
6.0	0.023	0.073	1.370	3.458
6.5	0.025	0.085	1.485	3.803
7.0	0.028	0.106	1.651	4.085
7.5	0.030	0.129	1.834	4.370
8.0	0.033	0.144	1.971	4.739
8.5	0.036	0.171	2.180	5.034
9.0	0.038	0.200	2.407	5.338
9.5	0.042	0.217	2.509	5.736
10.0	0.045	0.251	2.760	6.058
10.5	0.047	0.285	2.957	6.385
11.0	0.051	0.307	3.197	6.814

Table 0: Computed flexural toughness for reinforced concrete bridge decks for different spans (CL_{top} = 2.75 in)

S (ft)	E_{cr} (kip.in)	E_d (kip.in)	E_y (kip.in)	E_u (kip.in)
11.5	0.054	0.346	3.460	7.159
12.0	0.058	0.371	3.584	7.595

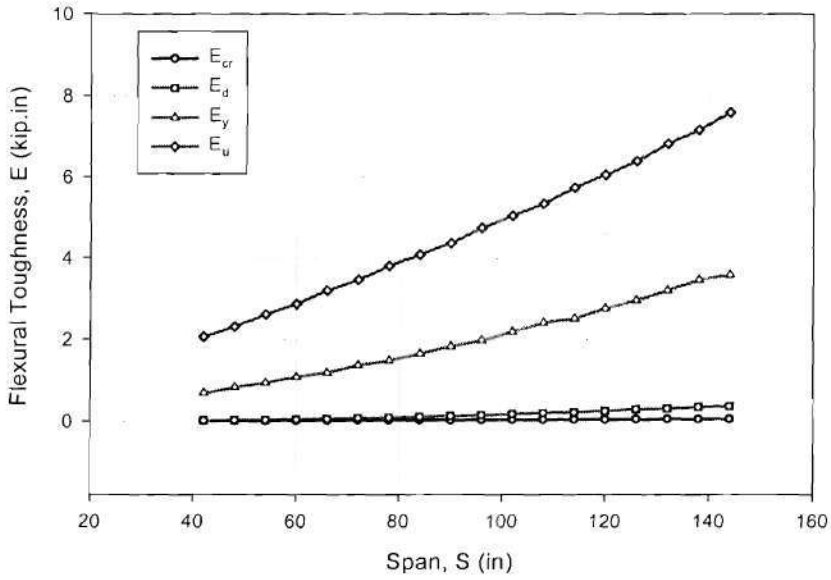

Figure 32. Flexural toughness of reinforced concrete bridge decks (CL_{top}=2.75 in)

Strength and deflection acceptance limits for FRP bridge deck panels: As a minimum a polymeric composite bridge deck panel tested in accordance with Section 2.2.1 should have at the least the following strength and toughness requirements:

$$P_u^{FRP} \geq P_u^{RC} \tag{73}$$

$$E_u^{FRP} \geq 1.25 E_u^{RC} \tag{74}$$

The values P_u^{RC} and E_u^{RC} are found in Tables 0 and 0, respectively. These values do not account for any degradation in the strength as a result of combined environmental and mechani-

cal loads over time. The number 1.25, toughness factor, is proposed at this point to account for the lack in ductility of FRP structural members.

Regarding the stiffness requirement, it is proposed at this time that a minimum deflection value of (S/300) be adopted. Therefore, when one accounts for possible material degradation of at most 25% coupled with the increase of deflection values resulting from creep (Zureick and Kang 2000), a deflection requirement at service load (approximately 30% of ultimate) of S/500 should be met. The S/500 value does not account for vibration effects.

Appendix I- Standard Methods of Testing Fiber Reinforced Polymeric Bridge Decks in Flexure

1. Scope

1.1 This test method determines the flexural properties of fiber-reinforced polymer matrix composite bridge decks. The composite material forms used for fabrication of the elements comprising the bridge deck cross section can be in the form of continuous fibers, fabrics, or braided preforms.

1.2 The flexural properties can be determined by loading the deck under one of two possible scenarios. The deck can be loaded by one uniformly distributed line load at midspan ("Uniformly distributed line load at midspan" on page 90), or by two equal, uniformly distributed line loads, each of which are one third the span distance from their respective support ("Two equal, uniformly distributed line loads" on page 90).

1.3 *This standard does not purport to address all of the safety problems, if any, associated with its use. It is the responsibility of the user of this standard to establish appropriate safety and health practices and determine the applicability of regulatory limitations prior to use.*

1.4 The values stated in either SI units or inch-pound units are to be regarded separately as standard. Within the text the inch-pounds units are shown in brackets. The values stated in each system are not exact equivalents; therefore, each system must be used independently of the other. Combining values from the two systems may result in nonconformance with the standard.

1.5

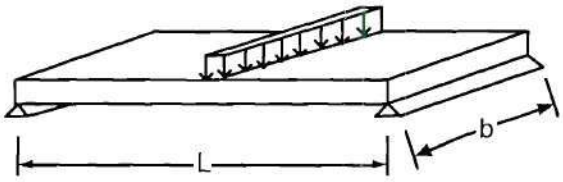

Figure 33. Uniformly distributed line load at midspan

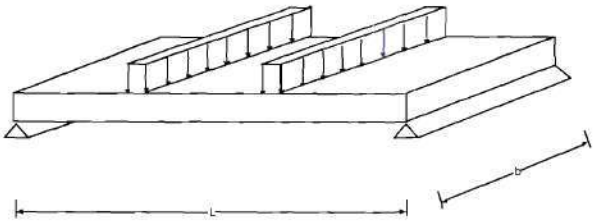

Figure 34. Two equal, uniformly distributed line loads

2. Reference Documents

2.1 *ASTM Standards*

D792 Test Method for Specific Gravity (Relative Density) and Density of

Plastics by Displacement[1]

D883 Terminology Relating to Plastics "Annual Book of ASTM Standards, Vol 8.01" on page 91

D3171 Standard Test Method for Fiber Content of Resin-Matrix Composites by Matrix Digestion[2]

D3878 Terminology of High-Modulus Reinforced Fibers and Their Composites "Annual Book of ASTM Standards, Vol 15.03" on page 91

D5229/D5229M Test Method for Moisture Absorption Properties and Equilibrium Conditioning of Polymer Matrix Composite Materials "Annual Book of ASTM Standards, Vol 15.03" on page 91

D5379/D5379M Test Method for Shear Properties of Composite Materials by the V-Notched Beam Method "Annual Book of ASTM Standards, Vol 15.03" on page 91

E4 Practices for Load Verification of Testing Machines[3]

E6 Terminology Relating to Methods of Mechanical Testing "Annual Book of ASTM Standards, Vol 3.01" on page 91

E83 Practice for Verification and Classification of Extensometers "Annual Book of ASTM Standards, Vol 3.01" on page 91

E111 Test Method for Young's Modulus, Tangent Modulus, and Chord Modulus "Annual Book of ASTM Standards, Vol 3.01" on page 91

E177 Practice for Use of the Terms Precision and Bias in ASTM Test Methods[4]

E456 Terminology Relating to Quality and Statistics "Annual Book of ASTM Standards, Vol 14.02" on page 91

E1237 Guide for Installing Bonded Resistance Strain Gages "Annual Book of ASTM Standards, Vol 3.01" on page 91

E6308 Guide for the Identification of Composite Materials in Computerized Material Property databases "Annual Book of ASTM Standards, Vol 15.03" on page 91

E6309 Guide for the Development of Standard Data Records for Computerization of Mechanical Test Data for High-Modulus Fiber-Reinforced Composite Materials "Annual Book of ASTM Standards, Vol 15.03" on page 91

E1471 Guide for the Identification of Fibers, Fillers, and Core Materials in Computerized Material Property Databases "Annual Book of ASTM Standards, Vol 15.03" on page 91

3. Terminology

3.1 Terminology D3878 defines terms relating to high-modulus fibers and their composites. Terminology D883 defines terms relating to plastics. Terminology E6 defines terms relating to mechanical testing. Terminology E456 and Practice E177 define terms relating to statistics. In

1. Annual Book of ASTM Standards, Vol 8.01
2. Annual Book of ASTM Standards, Vol 15.03
3. Annual Book of ASTM Standards, Vol 3.01
4. Annual Book of ASTM Standards, Vol 14.02

the event of a conflict between terms, Terminology D3878 shall have precedence over the other Terminology standards.

3.2 *Descriptions of Terms Specific to This Standard*:

3.2.1 *specimen,*- a fiber reinforced polymetric (FRP) bridge deck section used in testing to determine the flexural properties.

3.2.2 *span,*--the total distance between reactions on which a specimen is supported to accommodate a transverse load.

3.2.3 *shear span,*--two times the distance between a reaction and the nearest load point for a symmetrically loaded specimen.

3.2.4 *depth of specimen,*--that dimension of the specimen which is perpendicular to the span and parallel to the direction in which the load is applied.

3.2.5 *span-depth ratio,*--the numerical ratio of total span divided by specimen depth.

3.2.6 *shear span-depth ratio,*--the numerial ratio of shear span divided by specimen depth.

3.2.7 *nominal value,* –a value, existing in name only, assigned to a measurable property for the purpose of convenient designation. Tolerances may be applied to a nominal value to define an acceptable range for the property.

3.2.8 *principal bridge deck coordinate system,*- a coordinate system with axes that are normal to the planes of symmetry that exist within the bridge deck.

3.3 *Symbols*:

3.3.1 A—cross-sectional area of specimen,

3.3.2 CV—sample coefficient of variation, in percent,

3.3.3 E^b—apparent flexural stiffness,

3.3.4 F^b—ultimate flexural strength,

3.3.5 n—number of specimens,

3.3.6 P—load carried by test specimen,

3.3.7 P^f—load carried by test specimen at failure,

3.3.8 P^{max}—maximum load prior to failure,

3.3.9 s_{n-1}—sample standard deviation,

3.3.10 x_i—measured or derived property,

3.3.11 x—sample mean (average),

3.3.12 ε–indicated normal strain from strain transducer,

4. Summary of Test Method

4.1 A fiber reinforced polymer (FRP) bridge deck is mounted in a mechanical testing machine and monotonically loaded in flexure by either a uniformly distributed line load at midspan, or by two equal, uniformly distributed line loads placed at one third span from their respective support. The deck is loaded to failure while recording the load, midspan deflection, and strain.

5. Significance and Use

5.1 This test method is designed to produce flexure property data for material specifications, research and development, quality assurance, and structural analysis and design. From a flexure test a variety of data are acquired that are needed for design purposes. Factors that influence the flexural response and should therefore be reported include the following: material, methods of material preparation and reinforcement architecture, specimen preparation, specimen conditioning, environment of testing, speed of testing, and time and temperature. The void content and volume percent reinforcement of elements comprising the total cross section should also be reported. Properties, in the test direction, that may be obtained from this test method include

5.1.1 Flexural Strength

5.1.2 Flexural Strain

5.1.3 Flexural Stiffness

5.1.4

6. Interferences

[2] *The results from the procedures presented are limited to the material and test factors listed in 5.1.*

7. Apparatus

7.1 *Testing Machine--* A device that provides (1) a rigid frame to support the specimen yet permit its deflection without restraint, (2) a loading head through which the force is applied without high-stress concentrations in the specimen, and (3) a force-measuring device that is calibrated to ensure accuracy in accordance with Practices E4.

7.2 *Drive Mechanism*— The testing machine drive mechanism shall be capable of imparting to the movable head a controlled displacement rate with respect to the stationary head. The displacement rate of the movable head shall be capable of being regulated as specified in "Speed of Testing—Set speed of testing to effect a nearly constant strain rate. If strain control is not available on the testing machine, this may be approximated by repeated monitoring and adjusting of the rate of load application to maintain a nearly constant strain rate, as measured by strain transducer response versus time. Select the strain rate so as to produce failure within 1 to 10 minutes from the beginning of load application. If the ultimate strain of the material cannot be reasonably estimated, conduct initial trials using standard speeds until the ultimate strain of the material and the compliance of the system are known, and the strain rate can be adjusted. The suggested standard speeds are:" on page 98.

7.3 *Load Indicator*—The testing machine load-sensing device shall be capable of indicating the total load being carried by the test specimen. This device shall be essentially free from inertia-lag at the specified rate of testing and shall indicate the load with an accuracy over the load range(s) of interest within ± 1% of the indicated value, as specified by Practices E4. The load range(s) of interest may be fairly low for modulus evaluation, much higher for strength evalua-

tion, or both, as required.

7.4 Support Apparatus:

7.4.1 *Reaction Bearing Plates--* The test specimen shall be supported by metal bearing plates extending over the entire width to prevent damage to the specimen at the point of contact between specimen and reaction support. The minimum thickness of the bearing plates shall be two inches.

7.4.2 *Reaction Bearing Roller--* The bearing plates shall be supported by either a single roller sandwiched between bearing plates ("Roller support" on page 94), rollers and a fixed knife edge reaction ("Rocker type knife edge support" on page 94), or a rocker type-knife edge reaction ("Fixed type knife edge support" on page 95) so that shortening and rotation of the specimen about the reaction due to deflection will be unrestricted.

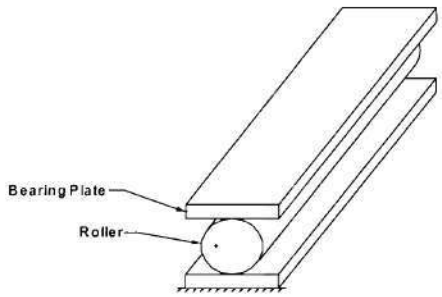

Figure 35. Roller support

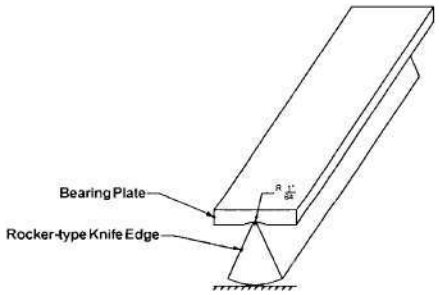

Figure 36. Rocker type knife edge support

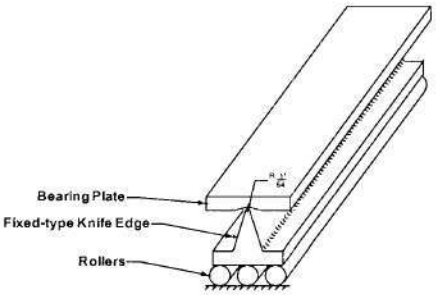

Figure 37. Fixed type knife edge support

7.4.3 *Reaction Bearing Alignment*-- Provisions shall be made at the reactions to ensure equal and even distribution of forces across the entire width of the specimen.

7.5 Load Apparatus:

7.5.1 *Load Bearing blocks*-- The load shall be applied through bearing blocks across the full specimen width which are of sufficient thickness to eliminate high-stress concentrations at places of contact between the specimen and bearing blocks. The loading surface of the blocks shall have a radius of curvature equal to two to four times the specimen depth for a chord length at least equal to the depth of the specimen. Load shall be applied to the blocks in such a manner that the blocks may rotate about an axis perpendicular to the span. Provisions such as rotatable bearings or shims shall be made to ensure full contact between the specimen and the loading blocks. In the case of third-span flexure, metal bearing plates and rollers shall be used in conjunction with one load bearing block to permit load deflection without restraint. The size of these plates and rollers may vary with the size and shape of the specimen.

7.5.2 Loading:

7.5.2.1 *Midspan Flexure*-- The total load on the test specimen shall be applied through a single, uniformly distributed line load across the entire width of the specimen, located at the mid-span.

7.5.2.2 *Third-Span Flexure*-- The total load on the test specimen shall be applied equally at two uniformly distributed line loads across the entire width of the specimen, equidistant from the reactions. The two load lines will normally be at a distance from their reaction equal to one third of the span, but for special purposes other distances may be specified.

Note 1 -One of the objectives of two-point loading is to subject the portion of the specimen between load points to a uniform bending moment, free of shear, and with comparatively small loads at the load points. For example, loads applied at one-third span length from reactions would be less than applied at one-fourth span length from reaction to develop a moment of similar magnitude. When loads are applied at the one-third points the moment distribution of the specimen simulates that for loads uniformly distributed across the span to develop a moment of similar magnitude. If loads are applied at the outer one-fourth points of the span, the maximum moment and shear are the same as the maximum moment and shear for the same total load uniformly distributed across the span.

7.6 *Deflection Apparatus*-- For the apparent flexural stiffness calculations, devices shall be provided by which the deflection of the bottom surface of the specimen at the center of the span is measured with respect to either the reaction or between cross sections free of shear deflections.

7.7 *Strain-Indicating Device*—Strain shall be measured by a strain transducer as long as the attachment of this devices does not cause damage to the specimen surface.

7.7.1 Select gages having larger resistances to reduce heating effects on low-conductivity materials. Resistances of 350 ohms or higher are preferred. Use the minimum possible gage excitation voltage consistent with the desired accuracy (1 to 2 volts is recommended) to further reduce the power consumed by the gage. Local heating of the specimen by the gage may affect the performance of the material directly, or it may affect the

indicated strain due to a difference between the gage temperature compensation factor and the coefficient of thermal expansion of the specimen material.

7.7.2 Temperature compensation is recommended when testing at Standard Laboratory Atmosphere. Temperature compensation is required when testing in non-ambient temperature environments. When appropriate, use a traveler specimen (dummy calibration specimen) with identical material and strain gage orientations for thermal strain compensation.

7.8 *Conditioning Chamber*--When conditioning materials in other than ambient laboratory environments, a temperature/vapor-level controlled environmental conditioning chamber is required that shall be capable of maintaining the required relative temperature to within ±3°C [±5°F] and the required relative vapor level to within ±5%. Chamber conditions shall be monitored either on an automated continuous basis or on a manual basis at regular intervals.

7.9 *Environmental Test Chamber*-- An environmental test chamber is required for test environments other than ambient testing laboratory conditions. This chamber shall be capable of maintaining the gage section of the test specimen within ±3°C [±5°F] of the required test temperature during the mechanical test. In addition, the chamber may have to be capable of maintaining environmental conditions such as fluid exposure or relative humidity during the test (see "Test Environment–Condition the specimen to the desired moisture profile and, if possible, test under the same conditioning fluid exposure level. However, cases such as elevated temperature testing of a moist specimen place unrealistic requirements on the capabilities of common testing machine environmental chambers. In such cases testing at elevated temperature with no fluid exposure control may be necessary, and moisture loss during mechanical testing may occur. This loss can be minimized by reducing exposure time in the test chamber although care should be taken to ensure that the specimen temperature is at equilibrium. This loss may be further minimized by increasing the relative humidity in an uncontrolled chamber by hanging wet, coarse fabric inside the chamber, and keeping it moist with a drip bottle placed outside the chamber. In addition, fixtures may be preheated, temperature may be ramped up quickly, and hold time at temperature may be minimized prior to testing. Environmentally conditioned traveler specimens may be used to measure moisture loss during exposure to the test environment. Weigh a traveler specimen prior to testing and place it in the test chamber at the same time as the specimen. Remove the traveler specimen immediately after fracture and reweigh it to determine moisture loss. Record modifications to the test environment." on page 98).

8. Sampling and Test Specimens

8.1 *Sampling*—Test at least six specimens per test condition unless valid results can be gained through the use of fewer specimens, such as in the case of a designed experiment. For statistically significant data the procedures outlined in E122 should be consulted. The method of sampling shall be reported.

8.2 Geometry:

8.2.1 *Cross-section and dimensions*-- The cross-sectional properties of the test specimen

shall be the same as that found in the manufactured FRP composite bridge decks. The depth of the specimen shall be equal to the depth of the manufactured FRP composite bridge decks. The width shall not be less than four times the depth of the specimen, nor greater than one half the span length.

8.2.2 *Overall Specimen Length*-- The total specimen length shall be the span plus an overhang beyond each reaction support so that the specimen can accommodate the bearing plates and rollers and will not slip off the reactions during test.

8.2.3 The span length of specimens intended primarily for evaluation of shear properties shall be such that the shear span is relatively short. Conversely, the span length of specimens intended primarily for evaluation of flexure properties shall be such that the shear span is relatively long.

8.3 *Labeling*—Label the specimens so that they will be distinct from each other and traceable back to the raw material, and in a manner that will both be unaffected by the test and not influence the test.

9. Calibration

9.1 The accuracy of all measuring equipment shall have certified calibrations that are current at the time of use of the equipment.

10. Conditioning

10.1 *Standard Conditioning Procedure*--Condition per Procedure C of Test Method D5229/D5229M; store and test at Standard Laboratory Atmosphere (23±3° C [73±5° F] and 50±10 % relative humidity) unless a different environment is specified as part of the experiment.

11. Procedure

11.1 Parameters To Be Specified Prior to Test:

11.1.1 Specimen type and geometry

11.1.2 Determine specific material property, accuracy, and data reporting requirements prior to test for proper selection of instrumentation and data recording equipment. Estimate operating stress and strain levels to aid in transducer selection, calibration of equipment, and determination of equipment settings.

11.1.3 The environmental conditioning test parameters.

11.2 General Instructions:Report any deviations from this test method, whether intentional or inadvertent.

11.2.1 Report any deviations from this test method, whether intentional or inadvertent.

11.2.2 If specific gravity, density, reinforcement volume or void volume of each element comprising the total cross-section are to be reported, then obtain these samples from the same bridge deck as the test specimens by means of Test Method D3171.

11.2.3 Determine the size of the specimen, the span, and the shear span in accordance with

"Loading:" on page 95 and "Geometry:" on page 96. Locate the specimen symmetrically on its supports with load bearing and reaction bearing blocks as described in "Load Apparatus:" on page 95. Set apparatus for measuring deflections in place. Full contact shall be attained between support bearings, loading blocks, and the specimen surface.

11.3 *Speed of Testing*—Set speed of testing to effect a nearly constant strain rate. If strain control is not available on the testing machine, this may be approximated by repeated monitoring and adjusting of the rate of load application to maintain a nearly constant strain rate, as measured by strain transducer response versus time. Select the strain rate so as to produce failure within 1 to 10 minutes from the beginning of load application. If the ultimate strain of the material cannot be reasonably estimated, conduct initial trials using standard speeds until the ultimate strain of the material and the compliance of the system are known, and the strain rate can be adjusted. The suggested standard speeds are:

11.4 *Test Environment*–Condition the specimen to the desired moisture profile and, if possible, test under the same conditioning fluid exposure level. However, cases such as elevated temperature testing of a moist specimen place unrealistic requirements on the capabilities of common testing machine environmental chambers. In such cases testing at elevated temperature with no fluid exposure control may be necessary, and moisture loss during mechanical testing may occur. This loss can be minimized by reducing exposure time in the test chamber although care should be taken to ensure that the specimen temperature is at equilibrium. This loss may be further minimized by increasing the relative humidity in an uncontrolled chamber by hanging wet, coarse fabric inside the chamber, and keeping it moist with a drip bottle placed outside the chamber. In addition, fixtures may be preheated, temperature may be ramped up quickly, and hold time at temperature may be minimized prior to testing. Environmentally conditioned traveler specimens may be used to measure moisture loss during exposure to the test environment. Weigh a traveler specimen prior to testing and place it in the test chamber at the same time as the specimen. Remove the traveler specimen immediately after fracture and reweigh it to determine moisture loss. Record modifications to the test environment.

11.4.1 Store the specimen in the conditioned environment until test time, if the testing area environment is different than the conditioning environment.

11.4.2 Monitor test temperature by placing an appropriate thermocouple within 25 mm [1.0 inch] of the specimen gage section. Maintain temperature of the specimen, and the traveler specimen, if one is being used for thermal strain compensation or moisture loss evaluation, within ±3° C [±5°F] of the required condition. Taping thermocouple(s) to the test specimen (and the traveler) is an effective measurement method.

11.5 *Loading* – Apply the load to the specimen at the specified rate until failure, while recording data.

11.6 *Data Recording*-Record load versus strain (or transducer displacement) continuously, or at frequent regular intervals. If a transition region is noted, record the load, strain, and mode of damage at such points. If the specimen is to be failed, record the maximum load, the failure load,

and the strain (or transducer displacement) at, or as near as possible to, the moment of rupture.

2.3 *Failure Modes*–Record the mode and location of failure of the specimen.

12. Calculations

12.1 Apparent Flexural Stiffness

12.1.1 Midspan Loading condition

$$D_a = \frac{PL^3}{48\Delta} \tag{75}$$

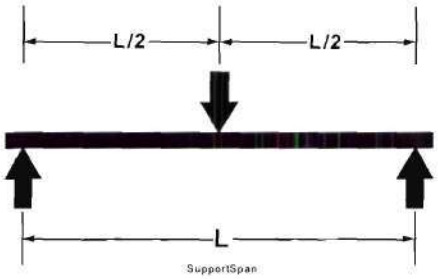

Figure 38. Midspan loading condition

12.1.2 Third-Span Loading Condition

$$D_a = \frac{Pa}{24\Delta} \cdot (3L^2 - 4a^2) \tag{76}$$

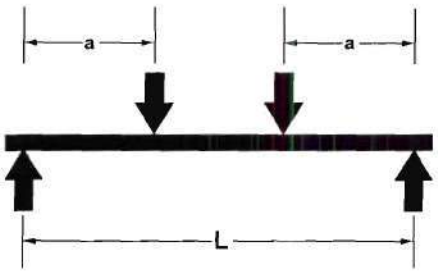

Figure 39. Third-span loading condition

where:

D_a = apparent flexural stiffness, kip·in^2 (N·mm^2),

P = load at observed deflection, kip (N),

L = span length, in (mm),

a = distance between load and nearest support, in (mm), and

Δ = deflection at midspan, in (mm)

12.2 *Statistics* - For each series of tests calculate the arithmetic mean, standard deviation and coefficient of variation (in percent) for each property determined:

12.2.1 Arithmetic Mean

$$\bar{x} = \frac{\left(\sum_{i=1}^{n} x_i\right)}{n} \tag{77}$$

12.2.2 Standard Deviation

$$s_{n-1} = \sqrt{\frac{\left(\sum_{i=1}^{n} x_i^2 - n(\bar{x})^2\right)}{(n-1)}} \tag{78}$$

12.2.3 Coefficient of Variation

$$CV = 100 \cdot \frac{s_{n-1}}{\bar{x}} \tag{79}$$

where:

$\bar{x}$ = sample mean (average)

s_{n-1} = sample standard deviation

CV = sample coefficient of variation, in percent

N = number of specimens, and

x_i = measured or derived property

13. Report

13.1 Report the following information, or references pointing to other documentation containing this information, to the maximum extent applicable (reporting of items beyond the control of a given testing laboratory, such as might occur with material details or panel fabrication param-

eters, shall be the responsibility of the requestor):

13.1.1 The revision level or date of issue of this test method.

13.1.2 The date(s) and location(s) of the test.

13.1.3 The name(s) of the test operator(s).

13.1.4 Any variations to this test method, anomalies noticed during testing or equipment problems occurring during testing

13.1.5 Identification of the material tested including: material specification, material type, material designation, manufacturer, manufacturer's lot or batch number, source (if not from manufacturer), date of certification, expiration of certification, filament diameter, tow or yarn filament count and twist, sizing, form or weave, and matrix type.

13.1.6 Description of the fabrication steps used to prepare the bridge deck including fabrication start date, fabrication end date, process specification, cure cycle, consolidation method, and a description of the equipment used.

13.1.7 Description of fiber architecture and surface deformation of each individual component of the bridge deck.

13.1.8 If requested, report density, volume percent reinforcement, and void content test methods, specimen sampling method and geometries, test parameters, and test results for each component of the bridge deck.

13.1.9 Method of preparing the test specimen, including specimen labeling scheme and method, specimen geometry, and sampling method. Identification of anchor material, geometry, bonding agent, and bonding agent preparation and curing information.

13.1.10 Calibration dates and methods for all measurement and test equipment.

13.1.11 Type of test machine, grips, jaws; grip pressure, alignment results, and data acquisition sampling rate and equipment type.

13.1.12 Dimensions of each test specimen.

13.1.13 Conditioning parameters and results, use of travelers and traveler geometry, and the procedure used if other than that specified in the test method.

13.1.14 Relative humidity and temperature of the testing laboratory.

13.1.15 Environment of the test machine environmental chamber (if used) and soak time at environment.

13.1.16 Number of specimens tested.

13.1.17 Speed of testing.

13.1.18 Transducer placement on the specimen and transducer type for each transducer used.

13.1.19 If strain gages were used, the types, resistance, size, gage factor, temperature compensation method, transverse sensitivity, lead-wire resistance, and any correction factors employed.

13.1.20 Load-deflection and load-strain curves and tabulated data for each specimen.

13.1.21 Individual strengths and average value, standard deviation, and coefficient of variation (in percent) for the population. Note if the failure load was less than the maximum

load prior to failure.

13.1.22 Individual strains at failure and the average value, standard deviation, and coefficient of variation (in percent) for the population.

13.1.23 Individual values of apparent flexural stiffness, and the average value, standard deviation, and coefficient of variation (in percent) for the population.

13.1.24 Failure mode and location of failure for each specimen.

13.1.25 Loading conditions to portray the load, support mechanics, and type of equipment.

13.1.26 Deflection apparatus.

13.1.27 Depth and width of the specimen or pertinent cross-sectional dimensions.

13.1.28 Span length and shear span distance.

13.1.29 Rate of load application.

13.1.30 Description of failure

14. Precision and Bias

14.1 *Precision*—The data required for the development of a precision statement is not available for this test method. Precision, defined as the degree of mutual agreement between individual measurements, cannot yet be estimated because of an insufficient amount of data.

14.2 *Bias*—Bias cannot be determined for this test method as no acceptable reference standard exists.

15. Keywords

2.4 Flexural properties, flexural strength, flexural strain, apparent flexural stiffness, bridge deck, composite materials.

16. References

ASTM D579-97 (1997). *Standard Specification for Greige Woven Glass Fibers.*

AASHTO (1994). AASHTO LRFD Bridge Design Specifications, Washington, D.C.

Ahmad, S. H. & Plecnik, J. M. (1989). "Transfer of Composite Technology to Design and Construction of Bridges." U.S. DOT Report, September.

AISC (1993). *Load and Resistance Factor Design Specification for Steel Buildings.* American Institute of Steel Construction, Chicago, IL.

AISI (1996). *Specification for the Design of Cold-Formed Steel Structural Members.* American Iron and Steel Institute, Washington, DC.

Ali-Khan, Mir Sajjad. (1991). "Transverse Joint and Connection Studies on a Fiber Reinforced Plastic Bridge Deck," Final Report Presented to the Federal Highway Administration, August.

Army (1966). Trilateral Design and Test Code for Military Bridging and Gap Crossing Equipment, US army Tank Automotive & Armament Command, AMSTA-TR-R(MS-21), Warren, MI.

ASTM D3039-95a (19956). *Standard Test Method for Tensile Properties of Polymer Matrix Composite Materials.*

ASTM D5083-96 (1996). *Standard Test Method for Tensile Properties of Reinforced Thermosetting Plastics using Straight-Sided Specimens.*

ASTM D5457-93 (1993*). Standard Specification for Computing the Reference Resistance of Wood-Based Materials and Structural Connections for Load and Resistance Factor Design.*

Azar, Waleed A. (1989). "Experimental and Analytical Study of Composite Bridge Decks," Structures Laboratory Report # 89-9-17, California State University, Long Beach, September.

Bain, L.J., and Engelhardt, M. (1991). *Statistical Analysis of Reliability and Life-Testing Models: Theory and Methods*. 2nd edition, Marcel Dekker, New York, NY.

Bakri, Pavan Anil (1989) Analysis and Design of Polymer Composite Bridge Decks, Thesis presented to the Department of Civil Engineering in partial Fulfilment of the Requirements for the Degree of Master of Science at the massachusetts Institute of Technology, September.

Bakeri, P. A. & Sunder, S. S. (1990). "Concepts for Hybrid FRP Bridge Deck System." Serviceability and Durability Of Construction Materials, edited By B. A. Suprenant, Proceedings of the First Materials Engineering Congress, ASCE, Denver, Colorado, August 13-15, Vol. 2, pp. 1006-1014.

Brown, R., and Zureick, A. (1999). "Lightweight composite truss section decking," Very Large Floating Structure Conference, VLFS 99, September 23, Paper 7-1-3.

Brown, R., and Zureick, A. (1998). " Truss section fiberglass reinforced composite causway deck," P30th International SAMPE Conference, San Antonio, Texas, October 24, pp. 303-315.

Chaterjee, S., Adams, D., and Oplinger, D. W. (1993). *Test Methods for composites-A status report volume III: Shear test methods,* DOT/FAA/CT-93/17, Springfield, Virginia.

Ditlevsen, O. *Uncertainty Modeling with Applications to Multidimensional Civil Engineering Systems.* McGraw-Hill, New York, NY.

Dodson, B. (1994). *Weibull Analysis.* ASQ Quality Press, Milwaukee, Wisconsin.

Ellingwood, B.R. (2000). *Load and Resistance Factor Design (LRFD) for Structures using Fiber-Reinforced Polymer (FRP) Composites.* NIST GCR 00-793, National Institute of Standards and Technology.

Elllingwood, B., Galambos, T.V., MacGregor, J.G., and Cornell, C.A. (1980). *Development of a Probability Based Load Criterion for American National Standard A58.* NBS Special Publication 577, National Bureau of Standards.

GangaRao, H. V. S. & Sotiropoulos, S. N. (1991). "Development of FRP Bridge Superstructural Systems." U.S. DOT Report, June.

GangaRao, Hota V.S., Thippeswamy, Hemanth K., Shekar, Vimala, and Craigo, Carl (1999). "Development of glass fiber reinforced polymer composite bridge deck, SAMPE Journal, Volume 35, Number 4, July/August, pp.12-24.

Gromala, D.S., Sharp, D.J., Pollock, D.G., and Goodman, J.R. (1990). "Load and resistance factor design for wood: the new U.S. wood design specification." *International Timber Engineering Conference*, Tokyo, Japan, 311-318.

Hayes, Michael D., Ohanehi, Don, Lesko, John, Cousin, Thomas and Dan Witcher (2000). "Performance of Tube and Plate Fiberglass Composite Bridge Deck," Journal of Composites for Construction, Vol. 4, No. 2, May, pp. 48-55.

Henry, J. A. (1985). "Deck Girders System for Highway Bridges Using Fiber Reinforced Plastics." M.S. Thesis, North Carolina State University.

Iosipescu, N., (1967). "*New Accurate Procedure for single Shear Testing of Metals*", J. of Mat., 2(3), 537-566.

Kang, J.O. (2001). *Behavior and Design of Pultruded Fiber Reinforced Polymeric Members and Beam-columns under Sustained Loads.* Ph.D. Dissertation, Georgia Tech University.

King, R.L. (1986). "Statistical methods for determining design allowable properties for advanced composite materials." *15th Reinforced Plastics Congress*, British Plastics Federation, Nottingham, England, 79-85.

Lee, S. and Munro, M., (

Lopez-Anido, Roberto, Hota V. S. GangaRao, Venkata Vedam, Nikki Overby (1997). "Design and Evaluation of a Modular FRP Bridge Deck," Proceedings of the International Composites Expo'97 Composite Institute , Nashville, TN, pp. 3-E(1-6).

McGhee, Kevin K. (1990). "Optimum Design of Bridge Deck Panels Using Composite Materials" A thesis presented to the faculty of the School of Engineering and Applied science, in Partial fulfillment of the Requirements for the Degree Master of Science, University of Virginia, May.

McGhee, K. K., Barton, F. W. & Mckeel, W. T. (1991). "Optimum Design of Composite Bridge Deck Panels." Advanced Composites Materials in Civil Engineering Structures, Proceedings of the Specialty Conference, A.S.C.E., Las Vegas, Nevada, Jan. 31-Feb. 1, pp. 360-370.

McNutt, J.A. (1998). *Reliability analysis of FRP composite columns.* Master's thesis, The University of Tennessee.

Mil-HDBK-17 (1997). "Polymer matrix composites." *Department of Defense.*

Mirza, S.A., Hatzinikolas, M., and MacGregor, J.G. (1979). "Statistical descriptions of strength of concrete." *Journal of the Structural Division*, ASCE, 105(ST6), 1021-1037.

Mongi, A. N. K. (1991). "Theoretical and Experimental Behavior of FRP Floor System." M.S. Thesis, West Virginia University, Morgantown, May.

Mottram, J.T. (1991). "Structural properties of a pultruded E-glass fibre-reinforced polymeric I-beam." *Composite Structures*, 6.

Murhpy, J.F., ed. (1988). Load and Resistance Factor Design for Engineered Wood Construction – A pre-Standard Report. American Society of Civil Engineers, New York, New York.

Naval Sea Systems Command (1992). Circular of Requirements for New Construction Strategic Sealift Ships, CSP/S-24.

Nowak, AS. (1995). "Calibration of LRFD bridge code." Journal of Structural Engineering, AWE, 121(8), 1245-1251.

Nowak, AS., Yamani, AS., and Tabsh, SW. (1994). "Probabilistic models for resistance of concrete bridge girders." ACI Structural journal, 91(3), 269-276.

Plecnik, J. M. & Azar, W. A. (1991). "Structural Components, Highway Bridge Deck Applications." International Encyclopedia of Composites, edited by I. Lee & M. Stuart, Vol. 6, pp. 430-445.

Sachs, L. (1984). *Applied Statistics, A Handbook in Techniques,* 2nd edition, Springer-Verlag, New York.

Sampaga, Reynaldo Estigoy (1991). "Mechanical Connection Studies on a Glass Fiber Reinforced Plastic Bridge Deck," Report Presented to the Federal Highway Administration, April.

Slepetz, J. M., Zagaeski, T. F., and Novello, R. F. (1978). "In-Plane Shear Test for Composite Materials", Report No. AMMRC TR 78-30, Army Materials and Mechanics Research Center, Watertown, MA.

Sotiropoulus, Sotiris, N. , GangaRao, Hota, V.S., and Mongi, Ahmed, N.K. (1994). "Theoretical and Experimental Evaluation of FRP Components and Systems," ASCE Journal of Structural Engineering, Vol. 120, No. 2, Feb., pp.464-485.

Tabsh, SW. and Nowak, A.S. (1991). "Reliability of highway girder bridges." Journal of Structural Engineering, ASCE, 117(8), 2372-2388.

Thoman, D.R., Bain, L.J., and Antle, C.E. (1970). "Maximum likelihood estimation, exact confidence intervals for reliability, and tolerance limits in the Weibull distribution." *Technometrics*, 12(2), 363-371.

Tsai, M. (1992). *Reliability Models of Load Testing*. Ph.D. Dissertation, University of Illinois at Urbana-Champaign, IL.

Wang, Y., and Zureick, A-H. (1994). "Characterization of the longitudinal tensile behavior of pultruded I-shape structural members using coupon specimens." *Composite Structures,* 29, 463-472.

Zanakis, S.H. (1979). "A simulation study of some simple estimators for the three-parameter Weibull distribution." *Journal of Statistical Computing and Simulation, 9, 101-116.*

Zureick, A. and Shih, B. (1992). "Preliminary Design of Fiber-Reinforced Polymeric Bridge Decks" Georgia Institute of Technology, Report No. SEM-94-1,

Zureick, A., Shih, B., and Munley, E. (1995). " Fiber-reinforced polymeric bridge decks," Structural Engineering Review, Vol. 7, No. 3, pp. 257-266.

Zureick, A. and Scott, D. (1997). "Short-term behavior and design of fiber-reinforced polymeric slender members under axial compression." *Journal of Composites for Construction.* 1(4), 140-149.

Zureick, A., Berghaus, D., Park, J., and Cho, B. (1997). "Shear Properties of Pultruded Composite Materials," SEM 97-2, School of Civil & Environmental Engineering, Georgia Institute of Technology.

Zureick, A. and Steffen, R. (2000). "Behavior and Design of Concentrically Loaded Pultruded Angle Struts," Journal of Structural Engineering, ASCE, Vol. 126, No. 3, pp. 406-416.

Georgia Institute of Technology

School of Civil and Environmental Engineering

Structural Engineering, Mechanics and Materials
Research Report No. 02-4

SHEAR STRENGTH OF HORIZONTALLY CURVED STEEL I-GIRDERS – EXPERIMENTAL TESTS

Final Report

Prepared for

Professional Service Industries, Inc.
and
Federal Highway Administration

by

A. Zureick, D.W. White, N. Phoawanich and J. Park

March 2002

SHEAR STRENGTH OF HORIZONTALLY CURVED STEEL I-GIRDERS – EXPERIMENTAL TESTS

Abdul-Hamid Zureick, Donald W. White, Narin Phoawanich and Jin Park

School of Civil and Environmental Engineering
Georgia Institute of Technology

This report presents the results of four full-scale curved steel I-girder component tests conducted to examine their shear behavior and to determine their maximum shear strengths. The girders were made of AASHTO M270 Grade 345 steel and had a nominal web depth and web thickness of 1,219 mm (48 in) and 8 mm (5/16 in) respectively. The resulting nominal web slenderness ratio D/t_w was 154. Two of the girders, labeled as S1 and S1-S, had a nominal radius R = 63,630 mm (208.75 ft) and a transverse stiffener spacing such that the ratio d_o/D was 3 for S1 and 1.5 for S1-S (producing $d_o/R = 0.0575$ and 0.0287). The other two test components, labeled as S2 and S2-S, were identical to S1 and S1-S except that their radii were 36,580 mm (120 ft), resulting in $d_o/R = 0.10$ and 0.050. All of the girders were braced against radial deflections at intervals of 3,658 mm (12 ft) along the girder arc. Therefore, the ratio L_b/R was equal to 0.0575 for S1 and S1-S and 0.10 for S2 and S2-S, where L_b is the distance between the bracing systems along the girder arc. All the test girders were instrumented to determine their maximum shear resistance as well as the mechanisms associated with the development of their shear strengths. Of particular interest was the extent to which the curved webs were capable of developing post-buckling strength, and the influence of the horizontal curvature and panel aspect ratio on the development of this strength.

ACKNOWLEDGEMENTS

The authors express their sincere thanks to Professional Service Industries, Inc. (PSI) and the Federal Highway Administration (FHWA) for their support of this work. Dr. Mohammad S. Kahn is the technical contact at PSI and Mr. William Wright is the technical contact at FHWA. Also, the assistance from Professor Roberto Leon of Georgia Tech, Mr. Joey Hartmann of FHWA, and Mr. Se-Kwon Jung of Georgia Tech is gratefully acknowledged. The opinions, findings and conclusions expressed in this report are those of the authors and do not necessarily reflect the views of the individuals and groups acknowledged here.

TABLE OF CONTENTS

TABLE OF CONTENTS
(continued)

LIST OF FIGURES

LIST OF FIGURES (continued)

LIST OF FIGURES (continued)

LIST OF FIGURES (continued)

LIST OF TABLES

CHAPTER I - INTRODUCTION

With the increased usage of horizontally curved steel I-girder bridges, the interest in understanding the behavior of and developing rational design guidelines for these types of structures has grown rapidly. One particular interest is the shear strength of curved I-girders, an issue that has been studied analytically and experimentally by a number of investigators.

Prior research has shown that the elastic buckling strength of a curved web panel is greater than that of a straight girder panel with the same aspect ratio, material properties, web slenderness ratio and boundary conditions (Mozer et al. 1971 and 1973; Culver et al. 1972c; Mariani et al. 1973, Abdel-Sayed 1973; Davidson 1996; Lee and Yoo 1999b; White et al. 2001). However the increase in strength due to horizontal curvature is typically small relative to the shear capacity, and thus the *Guide Specifications for Horizontally Curved Highway Bridges* (AASHTO 2002), hereafter referred to as the *2002 Guide Specifications*, ignore this benefit and utilize the same shear buckling strength equations as in the AASHTO LFD and LRFD provisions for straight I-girders (AASHTO 1996 and 1998).

The experimental research by Mozer et al. (1970, 1971 and 1973) and by Nakai (1984a and b, 1985) showed that horizontal curvature reduces the maximum shear strength of curved web panels from that of equivalent straight panels; however, this reduction was found to be insignificant for the horizontal curvatures studied, i.e., $L_b/R \leq 0.10$ and $d_o/R \leq 0.08$. Lee and Yoo (1999b) and White et al. (2001) have confirmed these findings analytically.

Despite the available analytical and numerical studies on the shear behavior and strength of curved I-girders, no experimental tests of transversely-stiffened I-girders with web slenderness $D/t_w > 70$ and panel aspect ratio $d_o/D > 1.33$ have been conducted (Zureick 1998; Hall et al.

1999). Mozer and Culver (1970) did test girders with ($D/t_w = 188$, $d_o/D = 1$) and with ($D/t_w = 150$, $d_o/D = 1.33$), and I-girders with similar parameters have been tested in Japan (Nakai et al. 1984a and b, 1985). These test limits appear to be related to the fact that the AASHTO design specifications in effect for straight I-girders at the time of the earlier research limited the panel aspect ratio to $d_o/D \leq 1$.

As a result of the above limits on the prior experimental testing, the *2002 Guide Specifications* place the following significant restrictions on the design of curved I-girder webs:

- The maximum web slenderness is limited to

$$\frac{D}{t_w} \leq 100 \tag{1}$$

for curved girders with unstiffened web panels (defined by $d_o/D > 1$) and a radius of curvature less than 213 m (700 ft). This restriction is relaxed to $D/t_w \leq 150$ for $R \geq 610$ m (2000 ft), with a linear transition in the D/t_w limit between these two radii. That is, for $R \geq 213$ m,

$$\frac{D}{t_w} \leq 100 + 0.125(R - 213) \leq 150 \tag{2}$$

where R is expressed in meters. The limit $D/t_w \leq 150$ is the maximum web slenderness permitted for unstiffened web panels in the LRFD straight girder Specifications (AASHTO 1998), and is intended to facilitate handling during fabrication and erection[1]. The limit of 100 is selected to satisfy approximately the web compactness provisions in AASHTO LRFD for $F_y = 345$ MPa (50 ksi). The value $F_y = 345$ MPa is the maximum yield strength allowed for the use of compact flange flexural strength equations in the *Guide Specifications* (AASHTO 2002).

---

1. Panels with $d_o/D \leq 3$ are considered as stiffened in (AASHTO 1998).

- The ratio d_o/D is restricted to be less than or equal to one in girders designed with stiffened web panels[2].
- The maximum web flexural stresses are limited to the elastic bend buckling stress under all loading conditions. In addition, potential postbuckling contributions to the shear strength are neglected.

Hall et al. (1999) state in their discussion of new recommended research:

> **"Relief from this requirement [the limit of $d_o/D \leq 1$] for some curvatures can be justified with additional testing. Neither fatigue behavior nor strength of curved-girder webs is well understood at this time, and it would be risky to reduce the stiffening requirements without further analytical and experimental research.... Reduction of required web stiffening is one area where gains are possible.... Investigation of various types of web stiffening should be expanded for bending, shear, and combined bending and shear conditions.... The effect of stiffener spacing on the bend-buckling strength of curved girders with varying details is needed."**

1.1 OBJECTIVE AND SCOPE

This report presents the results of four full-scale curved steel I-girder component tests conducted to examine their shear behavior and to determine their maximum shear strengths. The girders were made of AASHTO M270 Grade 345 steel and had a nominal web depth and web thickness of 1,219 mm (48 in) and 8 mm (5/16 in) respectively. The resulting nominal web slenderness ratio D/t_w was 154. This web slenderness is slightly smaller than the maximum D/t_w permitted for Grade 345 transversely stiffened I-girders in the AASHTO LRFD (1998) straight I-girder specifications. Two of the girders, labeled as S1 and S1-S, had a radius R = 63,630 mm (208.75 ft) and a transverse stiffener spacing such that the ratio d_o/D was 3 for S1 and 1.5 for

2. At the time of the final editing of this manuscript (February 2002), AASHTO T-14 approved a change to the *2002 Guide Specifications* permitting an increase in the maximum d_o/D allowed in stiffened web panels. The new provisions specify a linear increase in the maximum d_o/D from a value of one at a radius of 213 m (700 ft) to three at a radius of 610 m (2000 ft).

S1-S (producing $d_o/R = 0.0575$ and 0.0287). The other two test components, labeled as S2 and S2-S, were identical to S1 and S1-S except that their radii were 36,580 mm (120 ft), resulting in $d_o/R = 0.10$ and 0.050. All of the girders were braced against radial deflections at intervals of $L_b = 3658$ mm (12 ft) along the girder arc. Therefore, the ratio L_b/R was equal to 0.0575 for S1 and S1-S and 0.10 for S2 and S2-S.

All the test girders were loaded while instrumented with electrical resistance strain gages, linear variable differential transformers, wire potentiometers and load cells to determine their maximum shear resistance as well as the mechanisms associated with the development of their shear strengths. Of particular interest was the extent to which the curved webs were capable of developing postbuckling strength, and the influence of the horizontal curvature and panel aspect ratio on the development of this strength.

1.2 ORGANIZATION

In Chapter II, a detailed outline of issues associated with curved I-girder webs is presented. Prior research on the behavior of curved web panels is reviewed, and current specification provisions for proportioning of these elements are summarized. Although the complete range of issues associated with curved I-girder web design is beyond the scope of this specific research, it is essential to understand the broad context within which the current research on maximum shear strength of curved I-girder webs fits.

Chapter III summarizes the geometry and material properties of the four curved I-girders tested in this work, describes the overall layout and the specific loading and displacement boundary conditions for these tests, details the instrumentation of the test girders, and outlines the test procedure. Chapter IV then presents the test data. The overall load-deflection and load-web

distortion behavior is discussed, and strain measurements that provide insight into the load transfer mechanisms are provided. Chapter V outlines several design models for predicting the shear strength, and compares the maximum strengths and other data attained experimentally to corresponding predictions of the different idealized models. The findings from this research are summarized and conclusions are stated in Chapter VI.

CHAPTER II BACKGROUND

Requirements for proportioning of horizontally curved I-girder web panels have been established in the past based on elastic stress limits (including consideration of fatigue) as well as maximum strength considerations. Prior work concerning these requirements is reviewed below.

2.1 ELASTIC STRESS BASED WEB SLENDERNESS LIMITS (INCLUDING CONSIDERATION OF FATIGUE)

Culver et al. (1972a, b) were the first to develop recommended web slenderness limits for curved I-girder webs. These investigators analyzed a range of cylindrically curved web panels in doubly symmetric girders with D/t_w up to 300, d_o/D from 0.67 to 1.5 and d_o/R up to 0.167. They then determined the values of D/t_w at various curvatures, quantified by the parameter d_o/R, to limit the calculated web longitudinal plate bending stresses at the transverse stiffeners. Culver et al. selected a criterion of limiting these stresses to the same magnitude as in imperfect straight girder web panels with the same panel aspect ratio d_o/D, a web slenderness $D/t_w = 200$, and an out-of-flatness representative of AWS (1966) fabrication tolerances. The web slenderness of 200 was selected as a base in their studies since this value was approximately the upper limit on the D/t_w of straight bridge girders at the time of their research. The resulting equation for the maximum web slenderness allowable within curved web panels can be written as

$$\frac{D}{t_w} \le 6.78 \sqrt{\frac{E}{F_y}} \left[1 - 8.6 \frac{d_o}{R} + 34 \left(\frac{d_o}{R} \right)^2 \right] \qquad (3)$$

In the limiting case in which R approaches infinity, this equation reduces to the restriction on the maximum slenderness of straight I-girder webs within (AASHTO 1996, 1998). This restriction represents an upper bound below which fatigue due to excessive web lateral deflections is not an issue, and is based on the research by Yen and Muller (1966) and Muller and Yen (1968). The dependency of Eq. (3) on F_y indirectly reflects the tendency of bridges designed with higher yield strength steels to be subjected to larger applied stresses. Culver et al. (1972c) stated that, "Until fatigue test data are obtained for curved girders, this reduction [Eq. (3)] or essentially limiting D/t_w for highly curved girders to existing limits in the working stress portion of the AASHO specifications appears to be warranted."

In the analyses conducted by Culver et al. (1972a, b), the web panel was modeled as a series of isolated unit cylindrical strips on an elastic foundation, subjected to a radial pressure loading per (Wachowiak 1967) to simulate the effect of horizontal curvature. The radial displacements at the web boundaries were assumed to be zero. An extension of this work was published a year later, when Culver et al. (1973) used a shell model to examine the accuracy of the cylindrical strip idealization. This work also included consideration of longitudinal stiffeners. In both (Culver 1972a, b) and (Culver et al. 1973), the investigators showed that the magnitude of the longitudinal web plate bending stresses was significantly affected by the spring constant of the equivalent elastic foundation associated with the plate action between the girder flanges (or the flanges and the longitudinal stiffeners). Also, both Culver et al. (1972a, b) and Culver et al. (1973) showed a significant increase in the calculated longitudinal web plate bending stresses at the transverse stiffeners with decreasing panel aspect ratio d_o/D. However, they found that the required reduction in D/t_w (for the above stresses to be the same magnitude in curved web panels as in imperfect straight girder panels with the same d_o/D and $D/t_w = 200$) was insensitive to

the spring constant and the value of d_o/D. Nevertheless, their computed web plate bending stresses ranged from as low as nine percent to as high as 44 percent of the yield strength of A36 steel (for $d_o/D = 1.5$ and their largest assumed spring constant versus $d_o/D = 0.67$ and their smallest assumed spring constant (Culver et al. 1973)). Since the web fatigue behavior should be related to the stress magnitude, it is possible that a more rational assessment of fatigue might be attained with a basis different than that of equating web plate bending stresses in curved and straight web panels without regard for the magnitude of the stresses.

Daniels and Herbein (1980) conducted the only experimental research in the United States regarding fatigue of curved steel bridge I-girders. These investigators studied the performance of thin webs in a number of homogeneous noncomposite doubly symmetric I-girders. Based on this research, Daniels et al. (1980) concluded that Eq. (3) was too severe and proposed the following more liberal equations (expressed here in a nondimensionalized form):

$$\frac{D}{t_w} \le 4.27 \sqrt{\frac{E}{f_b}} \left[1 - 4\frac{d_o}{R} \right] \le 170 \tag{4}$$

for allowable stress design and

$$\frac{D}{t_w} \le 6.78 \sqrt{\frac{E}{F_y}} \left[1 - 4\frac{d_o}{R} \right] \le 192 \tag{5}$$

for load factor design.

Daniels et al. (1980) arrived at Eqs. (4) and (5) by observing that the radial deflections at the web-to-flange boundaries in curved I-girders tend to reduce the relative web transverse displacements and the corresponding plate bending stresses. The analyses by Culver et al. (1972a, b, 1973) did not consider these effects. The girders tested by Daniels and Herbein (1980) exceeded the Eq. (3) limits in all cases, but no fatigue crack developed along the web boundaries. The web

slenderness D/t_w ranged from 139 to 192 and the panel aspect ratio d_o/D ranged from to 2.03 to 2.36 in these girders. In the development of their design recommendations Daniels et al. (1980) stated, "To estimate the lateral deflections of the web boundaries would be mathematically highly involved, if not impossible. Thus, a rigorous reexamination of the web boundary bending stresses is not warranted for the sake of establishing web slenderness ratios. A relatively simple although empirical way to liberate the slenderness reduction factor is to reduce the (CURT) [i.e., the (Culver et al. 1972a, b and 1973)] adopted initial out-of-straightness." Daniels et al. (1980) developed Eqs. (4) and (5) simply by assuming an initial web out-of-flatness of one-half that assumed by Culver et al. (1972a, b, 1973). Equation (4) is adopted within the allowable stress design portion of the *AASHTO Guide Specifications for Horizontally Curved Highway Bridges* (AASHTO 1993). However, the load factor design portion of these specifications still retains Eq. (3).

More recently, Davidson et al. (1999a and b) developed a conservative multiplier that can be applied to the stress at the web-flange juncture of a curved I-girder (calculated by beam theory as $f = -My/I$) to obtain an estimate of the maximum von Mises stress in the web, located at the web-flange juncture, including geometric nonlinear plate bending effects. This multiplier takes the form

$$\psi_w = \left[1 + 1.5\sqrt{\frac{D_c}{R}}\right]\sqrt{1 + 0.161\frac{D_c}{t_w}\frac{D_c}{R} + 0.128\left(\frac{D_c}{t_w}\right)^2\left(\frac{D_c}{R}\right)^2} \qquad (6)$$

where D_c is the depth of the web in compression. The analyses leading to this multiplier were conducted on isolated curved web panels with the vertical bending moments applied as an idealized linear stress distribution through the depth of the cross-section at the ends of the panel.

Davidson et al. (1999b) also proposed a reduction factor on the web slenderness D/t_w that can be utilized as an alternative to the bracketed terms in Eqs. (3) through (5). They obtained this factor by taking the inverse square root of Eq. (6), i.e.,

$$R_s = \sqrt{\frac{1}{\psi_w}} \tag{7}$$

Although there is no theoretical basis for this equation, Davidson et al. showed that it fits closely with the reduction proposed by Daniels et al. (1980) and with a separate equation for the maximum D/t_w in curved I-girders proposed by Nakai et al. (1986) and reviewed in (Nakai and Yoo 1988). The D/t_w limit suggested by Nakai et al. (1986) was based on equating the plate bending stresses within curved and equivalent imperfect straight girder web panels, similar to the basis for the equations proposed by Culver et al. (1972a, b, 1973).

Davidson et al. (2000) extended the above research on behavior of curved webs subjected to uniform vertical bending to include the effects of combined bending and shear. The shear was induced by applying shear tractions along the four edges of isolated web panels and the bending stresses were applied as in Davidson et al. (1999a and b). They found that the addition of shear tends to give a small increase in the transverse "bulging" displacements within the panel and the maximum stress at the top of the web, along with a further reduction in the girder moment at first yield (with first yield calculated including the effect of plate bending stresses). However, since the increase in the maximum stress due to added shear was small, they found that Eq. (6) from (Davidson et al. 1999b) was still conservative.

The general trends observed by (Davidson et al. 1999a, b and 2000) were also observed by Mikami and Furunishi (1984), who also studied the nonlinear behavior of isolated cylindrical web panels subjected to uniform vertical bending and combined bending and shear edge trac-

tions. Unfortunately, Mikami and Furunishi showed only a limited number of solutions, and they did not provide any design recommendations. In summary, both Davidson et al. (1999b and 2000) and Mikami and Furunishi (1984) found that:

- The web membrane stresses associated with the overall bending of the girder tend to decrease as the horizontal curvature increases, and as a result, the bending moment carried by the web panel is reduced.
- A web panel subjected to combined bending and shear has smaller web membrane stresses due to vertical bending compared with the same panel under uniform vertical bending.
- The web plate bending stresses under combined bending and shear are larger than those under uniform vertical bending.

It is also unfortunate that Davidson et al. (1999b and 2000) applied Eq. (6) in calculating the maximum girder flexural strength, effectively basing the vertical bending strength of a curved I-girder on first yielding at the web-flange juncture (including the effect of estimated plate bending stresses but neglecting initial residual stresses). Their approach for estimating web plate bending stresses may be valuable for assessment of fatigue. However, in the view of the authors, there is no reason why an I-girder web needs to be limited to nominal first yield under maximum strength loading conditions. In general, it can be shown that the overall contribution of the web to both vertical and lateral bending is relatively small compared to that of the flanges of an I-girder. It should be possible to allow some yielding within a noncompact or slender curved web at maximum strength load levels without any significant detriment to the overall girder vertical and/or lateral bending capacity. This issue is addressed within the context of curved homogenous I-girders in the parametric studies by White et al. (2001). Also, an analogy can be drawn with the design of straight hybrid I-girders. In hybrid I-girder design, the web is allowed to yield

under the maximum design loading conditions, regardless of whether it is compact or not (Frost and Schilling 1964; Schilling 1968; ASCE 1968). The reduction in the flexural capacity due to web yielding and bend buckling is accounted for within the hybrid R_h and load-shedding R_b factors of the AASHTO (1998) Specifications. The capacity of a hybrid girder does not need to be limited to nominal first yielding of the web.

The *2002 Guide Specifications* (AASHTO 2002) do not adopt any of the above equations for the maximum permitted D/t_w. Rather, these specifications limit the nominal web stress due to overall vertical bending of the I-girder to the web bend buckling stress. Furthermore, they limit the web shear force to the elastic or inelastic shear buckling load. Hall et al. (1999) evaluated prior research pertaining to the fatigue of curved I-girder webs, and concluded that fatigue issues due to web plate bending could be avoided if the web stresses were maintained below these buckling strengths (Hall 2000). There is precedent for limiting the web to its elastic bend buckling and elastic/inelastic shear buckling strength to avoid fatigue issues in straight I-girder webs (Patterson et al. 1970, Galambos et al. 1977, Fisher et al. 1979, Montgomery 1987, Nowak et al. 1993, Okura et al. 1993, Duchene and Maquoi 1995, Remadi et al. 1995 and AASHTO 1998). However, the *2002 Guide Specifications* restrict the web to these buckling strengths under all loading combinations, whereas the LRFD Specifications (AASHTO 1998) apply this limit only under fatigue loading conditions.

The theoretical web elastic bend buckling stress is expressed in the *2002 Guide Specifications* as

$$f_{bw} \le \left[\frac{\pi^2 E k}{12(1-\nu^2)\left(\frac{D}{t_w}\right)^2} = \frac{0.9Ek}{\left(\frac{D}{t_w}\right)^2} \right] \le F_y \qquad (8)$$

where

$$k = 7.2\left(\frac{D}{D_c}\right)^2 \geq 7.2 \tag{9}$$

for unstiffened webs (i.e., $d_o/D > 1$) and

$$k = 9\left(\frac{D}{D_c}\right)^2 \geq 7.2 \tag{10}$$

for stiffened web panels. The multiplier 7.2 in the middle expression of Eq. (9) results in a bend buckling coefficient of 28.8 for doubly symmetric girders. This is close to the theoretical value of k = 24 for webs with $D_c = D/2$ and simply supported boundary conditions on their longitudinal edges. The multiplier 9 in Eq. (10) gives a k of 36 for a doubly symmetric girder, which is approximately $k_{ss} + 0.8\,(k_{sf} - k_{ss})$, where k_{ss} and k_{sf} are the bend buckling coefficients for simply supported and fully restrained longitudinal edge conditions respectively. Equation (9) is used implicitly in the current AASHTO LRFD Specifications for sections with $D_c > D/2$, to represent the bend buckling resistance within the load-shedding parameter R_b. Furthermore, Eq. (10) gives the bend buckling coefficient implicitly used within (AASHTO 1998) R_b equation for sections with $D_c \leq D/2$. Hall et al. (1999) explain that the smaller bend buckling coefficient is used for unstiffened webs in (AASHTO 2002) to account for potential moment-shear interaction effects. Also, they explain that the more liberal value is utilized for stiffened web panels since the reserve postbuckling strength of stiffened panels is ignored. The lower limit of 7.2 on the value of k in Eqs. (9) and (10) is approximately equal to the theoretical buckling coefficient for a web plate under uniform compression, assuming clamped boundary conditions at the flanges (SSRC 1998).

For $d_o/D \leq 1$, the limit on D/t_w based on Eq. (8), applied to all loading conditions, is typically more restrictive than that required by the Daniels et al. (1980) load factor design formula (Eq. (5)). However, for $d_o/D > 1$, the Daniels equation can be more restrictive than the Eq. (8) limit on D/t_w. The reader can verify these observations by assuming an upper bound of $f_{bw} = F_{yc}$ = 345 MPa (50 ksi) under the maximum strength loading conditions along with Eq. (8), solving for D/t_w, and comparing the result to Eq. (5). Based on the above assumed f_{bw} and $d_o/D \leq 1$, the limit on D/t_w from Eq. (8) (i.e., $D/t_w \leq 137$) is more restrictive when $d_o/R \leq 0.040$, which is typically the case for these small stiffener spacings. Conversely, for $d_o/D > 1$, the limit on D/t_w from Eq. (5) is more restrictive (and the web slenderness is limited to values smaller than $D/t_w = 122$), when $d_o/R > 0.063$. One should note that although Eq. (5) can be more restrictive than Eq. (8) for $d_o/D > 1$, Eqs. (1) and (2) still can be more critical than Eq. (5). Also, one should note that by restricting the web slenderness based on Eq. (8), the *2002 Guide Specifications* account for the effect of girder monosymmetry in limiting the web slenderness that can be used in design. The Daniels et al. (1980) and Culver et al. (1972a and b, 1973) equations do not address this issue.

The current LRFD Specifications (AASHTO 1998) limit the web in straight I-girders to the elastic bend and shear buckling strengths only under fatigue and under some construction loading conditions. With further research, it may be possible to liberalize the limits specified by the *2002 Guide Specifications* and by Daniels et al. (1980). For instance, it may be possible to avoid fatigue issues by restricting the web stresses to the buckling stress only under fatigue loading conditions, at least up to some curvature limit. However, combined shear and bending may need to be considered, e.g., by using a reduced value for the buckling coefficient as in Eq. (9), if fatigue issues are to be addressed based on a buckling limit under fatigue loading conditions only.

2.2 WEB REQUIREMENTS BASED ON STRENGTH

The issues associated with horizontally curved I-girder web panels and maximum strength include:

- The shedding of flexural stresses due to radial plate bending deformations of the curved web.
- The potential distortion of thin webs associated with flange raking; these distortions result in an increase in lateral flange bending and a reduction in the lateral-torsional stiffness and resistance.
- Shear buckling of curved web panels and the potential development of additional postbuckling strength (typically idealized as tension field action).
- Potential interactions between the load carrying mechanisms associated with the flexural and shear strengths. For instance, it is possible that the shear capacity of a curved I-girder could be reduced because of the loss of lateral restraint and/or tension field anchorage from a compression flange subjected to high vertical and/or lateral bending stresses or significant lateral bending deformations. Conversely, the vertical bending capacity of an I-girder might be reduced due to destabilization of the compression flange associated with the buckling and/or postbuckling response of the web in shear.
- Bending of transverse stiffeners due to the tendency of the curved web to deflect outward, for girders designed based on a web shear buckling limit, and due to potential additional demands associated the development of postbuckling strength, if tension field action is utilized in the calculation of the shear strength.

With respect to the first issue, Culver et al. (1972b) show in Table 1 of their paper that, for doubly symmetric I-girders, the reduction in the yield moment capacity M_y due to web plate bending is approximately the same as that predicted by a simplified form of Basler and Thurli-

mann's (1961) web load shedding parameter R_b specified in (Vincent 1969). More recently, White et al. (2001) performed a finite element parametric study of a wide range of doubly and monosymmetric curved I-girders with $2D_c/t_w$ values up to 208 and reviewed experimental tests with $2D_c/t_w$ up to 188. They proposed unified flexural strength equations which involve a simple extension of current LRFD (AASHTO 1998) straight I-girder strength formulae, and found that these equations adequately predict the maximum flexural capacities. These equations use the current LRFD load shedding parameter R_b (with F_{yc} used in the R_b equation instead of f_b, for simplicity of the design calculations).

Regarding the second issue, there is some evidence that transverse stiffeners can improve the bending resistance of curved I-girders (Mozer et al. 1970, 1971 and 1973; Nakai et al. 1984b). Nevertheless, to the knowledge of the authors, this beneficial effect is generally not included in any formulae for the nominal flexural strength of these types of members. White et al. (2001) considered this effect parametrically for girders with $D/t_w = 160$, and found that the increase in the flexural resistance with decreasing d_o/D (for $d_o/D = 1$, 2 and 3) is noticeable in some cases, but that it is generally small. However, they noted that the transverse stiffeners were not attached to the tension flange in their analyses, and that the effects of close stiffener spacing may be more significant for smaller D/t_w values.

Overall, in their finite element parametric studies, White et al. (2001) found that the vertical bending strength of I-girders is somewhat less sensitive to flange lateral bending than implied by a number of previously developed strength equations for curved I-girder bridge design. As a result, the vertical bending resistance is also less sensitive to design analysis estimates of flange lateral bending stresses – including estimates of the increases in flange lateral bending moments due to distortion of the web – than implied by some of the prior design resistance formulations.

It is believed this behavior is due in part to a requirement in the procedure suggested by White et al. (2001) that L_b must be less than or equal to L_r in members that are subjected to sustained lateral bending, where L_r is the unsupported length corresponding to the transition from inelastic to elastic lateral torsional buckling in the equivalent straight girder strength equations. This requirement corresponds approximately to the limit of $L/b_f \leq 25$ in (AASHTO 2002). The $L_b \leq L_r$ limit, combined with the fact that there is typically some end restraint at at least one end of a critical unsupported segment, tends to prevent large second-order amplification of lateral bending stresses and displacements until the girder is close to its strength limit.

White et al. (2001) proposed a base lateral-torsional buckling (LTB) strength equation that includes the destabilizing effect from flexural compression in the web (through the calculation of a radius of gyration r_t associated with the compression flange and one-third of the depth of the web in compression), and they did not include any contribution from the St. Venant torsional rigidity GJ in their calculation of the LTB strength (due to potential web distortion and corresponding raking of the flanges). Of the formulae considered in (White et al. 2001), the resulting flexural strength equations were shown to provide the best correlation with refined finite element analysis and experimental test strengths.

The third issue, the maximum shear strength of curved web panels, is the primary subject of this research. Lee and Yoo (1999b) recently considered the strength of curved web panels subjected to pure shear loading, via finite element analysis. Similar to Davidson (2000), they applied the web shear to isolated panels by placing shear tractions along the four panel edges. Based on their studies, Lee and Yoo concluded that shear strength models developed for straight I-girders, including postbuckling resistance, are also adequate for estimating the nominal strength of curved web panels when the curvature parameter

$$c = \frac{d_o^2}{8Rt_w} \tag{11}$$

is less than or equal to one[1]. This limit was the maximum value of c considered in their studies; also, Nakai (1981) concluded that c = 1 was a practical upper bound for curved bridge design. Furthermore, Lee and Yoo (1999b) found that the elastic shear buckling strength of curved girder web panels was typically much higher than that associated with traditional shear buckling equations based on equivalent flat plates with simply supported edge conditions. However, these strengths were only slightly greater than those calculated using an equation suggested for straight girder web panels by Lee et al. (1996). Lee et al. (1996) developed a simple set of formulae for calculation of the web shear buckling coefficient, accounting for realistic restraint conditions from the girder flanges. Bradford (1996) independently derived web shear buckling charts that predict essentially the same shear strengths as Lee's equations. Based on the above research, it is clear that the assumption of simply supported boundary conditions on all four edges is typically quite conservative in both flat and curved web panels, particularly for panels with d_0/D significantly greater than one.

Regarding the postbuckling strength under pure shear, Lee and Yoo (1999b) showed that curved girder web panels with $c \leq 1$ can support shear loadings well beyond the elastic buckling limit, similar to the levels supported by straight I-girder webs, despite the presence of out-of-plane bending from the inception of the loading.

White et al. (2001) studied parametrically the shear strength of complete curved I-girders with the same support and loading conditions as utilized in the experimental shear tests addressed in this report. The results of their parametric study indicate that:

1. The curvature parameter c given by Eq. (11) is a small-angle approximation of the maximum eccentricity of the curved web from a straight chord between the ends of the panel, divided by the web thickness.

- The current AASHTO LRFD shear strength equations provide a reasonably good characterization of the maximum shear strength for girders with D/t_w up to 160 and $L_b/R \leq 0.10$ (the limits of the design parameters considered in their study), even though the AASHTO LRFD shear strength model, which is based on Basler's (1961) research, is not very realistic in characterizing the physical shear limit state behavior.
- The accuracy of the AASHTO LRFD shear strength equations is improved by basing the web shear buckling coefficient on the equations developed by Lee et al. (1996). Although the strengths for slightly less than half of the 133 girders considered in their parametric study are overpredicted when the equations developed by Lee et al. (1996) are used for the shear buckling coefficient in the LRFD shear strength formulae, the coefficient of variation of the ratio between the predicted and the finite element based strengths is significantly reduced by the use of the more refined shear buckling coefficient.
- The shear buckling coefficient equations developed by Lee and Yoo (1996) provide an accurate characterization of shear buckling loads obtained via elastic linear buckling finite element analysis.
- The typical increases in the web elastic shear buckling strength and decreases in the ultimate shear capacity due to horizontal curvature are small compared to the effects of various other factors that lead to variability in nominal strength predictions relative to experimental tests and refined finite element solutions.
- Based solely on maximum strength considerations, the maximum limit on transverse stiffener spacing of $d_o/D = 3$ in the AASHTO LRFD straight girder Specifications is also sufficient for horizontally curved I-girders with $L_b/R \leq 0.10$ and $D/t_w \leq 160$.

Of the shear strength equations considered by White et al. (2001), the AASHTO LRFD (1998) equations with the shear buckling coefficient calculated per Lee et al. (1996) give the best estimates relative to refined finite element strength solutions. In the interest of maintaining levels of simplicity similar to those of the current AASHTO provisions, White et al. (2001) limited their study to formulae that do not require consideration of girder flange proportions and flexural stresses. Therefore, they focused on the current (AASHTO 1998) equations, the formulae proposed by Lee and Yoo (1998, 1999a and b), and the current AASHTO equations modified by the use of Lee's shear buckling coefficient. Chapter II of White et al. (2001) provides detailed discussions of the concepts associated with these different strength predictors, and discusses their individual qualities and limitations.

In subsequent research, White et al. (2002a) have studied various nominal strength predictors for more than 140 experimental shear tests of straight and curved I-girders. These researchers considered the three models investigated in White et al. (2001) as well as a number of additional shear strength models including: (1) one form of the Cardiff shear strength model (Davies and Griffith 1999, Porter et al. 1975, Evans et al. 1978 and Evans 1983) combined with the use of Lee's shear buckling coefficient, and (2) a modified form of a model proposed by Höglund (1971, 1995, 1996) and studied by Davies and Griffith (1999). White et al. (2002a) found that, similar to the predictions relative to refined finite element solutions in White et al. (2001), the correlation of the AASHTO shear strength equations with the experimental data is improved by the use of Lee's buckling coefficient. However, the improvement was found to be less significant than that determined in the above finite element study. In addition, the Cardiff equations combined with the use of Lee's shear buckling coefficient were found to provide the best overall correlation with the test data for girders with $d_o/D \leq 3$, and Höglund's (1971, 1995,

1996) equations were found to give the best prediction of the test strengths for unstiffened girders. Of the shear strength equations that do not require explicit calculation of a contribution from the girder flanges, the modified AASHTO equations exhibited the best correlation with the physical data, followed closely by the current AASHTO (1998) LRFD equations. Höglund's model arguably provides the best combination of simplicity and accuracy. The reader is referred to (White et al. 2002a) for a detailed assessment of these results. Chapter V of this report evaluates the predictions by each of the above models relative to the experimental results for the four curved I-girders tested in this research.

The fourth issue listed above, potential interaction between web shear strength and I-girder flexural capacity, was also addressed in the parametric studies by White et al. (2001). These authors found that curved I-girder capacities can be predicted adequately by a combination of the AASHTO (1998) or modified AASHTO shear strength equations discussed above with the flexural resistance equations proposed in their research, without the need for consideration of any interaction between these strengths (as long as the maximum panel moment is used in the flexure check). In fact, the flexural strength equations proposed in their research, which include the effect of lateral flange bending due to any source (i.e., horizontal curvature as well as applied loadings and torsion within curved and/or straight I-girder bridges), tend to give conservative predictions of the flexural capacity in cases involving high shear and *high moment*, when the strength is controlled by flexure. This is not surprising once it is understood that the combination of high moment gradient (equal to the web shear force) with smaller flange lateral bending moments (because of the rapid reduction in vertical bending moment as we move away from the maximum moment location, due to the high shear) tends to increase the flexural capacity in high-shear high-moment loading cases. In addition, the maximum moment occurs at a brace location

in the high-shear high-moment tests studied by White et al. (2001), as well as in typical cases of high-shear high-moment in bridge structures. Hash (2001), White and Aydemir (2002) and White et al. (2002b) have extended these conclusions to homogeneous and hybrid straight I-girders.

In the study conducted by White et al. (2001), the unsupported length and flange proportions in some of the girders subjected to high-shear low-moment loadings (i.e., loaded such that an inflection point occurs at the middle of the test segment) were such that significant lateral flange bending was evident at their maximum strength limit state. The strengths of these girders were adequately predicted by the combined flexural and shear strength equations proposed by White et al. (2001), without any requirement for consideration of moment-shear strength interaction. White et al. (2001) also found that for girders in which the calculated resistance was controlled by the suggested *shear* strength equations, the statistical distribution of the strength ratio for high bending moment (defined as the ratio of the predicted to the finite element based strength) was similar to the distribution for low bending moment. Furthermore, as noted above, in girders controlled by the proposed *flexural* strength equations, the strengths tended to be predicted more conservatively for high-moment high-shear than for uniform vertical bending cases, i.e., zero shear.

It should be noted that Nakai et al (1984a and b, 1985) reported significant moment-shear interaction in their tests of several horizontally curved I-girders subjected to high moment and high shear. However, the strengths of the girders tested by Nakai et al. are predicted quite adequately with the equations proposed by White et al. (2001). There was some reduction in the strength of the high-shear *low-moment* specimens tested by these researchers relative to straight I-girder based shear strength equations. However, as observed by Nakai et al. (1984a), this

reduction was small. Some further reduction in the strength occurred in one of their high-shear *high-moment* tests relative to strength estimates using just the base straight-girder equations in White et al. (2001) and neglecting horizontal curvature effects. However, the strength of this test is predicted well when the effect of the lateral flange bending is included within the vertical bending strength check per the recommendations by White et al. (2001). The results of these tests were included in the studies by White et al. (2002a), and also in a study of high-moment high-shear cases by White et al. (2002b).

The fifth issue listed above, failure of transverse stiffeners, was addressed originally by Culver et al. (1972c) and Mariani et al. (1973). These researchers studied curved web panels under pure shear analytically using the Donnell shell equation and the Galerkin method. They concluded that the required stiffener rigidity for a curved web is less than that for a straight web if the panel aspect ratio d_o/D is less than 0.78. However, for $0.78 \leq d_o/D \leq 1$, they found that the required stiffener rigidity increases with the curvature by the ratio

$$X = 1 + \frac{1}{1775}\left(\frac{d_o}{D} - 0.78\right)Z^4 \tag{12}$$

where Z is a curvature parameter defined as

$$Z = \frac{d_o^2}{Rt_w}\sqrt{1-\nu^2} = 8c\sqrt{1-\nu^2} \tag{13}$$

This study was limited to $0 \leq Z \leq 10$. Its design recommendations were limited to $d_o/D \leq 1$, although panel aspect ratios up to $d_o/D = 1.5$ were considered. The limit of $d_o/D \leq 1$ appears to be related to: (a) the fact that the AASHTO Standard Specifications in effect at the time of the research limited the panel aspect ratios of transversely stiffened straight I-girders to this value and (b) their research indicated that a function different than Eq. (12) would be needed for d_o/D

= 1.5. Mariani et al. (1973) found that for a girder with $d_o/D = 1.5$, a maximum rigidity of 2.4 times that required for the corresponding straight-girder web was necessary, and that this requirement occurred at Z = 5. However, the required rigidity for this panel aspect ratio reduced to the same limit as for transverse stiffeners in straight I-girder webs as Z approached 0 or 10. Equation (12) gives a maximum required value of X = 2.24 for $d_o/D = 1$ and Z = 10. As a result, the maximum rigidity requirement determined by Mariani et al. (1973) for panels with $d_o/D = 1.5$ is not significantly larger than the maximum for $d_o/D = 1$.

The above research only addressed the development of web buckling strength; web postbuckling behavior and its influence on the transverse stiffeners was not considered. Equations (12) and (13) are adopted within the *2002 Guide Specifications*, which as noted previously do not allow consideration of the web postbuckling actions.

Nakai et al. (1984c and 1985b) studied the demands placed on transverse stiffeners in curved I girders for development of postbuckling strength in the context of tension field theory. These researchers developed an analytical beam-column model to estimate the strength of transverse stiffeners in curved I-girders, including the influence of web tension-field action. They compared their analytical predictions to the results from experiments conducted by Nakai et al. (1984a), in which premature buckling of a transverse stiffener occurred in one of the tests. Based on the above research, these authors recommended that the relative rigidity parameter X must be the following:

For stiffeners attached to one side of the web plate:

$$X = \begin{cases} 1.0 + (\alpha - 0.69)Z[9.38\alpha - 7.67 - (1.49\alpha - 1.78)Z] & \text{for } 0.69 \le \alpha \le 1.0 \\ 1.0 & \text{for } \alpha < 0.69 \end{cases} \qquad (14)$$

and for stiffeners attached to both sides of the web:

$$X = \begin{cases} 1.0 + (\alpha - 0.65)Z[12.67\alpha - 10.42 - (1.99\alpha - 2.49)Z] & \text{for } 0.65 \le \alpha \le 1.0 \\ 1.0 & \text{for } \alpha < 0.65 \end{cases} \quad (15)$$

where $\alpha = d_o/D$.

Nakai et al. (1984c and 1985b) considered maximum values of $Z = 10$ and $\alpha = 1.0$ in their studies. Nakai and Yoo (1988) stated that in deriving the above limits, the panel aspect ratio d_o/D was limited to a value less than or equal to one because the required rigidity of the transverse stiffeners was otherwise too large for use in design practice. Also, they stated that the same conclusion was reached by Mariani et al. (1973). The Mariani et al. paper does not contain any evidence of this conclusion. For $Z = 10$ and $\alpha = 1.0$, Eq. (14) gives a required value for X of 15.3. Although this is a significant requirement beyond that for transverse stiffeners in a straight I-girders, it can often be met with reasonable stiffener proportions. The authors are not aware of any studies to date that investigate the transverse stiffener requirements for curved web panels with $d_o/D > 1$.

Recent research by Lee et al. (2002) indicated that transverse stiffeners do not need to be designed for compressive forces from a theoretical tension field in order for straight I-girder web panels to develop their nominal calculated postbuckling strengths. These conclusions would seem to invalidate one of the premises on which the equations for the stiffener requirements developed by Nakai et al. (1984c and 1985b) are based. In either case, Nakai's equations were proposed only for $d_o/D \le 1$. The present equations for stiffener requirements in the AASHTO *2002 Guide Specifications* are targeted only at development of the shear buckling strengths for $d_o/D \le 1$.

White et al. (2001) included the influence of stiffener size indirectly in their finite element parametric studies. These investigators utilized transverse stiffeners sized based on the

AASHTO LRFD (1998) straight I-girder stiffener requirements and with a stiffener width equal to $0.3b_f$ as the initial design in all of their parametric tests. They found that these stiffener sizes were adequate in all of their parametric study girders with $L_b/R = 0.05$ and 0.075. These studies included cases with $d_o/D = 2$ and 3. However, in some of their parametric study girders with $L_b/R = 0.10$, the stiffener sizes had to be increased beyond the straight I-girder minimum requirements to avoid a failure mode involving significant bending of the transverse stiffeners. Unfortunately, this research did not provide any definitive guidelines on minimum requirements for transverse stiffeners within curved I-girder webs.

CHAPTER III - TEST SPECIMENS, APPARATUS AND PROCEDURE

Four curved I girder test components, labeled hereafter as S1, S1-S, S2 and S2-S, were fabricated from AASHTO M270 Grade 345 steel. Each of the test girders had a total arc length of 11,580 mm (38 ft) and a doubly symmetric cross section with nominally 544.5 x 22.2 mm (21-7/16 x 7/8 in) flange plates curve cut and 1219 x 8 mm (48 x 5/16 in) web plates heat curved. The resulting web slenderness D/t_w was 154, the flange slenderness $b_f/2t_f$ was 12.25 and the ratio of the web-to-flange area A_w/A_f was 0.80 based on these nominal dimensions. The value of $D/t_w = 154$ was selected to be slightly smaller than the maximum value permitted for Grade 345 transversely stiffened I-girders in the AASHTO LRFD (1998) straight girder specifications. The radii R were 63,630 mm (208.75 ft) for S1 and S1-S and 36,580 mm (120 ft) for S2 and S2-S. All the girders had four 229 x 25.4 mm (9 x 1 in) bearing stiffeners placed in pairs at 305 mm (1 ft) from their ends and at 3,660 mm (12 ft) intervals along their length. The girders were braced radially at each of the bearing stiffener locations such that the unsupported lengths along the girder arc were all $L_b = 3658$ mm (12 ft) and the ratio L_b/b_f was 6.7. The geometry and longitudinal dimensions of these test girders are illustrated in Figs. 1 and 2.

The objectives of each of these tests were as follows:

Girder S1: This test was targeted to examine the shear strength of a curved web panel having an aspect ratio $d_o/D = 3$, a ratio of the web panel length to the radius of curvature of $d_o/R = 0.0575$, and a subtended angle between the cross frame locations of $L_b/R = 0.0575$. The angle $L_b/R = 0.0575$ is slightly greater than one-half of the maximum value 0.10 permitted by the *2002*

AASHTO Guide Specifications. The web of this girder contained only the four bearing stiffeners described above without any intermediate transverse stiffeners between.

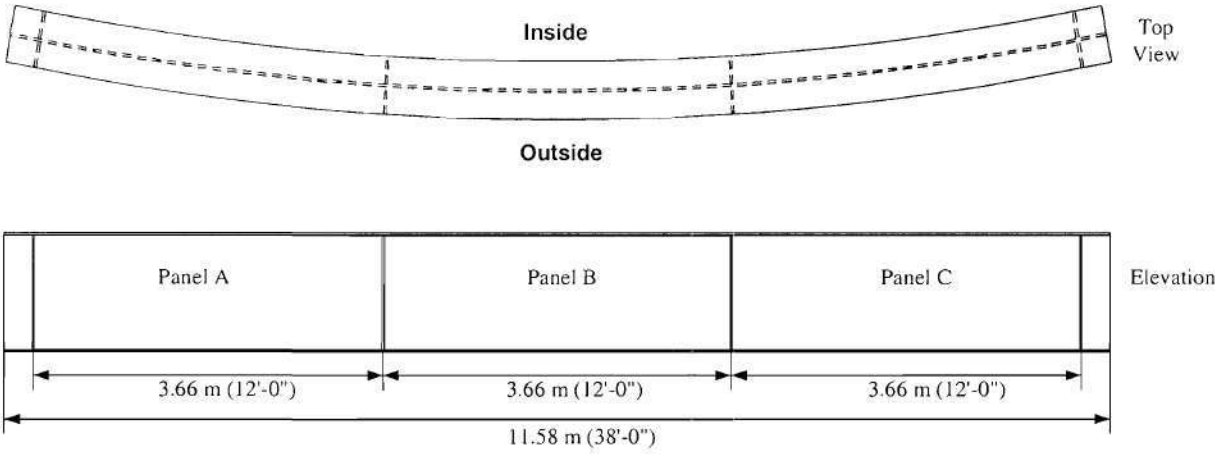

Figure 1 Geometry and longitudinal dimensions of test girders S1 and S2

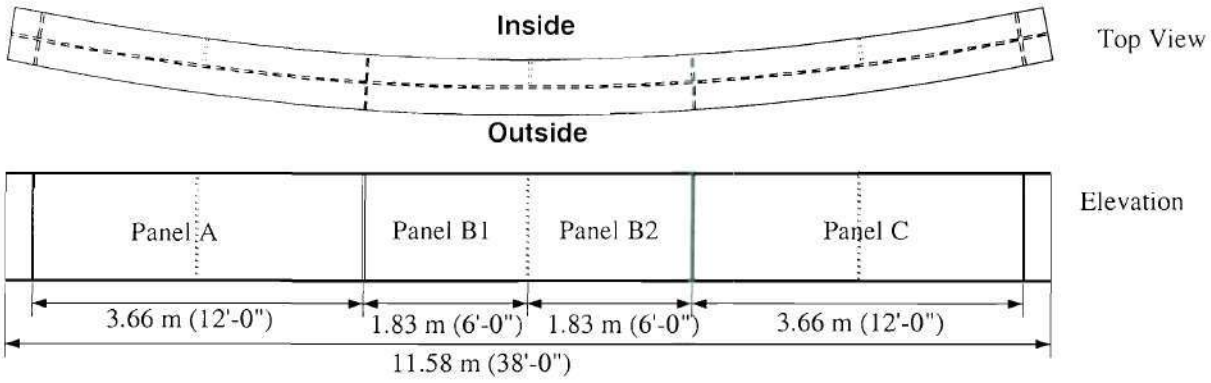

Figure 2 Geometry and longitudinal dimensions of test girders S1-S and S2-S

Girder S1-S: This girder was identical in length and curvature to S1, but had an additional 165 x 16 mm (6-1/2 x 5/8 in) intermediate transverse stiffener located at the center of each panel between the bearing stiffeners. The intermediate transverse stiffeners were cut back 25.4 mm

(1 in) from one of the flanges, and were placed on the side of the web closest to the center of curvature only. The resulting web panel aspect ratio was 1.5, and the value of d_o/R was 0.0287. Although the above transverse stiffeners had reasonable proportions relative to the girder geometry, their moment of inertia about the edge in contact with the web plate was 52 times that required by the (AASHTO 1998) straight-girder specifications. The above transverse stiffener size was selected conservatively to ensure that the shear strength would not be limited by a failure of the stiffener; the stiffener requirements discussed in Chapter II apply only for $d_o/D \leq 1$.

Girder S2: This component was similar to S1 in that it only had bearing stiffeners at 3658 mm (12 ft) intervals along its length and a resulting panel aspect ratio of $d_o/D = 3$. However, it differed from S1 in that it had a radius of 36,580 mm (120 ft), thus representing a case in which $L_b/R = 0.10$, the maximum subtended angle between the cross frame locations allowed by the *2002 AASHTO Guide Specifications*. The corresponding d_o/R for this girder was 0.10.

Girder S2-S: This girder was identical to S1-S, but with a radius of 36,580 mm (120 ft). Therefore, its normalized dimensional parameters were $d_o/D = 1.5$, $d_o/R = 0.050$ and $L_b/R = 0.10$.

Table 1 presents a matrix of nondimensional parameters associated with the four tests, including the parameters c and Z given by Eqs. (11) and (13), calculated using the nominal girder dimensions. It can be observed that the value of c for all but one of these designs is significantly greater than one. This is due to the large panel aspect ratios d_o/D and web slenderness D/t_w relative to current practice, as reflected in the *2002 Guide Specifications* and in Nakai (1981).

Table 1 Summary of test girder nondimensional parameters

Girder	L_b/R	d_o/D	d_o/R	$c = d_o^2/8Rt_w$	$Z = d_o^2\sqrt{1-\upsilon^2}/Rt_w$
S1	0.0575	3	0.0575	3.31	25.3
S1-S	0.0575	1.5	0.0287	0.83	6.3
S2	0.10	3	0.1000	5.76	44.0
S2-S	0.10	1.5	0.0500	1.44	11.0

3.1 MEASURED DIMENSIONS

The top and bottom flange widths and thicknesses of the test girders were measured at seven locations along their lengths using a precision caliper. These measurements were taken adjacent to each of the four bearing stiffeners, and close to the middle of each of the three lengths between these stiffeners. The flange thicknesses were determined at the flange tips on each side of the web at each of these locations, giving a total of 14 thickness values for each flange. The web thicknesses were measured with an ultrasonic time-of-flight device at the same seven locations as above, and at approximately 1/3 and 2/3 of the web height, giving a total of 14 web thickness values for each girder. The web thickness measurements from the ultrasonic device were checked versus direct measurements using a precision caliper at three edge locations through the web depth at both ends of the girders. The ratio of the average web thickness measured by the ultrasonic device and by the caliper for these 24 locations was 1.007. The web depths were measured with a tape at the ends of the girders and at each of the interior bearing stiffener locations. At the interior bearing stiffener locations, the total girder depth (including the flange thick-

nesses) was measured at the flange tips on each side of the web. The total depth at the centerline of the flanges was then estimated by taking the average of these two measurements. At the girder ends, the total depth was measured directly at the centerline of the flanges. The depth of the web plate D was then calculated by subtracting the average flange thicknesses measured at each of the above locations from the corresponding total depths.

The data from the above cross-section measurements are summarized in Table 2. The flange widths b_f at the girder ends were consistently about 1.5 mm (0.06 in) smaller in Girders S1 and S1-S and about 5 mm (0.20 in) smaller in Girders S2 and S2-S than the average of the flange widths measured at the other locations. Therefore, the end measurements for the flange widths are not included within the statistics reported in the table.

Table 3 presents several measured and nominal computed distances from a straight chord taken from the inside flange tip at the bearing stiffener at one end of the girders to the same flange tip at the opposite end. The distances from this chord to the inside flange tips at the interior bearing stiffeners, taken perpendicular to the chord, are denoted by the symbols d_{2L} and d_{2R} in the table. In addition, the distance from this chord to the inside flange tip at the mid-length of the girders, denoted by the symbol d_{mid}, is presented. These distances were measured by pulling a wire taut between the flange tips at the end bearing stiffeners, then using a scale to determine the distance from this wire to the above locations to the nearest mm. The girders were resting on a flat surface when these measurements were taken. The nominal distances were computed by assuming the specified nominal radii of 63,630 mm (208.75 ft) for girders S1 and S1-S and 36,580 mm (120 ft) for girders S2 and S2-S, and back-calculating the corresponding radius to the inside flange tips at the stiffener and mid-length locations based on the actual measured flange widths at these locations. Therefore, the nominal computed distances were effectively deter-

mined by assuming the specified nominal radii to the centerline of the flange widths. One can observe that in girders S1 and S1-S, most of the nominal and measured distances did not differ by more than 2 mm (0.08 in). The maximum deviation between the nominal and measured

Table 2 Measured cross-section dimensions

Girder		D (mm)	t_w (mm)	Top Flange		Bottom Flange	
				b_f (mm)	t_f (mm)	b_f (mm)	t_f (mm)
S1	Average	1217	8.53	546.6	22.99	546.4	23.04
	COV (%)	0.08	0.78	0.15	0.22	0.09	0.25
	Maximum	1218	8.64	547.9	23.06	546.9	23.14
	Median	1217	8.53	546.4	23.01	546.4	23.01
	Minimum	1216	8.46	545.6	22.89	545.6	22.94
	N	4	14	5	14	5	14
S1-S	Average	1218	8.46	546.4	22.91	546.9	22.96
	COV (%)	0.04	1.02	0.05	0.25	0.11	0.50
	Maximum	1218	8.61	546.6	22.99	547.9	23.16
	Median	1218	8.43	546.1	22.94	546.9	22.94
	Minimum	1217	8.31	546.1	22.81	546.4	22.76
	N	4	14	5	14	5	14
S2	Average	1217	8.31	557.3	22.83	556.8	22.76
	COV (%)	0.08	0.60	0.16	0.33	0.26	0.24
	Maximum	1218	8.38	558.3	22.99	558.5	22.83
	Median	1217	8.31	557.0	22.83	556.8	22.76
	Minimum	1216	8.23	556.5	22.73	554.5	22.63
	N	4	14	5	14	5	14
S2-S	Average	1217	8.23	556.3	22.81	556.5	22.81
	COV (%)	0.05	0.51	0.24	0.21	0.21	0.29
	Maximum	1218	8.31	557.5	22.94	558.0	22.91
	Median	1217	8.23	556.8	22.83	556.5	22.83
	Minimum	1217	8.18	554.7	22.68	555.0	22.68
	N	4	14	5	14	5	14

distances was 5 mm (0.2 in) or 2.4 percent in these girders. The deviations were slightly larger in girders S2 and S2-S, with a maximum of 13 mm (0.51 in) or 3.3 percent.

Table 4 presents the measured radial distances from the inside and outside faces of the web to the corresponding flange tips. These distances were also measured with a scale to the nearest mm. One can observe that the maximum deviation of the web from the centerline of the flanges was approximately 5/2 = 2.5 mm (0.1 in), corresponding to the bottom flange at the mid-length in girder S1 and 6/2 = 3 mm to the top flange at the mid-length in girder S1-S.

Table 3 Measured and nominal computed distances from a straight chord between the inside flange tips at the end bearing stiffeners to the corresponding flange tips at the interior bearing stiffeners and at the mid-length of the girders (distances taken perpendicular to the chord)

Position	d_{2L} [1]		d_{mid} [1]		d_{2R} [1]	
	Nominal (mm)	Measured (mm)	Nominal (mm)	Measured (mm)	Nominal (mm)	Measured (mm)
S1 top flange	209	210	234	235	208	207
S1 bottom flange	208	206	234	232	208	206
S1-S top flange	208	208	234	233	209	213
S1-S bottom flange	208	211	234	238	208	213
S2 top flange	360	354	404	396	359	354
S2 bottom flange	359	353	404	398	359	354
S2-S top flange	359	354	404	400	359	356
S2-S bottom flange	360	352	404	391	360	352

[1] d_{2L} and d_{2R} are the distances from a straight chord between the inside flange tips at the end bearing stiffeners to the inside flange tips at the interior bearing stiffeners, measured perpendicular to the chord; d_{mid} is the distance to the inside flange tip at the mid-length.

Table 4 Measured radial distances from the face of the web to the corresponding flange tips at the interior bearing stiffeners and at the mid-length of the girders

Location	b_{2L} [1] top (mm)	b_{mid} [1] top (mm)	b_{2R} [1] top (mm)	b_{2L} [1] bottom (mm)	b_{mid} [1] bottom (mm)	b_{2R} [1] bottom (mm)
S1 Outside	268	268	266	270	265	269
S1 Inside	268	271	272	269	270	270
S1-S Outside	269	265	268	269	269	269
S1-S Inside	268	271	270	270	269	270
S2 Outside	275	273	274	274	274	274
S2 Inside	272	272	271	274	275	275
S2-S Outside	274	274	273	274	274	273
S2-S Inside	274	272	272	275	276	275

[1] b_{2L} and b_{2R} are the radial distances from the face of the web to the corresponding flange tips at the interior bearing stiffeners; b_{mid} is the corresponding distance at the mid-length.

Lastly, Table 5 shows the values for the maximum out-of-flatness of the web relative to a straight chord between the top and bottom of web panels. These imperfections were estimated by placing a straight edge between the top and bottom of the web in a vertical position at various locations along the length, and measuring the gap between the straight edge and the web panel with a scale to the nearest mm. The largest imperfections were located between the interior bearing stiffeners in each of the girders, and were all oriented toward the inside direction, i.e., toward the center of curvature. The ratio of these out-of-flatness values to the web thickness, and to the maximum value permitted by the AWS Structural Welding Code (AWS 2000) in interior girders with one-sided stiffeners, (equal to d/67 where d is the least panel dimension), are also shown in the table. One should note that this web out-of-flatness imperfection is the same order of magnitude as the out-of-flatness associated with the horizontal curvature in girders S1-S and S2-S, and

it is one order of magnitude smaller than the out-of-flatness due to the horizontal curvature in girders S1 and S2.

Table 5 Maximum initial web out-of-flatness

Girder	Out-of-flatness δ_0 (mm)	$\frac{\delta_0}{t_w}$	$\frac{\delta_0}{(d/67)}$
S1	3	0.352	0.165
S1-S	3	0.339	0.158
S2	5	0.602	0.275
S2-S	8	0.972	0.440

In girder S1-S, the girder out-of-flatness was also measured between the interior bearing stiffeners with a dial gage instrument. This instrument was constructed by attaching dial gages to a straight bar at 38.1 mm (1.5 in) above the top surface of the bottom flange, at 1/4, 1/2 and 3/4 of the depth of the web, and at 38.1 mm (1.5 in) below the bottom surface of the top flange. The bar was placed against the outside tips of the flanges at 11 locations between the interior bearing stiffeners, starting at 304.8 mm (1 ft) from the left-side bearing stiffener and continuing at increments of 304.8 mm (1 ft) along the length. Readings were taken to the outside surface of the web plate at each of these positions from each of the dial gages. Figure 3 shows a contour plot of the corresponding web imperfections measured relative to a straight chord between the web surface at the top and bottom dial gage locations at 0.97 and 0.03D. This figure shows that: (1) the web imperfections in girder S1-S were oriented toward the inside direction with the exception of some small imperfections in the vicinity of the middle transverse stiffener, (2) the imperfections increased in magnitude from small values at the top and bottom edges of the stiffened panels B1 and B2 to a maximum at approximately the mid-depth of these panels, and (3) the imperfections were largest in the right-side panel, with the maximum out-of-flatness occur-

ring at approximately 50.8 mm (2 ft) from the right-hand end (at position 10). The maximum out-of-flatness in Fig. 3 is 2.87 mm (0.113 in).

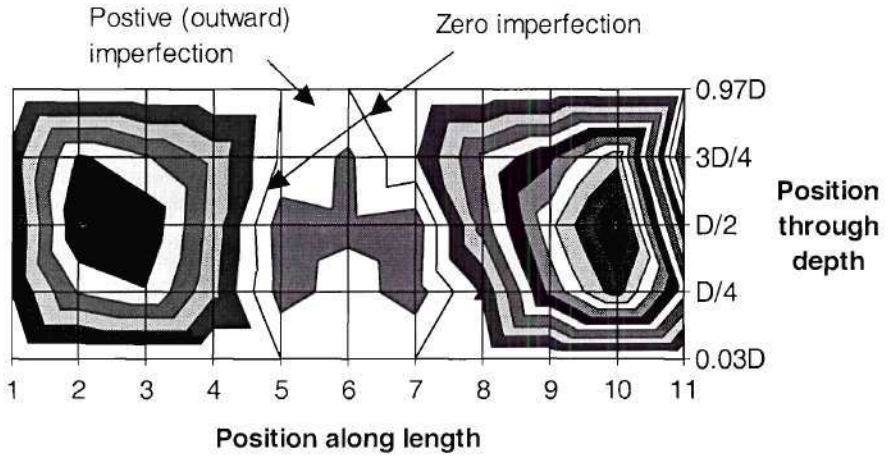

Figure 3 Contour of web imperfections relative to a straight chord between the top and bottom dial gage locations at 0.97 and 0.03D in girder S1-S

3.2 MATERIAL PROPERTIES

The material properties of the steel used for fabricating the components were determined from tensile coupon tests conducted in accordance with ASTM E8-00b (ASTM 2000). The four flanges for S1 and S1-S were cut-curved from one 2,896 x 13,260 mm (114 in x 43.5 ft) plate, and the four flanges for S2 and S2-S were cut-curved from another similar plate. Three 305 x 610 mm (12 x 24 in) coupon samples were cut from each of these plates, one at each end at the centerline radius of the four flange cut outs, and one at the mid-length of the ordered plate on the side toward the center of curvature of the flange cutouts. The long direction of the coupons was oriented tangent to the arc of the flange plates at the ends, and in the long direction of the plate, i.e., in the primary mill rolling direction, at the mid-length. The webs of S1 and S1-S were cut from a 1,830 x 24,540 mm (72 in x 80.5 ft) plate, and the webs of S2 and S2-S were taken from

another similar plate. Six 305 x 610 mm (12 x 24 in) web coupons were cut from each of these plates, two at each end and two on one side of the plate at the center of the overall length. At each of these locations, one of the coupons had its long direction aligned with the long direction of the ordered plate, which was the primary mill rolling direction, and one was cut with its long direction at 90^{o} to this orientation.

Three plate-type rectangular tension specimens were prepared from each of the above coupons per ASTM E8-00b (ASTM 2000). The specimens were 38.1 mm (1.5 in) wide and had a 203 mm (8 in) gage length. From these specimens, a total of 12 and 8 tests were conducted for the web and flange plates of girders S1 and S1-S, respectively, and a total of 18 and 9 tests were conducted for the web and flange plates of girders S2 and S2-S, respectively. The tension specimens were loaded under displacement control at a rate of about 0.02 mm/s up to a strain level slightly higher than that at the onset of strain hardening. The rate was then increased to approximately 0.09 mm/s throughout the remainder of the tests. The upper and lower yield strengths were determined by the autographic diagram method defined in ASTM E8-00b. In the majority of the tests, the SSRC Technical Memorandum No. 7 procedure (SSRC 1998) was utilized to determine static yield strengths. In this procedure, the test was interrupted by stopping the cross head motion when the strain reached a value corresponding to approximately 0.2 percent offset. This condition was maintained until the load stabilized, and the lowest value of the load and the corresponding strain was recorded. Straining was then resumed at the specified rate. The tests were interrupted and static load values were recorded at approximately 0.005 increments of strain until strain hardening began.

Table 6 summarizes the key coupon stress-strain data: the modulus of elasticity E, static yield F_y, strain hardening modulus E_{st} and strain at the onset of strain hardening e_{st}, the ultimate

tensile strength F_u as defined in ASTM E8-00b, and the strain at ultimate e_u. No effects of coupon orientation or of small differences in loading rates among the different tests could be discerned statistically from the data. Figure 4 shows typical stress-strain curves for the flange and web plates of girders S2 and S2-S. The static yield strength was not measured in the coupon tests corresponding to the stress-strain curves shown in this figure.

The procedure for calculation of the strain hardening strain and strain hardening modulus is discussed in Appendix I. These parameters do not appear to be of any primary significance in the girder shear tests conducted in this research since the measured strains were typically smaller than the strain-hardening strain. Young's Modulus (E) was calculated by a linear regression analysis of the data between a pre-load, selected high enough such that errors at small load could be neglected, and the upper yield strength. It is well known that E is sensitive to numerous attributes of the test procedures (ASTM 1997; Adams et al. 1964; Galambos and Ravindra 1978). The average E for all of the tension specimens reported in Table 6 is 203 GPa (29,440 ksi) with a coefficient of variation of 2.6 percent. This coefficient of variation is somewhat higher than that reported for each of the separate flange and web plates in the table. Galambos and Ravindra (1978) report average test values for E from various investigations ranging from 202 to 215 GPa (29,360 to 31,200 ksi). It is likely that the differences in elastic moduli for the different plate tests shown in Table 6 are due to measurement error, and therefore one value should be selected for Young's modulus to represent all of the tests. The average value determined from the full set of the tension coupon tests is certainly reasonable, and thus this value is selected for further analysis of the girder test data in this research.

Table 6 Stress-strain data from tension coupon tests

Girders	Coupon Location	N		E (GPa)	Avg. Static F_y (MPa)	E_{st} (GPa)	e_{st} (%)	F_u (MPa)	e_u (%)
S1 and S1-S R = 63,630 mm (208.75 ft)	Web	12	Average	208	410	3.44	1.95	567	14.6
			COV (%)	1.4	3.3	5.9	8.9	1.4	11.1
			Maximum	213	423	3.78	2.13	575	16.0
			Median	209	416	3.43	1.99	569	15.2
			Minimum	203	384	3.07	1.57	548	11.1
	Flanges	8	Average	196	377	3.59	1.59	542	15.6
			COV (%)	1.5	1.4	6.4	17.0	0.4	2.3
			Maximum	200	385	3.97	1.91	545	16.1
			Median	197	376	3.52	1.47	542	15.7
			Minimum	190	372	3.34	1.30	538	15.1
S2 and S2-S R = 36,580 mm (120 ft)	Web	18[1]	Average	202	411	3.36	1.87	564	15.6
			COV (%)	2.3	1.7	7.3	13.7	0.8	4.0
			Maximum	209	419	3.84	2.23	569	16.9
			Median	202	412	3.26	1.82	564	15.6
			Minimum	192	402	3.15	1.60	554	14.6
	Flanges	9[2]	Average	205	397	3.61	1.90	562	15.4
			COV (%)	1.4	0.7	2.9	5.8	0.3	3.8
			Maximum	208	400	3.72	2.00	564	16.3
			Median	206	396	3.63	1.93	562	15.5
			Minimum	200	394	3.47	1.74	559	14.2

[1]Static F_y was measured in six of the 18 tests.

[2]Static F_y was measured in three of the nine tests.

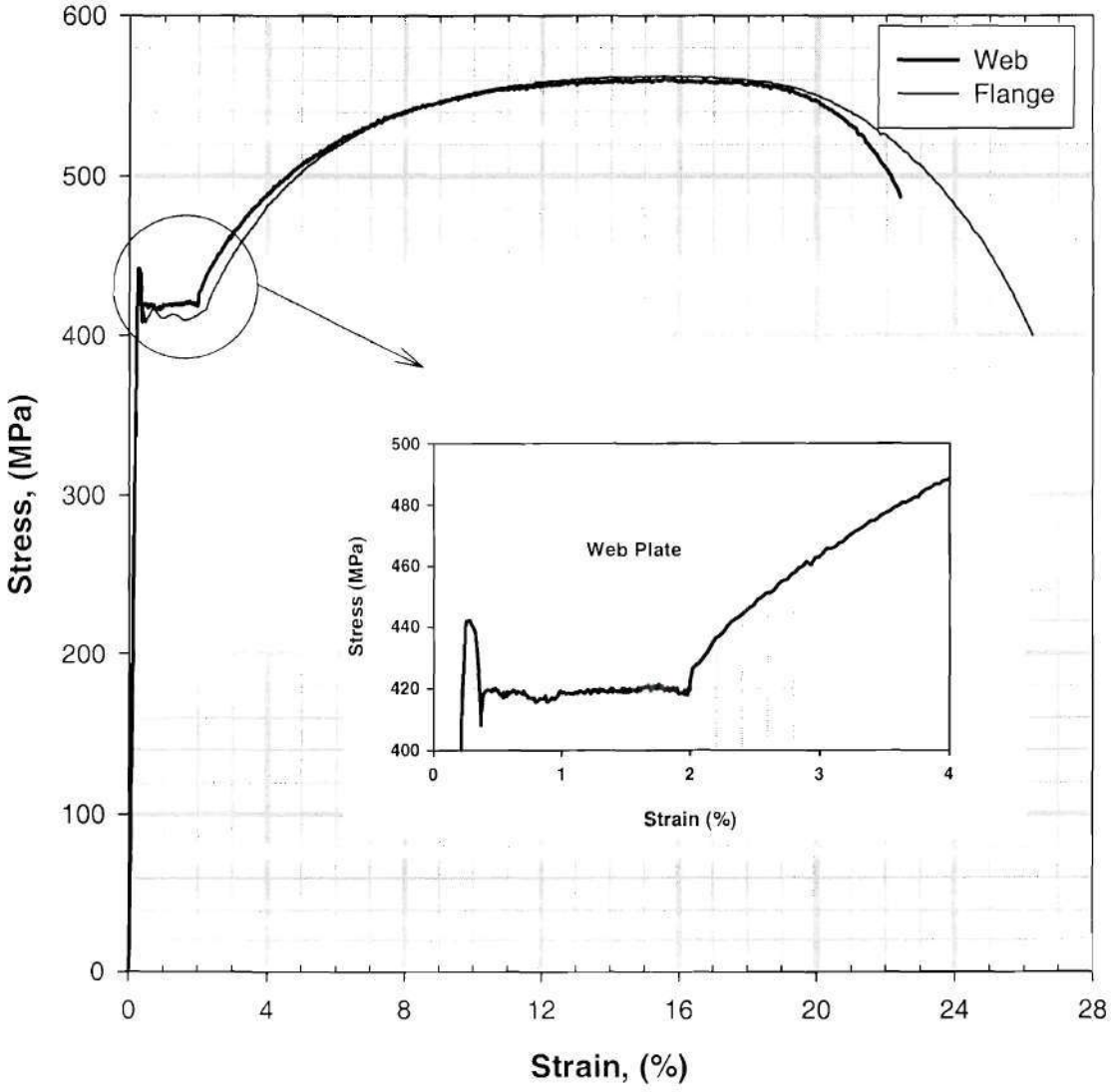

Figure 4 Representative stress-strain curves for flange and web plates – girders S2 and S2-S

3.3 TEST SETUP AND INSTRUMENTATION

All the girder tests were conducted in a steel reaction frame in which W920x446 (W36x300) 2,285 mm (7.5 ft) long beams were connected on one side to (20 ft) high W360x216 (W14x145) columns and on the other side to a 610 mm (2 ft) thick reinforced concrete reaction wall with 3,658 mm (12 ft) buttresses 3,658 mm (12 ft) on center. Figure 5 shows a schematic of the test setup and Fig. 6 shows a photograph taken from the right side of location 1R (defined in Fig. 5). The setup consisted of placing the girder on two steel pedestals located at a distance of 7,315 mm (24 ft) from center to center. The exterior end support was constructed by bolting a 890 kN (200-kip) load cell to the steel pedestal and attaching to the load cell button a 25.4-mm (1-inch) thick steel plate on which a 50.8-mm (2-inch) diameter round steel bar was welded. The round steel bar was aligned in the direction of the end bearing stiffeners as shown in Fig. 7. At the interior support, shown in Fig. 8, a 3,114-kN (700-kip) load cell having a 120.6-mm (4.75-inch) diameter flat load button was bolted to the interior pedestal and placed directly under the bearing stiffeners, with the center of the load button coinciding with the center of the web-flange juncture. A 12.7 x 203.2 x 406.4 mm (1/2 x 8 x 16 in) bearing plate was placed between the load button and the girder, with the 203.2 mm (8 in) dimension oriented along the girder length.

The test girders were braced radially at 3,658-mm (12-ft) intervals by means of two 101-mm (4-inch) diameter steel tubes connected to the bearing stiffeners at locations near the top and bottom flanges, as shown in Fig. 9. A detail of the top bracing member attachment is shown in Fig. 10. Double gusset plates were used at the ends of the tube bracing members, and their end attachments were accomplished through a pin that passed through a spherical bearing placed within the bearing stiffener on the girder and within a T-plate attached to the concrete reaction wall. Therefore, the bracing members restrained the girders essentially only along their

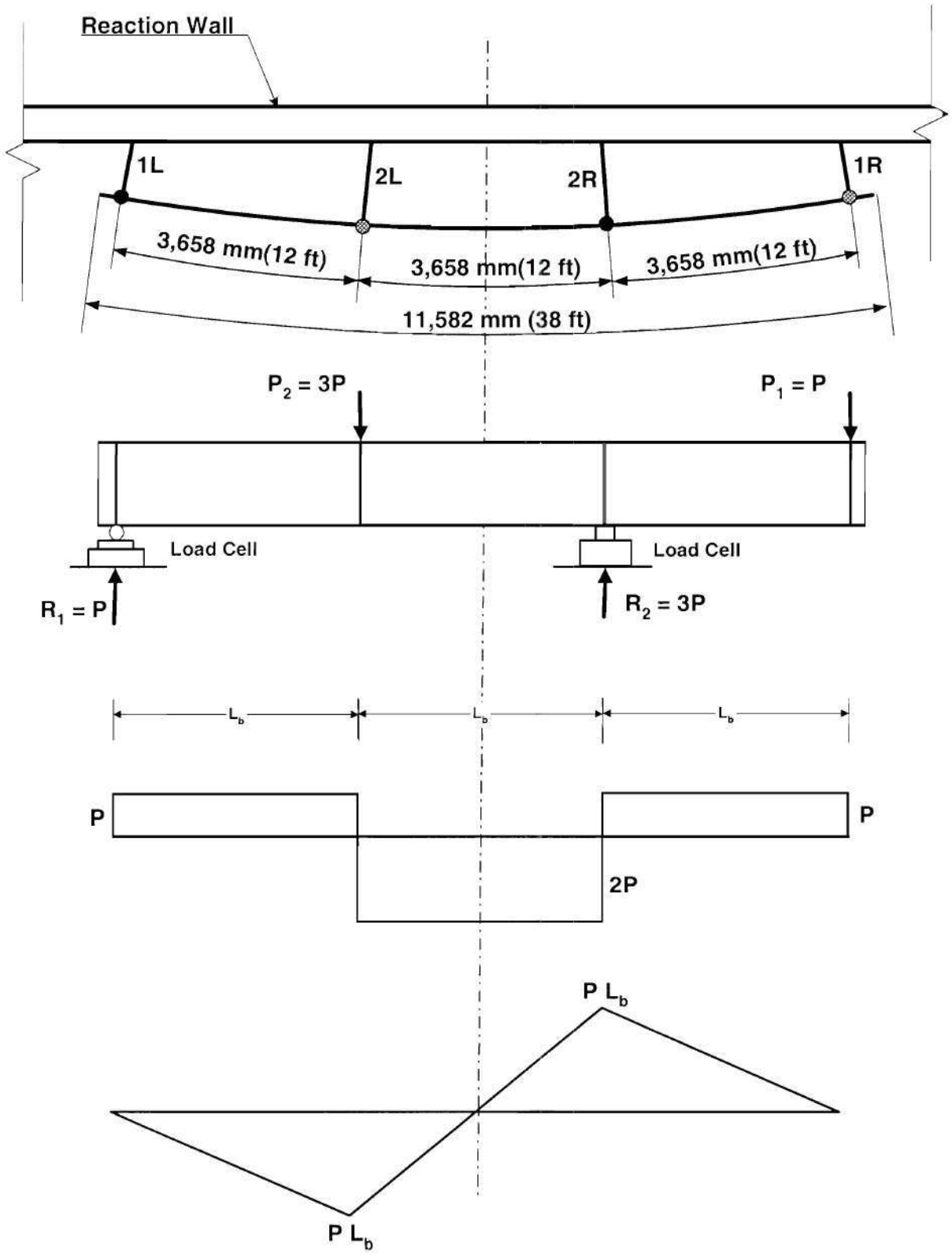

Figure 5 Test setup and shear and approximate moment diagrams

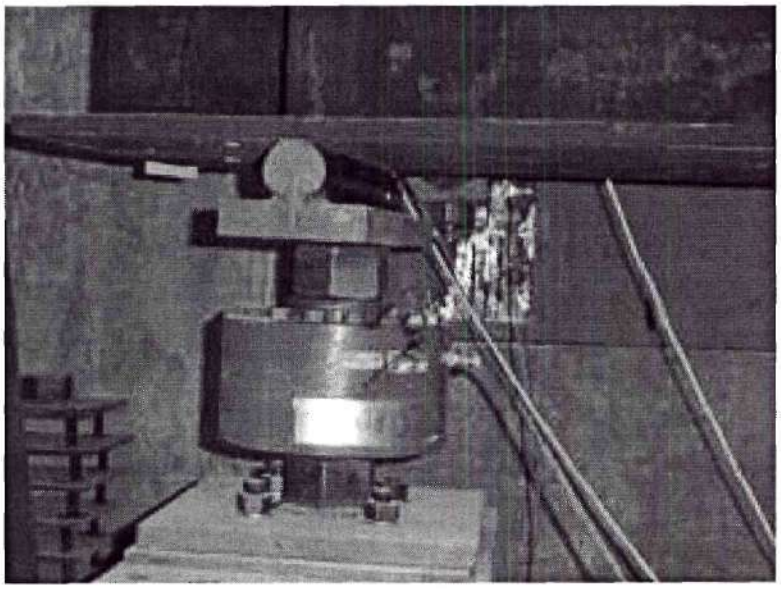

Figure 7 Detail of the exterior end support

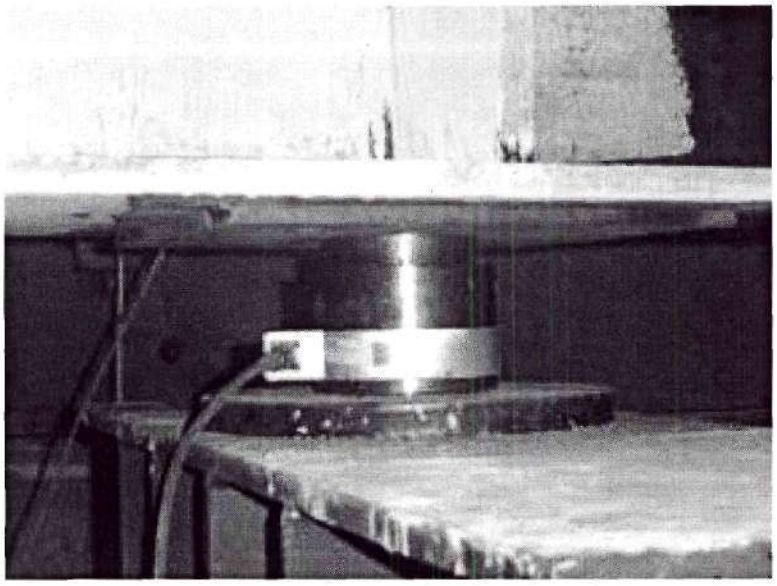

Figure 8 Detail of the interior support

longitudinal axes. The attachment of the bracing to the girders was placed approximately 50.8 mm (2 in) higher than the attachment to the reaction wall at the beginning of the tests, based on an estimated upper-bound displacement at the load points at maximum load equal to this value, and an estimated upper-bound required displacement at the load points of 101.6 mm (4 in) at the end of the tests. The length between the centerline of the spherical bearings at the ends of the bracing members was 1028.7 mm (40.5 in) at locations 1L and 1R and 1244.6 mm (49 in) at locations 2L and 2R. These lengths were sufficient to permit the bracing members to rotate through the above estimated vertical displacements with negligible lateral bending being induced within the girders. Refined finite element analyses were conducted during the design of the tests to verify that this bracing arrangement would have a negligible influence on the test behavior.

Two concentrated loads were applied to the girder, an internal load at the mid-length between the two supports and an external load near the tip of the cantilevered portion (see Fig. 5). The internal load was applied by means of a 4,448-kN (1,000-kip) double-acting hydraulic cylinder to which a 3,114 kN (700-kip) load cell was attached. A 12.7 mm (1/2 in) bearing plate was placed between the button of this load cell and the top flange of the girders, similar to the detail in Fig. 8. A heavy grease was applied to the contact surface between the load button and the bearing plate at this location, and at the interior support position, to minimize any longitudinal restraint within the tests. The torsional compliance within the reaction beam of the test frame and within the support pedestals was such that the longitudinal forces induced within the system were negligible even if slip did not occur between the button of the load cells and the corresponding bearing plates. The external load was applied by a closed-loop hydraulic actuator having a compressive capacity of 1,460 kN (328 kips). The above loading and vertical support

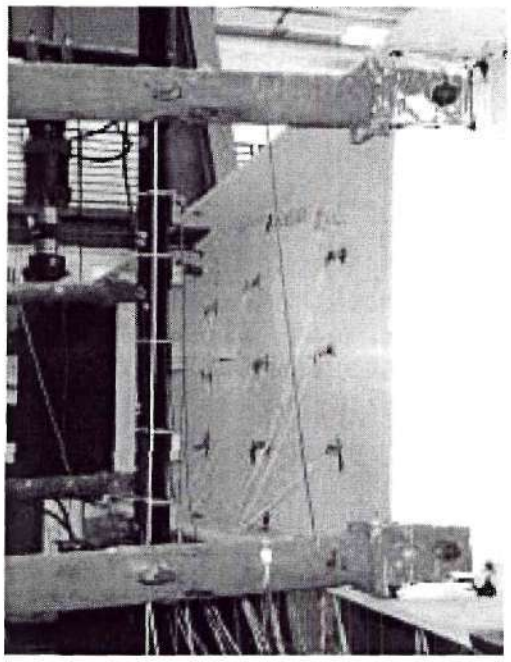

Figure 9 Top and bottom bracing members

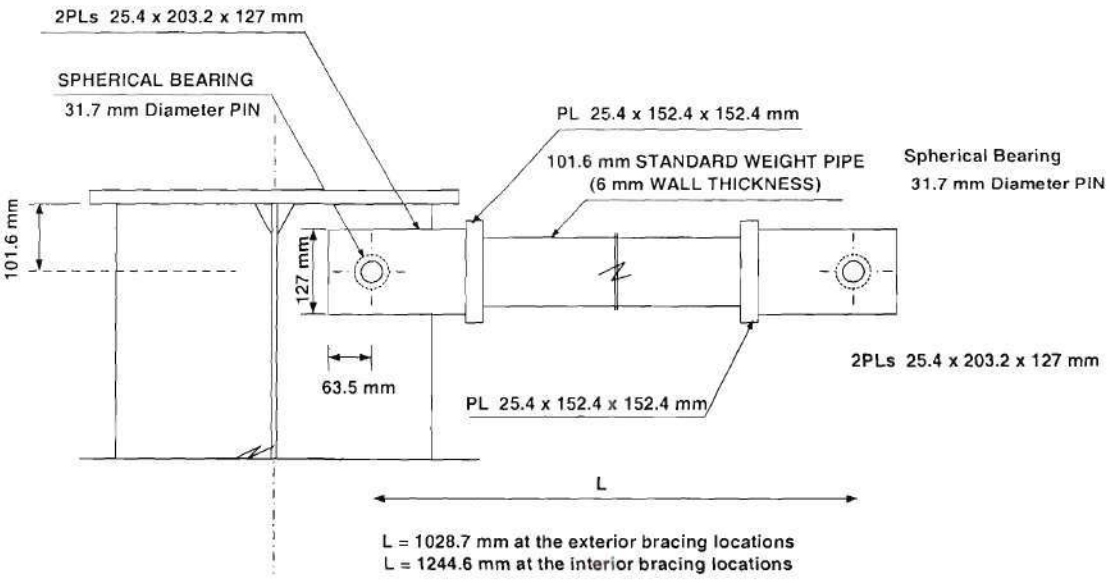

Figure 10 Detail of the top bracing members (bottom similar)

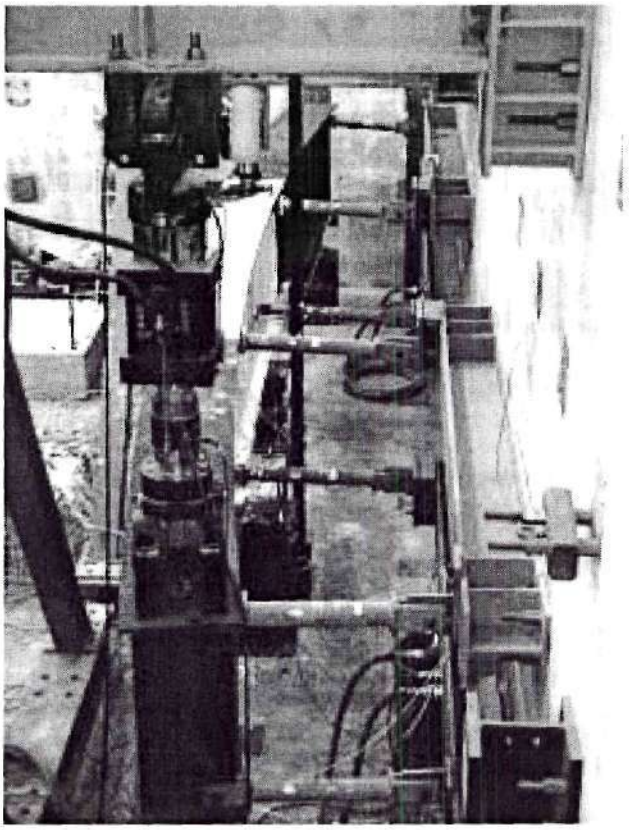

Figure 6 Longitudinal view of test setup from end 1R

arrangement produced a constant shear force in the web panel between the interior load and the interior support points, with an inflection point at the test girder centerline as illustrated in Fig. 5.

Applied loads, reactions, vertical deflections, radial deflections, and strains were recorded during the testing. The vertical deflections were recorded by means of linear variable differential transformers (LVDTs) centered under the bottom flange at the girder mid-length and at the locations of the applied loads as shown in Figs. 11 and 12. Radial deflections were measured by five wire potentiometers attached to the web of the test girders at the mid-depth and 1/4 and 3/4 depth locations and also at 38.1 mm (1.5 in.) from the inside face of the top and bottom flanges, as shown in Fig. 13. These measurements were taken at the mid-length of the web panels that were instrumented with rosette strain gages as explained below.

Each test component was instrumented with electrical resistance strain gages to measure strains in the web, flanges, and the bracing members. The web test panels (Panel B) for both components S1 and S2 were instrumented at nine locations with back-to-back three-arm rosettes arranged in the pattern shown in Fig. 14. These rosettes are labeled as Rnm where n = 1,2...9 represents the rosette location number, and m takes either the letter i or o to indicate the inside (toward the center of curvature) or outside, respectively. For components S1-S and S2-S, one of the two test panels was instrumented with back-to back three-arm strain rosettes at nine locations as shown in Fig. 15. Girder S1-S was instrumented in panel B1 and girder S2-S was instrumented in panel B2. In addition, back-to-back single-arm strain gages were mounted on the test panel adjacent to the instrumented one.

The longitudinal strains in the top and bottom flanges were measured at the cross-section associated with rosettes R7 through R9 in girders S1, S2 and S2-S. However, in girder S1-S, they were measured at the cross-section associated with rosettes R1 through R3, since panel B1

Figure 11 LVDT at location 2L

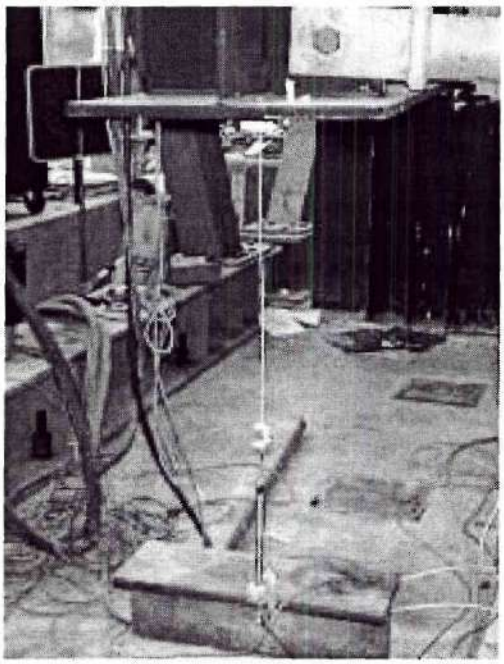

Figure 12 LVDT at location 1R

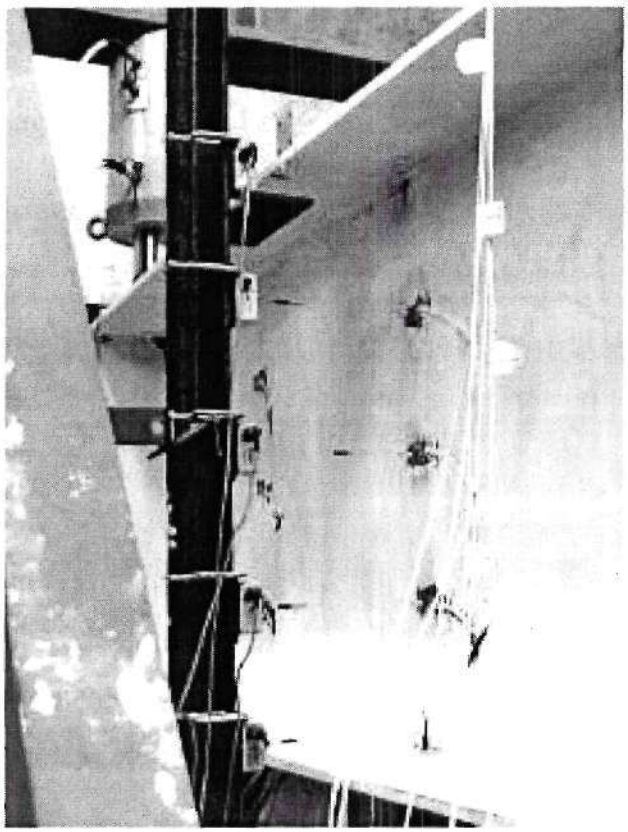

Figure 13 Wire potentiometers for measurement of web radial displacements

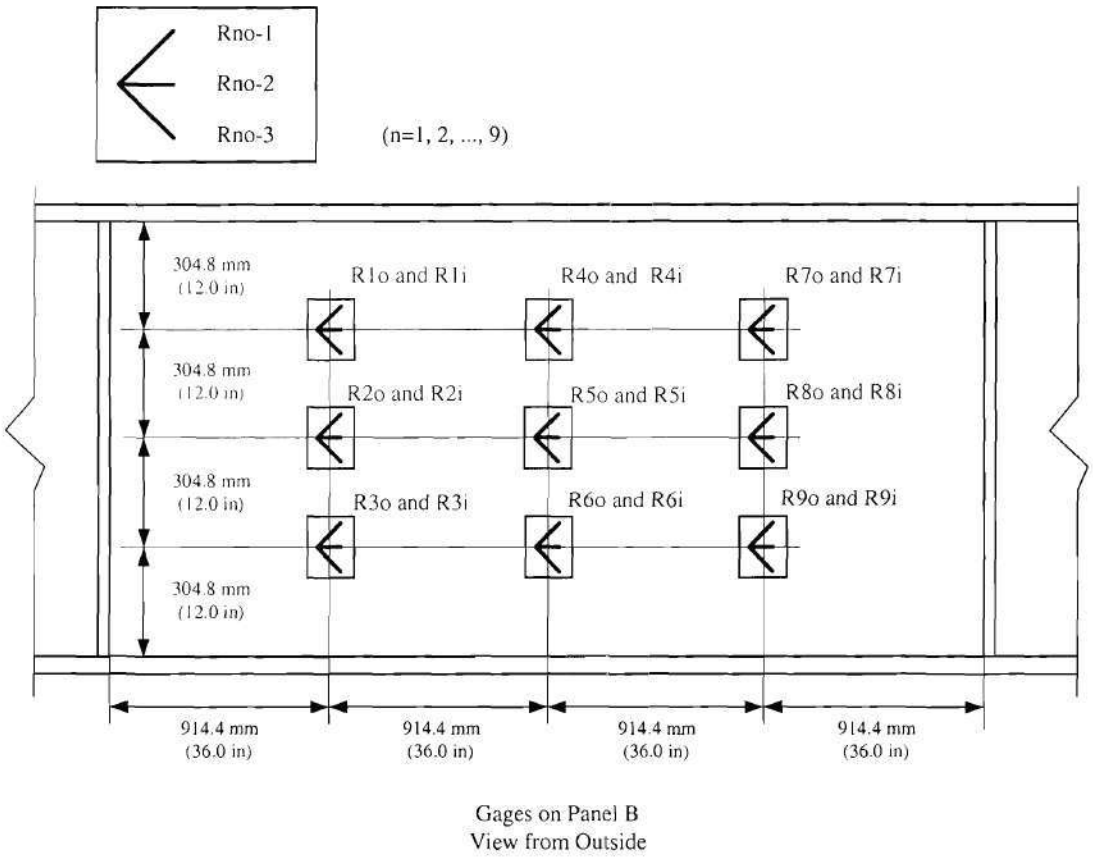

Figure 14 Strain rosette pattern for girders S1 and S2

CHAPTER IV - EXPERIMENTAL RESULTS

4.1 PANEL SHEAR FORCE

Theoretically speaking, if the small vertical components of force from the bracing members are neglected, the test panel shear force obtained from the difference ($V_R = R_2 - P_1$) between the interior support reaction and the applied external load on the right-hand side of the test must be the same as that computed from the difference ($V_L = P_2 - R_1$) between the applied internal load and the reaction at the exterior support on the left-hand side (see Fig. 5). However, due to unavoidable measurement error, the values of V_R and V_L will be different, even if the vertical components of force from the bracing members are included. Hereafter, the experimentally obtained panel shear force is reported as the average of V_R and V_L. The maximum values of V_R, V_L and $V_{avg} = (V_R + V_L) / 2$ and the ratio of the maximum values of V_R and V_L obtained in the four shear tests are reported in Table 7.

Table 7 Measured panel shear strengths

	V_R kN (kips)	V_L kN (kips)	V_{avg} kN (kips)	V_R/V_L
S1	1,210 (272)	1,190 (268)	1,200 (270)	1.015
S2	1,150 (258)	1,160 (261)	1,160 (260)	0.989
S1-S	1,410 (317)	1,320 (297)	1,370 (307)	1.067
S2-S	1,400 (315)	1,420 (320)	1,410 (317)	0.984

If the vertical components of force from the bracing members are included in the calculation of the shear forces, the difference between V_R and V_L is reduced in all the cases. However, the

the hydraulic cylinder (location 2L) and at the actuator (location 1R) were closed until the load readings stabilized. The loading was incremented by setting the actuator to increase the displacement at location 1R at a small constant rate while simultaneously pumping oil to the hydraulic cylinder by a manual control. The loading of each girder was terminated when the vertical deflection under the 3,114 kN (700 kip) hydraulic cylinder reached 51 mm (2 in). The test girders were then unloaded in a similar fashion. All loads, deflections and strains were recorded by a computer-based data acquisition system.

was instrumented in this test; this cross-section was the closest to location 2L. Each of the above cross-sections had four single arm strain gages mounted back-to-back on each surface of the flanges, i.e., a total of 16 gages. These gages are numbered 1 through 4, progressing from the outside to the inside tips of the flanges. That is, the gage numbers increase in the direction toward the center of curvature. Gages 1 and 4 were located at 76.2 mm (3 in) and gages 2 and 3 were located at 76.2 mm (3 in) from the corresponding face of the web. The gages on the outer surface of the flanges are referred to as the "outside" gages and those on the inside surface of the flanges, closest to the neutral axis of the cross-section, are referred to as the "inside" gages.

In addition, the mid-length of each tubular bracing member was instrumented with four-single arm gages placed at 90° intervals around the periphery. These gages were connected to create four legs of a Wheatstone-bridge configuration. The load output from this arrangement was checked against a calibrated load cell prior to the connection of the bracing members to the test girder.

3.4 TEST PROCEDURE

Prior to testing to failure, each girder was subjected to at least two preliminary cycles of loading and unloading to verify the operation of the testing equipment and ensure proper contacts between the girder and the loading and support fixtures. The maximum loads applied in these preliminary cycles were such that shear force in the test panel was approximately 178 kN (40 kips), which was less than 15 percent of the estimated shear capacity of girders S1 and S2. During the final sequence of loading to failure, the internal and external loads were incremented at a ratio of the interior load to the exterior load of three, as shown in Fig. 5. The shear capacity in each test was reached in 14 to 20 loading increments. At each load increment, the valves on

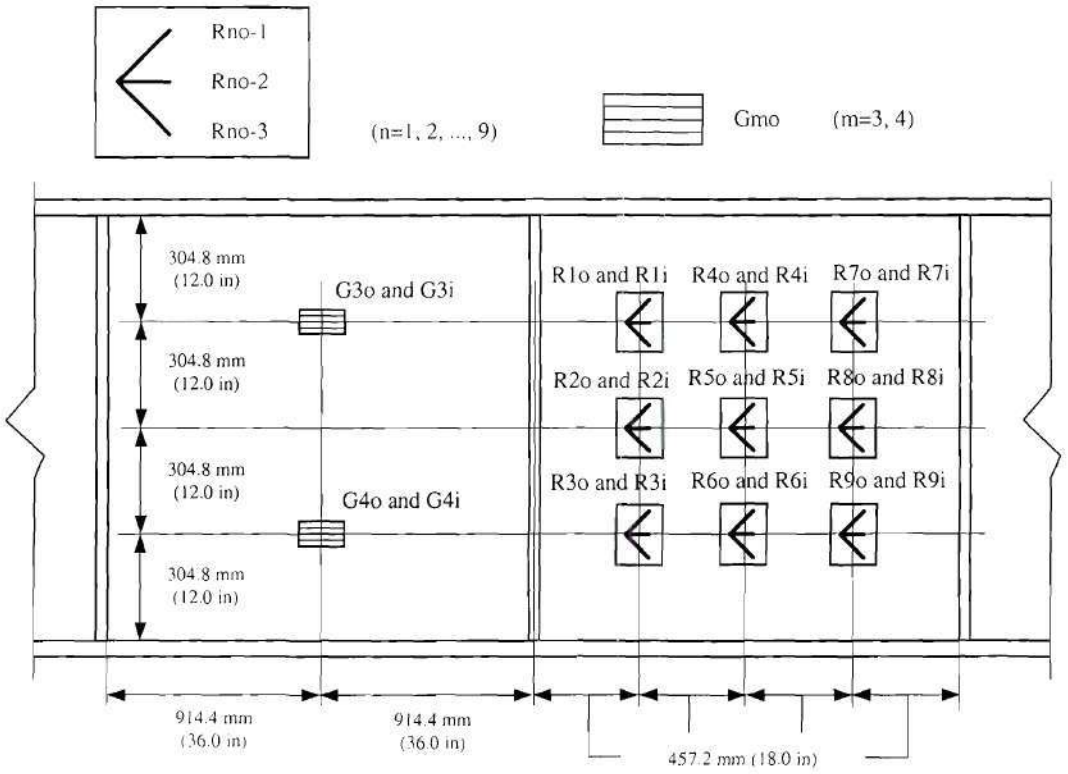

View from Outside

Figure 15 Strain rosette pattern for girder S2-S (S1-S similar)

largest change in V_{avg} by including the effect of the vertical components of the bracing forces is 0.5 percent (corresponding to test S1).

To examine the measurement error over the full range of loading and unloading, the ratio V_R/V_L versus the loading increment is plotted in Figure 16. The loading increments corresponding to the maximum shear force are labeled in the figure. For all the loading increments of all the tests, except in the early stages of the loading, the ratio of V_R/V_L is between 0.9 and 1.1. At the maximum panel shear strength, the difference between V_R and V_L is less than 2 percent in all the tests except for S1-S, for which the values of V_R and V_L are 317 kips and 297 kips, respectively.

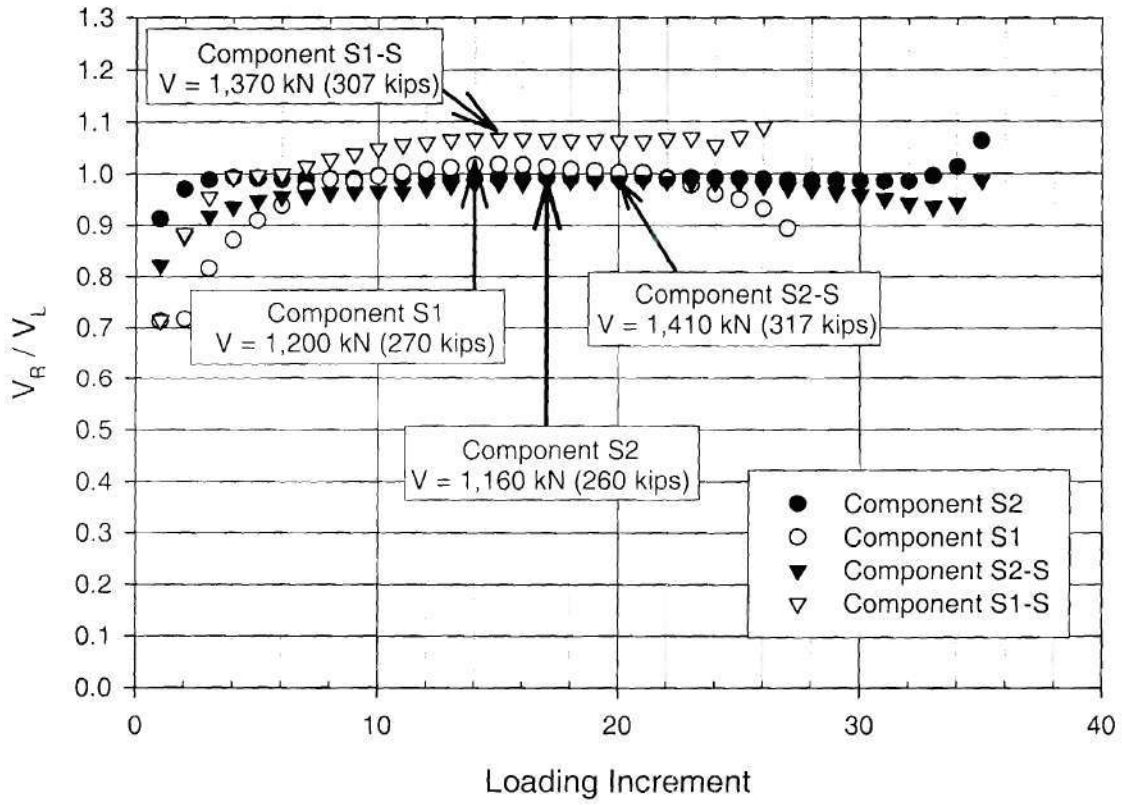

Figure 16 Ratio V_R/V_L versus loading step

4.2 LOAD-DEFLECTION RESPONSE

The vertical deflections at the applied load positions 1 and 2 and at the center of the test panel are plotted versus the panel shear force in Figs. 17 through 20. The deformed shapes of the web in the radial direction at the middle of the test segment in girders S1 and S2 and at the center of the instrumented web panel in girders S1-S and S2-S are shown at in Figs. 21 through 24. The corresponding radial deflections at D/4, D/2 and 3D/4 are plotted versus the panel shear force in Figs. 25 through 28.

One can observe that in all of the tests the load-vertical displacement response was only slightly nonlinear until just before the shear capacity was reached. In each case, the measured deflection under the interior applied load (and also under the exterior applied load) corresponding to 95 percent of the shear capacity was approximately twice that corresponding to 50 percent of the measured shear capacity. Furthermore, the loss in shear strength with increasing vertical deflections was small within the post-peak range of the response. The largest reduction in the shear strength in all of the tests was approximately 15 percent at the end of the post-peak loading, corresponding to girder S1 (see Figure 17). It is interesting that although girder S2 failed at a slightly smaller maximum load compared to S1, the shear resistance was larger at the end of the post-peak loading in this girder. As noted previously, all of the tests were terminated at approximately v_2 = 51 mm (2 in). This deflection ranged from 2.2 to 3.4 times the deflection at the maximum shear strength. The displacement at the middle of the test segment in girders S1 and S2 actually reversed direction, i.e., this point moved upward after the maximum shear capacity was reached. This behavior was associated with the bottom flange pushing up into the web, and with the development of compressive diagonal strains within the web plate as discussed subsequently.

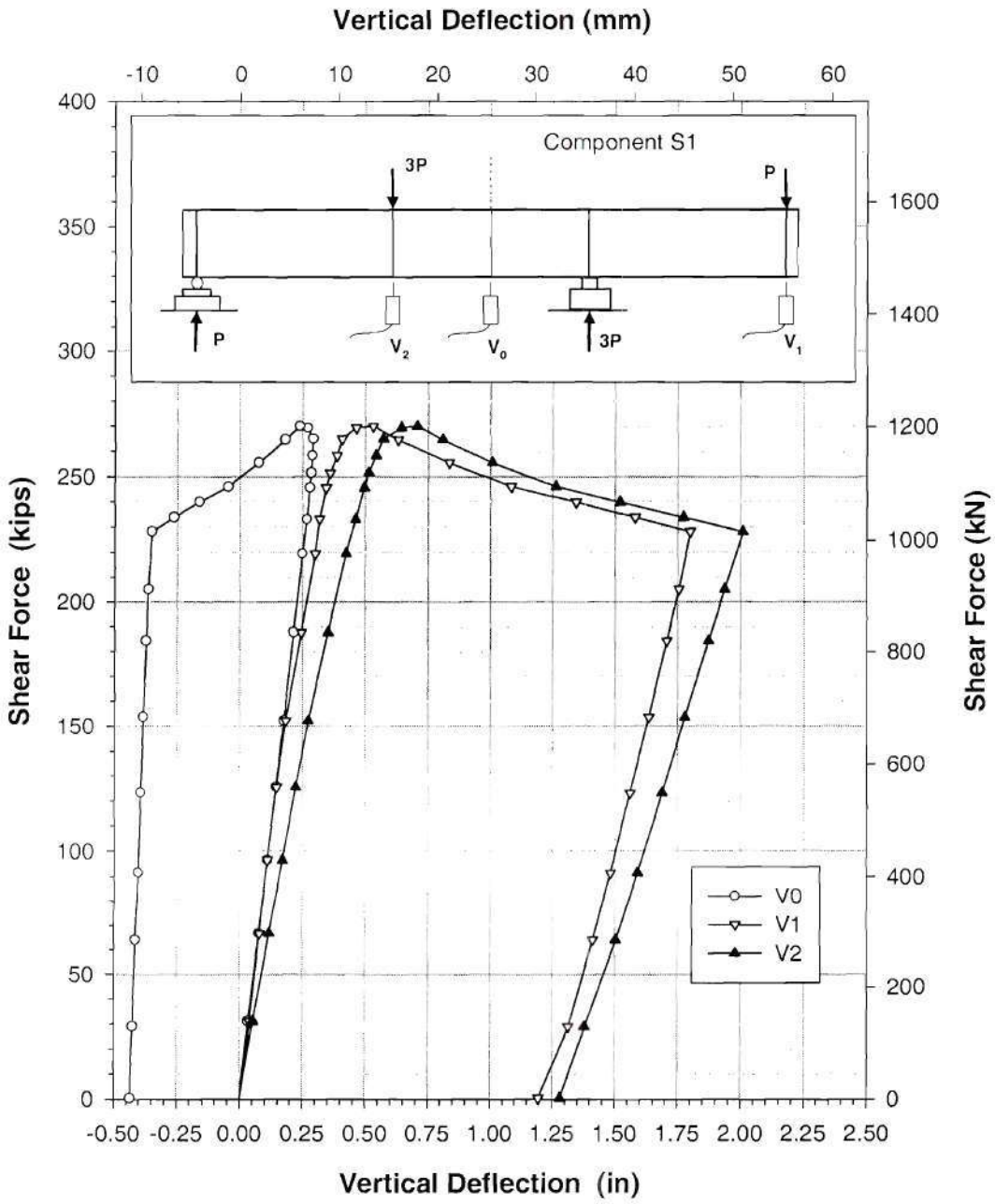

Figure 17 Girder S1 – load-vertical deflection curves

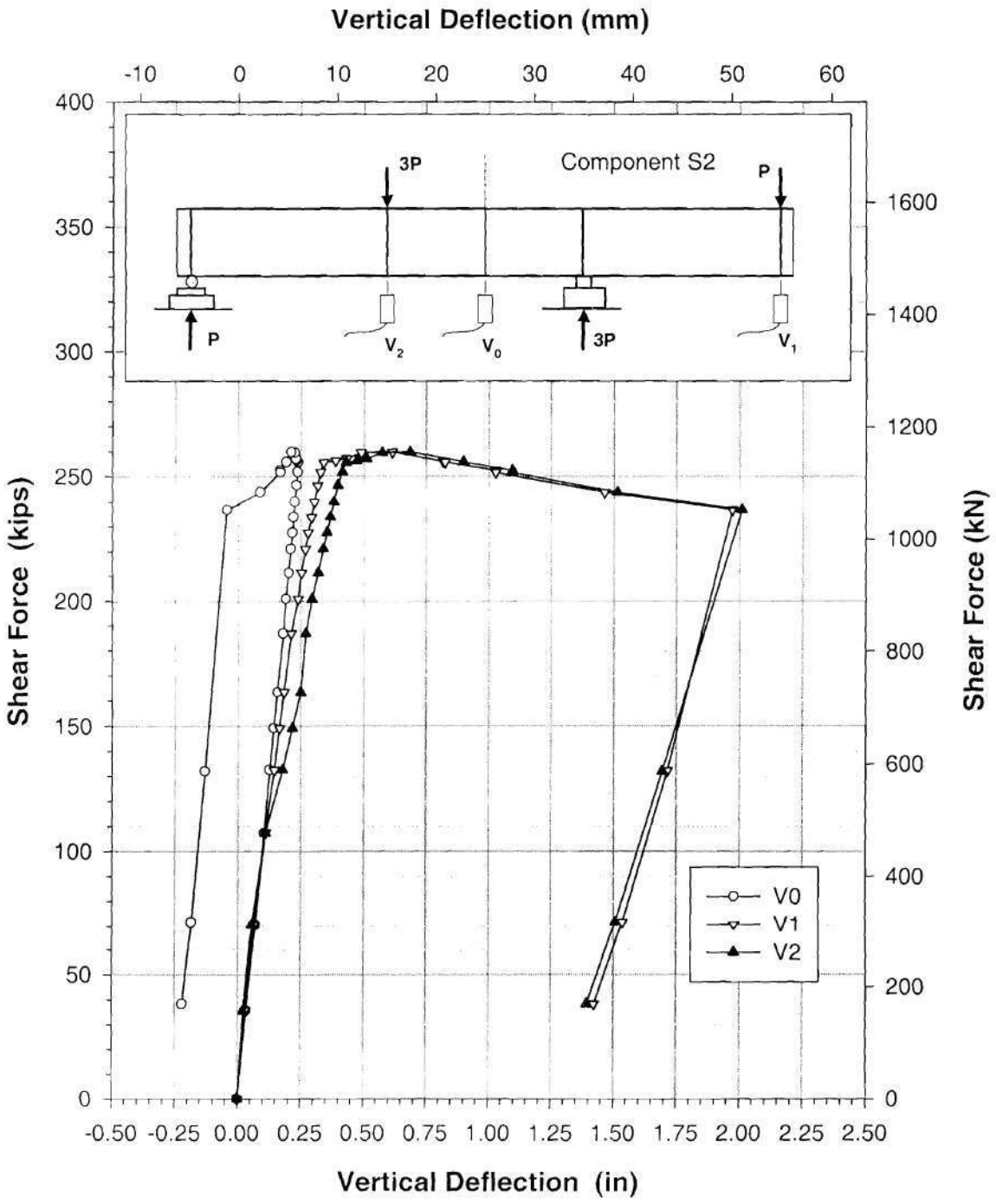

Figure 18 Girder S2 – load-vertical deflection curves

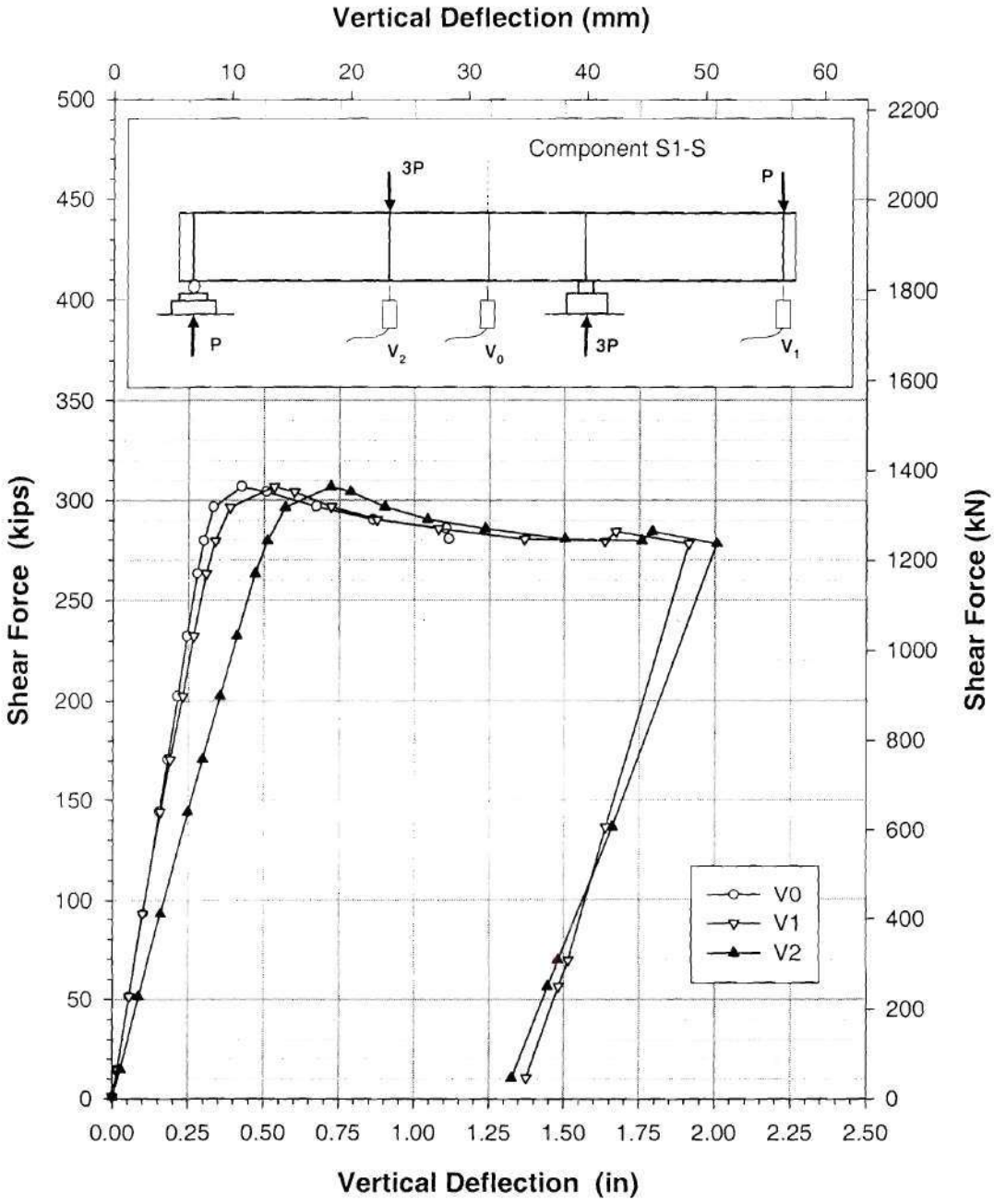

Figure 19 Girder S1-S – load-vertical deflection curves

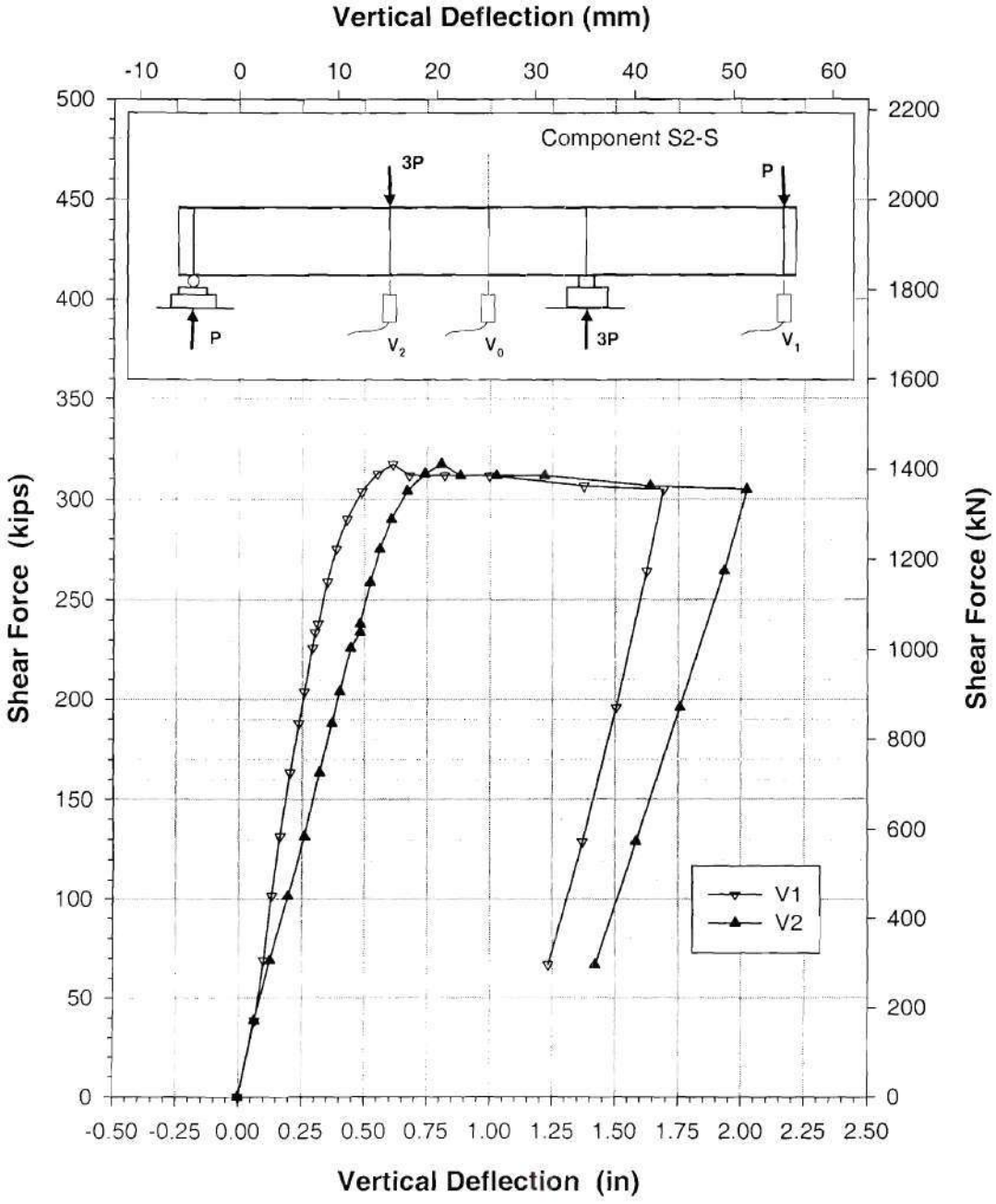

Figure 20 Girder S2-S – load-vertical deflection curves

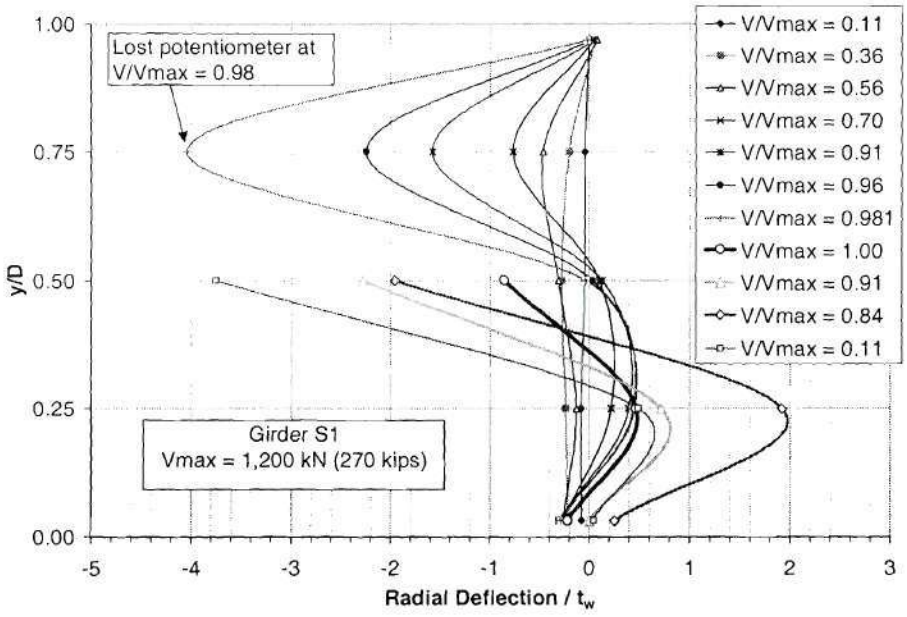

Figure 21 Girder S1– web radial deformations at the middle of the test segment

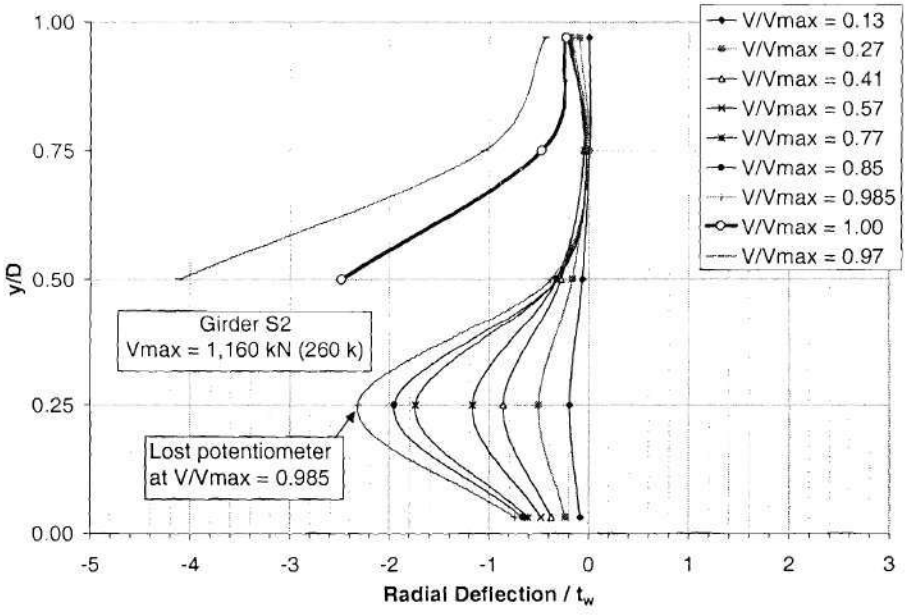

Figure 22 Girder S2 – web radial deformations at the middle of the test segment

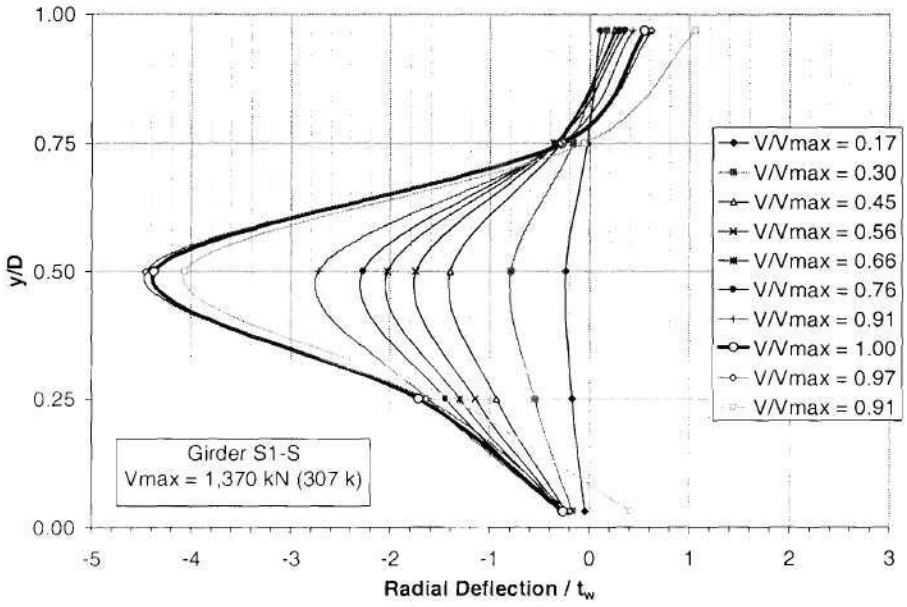

Figure 23 Girder S1-S – web radial deformations at the middle of the instrumented test panel

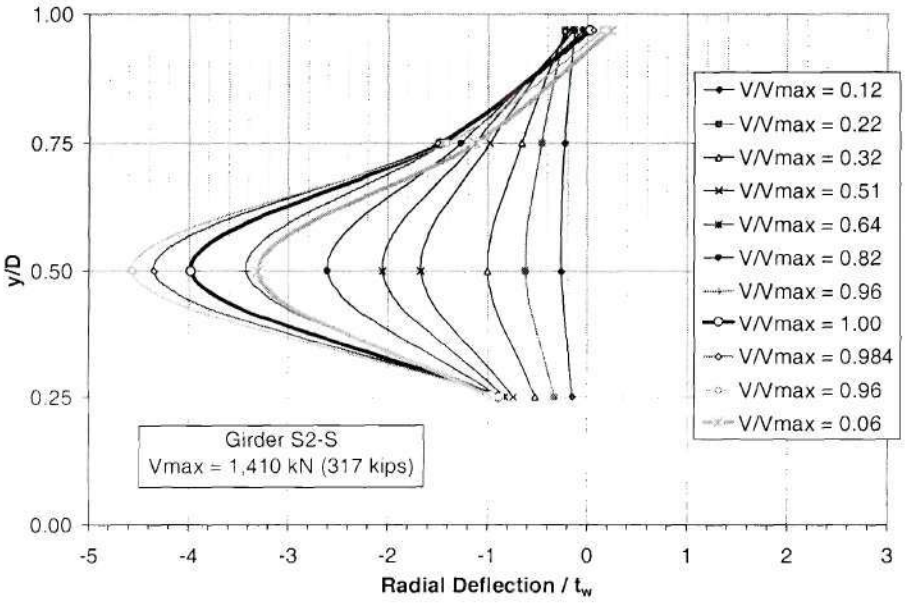

Figure 24 Girder S2-S – web radial deformations at the middle of the instrumented test panel

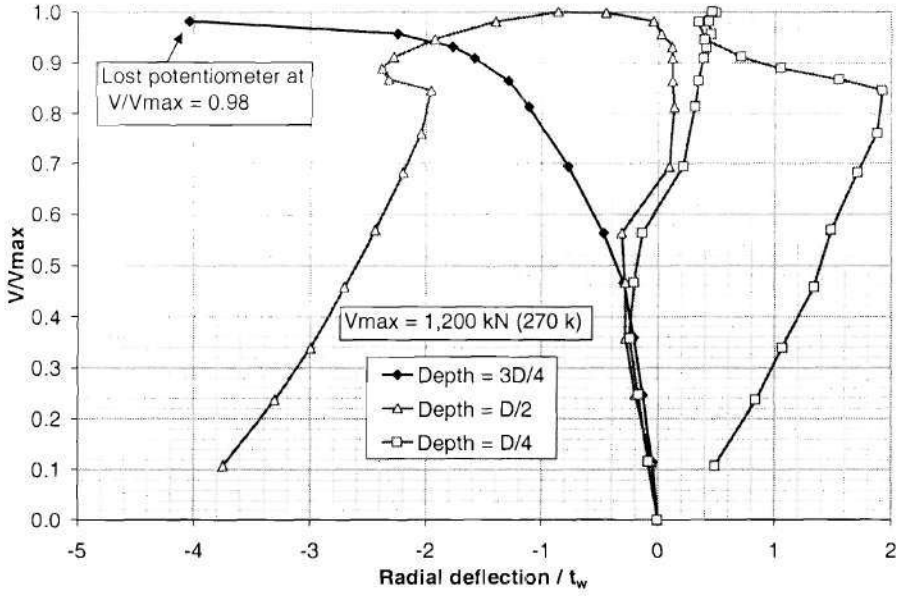

Figure 25 Girder S1 – radial displacement at locations D/4, D/2 and 3D/4 versus V/V_{max}

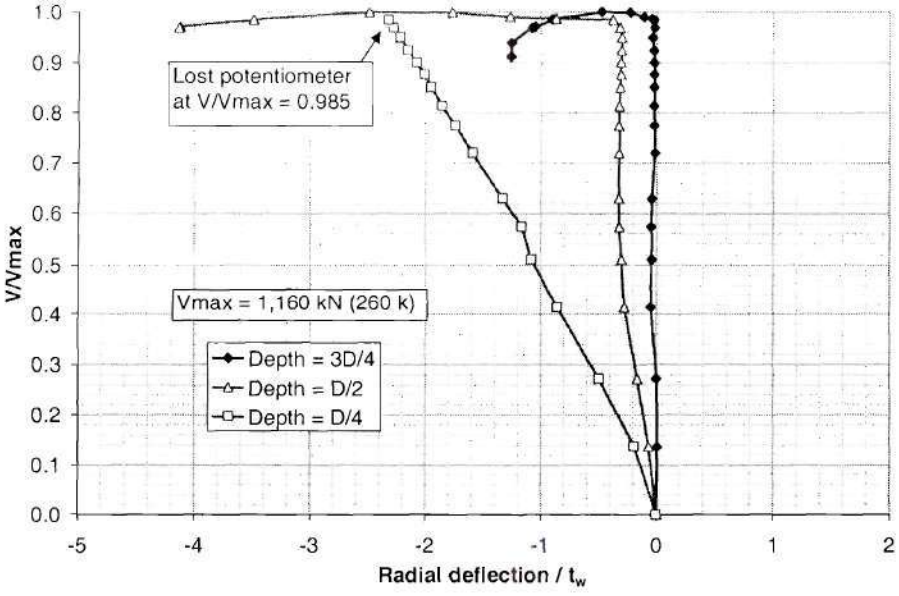

Figure 26 Girder S2 – radial displacement at locations D/4, D/2 and 3D/4 versus V/V_{max}

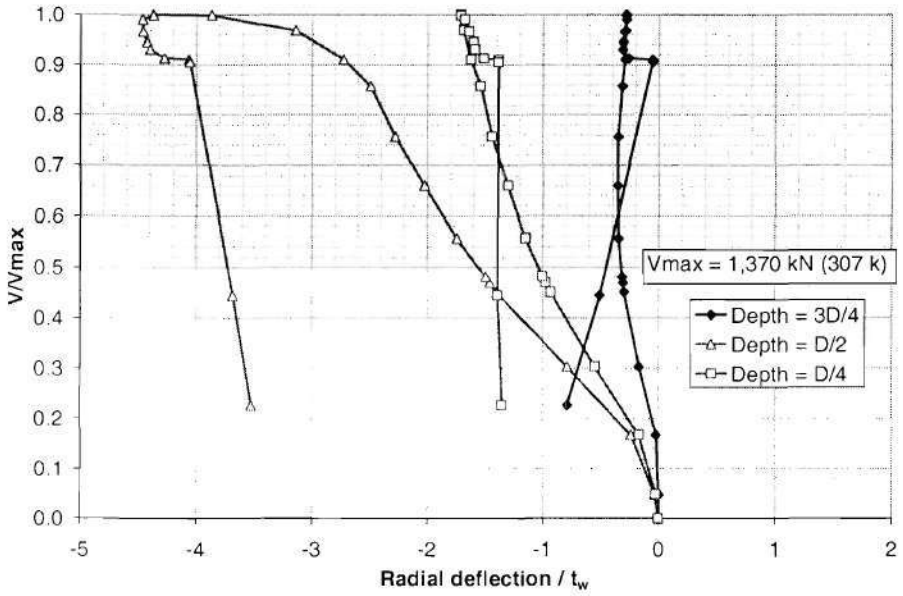

Figure 27 Girder S1-S – radial displacement at locations D/4, D/2 and 3D/4 versus V/V_{max}

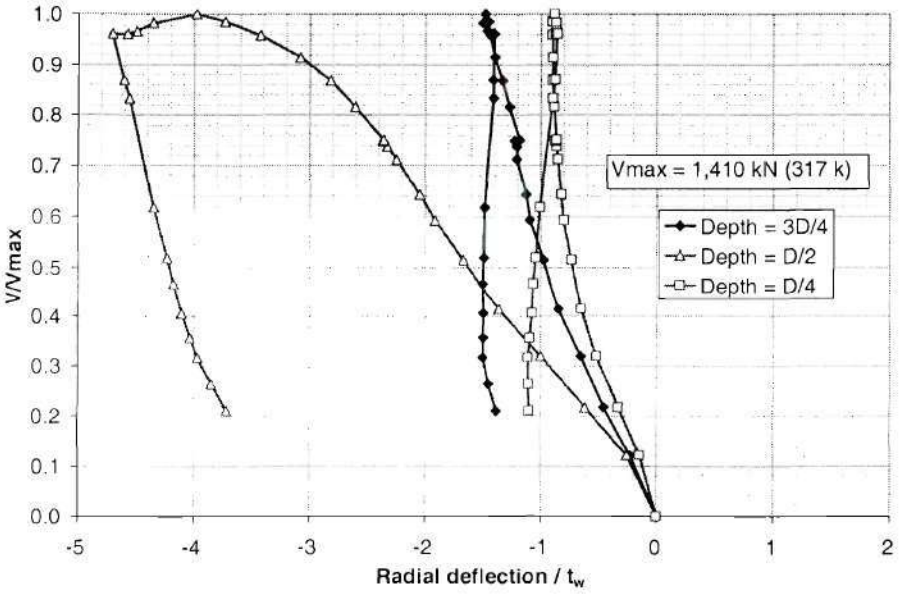

Figure 28 Girder S2-S – radial displacement at locations D/4, D/2 and 3D/4 versus V/V_{max}

The radial displacements of the webs were predominantly toward the inside direction, i.e., toward the center of curvature of the girders (plotted as negative displacements in Figs. 21 through 28). This was due to the initial tendency of the web panels to straighten out along the diagonal tension direction associated with the shear force. Also, as discussed previously, the predominant web initial out-of-flatness was toward the inside direction in the instrumented panels. As the shear force increased, stability effects associated with the diagonal compression in the web panels resulted in the gradual development of a dominant wave. This wave extended diagonally from one corner of the panel to a location on the opposite flange inside the panel length in girders S1 and S2, and essentially from the top-right to the bottom-left corner in girders S1-S and S2-S. This dominant wave is evidenced by the largest radial displacements shown in Figs. 21 through 28.

At the maximum shear capacity, the largest measured radial web displacement was approximately 38 mm (1.5 in, or $4.4t_w$) in girder S1-S and 33 mm (1.3 in, or $4.0t_w$) in girder S2-S. In addition, based on Figs. 21 and 22, one can infer that the maximum radial displacements at the potentiometer locations in girders S1 and S2 were of a similar magnitude at $V/V_{max} = 1.0$. These maximum panel radial displacements were somewhat larger than the initial offset of the web from a straight chord between the positions where the dominant wave intersected the top and bottom flanges. That is, the dominant wave within the web was deformed inward beyond the extent required to "straighten-out" the web panel along the diagonal tension direction. However, at 95 percent of the shear capacity, the maximum radial displacements were significantly smaller than the above values in all the girders except S2-S. At this load level, the measured radial deflections ranged from approximately 18 mm (0.73 in, or $2.1t_w$) in girder S1 to approximately 28 mm (1.10 in, or $3.4t_w$) in girder S2-S. One should note that girder S2-S had the

largest web initial out-of-flatness of all the test girders. Also, it is interesting that at 95 percent of the shear capacity, the radial displacements in the webs with $d_o/D = 1.5$ were somewhat larger than those with $d_o/D = 3$.

The shear-radial displacement curves shown in Figs. 25 through 28 range from essentially a linear load-deflection response up to the peak load level (see Fig. 26 for girder S2) to a somewhat nonlinear pre-peak load-deflection response in Fig. 25 for girder S1. The pre-peak load-radial deflection curves for both of the stiffened girders (see Figs. 27 and 28) exhibit only a mild nonlinearity. The load-radial deflection curves of all the tests indicate the gradual development of the dominant diagonal wave discussed above with increasing shear force. Upon careful inspection of the test data, there appeared to be no definitive bifurcation in the web load-deflection response as the shear force was increased above various theoretical web shear buckling levels (several theoretical web shear buckling loads are discussed in Chapter V). This was expected due to the presence of horizontal curvature plus additional initial imperfections in the web panels combined with the stable nature of the web postbuckling response. In fact, similar observations were documented by Basler et al. (1960) in tests of straight I girders.

The web shear-radial deflection behavior in girder S1 appeared to be the closest of all the tests to a theoretical bifurcation response. In this test (see Fig. 25), the slope of the shear-radial deflection curve at 3D/4 (the location of the maximum measured radial displacement) started to decrease noticeably at a shear force between 0.46 and 0.56 V_{max}, whereas the corresponding radial deflections at D/4 and D/2 actually decreased and then changed sign as the shear increased above this load level (i.e., the radial deflections at D/4 and D/2 were initially toward the center of curvature, but the web started to deflect outward from the center of curvature at these locations as the shear was increased above 0.46 to 0.56 V_{max}). In all of the other tests, the web radial dis-

placements at locations D/4, D/2 and 3D/4 either increased gradually or remained essentially constant in value as the shear force was increased within the pre-peak range of the response.

4.3 GIRDER DISTORTIONS AT MAXIMUM SHEAR CAPACITY AND IN POST-PEAK

Figures 29 to 32 show photographs of the girder test segments at the maximum shear capacity in each of the experiments. These figures illustrate the fact that the overall girder distortions were relatively small at the maximum shear strength. In each of these photos, one can observe that the white wash had started to flake off the web along a narrow diagonal strip. This strip extended from corner to corner of the left-most panel of the test segment in girders S1-S and S2-S, it extended from the bottom-left corner of the test segment through the rosette location R2 in girder S1, and it extended from the top-right corner of the test segment through the rosettes R6 in girder S2.

Figures 33 through 40 show outside views of the distorted girders at the end of the tests, when the girders were still located within the test frame, and inside views of the distorted test segments after the girders were removed from the test frame. Since the girder distortions grew significantly during the post-peak portion of the tests, these photos are useful in discerning the final failure modes of the girders. The white wash is flaked off the face of the web panels in these photographs primarily due to compressive surface strains. As noted by Basler et al. (1960), this flaking of the whitewash reveals surface conditions created by both membrane and bending strains, and therefore, it should not be identified with the width of a tension field. Dimensions are shown to the approximate locations of maximum plastic curvature and inflection points in the flanges associated with frame action of these elements. These dimensions were determined by

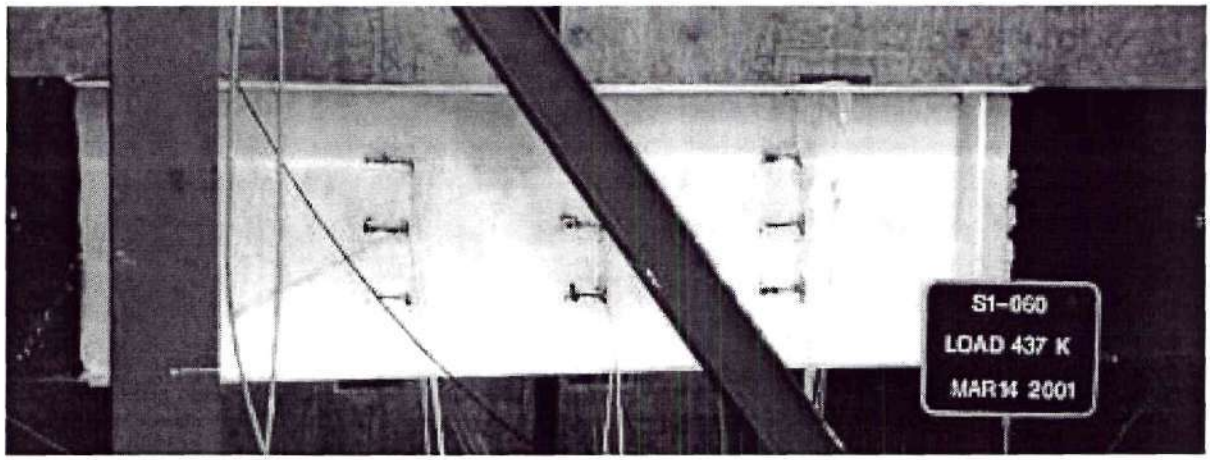

Figure 29 Girder S1 at peak load

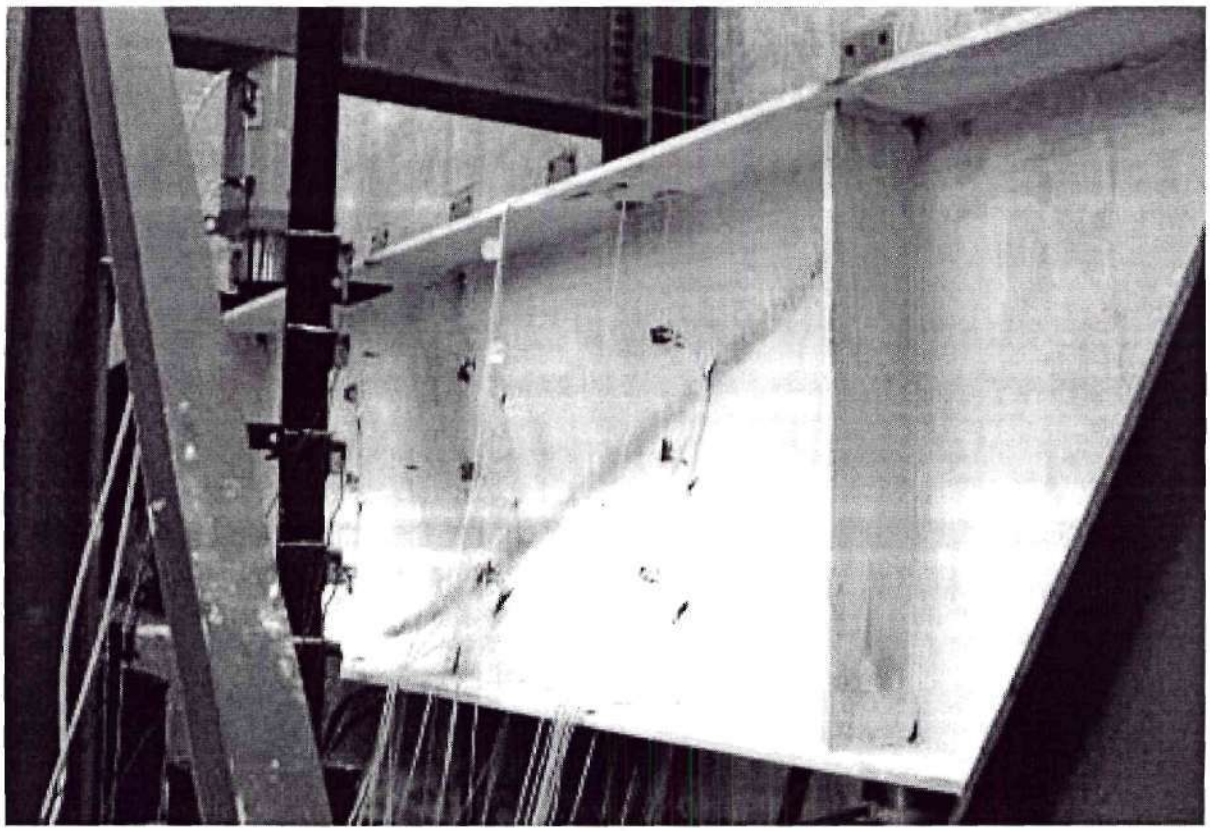

Figure 30 Girder S2 at peak load

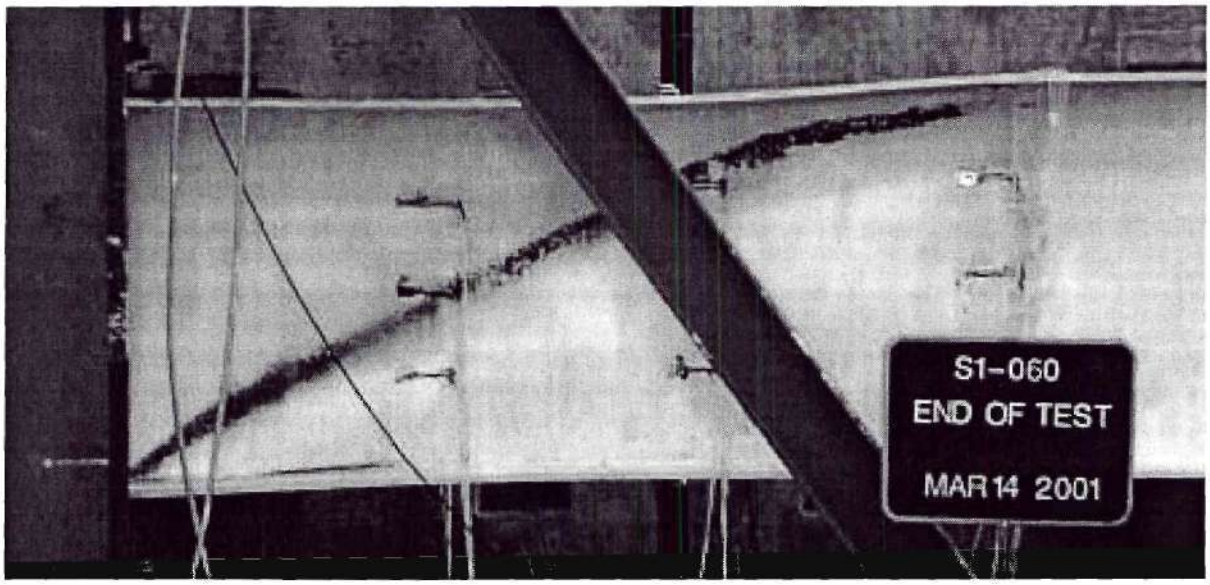

Figure 33 Girder S1 – outside view at end of test

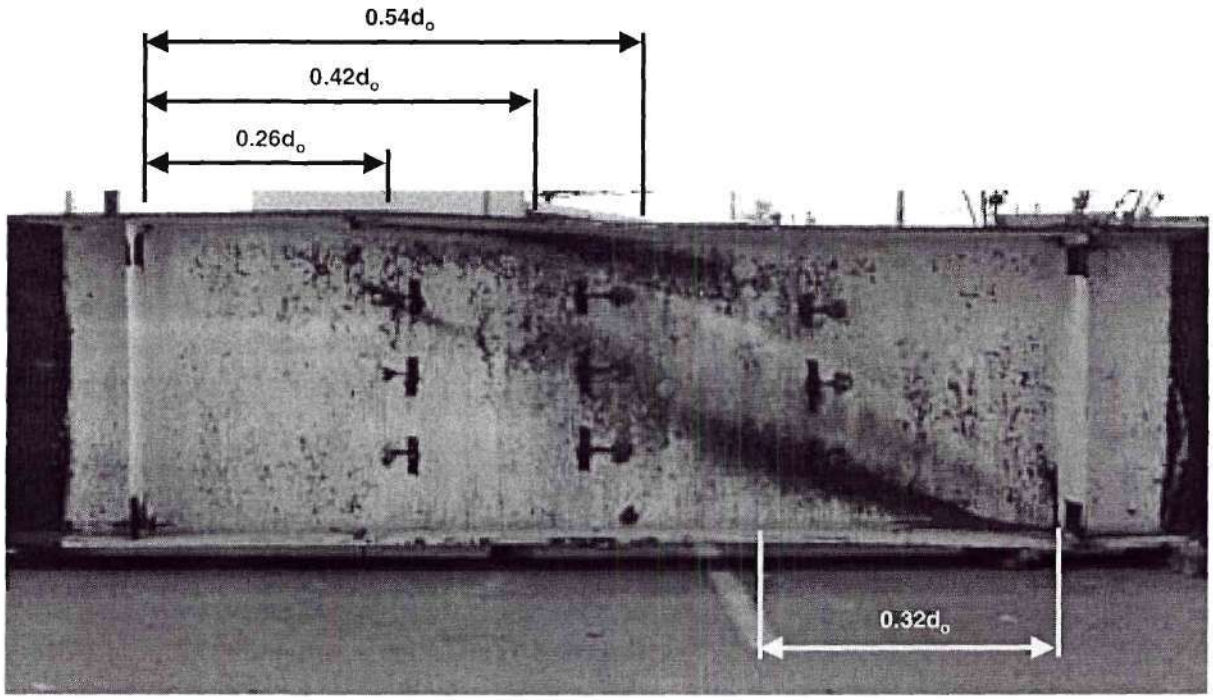

Figure 34 Girder S1 – inside view after test showing approximate locations of maximum curvature and inflection points within the flanges

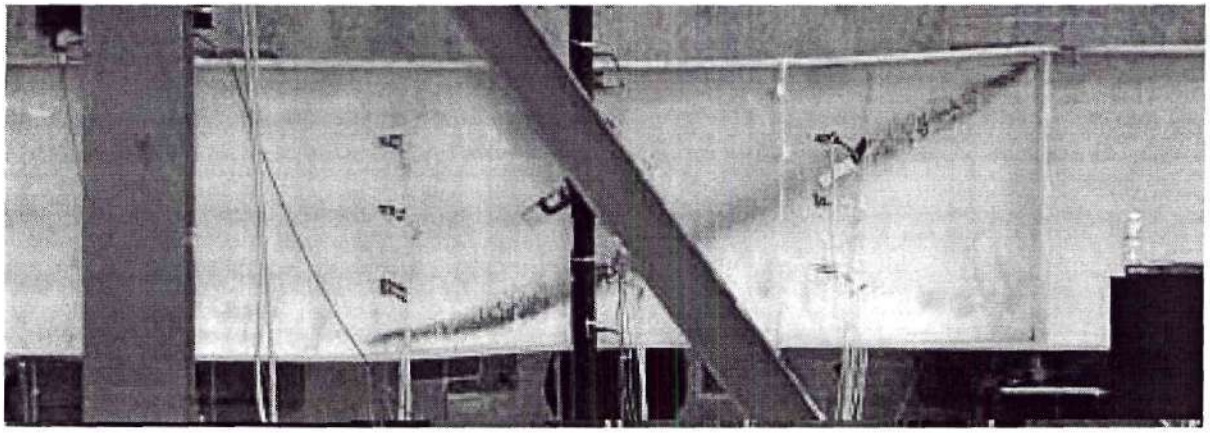

Figure 35 Girder S2 – outside view at end of test

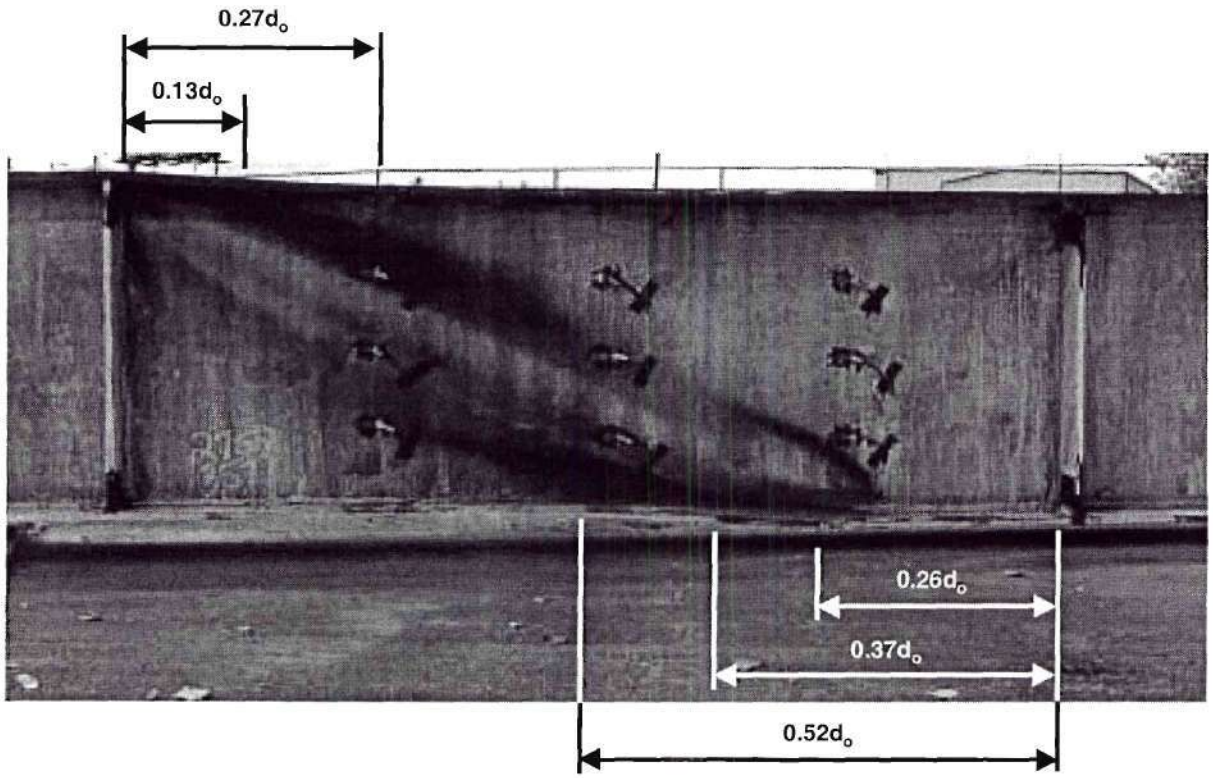

Figure 36 Girder S2 – inside view after test showing approximate locations of maximum curvature and inflection points within the flanges

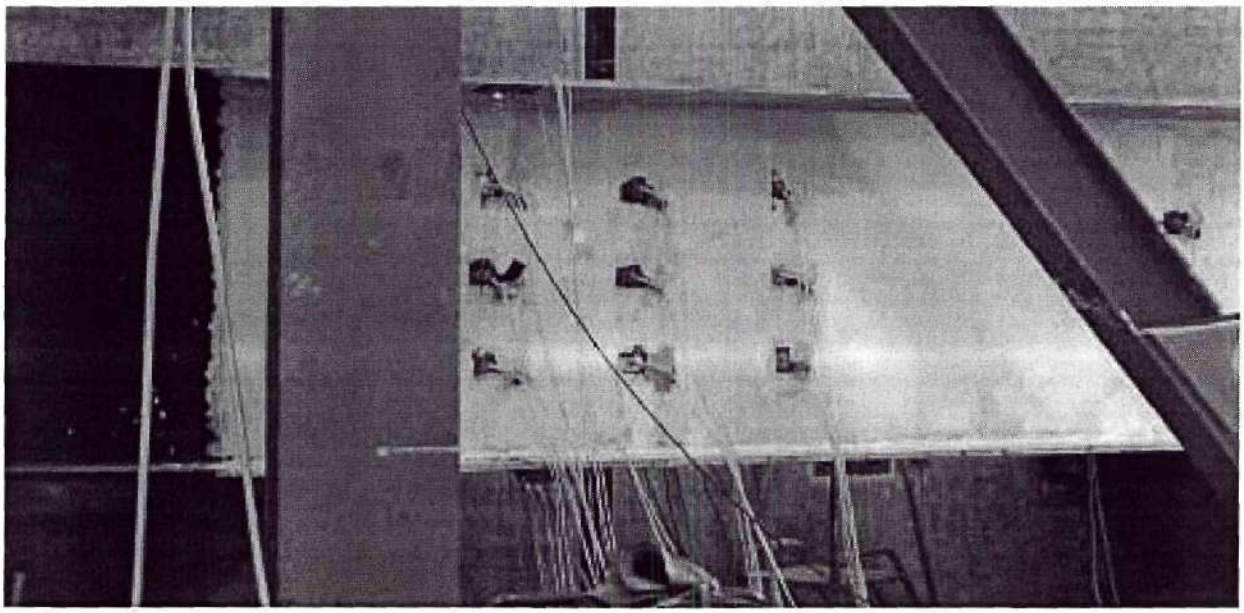

Figure 31 Girder S1-S at peak load

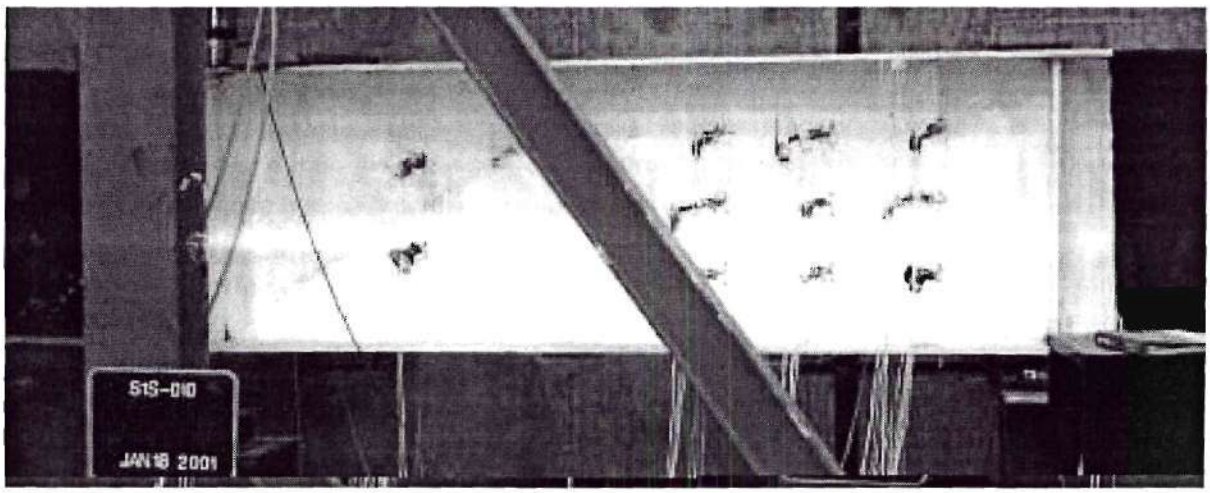

Figure 32 Girder S2-S at peak load

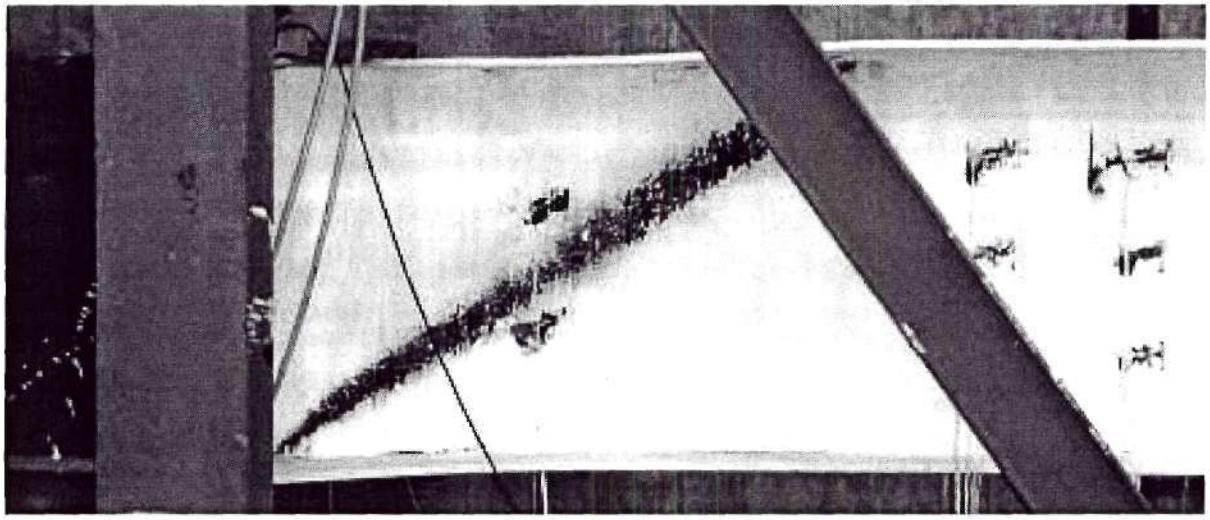

Figure 39 Girder S2-S – outside view at end of test.

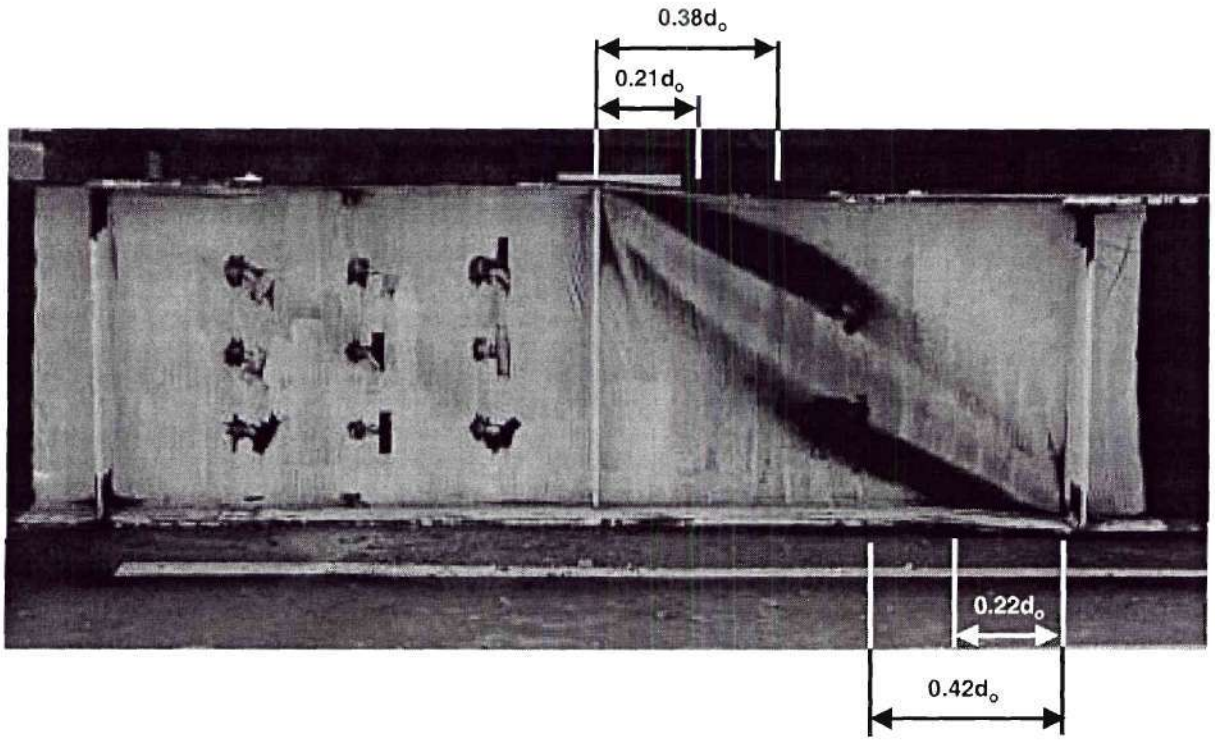

Figure 40 Girder S2-S – inside view after test showing approximate locations of maximum curvature and inflection points within the flanges

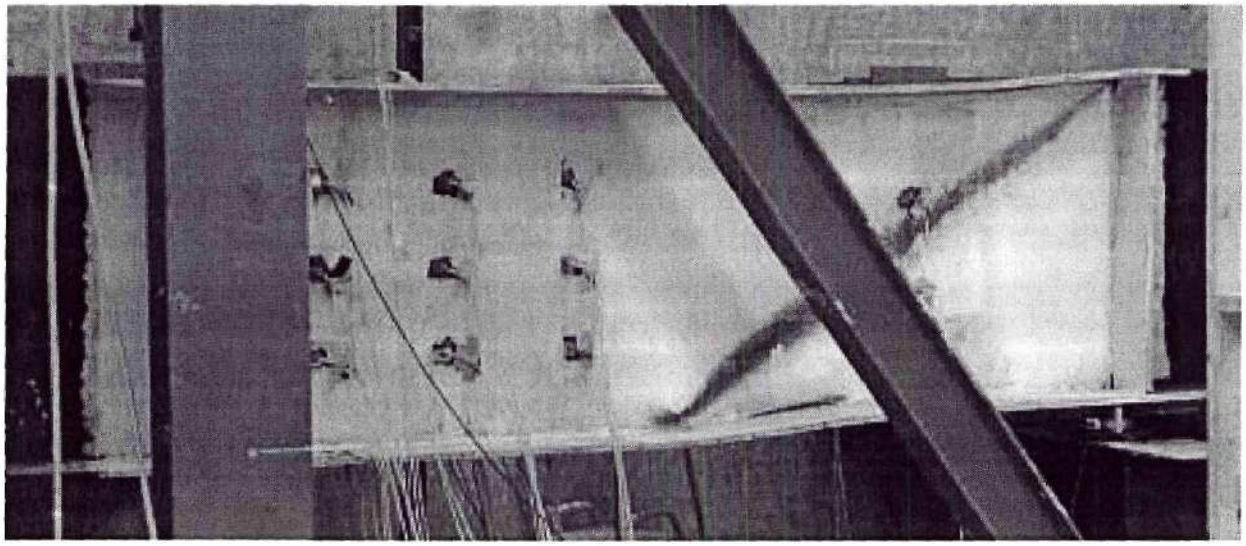

Figure 37 Girder S1-S – outside view at end of test

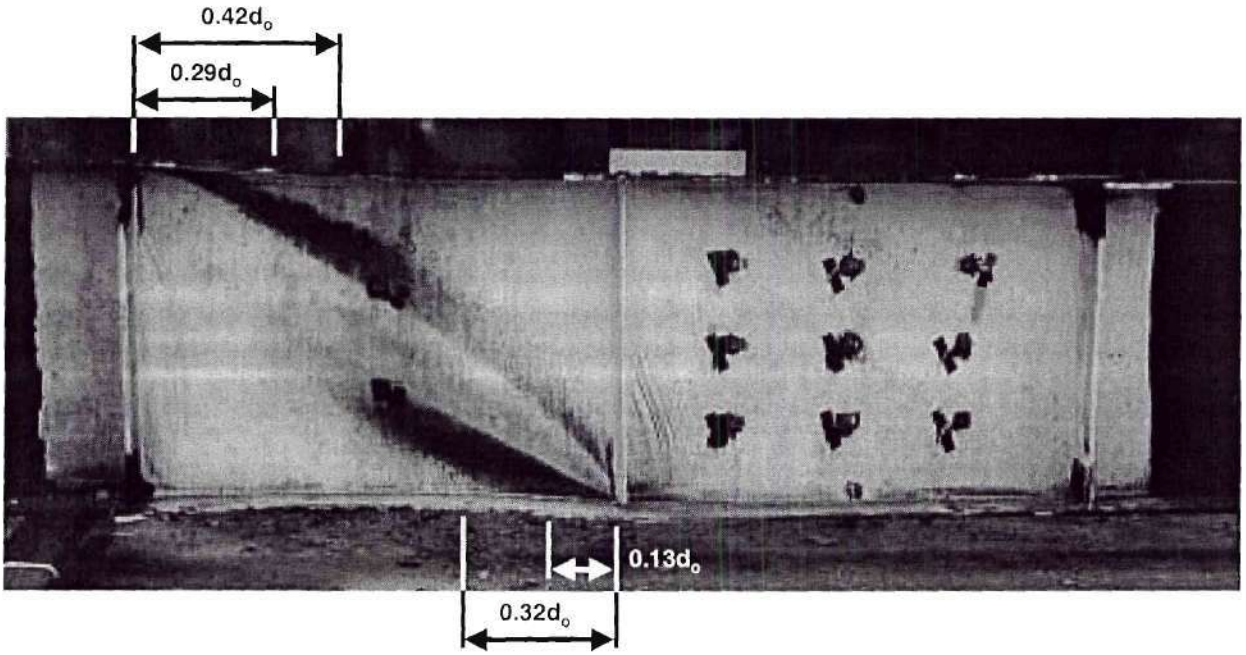

Figure 38 Girder S1-S – inside view after test showing approximate locations of maximum curvature and inflection points within the flanges

visual sighting along the flange tips on each side of the web in the final distorted girders, after they were removed from the test frame. The locations reported in the figures are the average of the positions determined at the flange tips on each side of the web.

In girder S1, the dominant wave in the web extended from the bottom-left corner of the test segment (in the outside view, Fig. 33) to a location on the top flange approximately $0.40d_o$ to the left of the top-right corner of this web panel (see Figs. 33 and 34). The center of this wave crossed the radial potentiometer locations at the middle of the test segment at approximately 0.80D, which is just above the rosette location R4. This is evidenced by the large negative (inward) deflection of the web panel at 3D/4 shown in Figs. 21 and 25. The center of this deformation also crossed approximately through the rosette location R2. The plastic curvature due to frame action in the top flange of this girder was largest at approximately $0.26d_o$ and $0.54d_o$ to the left of the top-right corner of the panel[1]; these locations corresponded roughly to the width at the top flange over which a significant amount of whitewash had spalled off the inside surface of the web (see Fig. 34). In the bottom flange of this girder, the flange plastic curvature due to frame action was highly localized under the bearing stiffener at location 2L, with the flange bent concave up over a length of only about 51 mm (2 in) under the stiffener. Otherwise, the bottom flange was bent concave downward within the test section, with the maximum plastic curvature occurring at approximately $0.32d_o$ from location 2L. One can observe from Figs. 33 and 34 that the flanges have deformed inward toward one another in the vicinity of this maximum plastic curvature location. This behavior is related to the upward (negative) displacement v_0 in Fig. 17.

1. Note that all the dimensions are discussed relative to the outside views. However, the dimensions to the maximum curvature locations and inflection points within the flanges are detailed on the inside view.

4.4 WEB PRINCIPAL STRAINS AND ELASTIC VON MISES STRESSES

Figures 41 through 44 and 47 through 50 illustrate the magnitudes and orientations of the principal strains e_1 and e_2 calculated from the average of the surface strains at rosettes R1 through R9, i.e., the web principal membrane strains in each of the tests. These figures show the principal membrane stains at the maximum shear capacity and at the end of the post-peak region of the response, just prior to removal of the loads. The tensile principal strains are indicated by the thin lines in these figures while the compressive principal strains are indicated by the thick lines. The locations at which yielding has occurred at these loading stages (outside surface, inside surface and/or mid-thickness), the level of V/V_{max} at which yielding first occurs at these locations, and the orientation of the principal direction Θ_{p1} with respect to the horizontal are shown next to the gage locations in each of these figures. In the figures illustrating the post-peak responses, the values of V/V_{max} are underlined for the locations at which yielding starts in the post-peak range. The onset of yielding was determined by calculating the elastic von Mises stress at each location based on the assumption of an isotropic elastic material and comparing this stress to the average yield strength of the web. This calculation neglects the influence of any initial residual stresses. The onset of yielding was taken as the first load increment at which the elastic von Mises stress exceeds the yield strength. The lines indicating the principal strain magnitudes are drawn to the same scale in Figs. 41, 42, 47 and 48, and are drawn to a scale 5.33 times larger in Figs. 43, 44, 49 and 50.

Figures 45 and 46 show the magnitudes and orientations of the outside surface strains in girders S1-S and S2-S at the maximum shear capacity. These figures are included to supplement Fig. 44, since the data was not available from several of the rosettes on the inside surface of

The dominant diagonal wave in girder S2 was similar to that in S1 except that it extended from the top-right corner to just below the mid-depth between rosettes R7 and R8 (located at $0.25d_o$ from the right-hand end of the panel in the outside view), and through rosettes R6 and the radial potentiometer location at /4 above the bottom of the web at the mid-length of the test segment (see Figs. 35 and 36). This wave intersected the bottom flange at approximately $0.30d_o$ from the bottom-left of this web panel (again in the outside view). The plastic curvature in the bottom flange due to frame action was largest at approximately $0.26d_o$ and $0.52d_o$ from the left side of this segment. However, the plastic curvature in the top flange was highly localized over the top of the bearing stiffener at location 2R in this girder, similar to the behavior under location 2L in girder S1 except that the flange was bent concave down over a length of about $0.13d_o$ within the test panel (see Fig. 36). The largest plastic curvature in the region of the top flange bent concave up occurred at about $0.27d_o$ from location 2R. One can observe that similar to girder S1, the flanges have deformed inward toward one another in the vicinity of this location.

The dominant wave in girders S1-S and S2-S extended essentially from corner to corner of the right-side web panel in S1-S and the left-side web panel in S2-S (see Figs. 37 and 38 for girder S1-S and Figs. 39 and 40 for girder S2-S). These panels were the opposite of the instrumented web panels in each of these girders. The behavior of the two web panels within the test segment of these girders was very similar up to the maximum load level (note the start of flaking of the white wash in the instrumented panel in Fig. 31). However, after the shear capacity was reached, the girder distortions localized within the panels that did not contain the strain rosettes. The estimated location of the maximum plastic curvature due to frame action (within the panels in which the distortions localized) was approximately the same in all the flanges of these girders, ranging from 0.32 to $0.42d_o$ from the ends of the failed panels.

localized at gage R2 (see Fig. 41). The membrane strains at R3 were also relatively large compared to the other gage locations at the maximum load level in this girder, although the web was not yielded through its entire thickness at this location when S1 reached its maximum capacity. In girder S2, the membrane strains were highly localized at R6 at the maximum load level.

The principal membrane tension orientations ranged from 16 degrees to 60 degrees relative to the horizontal direction in girder S1, with the largest angle of orientation occurring at gages R2 and R3 (where the strains were the largest), and from 25 to 37 degrees in girder S2, with the largest angle of orientation located at gage R6 (where the strains were the largest). In girders S1-S and S2-S, the principal membrane strains were oriented at 35 to 38 degrees for the gages along the tension band. This was approximately the same as the diagonal orientation between the corners of the web panel, $\Theta_d = 34$ degrees.

Figures 47 through 50 show the principal membrane strains at the end of the post-peak portion of the tests, just prior to removal of the load from the girders. Generally, in all of the tests, the principal strain orientation Θ_{p1} tended to decrease as the girders were deformed in post-peak. The angle Θ_{p1} ranged from 19 to 48 degrees for the gage locations that experienced plastic deformation in girder S1, and from 18 to 26 degrees for these gages in girder S2 at the end of the post-peak region. This angle reduced only slightly to a range of 30 to 35 degrees and 30 to 36 degrees in girders S1-S and S2-S respectively for the rosette locations that experienced plastic deformation. At the end of the post-peak region, the web was yielded through its entire thickness at all the rosette locations except R9 in girder S1, and at all the rosette locations except R1 and R2 in girder S2. The top-left region of the web panel experienced much smaller deformations in girder S1, and the bottom-right region of the panel experienced much smaller strains in girder S2. At the end of the post-peak region, the web was yielded through its entire thickness at

the web in the test of girder S2-S. The strains in these figures are drawn to the same scale as in the other figures corresponding to these girders.

Figures 51 through 58 give the magnitudes of the principal strain differences Δe_1 and Δe_2 and their orientations determined at the rosette locations at the above load stages. The principal strain differences Δe_1 and Δe_2 were determined by first calculating the strains e_x, e_y and γ_{xy} on the inside and outside surfaces at each of the rosette locations, then taking the difference between these strain components at the two surfaces, and finally calculating the principal values of these strain differences. The strain magnitudes in the figures corresponding to girders S1 and S2 are drawn to the same scale as displayed in the previous figures for these girders, whereas the strains in the plots corresponding to girders S1-S and S2-S are drawn to a scale 1.67 times larger.

Figures 41 to 44 indicate that at the maximum shear capacity in each of the tests, the web has just started to yield through its entire thickness along a diagonal tension band. It is interesting to note that Lee and Yoo (1998, 1999a) also observe this characteristic behavior in their studies of the shear strength of straight I girders. As would be expected, based on the locations at which the whitewash was starting to spall off in Figs. 29 through 32, this band cuts through gages R2 and R4 in girder S1, through gages R8 and R6 in girder S2, and through gages R3, R5 and R7 in girder S1-S. Although the strains at the inside rosettes at R3 and R5 were lost in girder S2-S, indications from the membrane strains at R7 and from the outside surface strains at R3 and R5 indicate that the web behavior in S1-S was very similar to that in girder S2-S. Both the tensile and compressive membrane strains were relatively large in magnitude at most of the gage locations along the tension band. In girder S1-S (and apparently also in S2-S, based on Fig. 46), these tensile and compressive membrane strains were fairly uniform at each of the gage locations along the tension band. However, in girder S1, the membrane strains were highly

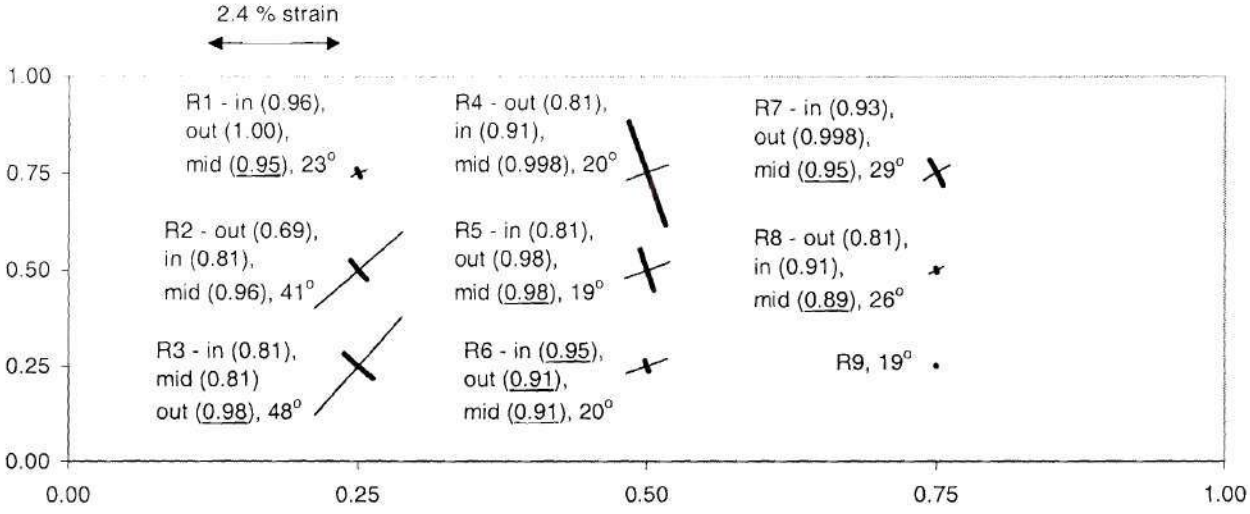

Figure 47 Girder S1 – yield locations and corresponding V/V_{max} values, and web principal membrane strain magnitudes and orientations at the end of the post-peak portion of the test

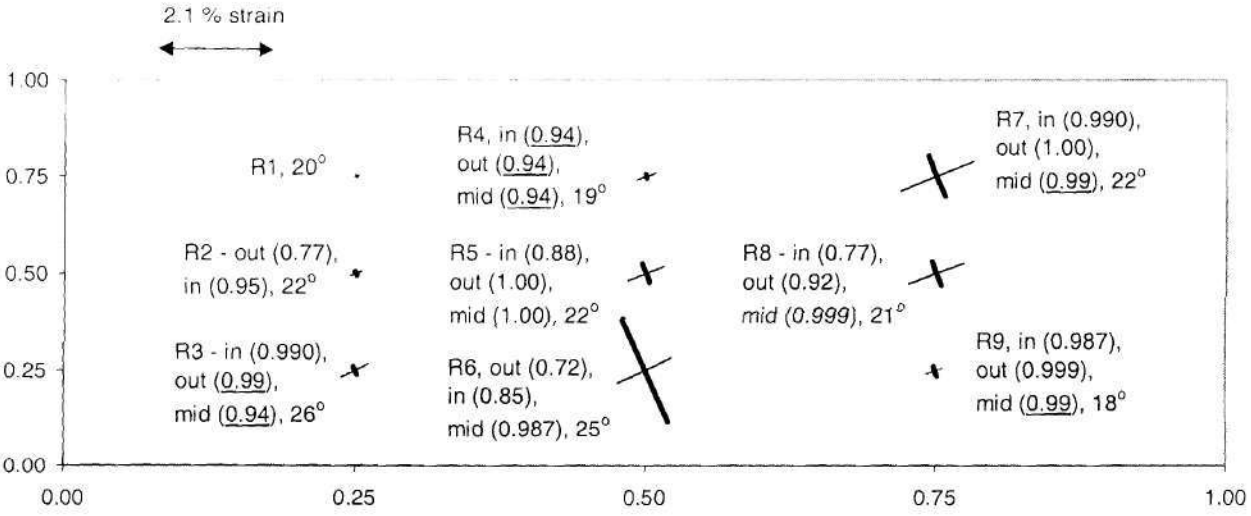

Figure 48 Girder S2 – yield locations and corresponding V/V_{max} values, and web principal membrane strain magnitudes and orientations at the end of the post-peak portion of the test

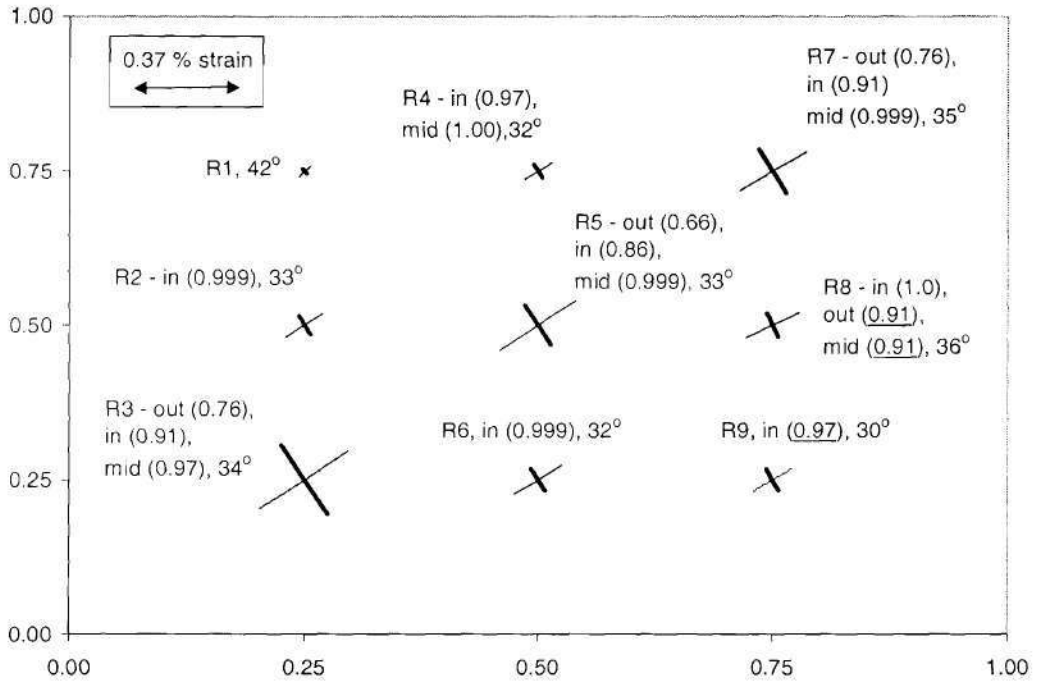

Figure 49 Girder S1-S – yield locations and corresponding V/V_{max} values, and web principal membrane strain magnitudes and orientations at the end of the post-peak portion of the test

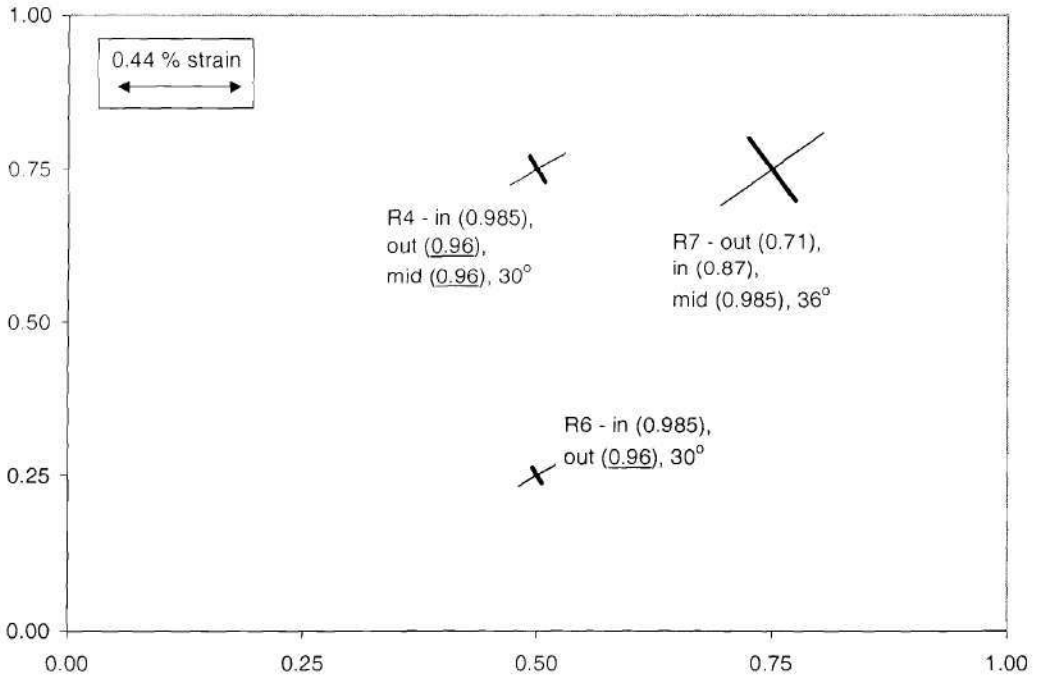

Figure 50 Girder S2-S – yield locations and corresponding V/V_{max} values, and web principal membrane strain magnitudes and orientations at rosettes R4, R6 and R7 at the end of the post-peak portion of the test

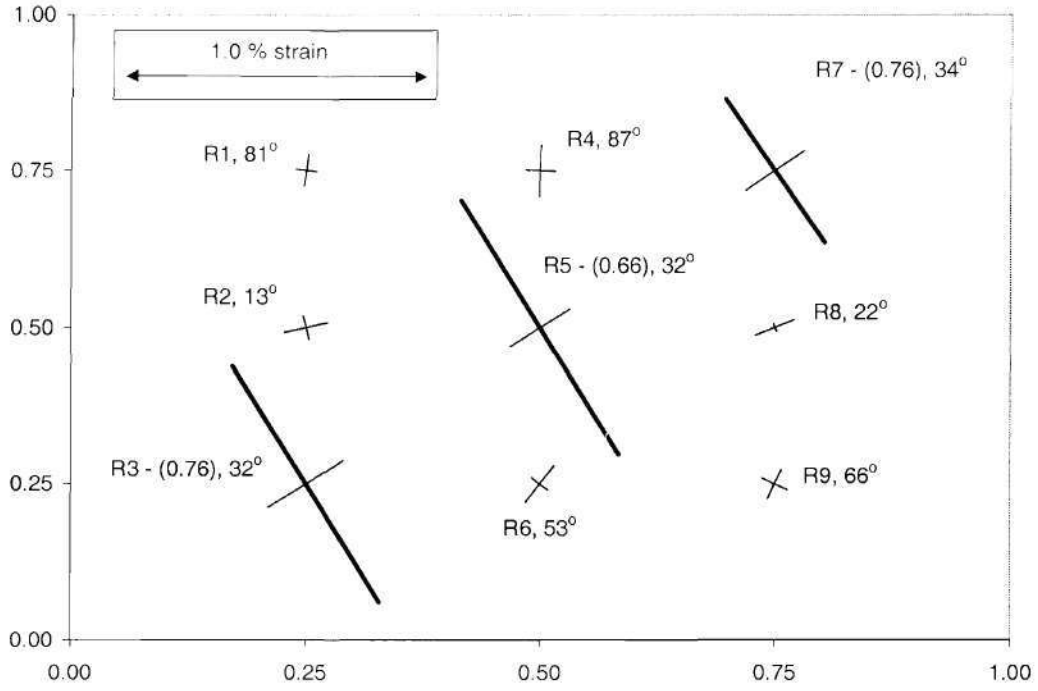

Figure 45 Girder S1-S – outside surface yield locations and corresponding V/V_{max} values, and principal strain magnitudes and orientations on outside surface at the maximum shear capacity

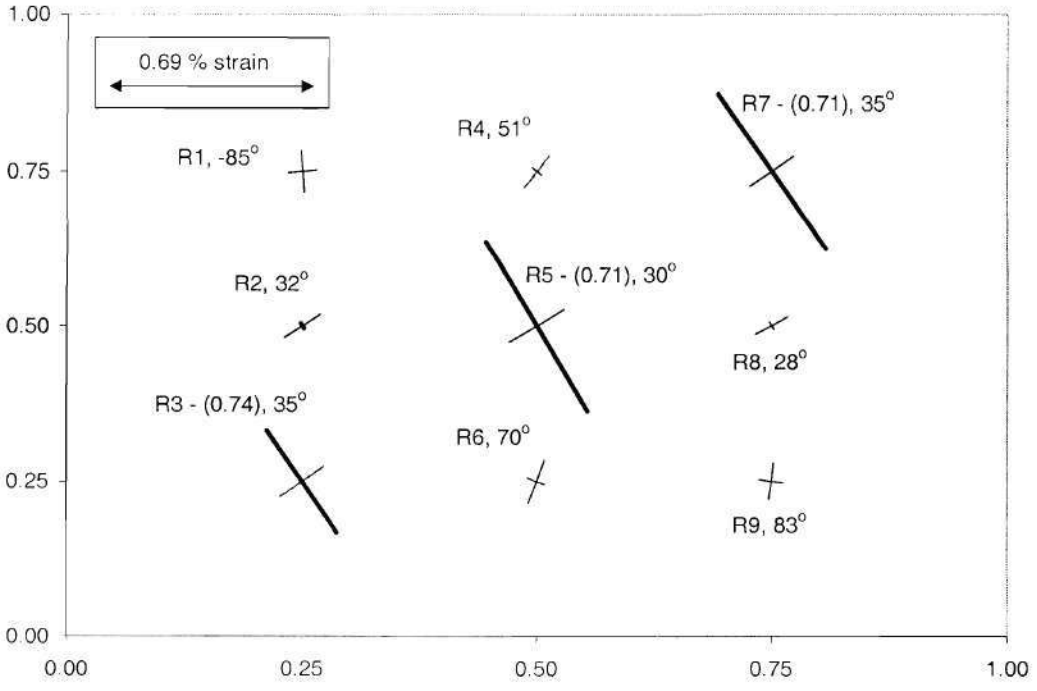

Figure 46 Girder S2-S – outside surface yield locations and corresponding V/V_{max} values, and principal strain magnitudes and orientations on outside surface at the maximum shear capacity

gages R3, R5, R7 and R8 in girder S1-S and at gages R4 and R7 (and likely also at gages R3 and R5, although the rosette data was incomplete at these positions).

At the end of the post-peak range of the response, the compressive principal membrane strain was significant at the rosettes R4 in girder S1 and at R6 in girder S2 (see Figs. 47 and 48). This is related to the fact that the distance between the flanges in the vicinity of the middle of the web panel was reduced to less than the original depth of the web as these girders were deformed in post-peak (see Figs. 33 and 34 for girder S1 and Figs. 35 and 36 for girder S2). Figures 47 and 48 indicate that this characteristic of the flange behavior was related in part to the diagonal compression within these web panels.

Figures 51 to 54 indicate significant web plate bending in the transverse diagonal direction along the diagonal tension band at the maximum shear capacity in girders S2, S1-S and S2-S. The heavy lines, indicating principal compression strain differences, are associated with compressive strains on the outside surface of the webs due to plate bending. The orientations of the principal strain differences at the maximum shear strength of girder S1 exhibit a complicated pattern, similar to the orientations of the principal membrane strain in this girder at this load stage (see Fig. 41). It is believed that the more complex nature of the web behavior in girder S1, compared to S2, was caused by the existence of different initial geometric imperfections and/or residual stresses in these two girders. However, there is no conclusive evidence to this effect.

Figures 55 to 58 show the principal strain differences in the web panels at the end of the post-peak range of the response. One can observe that the orientation of the largest strain differences in Fig. 55, corresponding to girder S1, were starting to line up with the direction of the maximum principal membrane strains at this load stage (see Fig. 47). For the other girders, the largest principal strain differences were compressive (causing compression on the outside

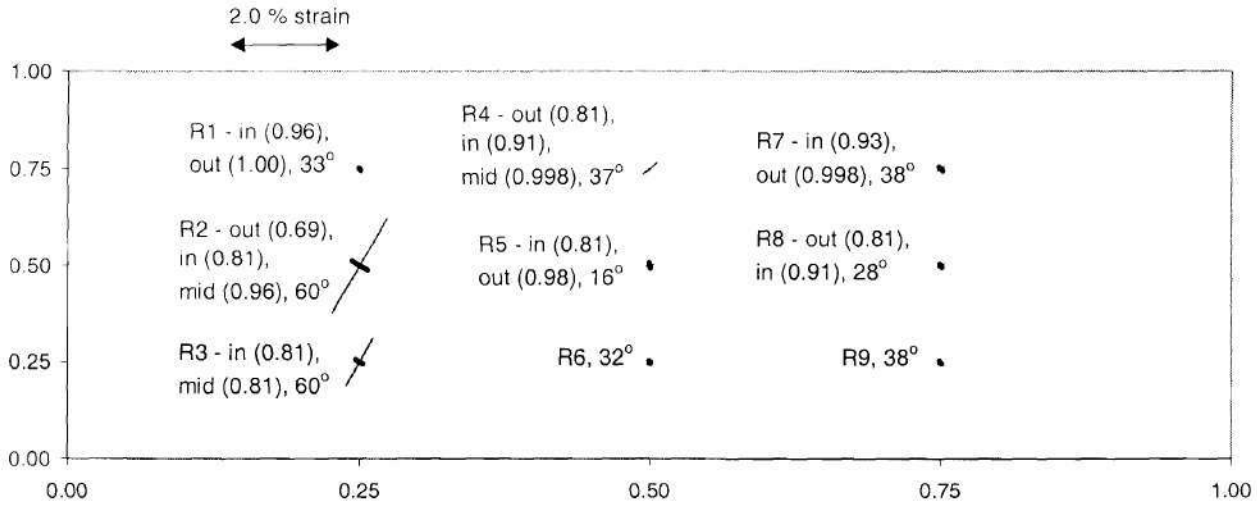

Figure 41 Girder S1 – yield locations and corresponding V/V_{max} values, and web principal membrane strain magnitudes and orientations at the maximum shear capacity

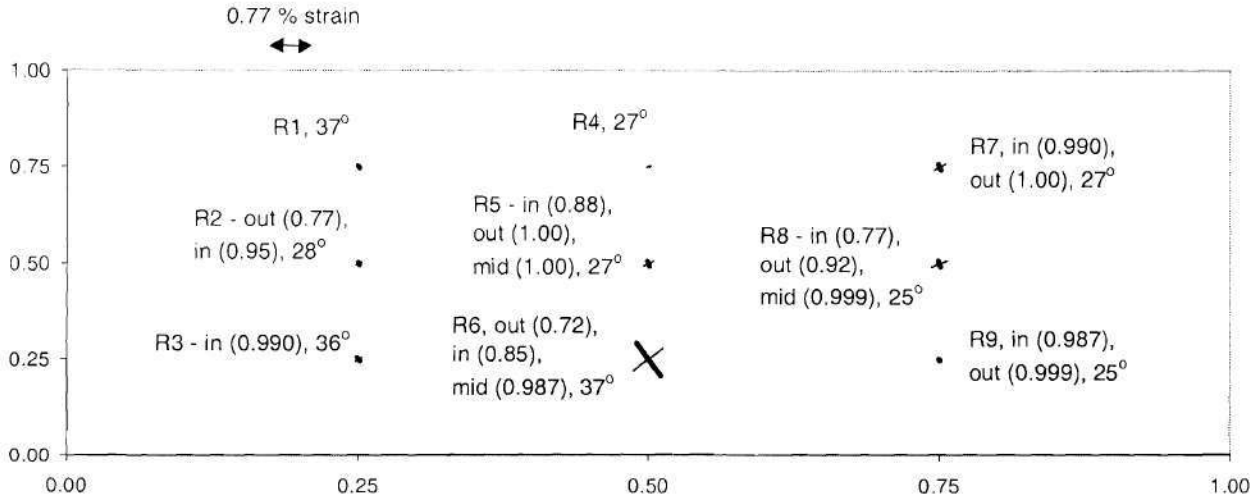

Figure 42 Girder S2 – yield locations and corresponding V/V_{max} values, and web principal membrane strain magnitudes and orientations at the maximum shear capacity

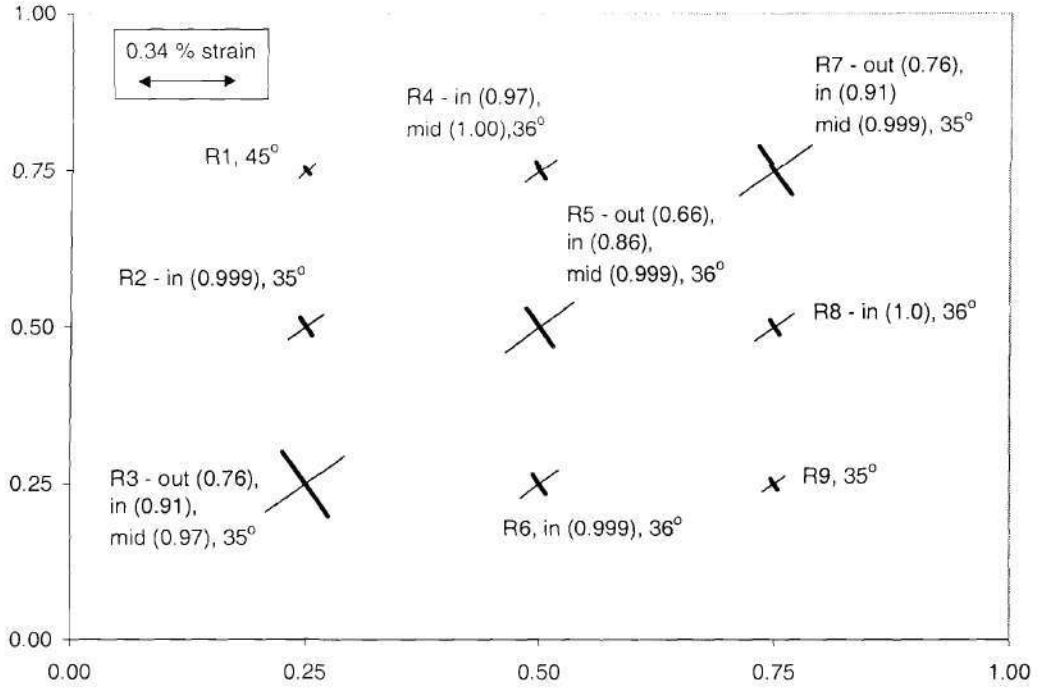

Figure 43 Girder S1-S – yield locations and corresponding V/V_{max} values, and web principal membrane strain magnitudes and orientations at the maximum shear capacity

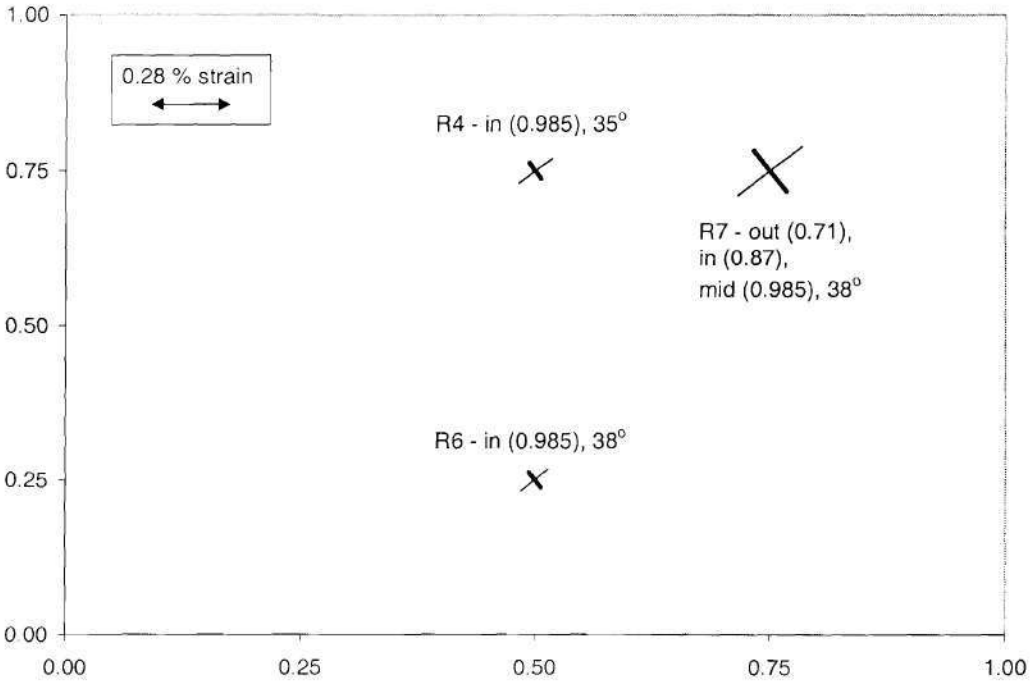

Figure 44 Girder S2-S – yield locations and corresponding V/V_{max} values, and web principal membrane strain magnitudes and orientations at rosettes R4, R6 and R7 at the maximum shear capacity

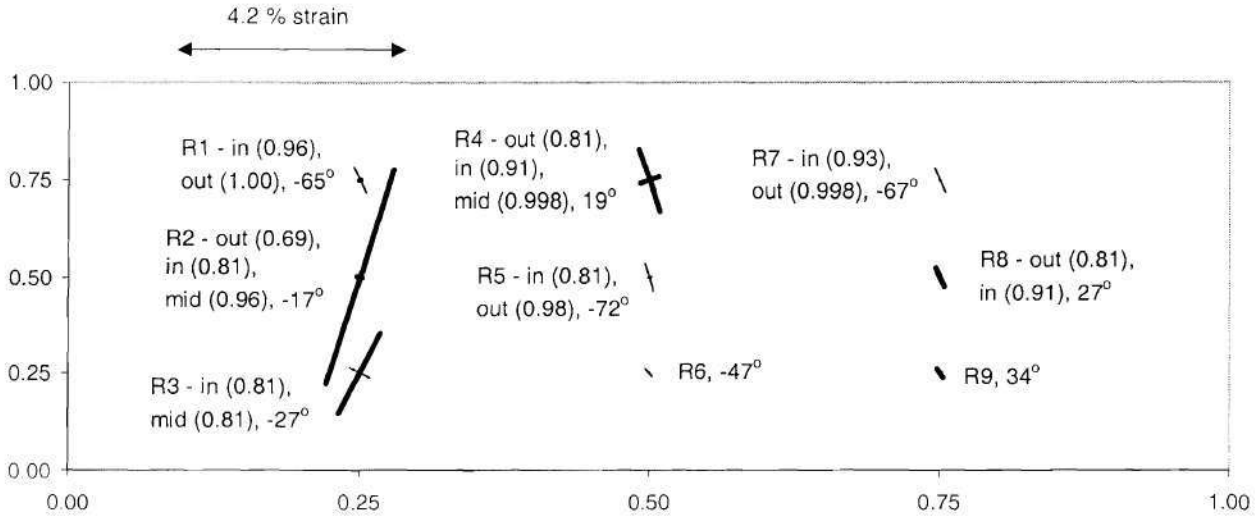

Figure 51 Girder S1 – yield locations and corresponding V/V_{max} values, and web principal strain difference magnitudes and orientations at the maximum shear capacity

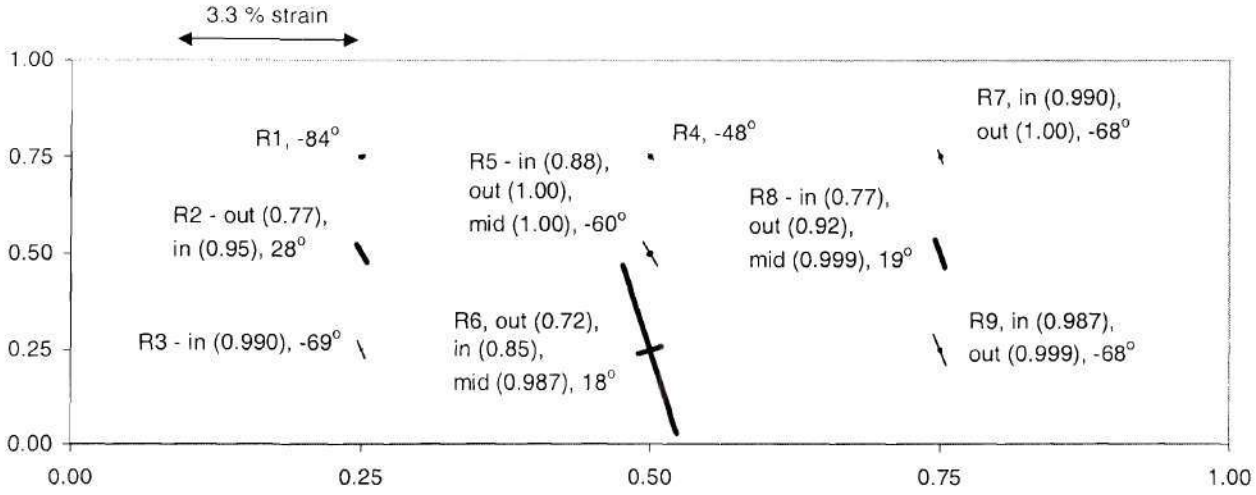

Figure 52 Girder S2 – yield locations and corresponding V/V_{max} values, and web principal strain difference magnitudes and orientations at the maximum shear capacity

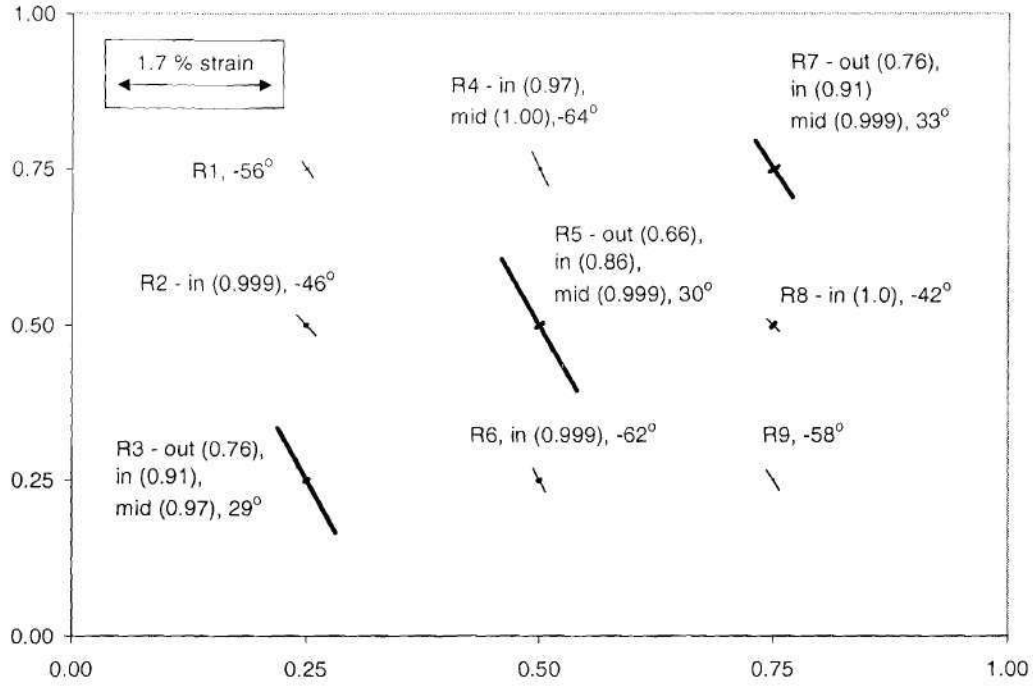

Figure 53 Girder S1-S – yield locations and corresponding V/V_{max} values, and web principal strain difference magnitudes and orientations at the maximum shear capacity

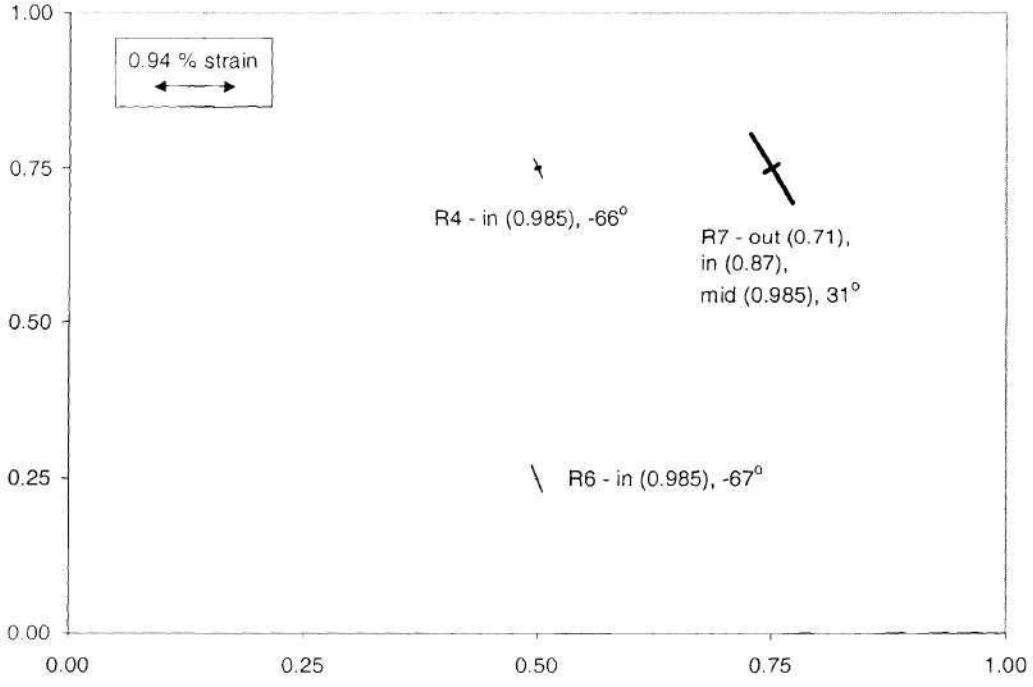

Figure 54 Girder S2-S – yield locations and corresponding V/V_{max} values, and web principal strain difference magnitudes and orientations at the maximum shear capacity

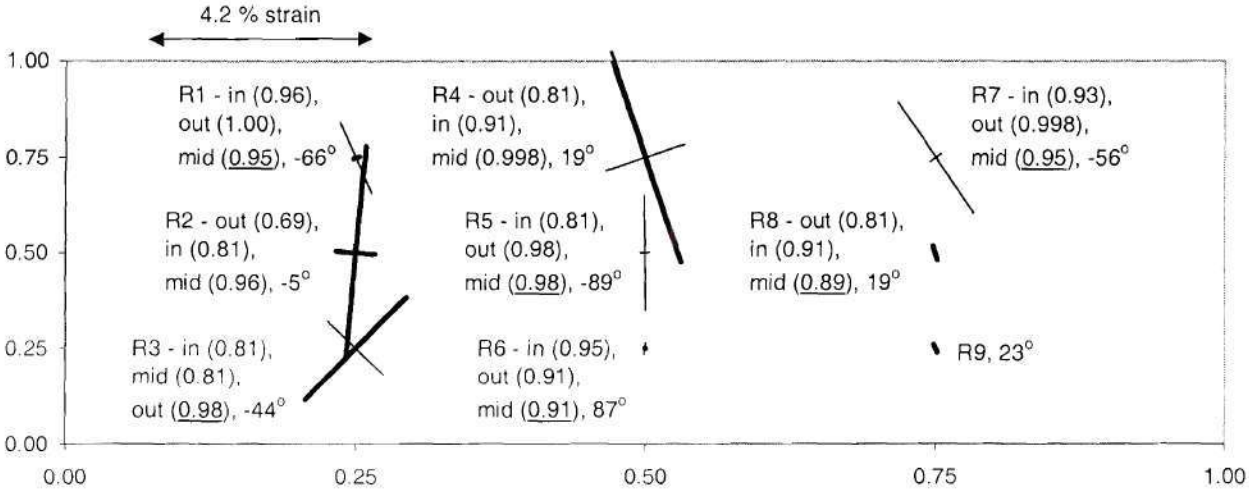

Figure 55 Girder S1 – yield locations and corresponding V/V_{max} values, and web principal strain difference magnitudes and orientations at the end of the post-peak portion of the test

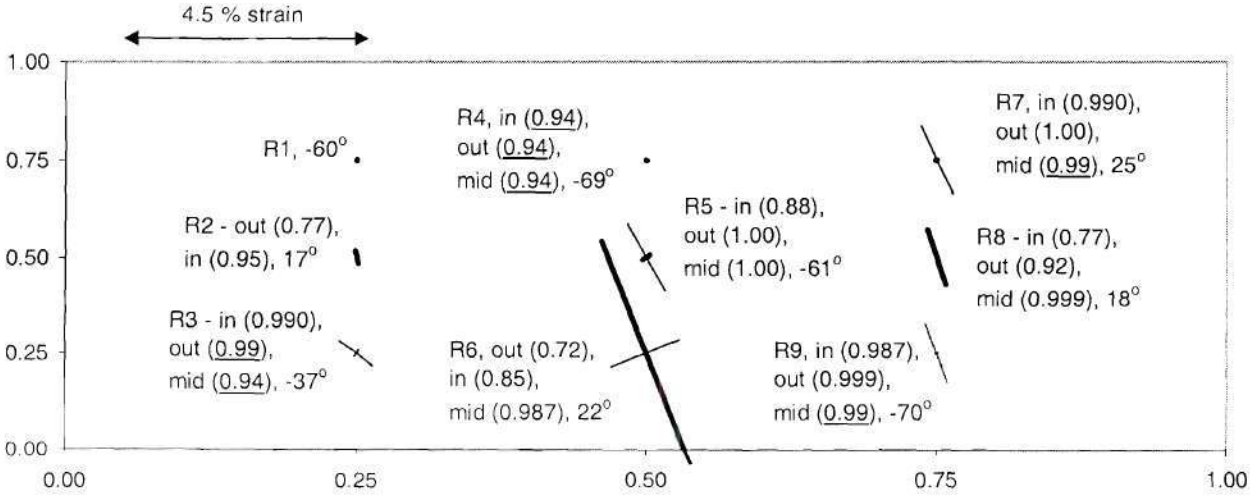

Figure 56 Girder S2 – yield locations and corresponding V/V_{max} values, and web principal strain difference magnitudes and orientations at the end of the post-peak portion of the test

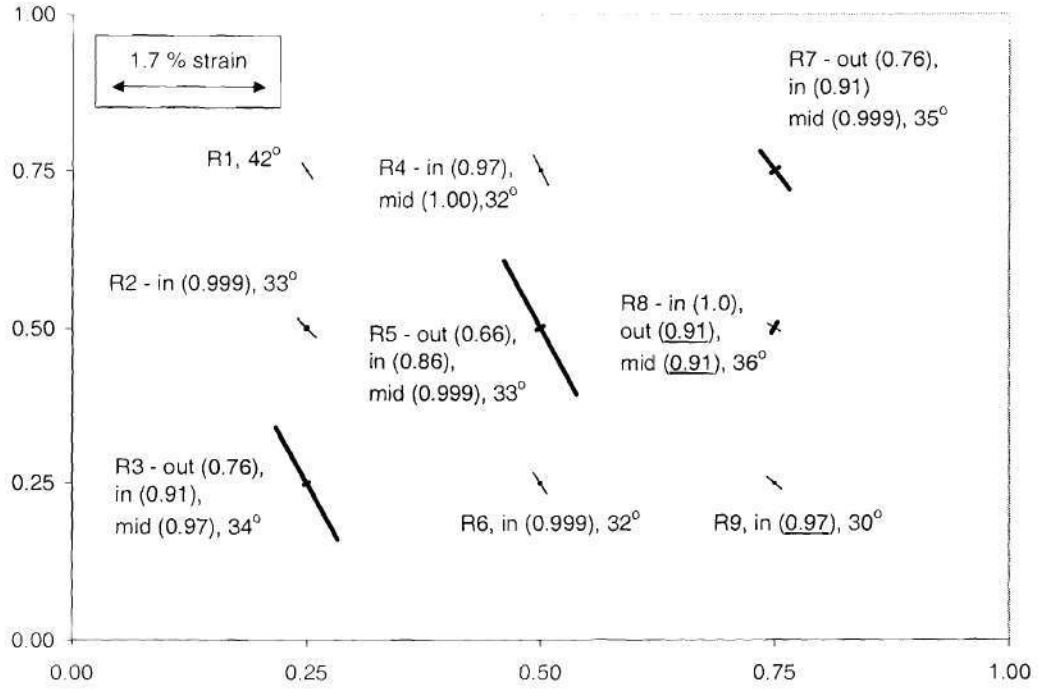

Figure 57 Girder S1-S – yield locations and corresponding V/V_{max} values, and web principal strain difference magnitudes and orientations at the end of the post-peak portion of the test

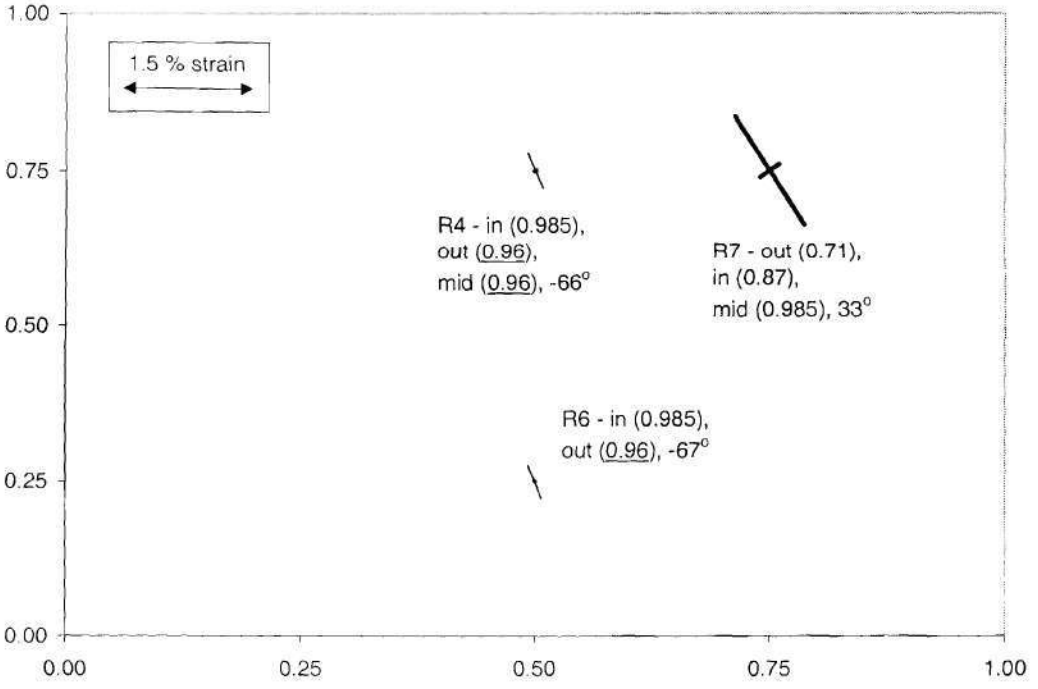

Figure 58 Girder S2-S – yield locations and corresponding V/V_{max} values, and web principal strain difference magnitudes and orientations at the end of the post-peak portion of the test

surface due to plate bending) and at orientations approximately orthogonal to the direction of the principal membrane tension in the web panels at the end of the post-peak range of the response. The deformation of the flanges inward toward one another in girders S1 and S2, visible in Figs. 33 and 34 for S1 and 35 and 36 for S2, and the upward (negative) displacement v_0 at the mid-length of these girders shown in Figs. 17 and 18, appears to be related to the plate bending of the web associated with the above compressive principal strain differences in addition to the compressive membrane strains at approximately the same orientation, discussed previously with respect to Figs. 47 and 48. Furthermore, it is evident that there were significant compressive principal strain differences orthogonal to the principal membrane tension direction in the instrumented panels of girders S1-S and S2-S at the end of the post-peak response. By inspection of Figs. 37 and 38 for girder S1-S and Figs. 39 and 40 for girder S2-S, one can observe that the flanges within the non-instrumented panels were deformed inward toward one another to a more significant degree, and that the corresponding post-peak strains in these panels were obviously larger than those in the instrumented ones.

Detailed plots of the variation of the web principal membrane strains and strain differences and their orientations are presented in Figs. 59 through 62 for girder S2. Figure 59 shows the variation in the principal membrane strain orientation Θ_{p1} at gages R1 through R9, Fig. 60 shows the variation in the principal membrane strain e_1, Fig. 61 shows the variation in the principal membrane strain e_2, and Fig. 62 shows the variation in the largest of the principal strain differences Δe_1 or Δe_2, all as a function of the normalized applied web shear force. In each of these plots, the load level corresponding to the onset of yielding at the first surface location is indicated by a large grey circle, the load level corresponding to the onset of yielding at both surface locations is indicated by a large grey square, and the load level corresponding to onset of yield-

panel, which when combined with the destabilizing effects in the diagonal compression direction, eventually result in the maximum strength of the web being reached. These figures emphasize the fact that a significant portion of the web plate was yielded prior to reaching the maximum shear strength. The maximum strength was reached due to a combination of the effects of progressive yielding and diagonal compression within the web panel. Figures 42, 52, 60 to 62 and 63 to 65 clearly show that the final failure of the web was associated with large increases in tensile and compressive membrane strains as well as large increases in web plate bending in a direction approximately transverse to the direction of principal membrane tension in the vicinity of the rosettes R6.

Figures 66 through 71 for girder S1-S are organized similarly to Figs. 59 through 65 for girder S2. The overall behavior in the strains as a function of the load level was similar to that for girder S1 except that the angles Θ_{p1} in Fig. 66 for girder S1-S were generally larger than those in Fig. 59 for girder S2. Also, the web membrane and plate bending strains subsequent to reaching the maximum shear capacity were relatively uniform along the diagonal of the web panel in girder S1-S whereas they were more localized to the region in the vicinity of rosettes R6 in girder S2. The pre-peak maximum principal strains and strain differences were similar in both girders, even though girder S2 has a larger panel aspect ratio and a smaller radius of curvature.

The overall behavior associated with the maximum shear capacity of the web of girder S1 was similar to that in girder S2. However, possibly because of the near bifurcation behavior as evidenced by the plots in Figs. 21 and 25, influenced by potentially different imperfections and residual stresses, the orientations of the web strains were not as simple as in girder S2. Based on the experimental data collected for these girders, it is not possible to identify any specific source of the slightly larger shear capacity achieved in girder S1 compared to girder S2. Obviously, one

ing at the mid-surface of the web plate is indicated by a black circle or square. A black circle indicates that yielding was detected at one of the surface gages and at the mid-surface of the plate and a black square indicates the onset of yielding throughout the thickness of the web, i.e., at the two surface gages and at the mid-thickness.

Figure 59 illustrates the tendency of the angle Θ_{p1} to reduce to some extent as the web shear increased within the pre-peak portion of the test. However, this figure also shows that the largest changes in Θ_{p1} occurred after the maximum shear capacity of the web was reached. Figures 60 and 61 show that the web membrane strains varied in a reasonably linear fashion with the web shear force essentially up to the point that the web shear capacity was reached. These curves started to exhibit a plateau at the most highly strained rosette locations at load levels slightly larger than about 95 percent of the capacity. By comparison of Figs. 61 and 62, one can observe that the web maximum principal strain differences at rosettes R2, R5, R6 and R8 were larger than the maximum web principal membrane strains within the pre-peak range of the response.

It is interesting that at the onset of yielding at either surface of the web plate, indicated by the large grey circles in Figs. 59 through 62, there was generally little change in the slope of the curves. In other words, the apparent onset of yielding does not have any significant impact on the response. This was the case even though the load level at initial yielding was calculated neglecting potential residual stress effects and even though first yield was defined by the first data point at which the elastic von Mises stress exceeded the average yield strength of the web plate – in some cases the elastic von Mises stress for this data point was significantly larger than F_y.

Figures 63 through 65 show the variation of the elastic von Mises stresses at locations R1 through R9 in girder S2. These figures help illustrate the progression of yielding within the web

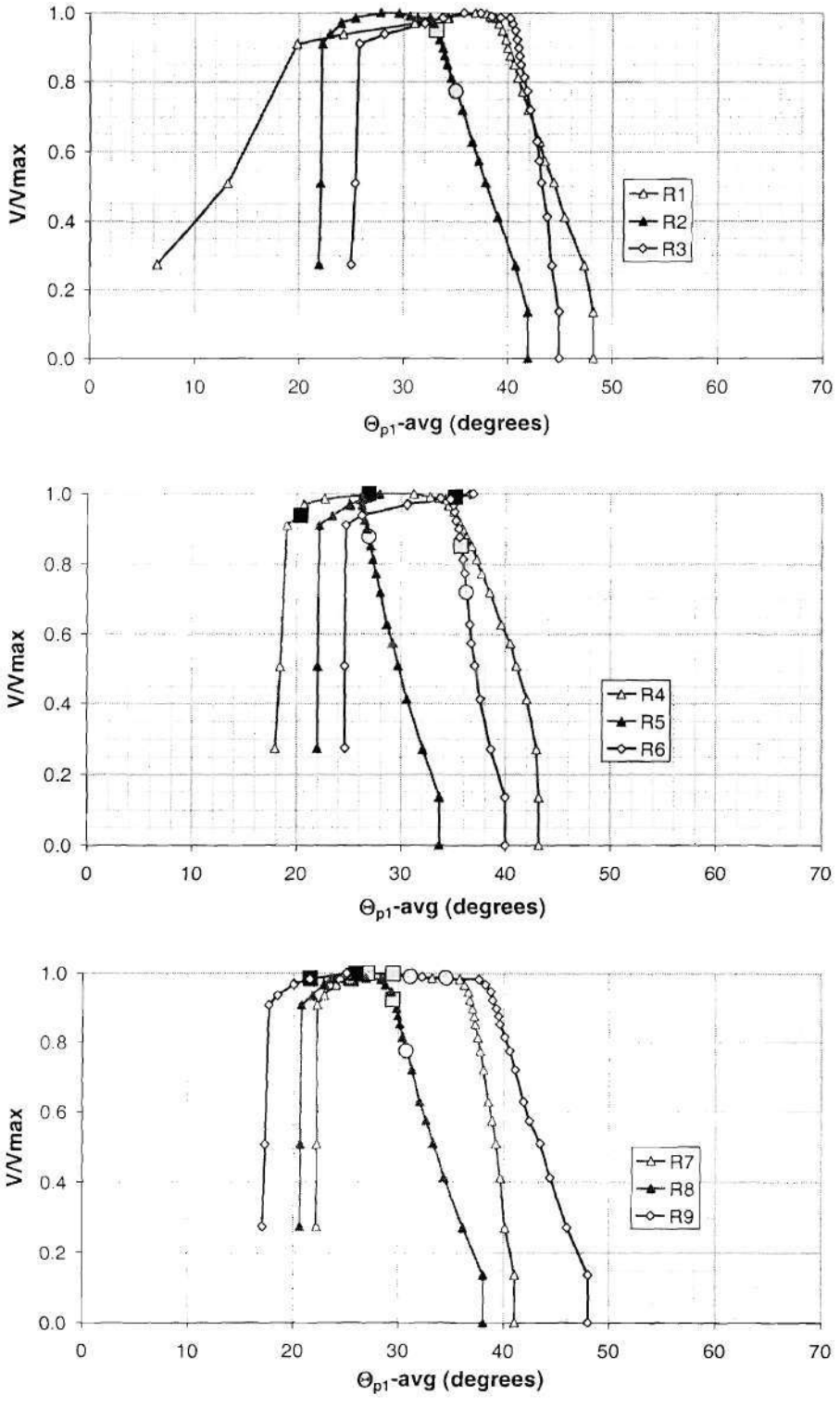

Figure 59 Orientation of maximum principal membrane strains Θ_{p1} versus V/V_{max} in girder S2

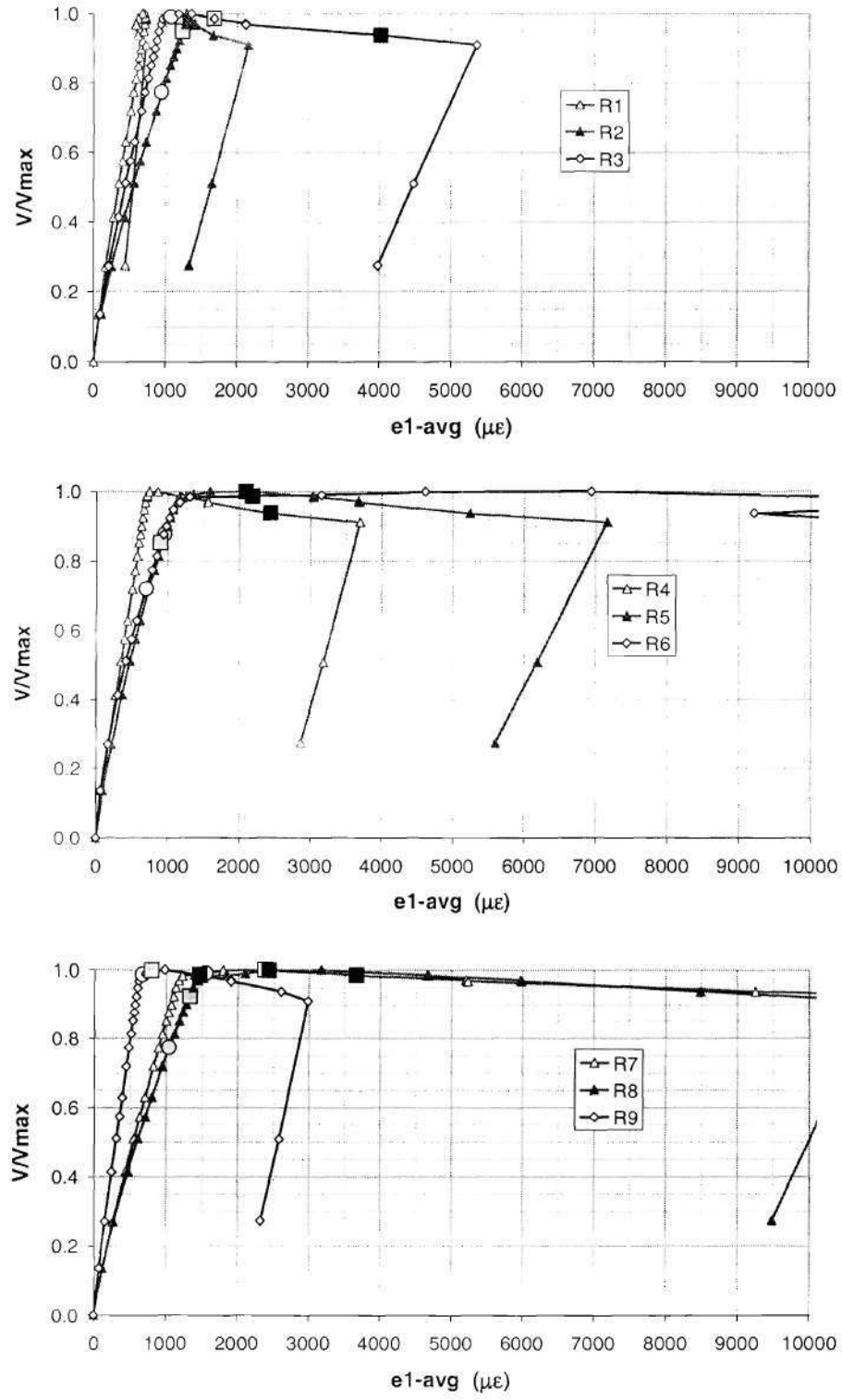

Figure 60 Maximum (tensile) principal membrane strains e_1 versus V/V_{max} in girder S2

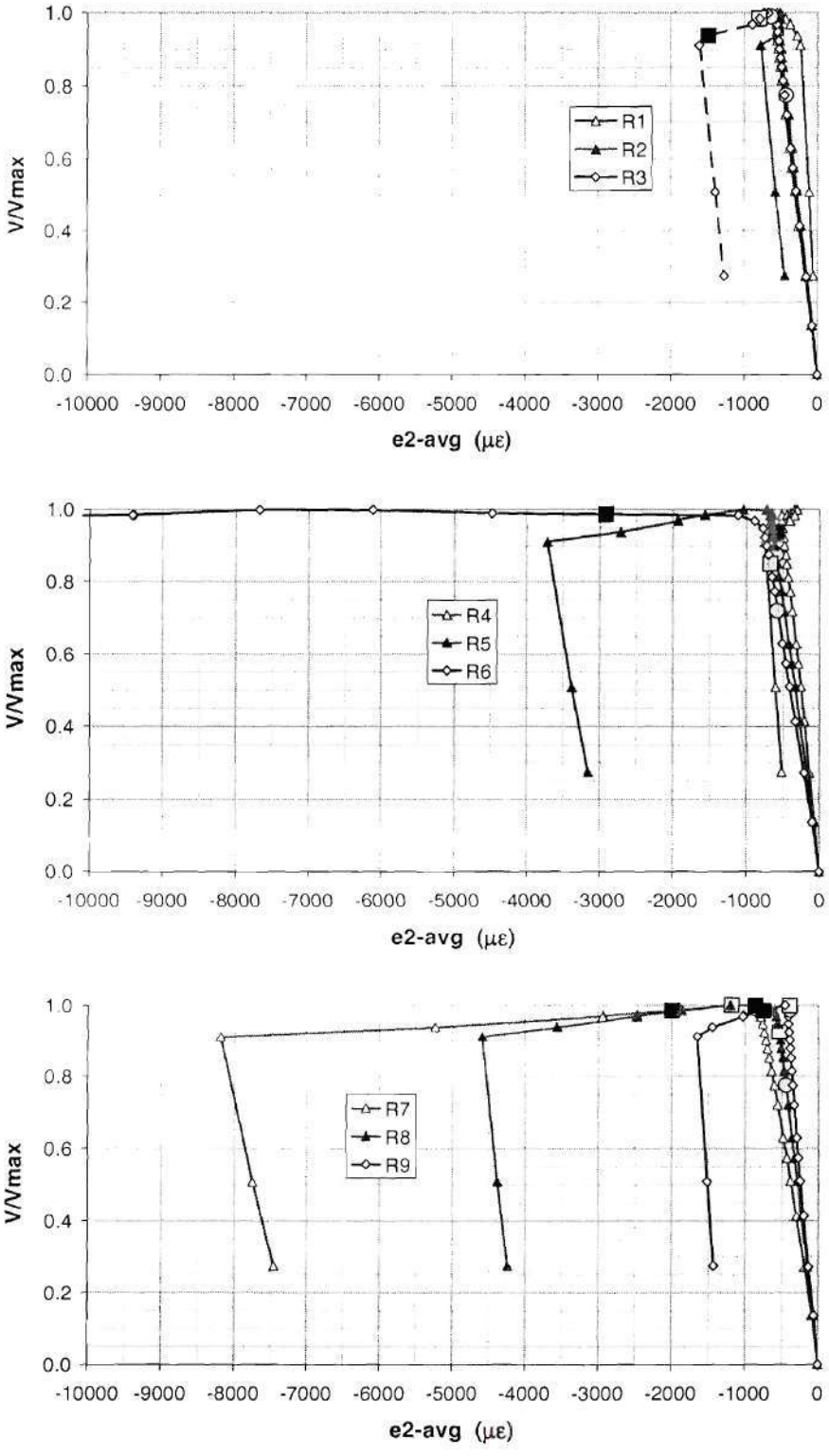

Figure 61 Minimum (compressive) principal membrane strains e_2 versus V/V_{max} in girder S2

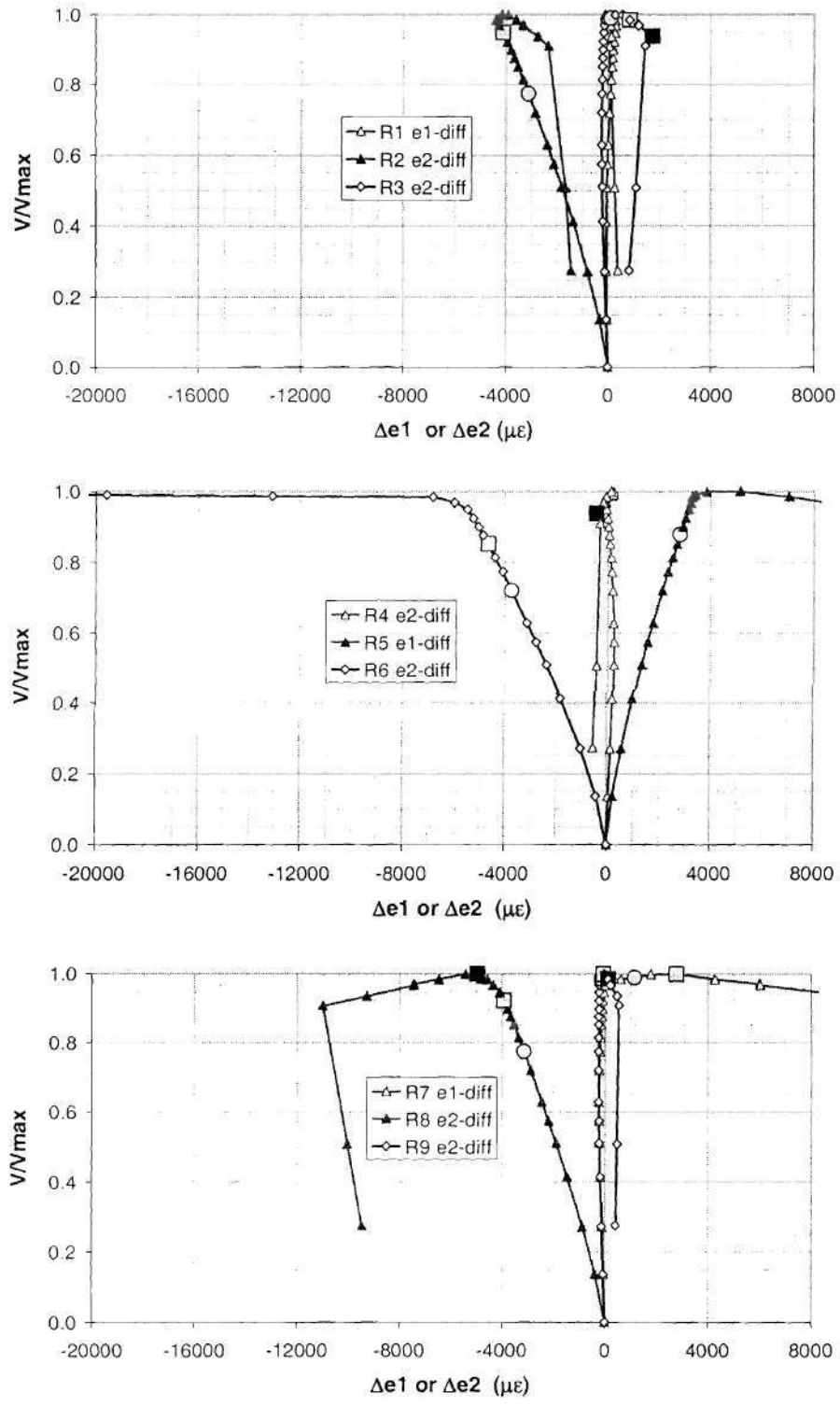

Figure 62 Largest magnitude of the principal strain differences Δe_1 and Δe_2 versus V/V_{max} in girder S2

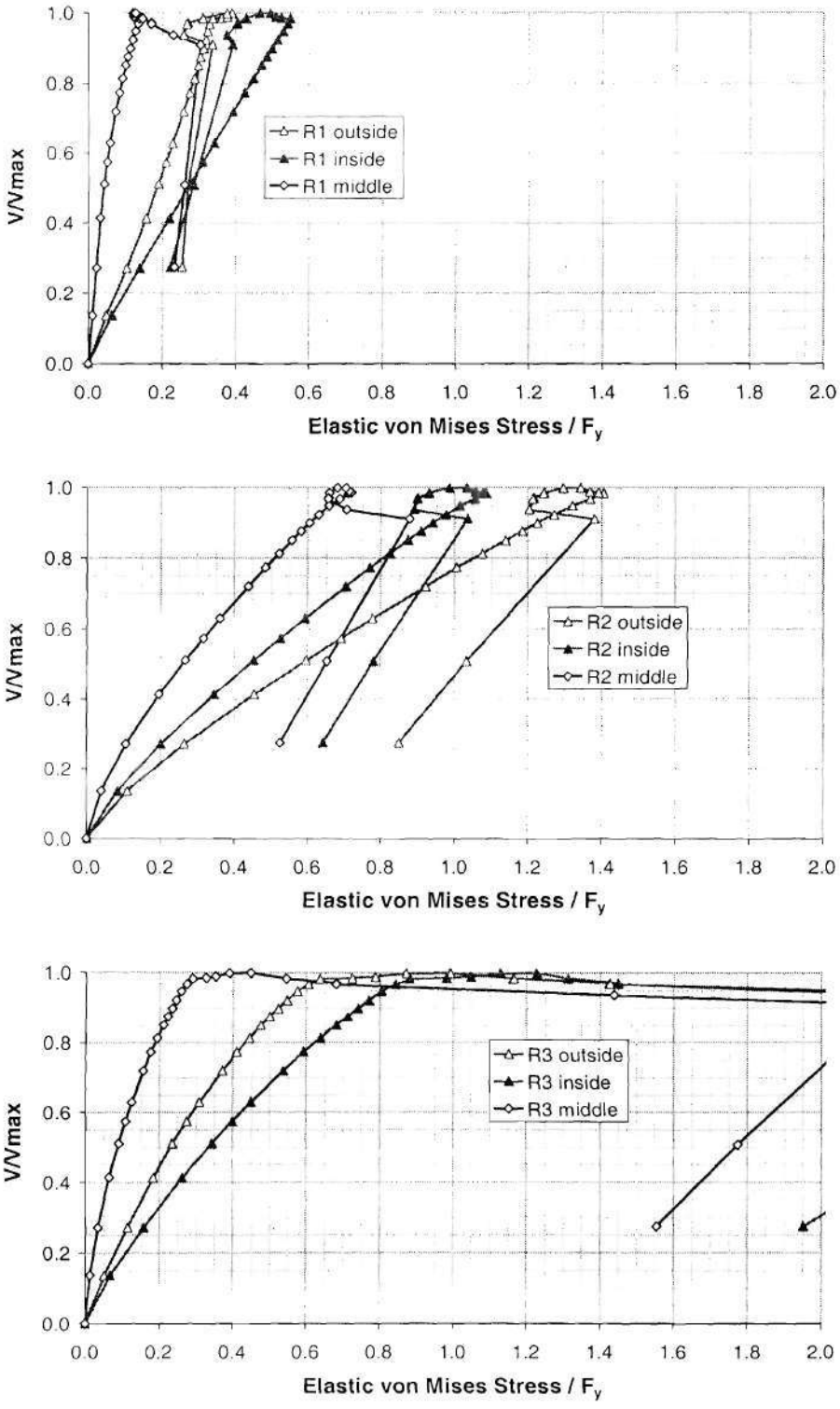

Figure 63 Normalized elastic von Mises stresses for gages R1 through R3 versus V/V_{max} in girder S2

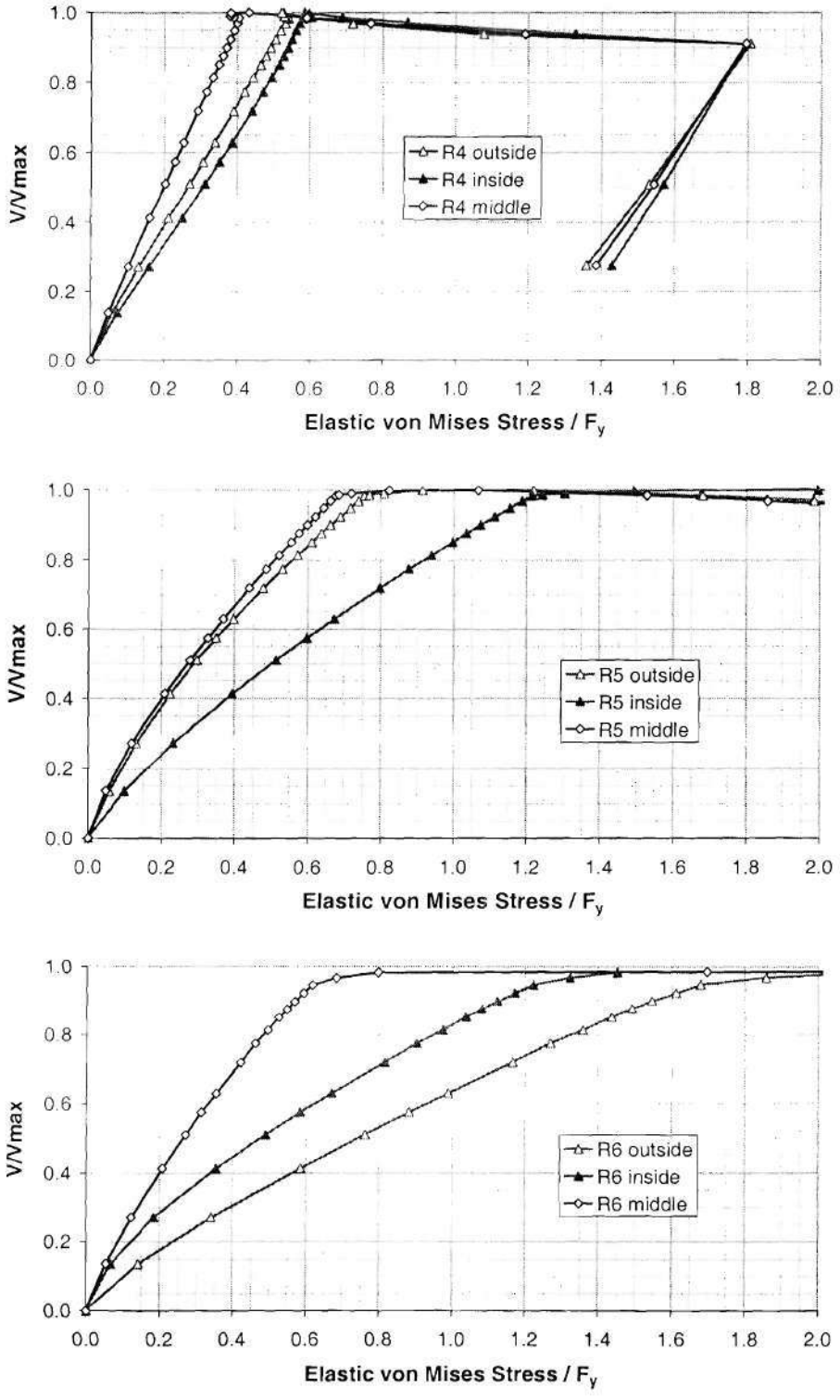

Figure 64 Normalized elastic von Mises stresses for gages R4 through R6 versus V/V_{max} in girder S2

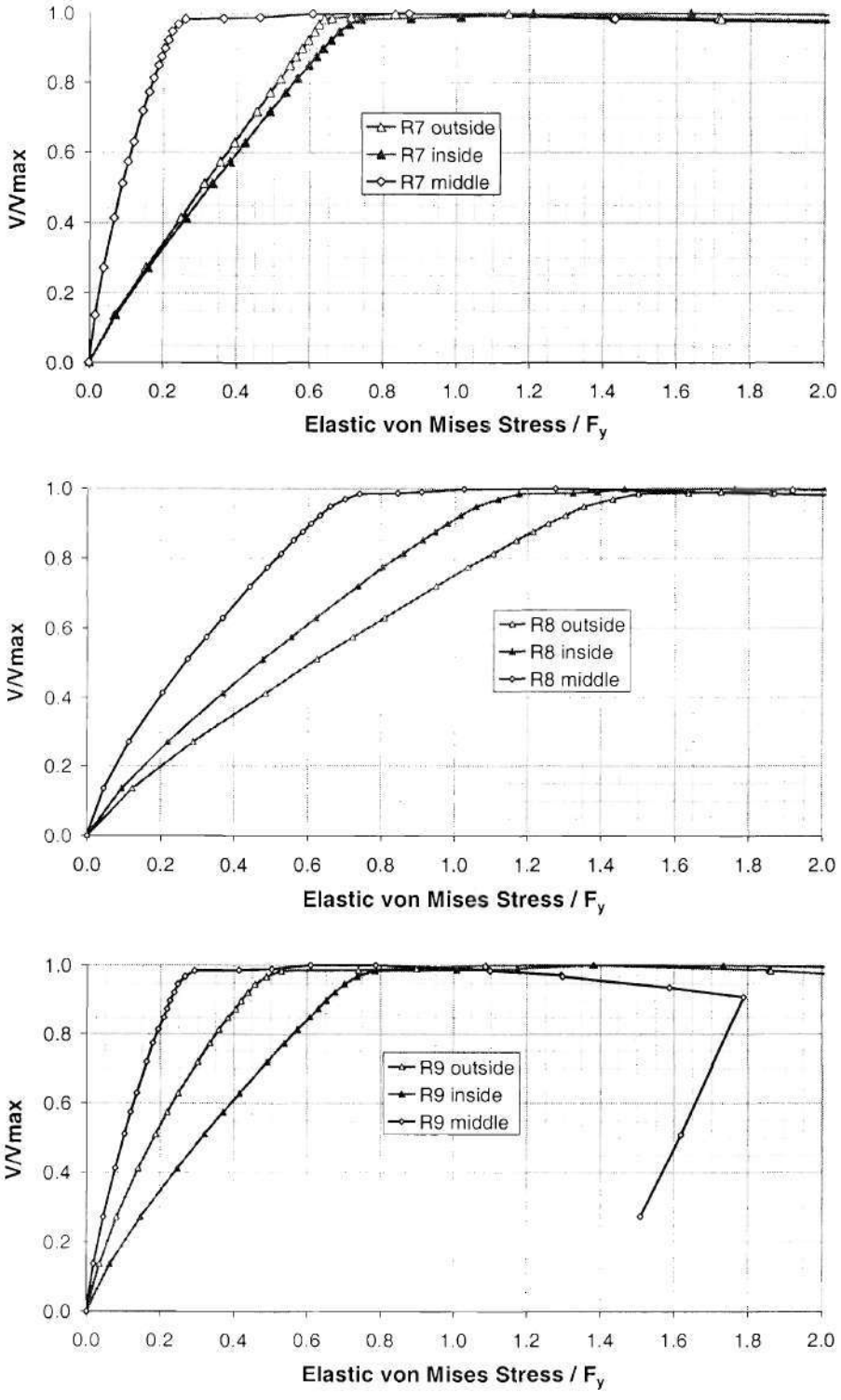

Figure 65 Normalized elastic von Mises stresses for gages R7 through R9 versus V/V_{max} in girder S2

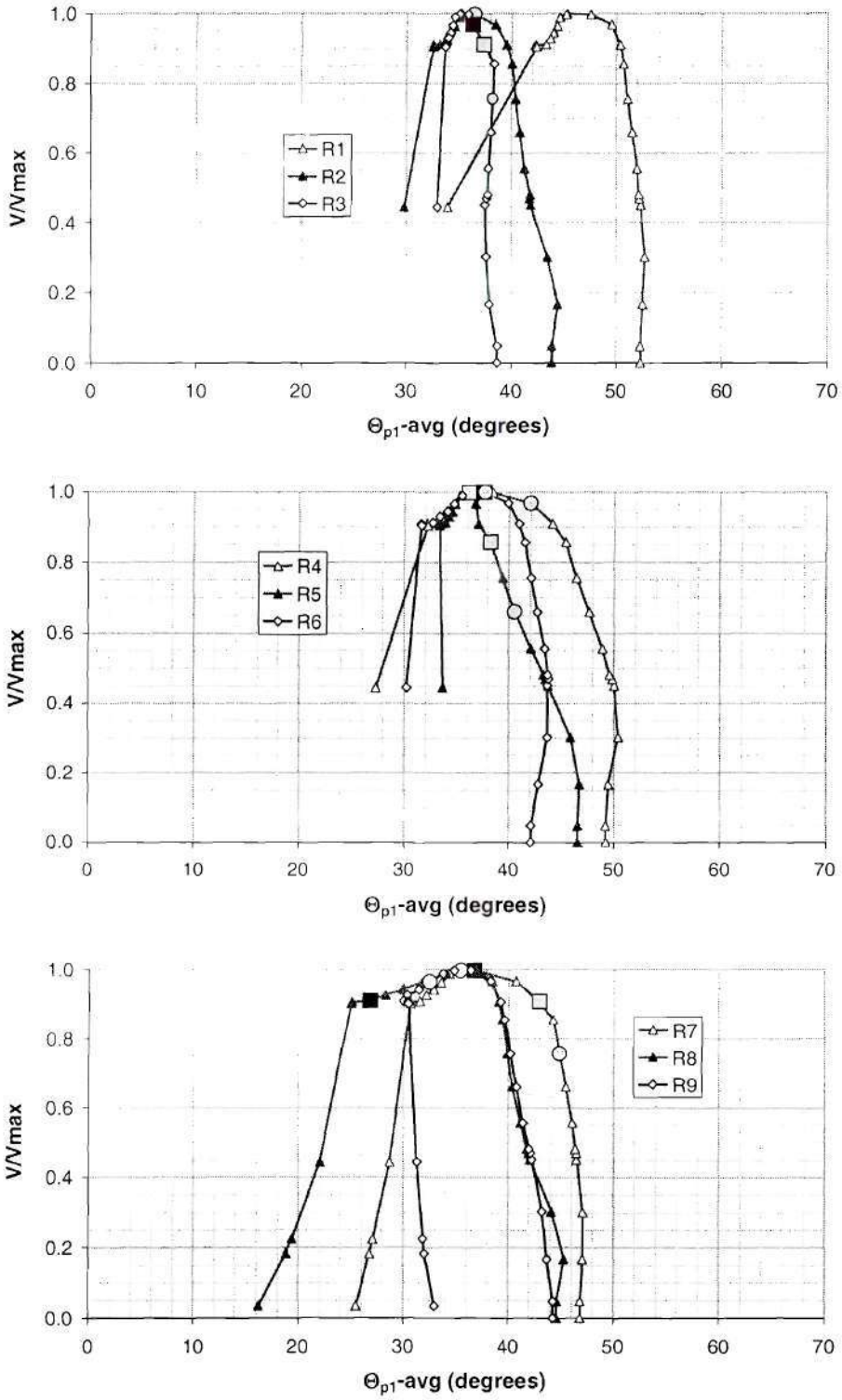

Figure 66 Orientation of maximum principal membrane strains Θ_{p1} versus V/V_{max} in girder S1-S

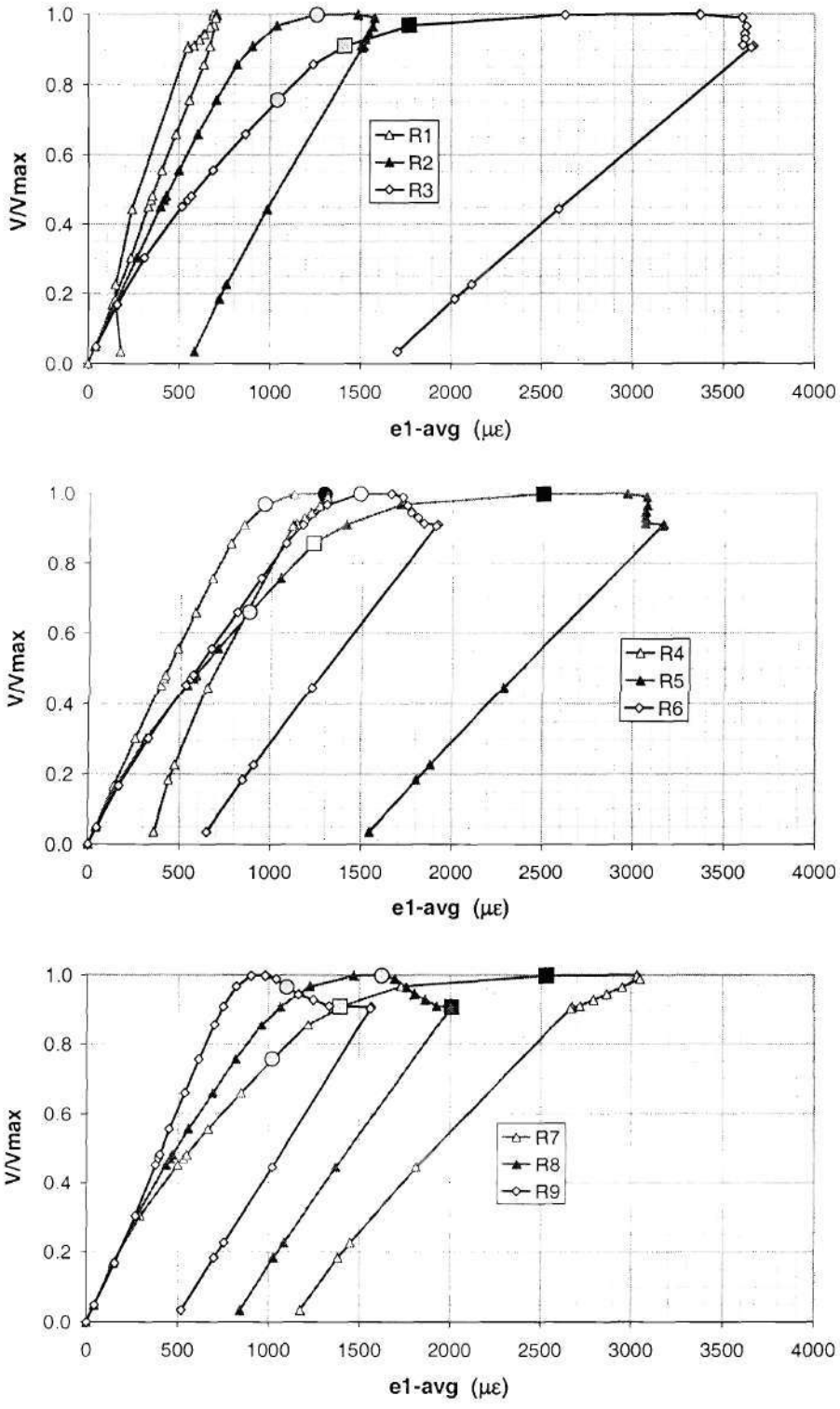

Figure 67 Maximum (tensile) principal membrane strains e_1 versus V/V_{max} in girder S1-S

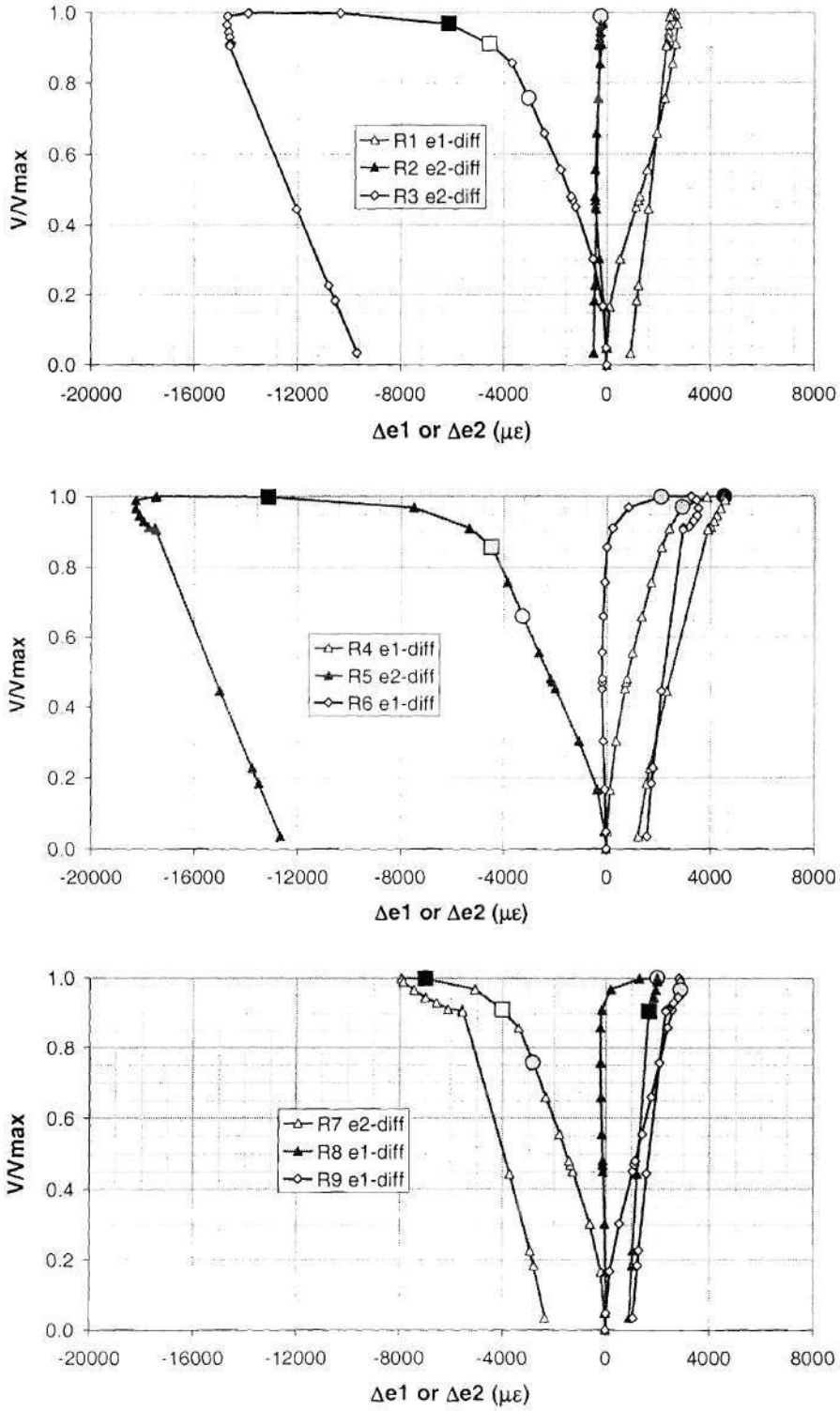

Figure 68 Largest magnitude of the principal strain differences Δe_1 and Δe_2 versus V/V_{max} in girder S1-S

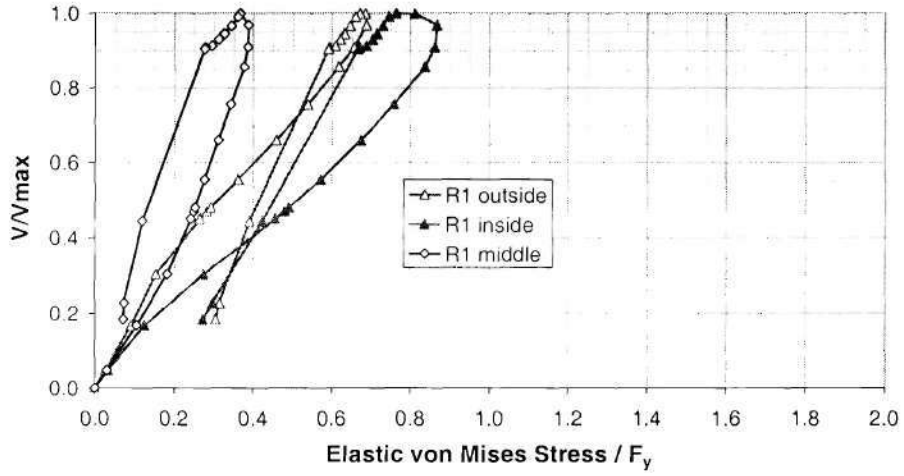

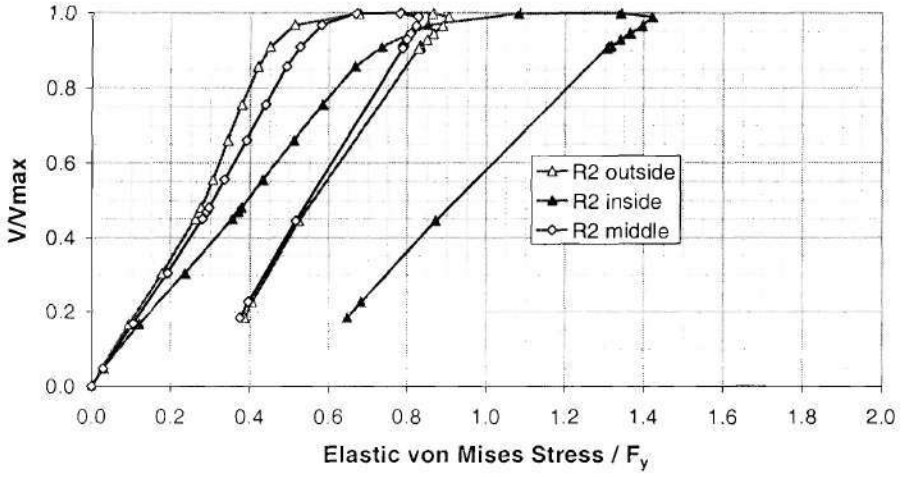

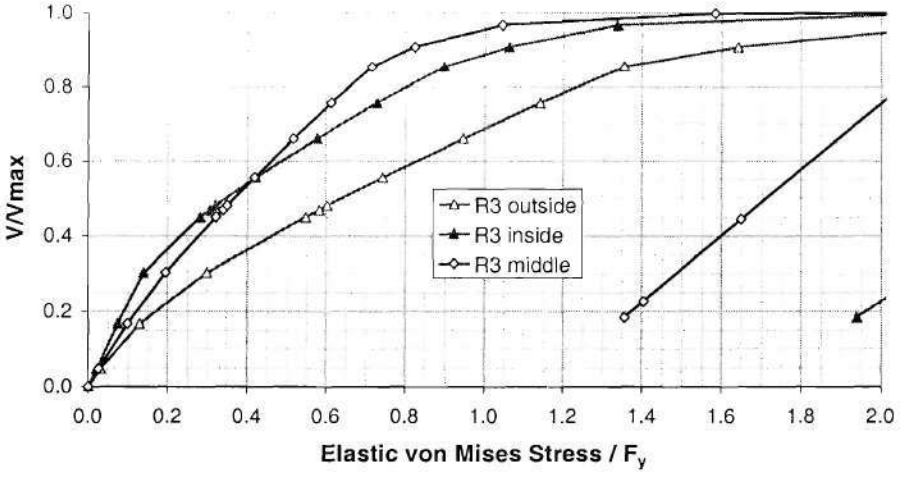

Figure 69 Normalized elastic von Mises stresses for gages R1 through R3 versus V/V_{max} in girder S1-S

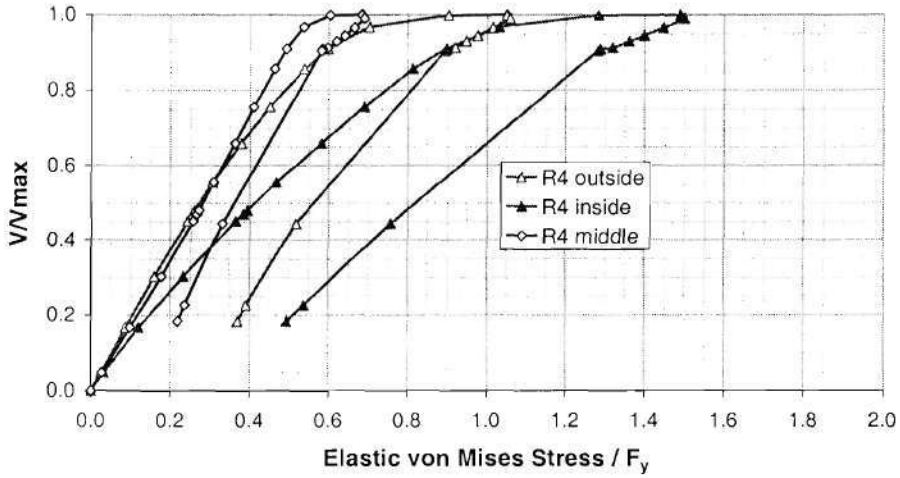

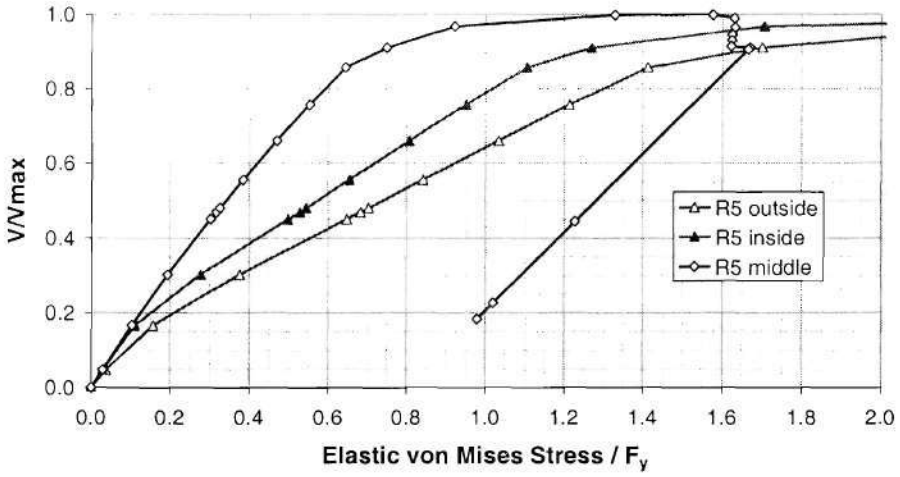

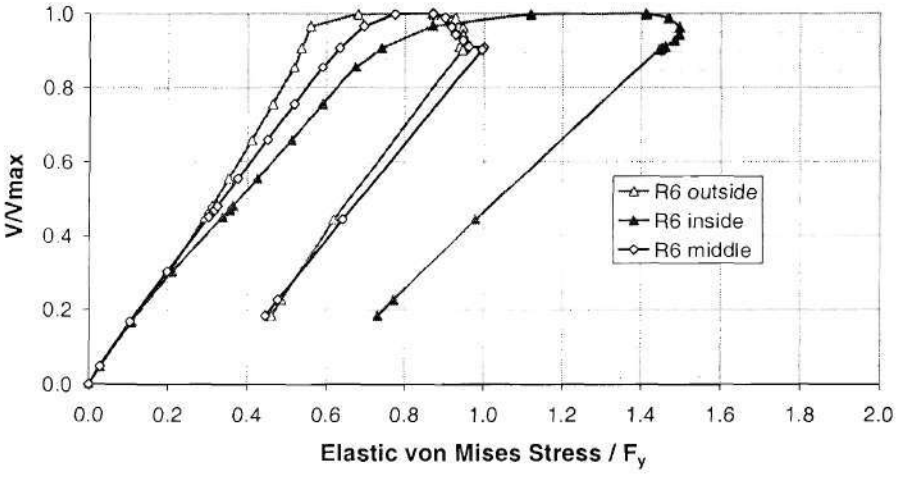

Figure 70 Normalized elastic von Mises stresses for gages R4 through R6 versus V/V_{max} in girder S1-S

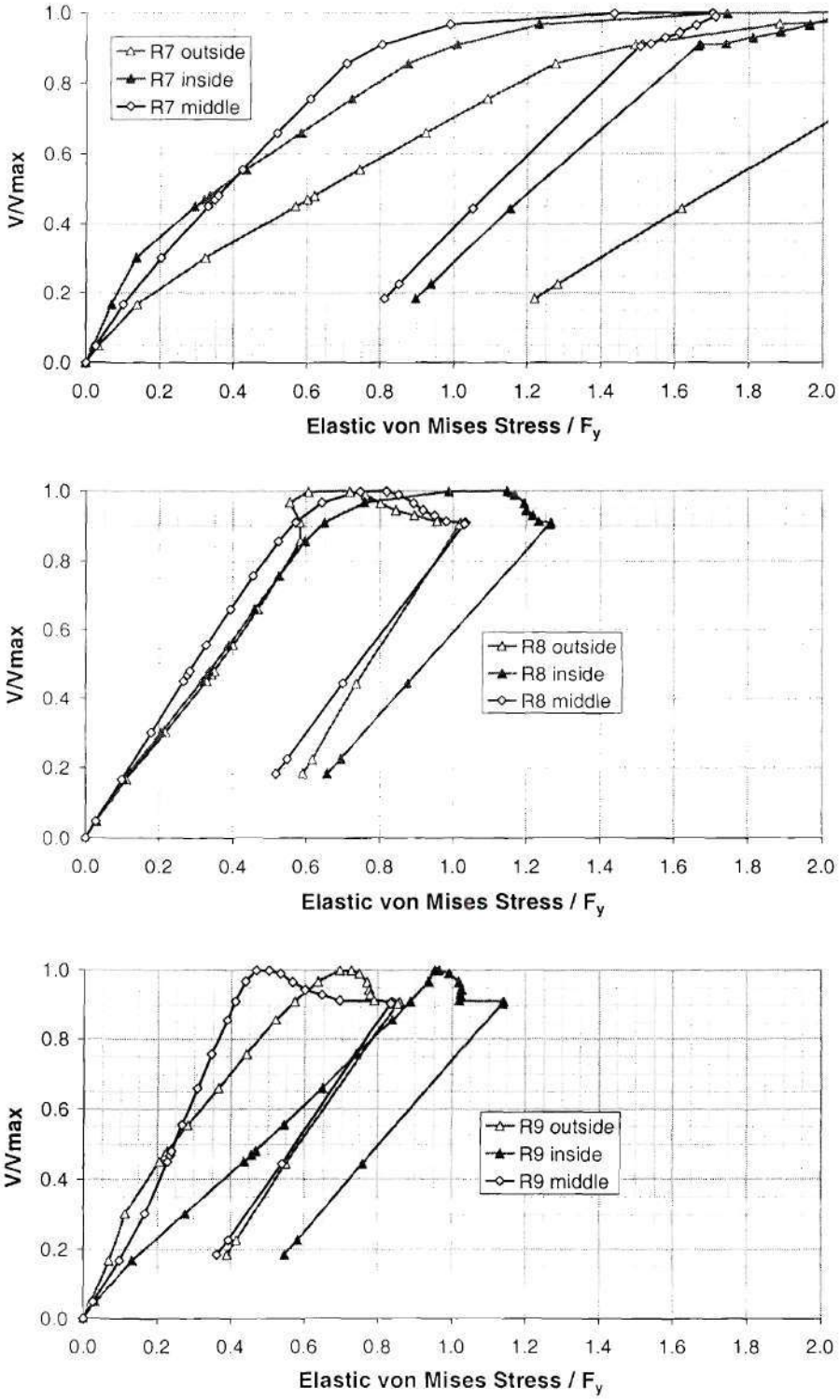

Figure 71 Normalized elastic von Mises stresses for gages R7 through R9 versus V/V_{max} in girder S1-S

might expect that the shear capacity of S1 would be larger than that of S2 due to the larger radius of curvature in S1.

The overall behavior in girder S2-S was also very similar to that in S1-S. However, the strains at the outside surface at rosettes R3 and R5 were somewhat larger in girder S1-S compared to girder S2-S at the maximum shear capacity (see Figs. 45 and 46). Also, the web radial deflections were somewhat larger at the peak load in girder S1-S (see Figs. 27 and 28). These differences are possibly due to different initial imperfections and residual stresses, and it can be inferred that the larger strength of girder S2-S was due to these effects. However, part of the differences between the shear capacities in these tests may be due to the small experimental error exhibited in the measurement of V_{max} in girder S1-S as discussed previously.

4.5 FLANGE STRAINS

Figures 72 through 75 show the flange longitudinal membrane strains and strain differences measured at $d_o/4$ from location 2R within the test panel of girder S2. By inspection of Figs. 35 and 36, one can observe that the maximum concave upward plastic curvature in the top flange (due to frame action of the flanges) occurred approximately at this location. Also, by inspection of Figs. 35 and 36, it is apparent that the deformation of the bottom flange was relatively minor at this cross-section. Figure 72 shows that the average membrane strain in the top flange was rather small but tensile within the pre-peak range of the response at the above location, as would be expected based on the loading of the girder (see Fig. 5). This figure also shows that the top flange membrane strains associated with lateral bending were the same order of magnitude as the average flange longitudinal strain, and that gage 4 (the gage closet to the inside flange tip) was actually in compression during the pre-peak portion of the test.

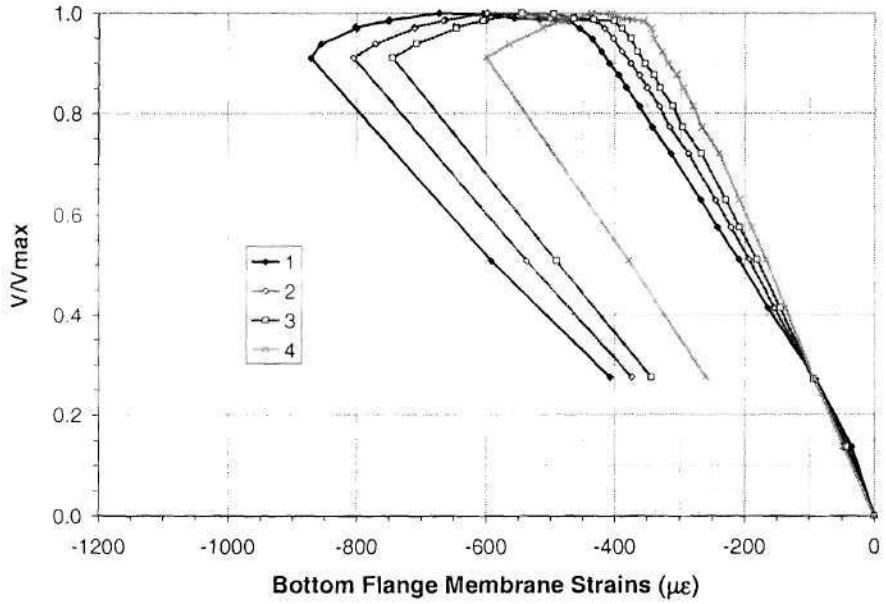

Figure 74 Bottom flange longitudinal membrane strains versus V/V_{max} in girder S2

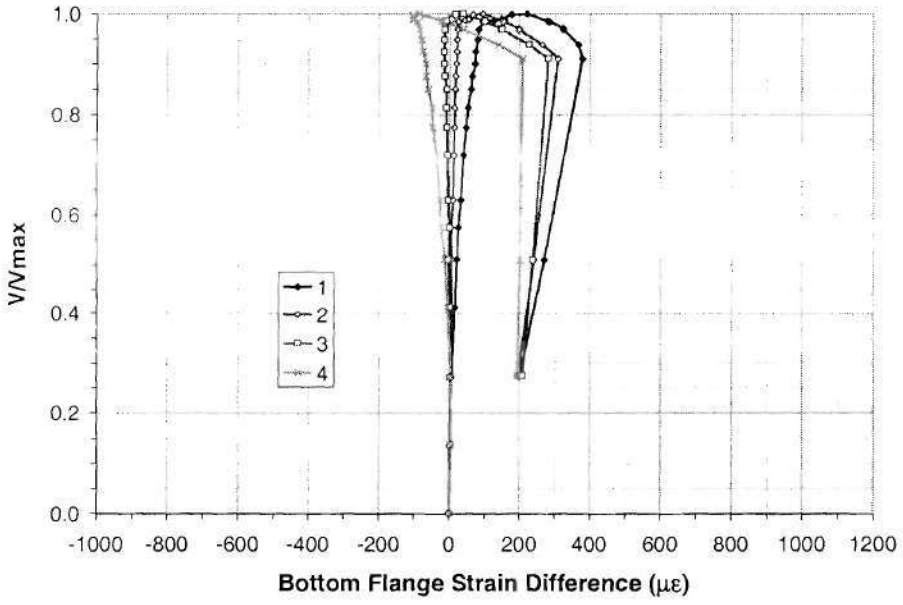

Figure 75 Bottom flange longitudinal membrane strain differences versus V/V_{max} in girder S2

Figure 73 shows that the bending of the top flange due to frame action was very minor until 98 percent of the shear capacity was reached, at which point an abrupt and dramatic increase in flange bending occurred at this location. The strain differences at all the top flange gage locations are negative from this stage of the loading onward, indicating that the flange was being bent concave upward. This behavior is confirmed by Figs. 35 and 36. One can observe from Fig. 72 that the longitudinal membrane strains at all the top flange gage locations also change abruptly and dramatically starting at $V/V_{max} = 0.98$. The resulting average membrane strain in the top flange at $d_o/4$ from location 2R reduces to a value close to zero at the maximum shear capacity of this girder, and becomes negative (i.e., compressive) as the girder is deformed in post-peak.

It appears that the increase in the shear from $V/V_{max} = 0.98$ to 1.0 may be associated with a change in the shear transfer mechanisms within the girder. The above figures seem to show that the flanges developed a small amount of additional shear strength via frame action as the contribution of the primary shear transfer element, the web, is exhausted. The behavior shown in Figs. 72 and 73 is consistent with both: (1) observations by Basler (1963), Lee and Yoo (1999) and others that the flange strains tend to be small up to the development of the maximum shear strength and (2) calculation of I girder shear capacity based on a plastic collapse mechanism as in (Porter et al. 1975, Evans et al. 1978 and Evans 1983).

As noted above, the bottom flange deformations at the location of the bottom flange gages was rather minor within girder S2. Figure 74 shows that this flange was in overall compression as would be expected based on the loading, and that there was an abrupt increase in these compressive membrane strains subsequent to $V/V_{max} = 0.98$. In addition, Fig. 75 shows an abrupt

increase in the bending of this flange due to frame action starting at the above load level, although the bending strains in this flange remain small throughout the test.

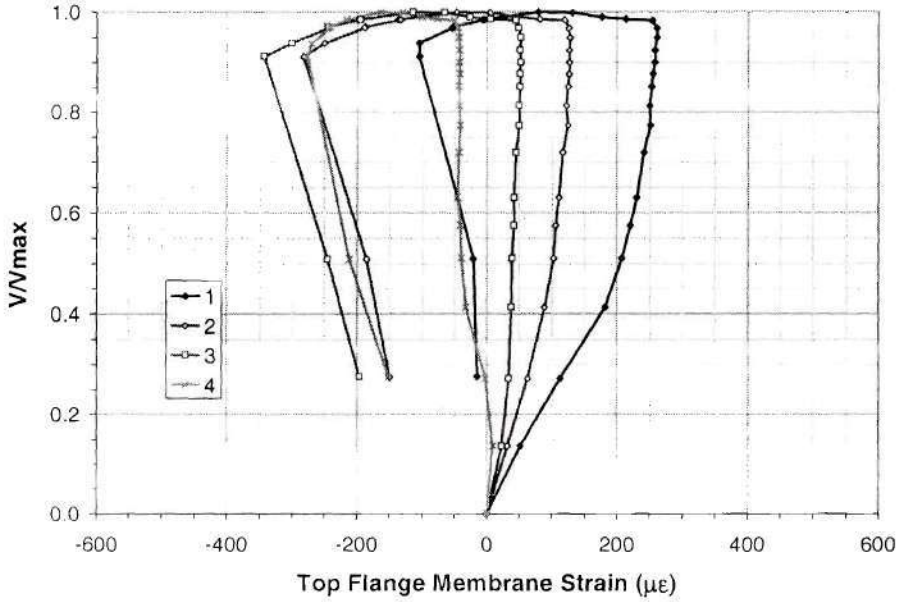

Figure 72 Top flange longitudinal membrane strains versus V/V_{max} in girder S2

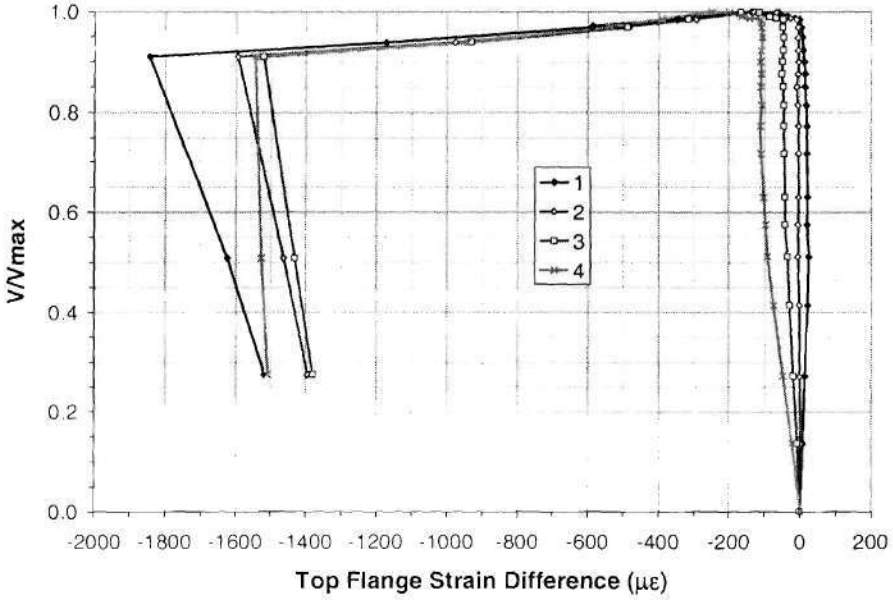

Figure 73 Top flange longitudinal membrane strain differences versus V/V_{max} in girder S2

The measured shear versus strain response of the flanges in girder S1 (not shown) were similar to those of S2 except that the flange gages in girder S1 were located approximately at the maximum (concave downward) plastic curvature location in the top flange near the intersection of the primary tension band with the top flange inside of the test panel. Conversely, in girder S2 the tension band intersected the bottom flange inside of the test panel nearly $d_o/2$ away from the location of the flange gages (compare Figs. 33 and 34 to Figs. 35 and 36). Also, there appeared to be less inelastic redistribution from the web to the flanges in girder S1 in that the abrupt change in the flange strains occurred essentially at the maximum load point.

Lastly, Figs. 76 to 79 show the longitudinal flange strains measured at $d_o/4$ from the location 2L in the left-most panel B1 of girder S1-S. These figures are organized in the same manner as Figs. 72 to 75 for girder S2. One can observe that the measured flange strain differences in girder S1-S were generally much smaller than those in the top flange of girder S2, and that the measured flange strains in this girder were predominantly elastic. This is of course expected since the deformations localized in the other test panel within the post-peak range of the response (see Figs. 37 and 38). However, some inelastic load redistribution and the beginning of the development of frame action is apparent within the pre-peak responses shown in these plots, particularly within the bottom flange plot in Fig. 79. In addition, one can observe that just after the peak shear capacity was reached in girder S1-S, the bottom flange response in Fig. 79 appears to be dominated by elastic unloading. The flange strain responses in girder S2-S were very similar to those presented for girder S1-S.

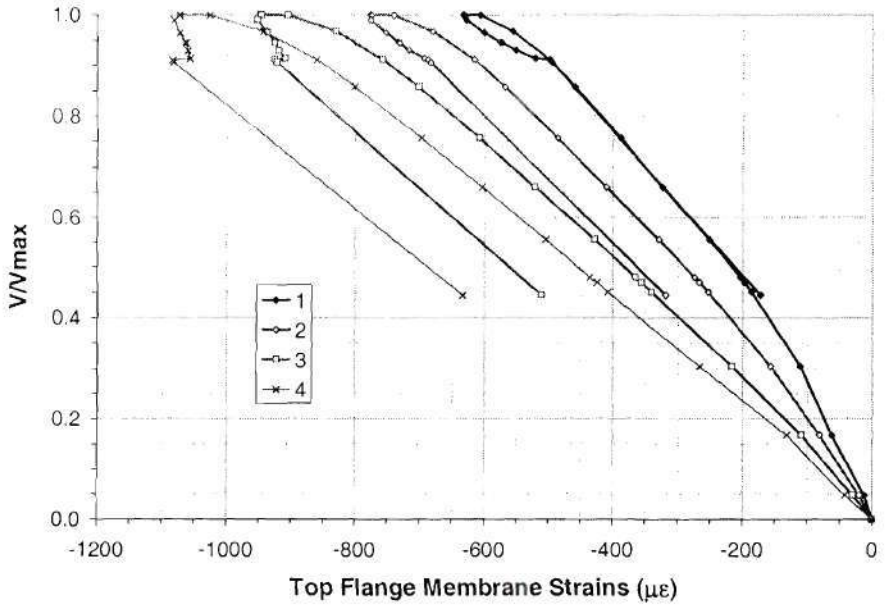

Figure 76 Top flange longitudinal membrane strains versus V/V_{max} in girder S1-S

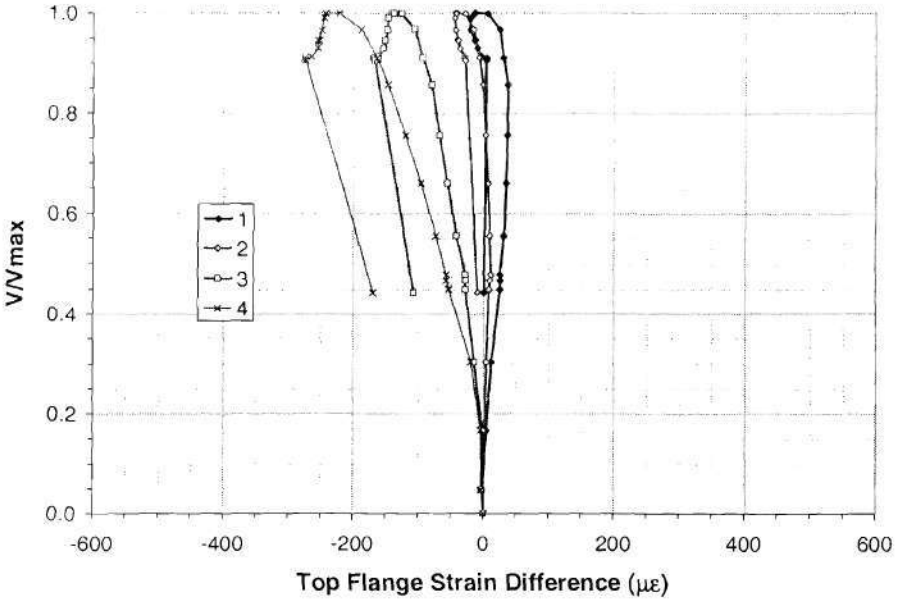

Figure 77 Top flange longitudinal membrane strain differences versus V/V_{max} in girder S1-S

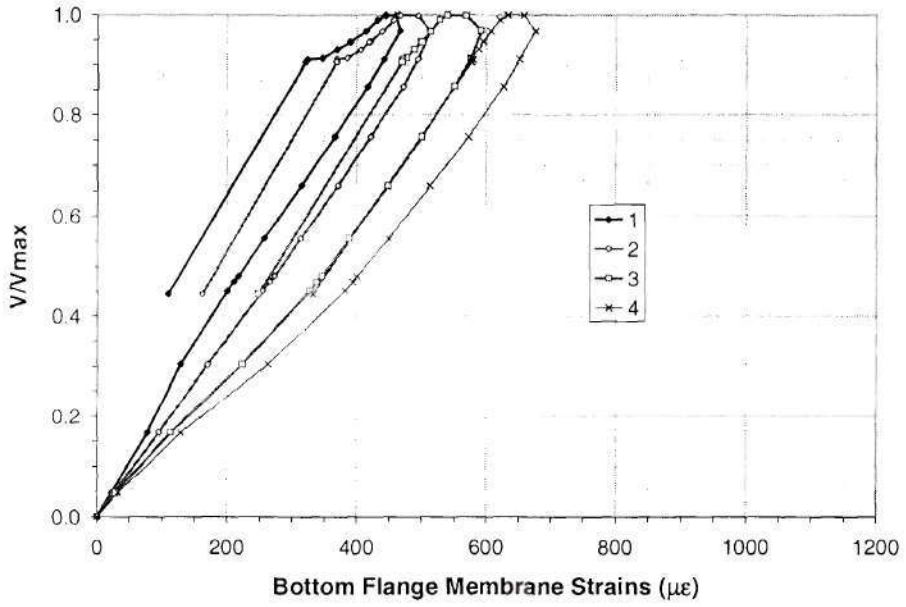

Figure 78 Bottom flange longitudinal membrane strains versus V/V_{max} in girder S1-S

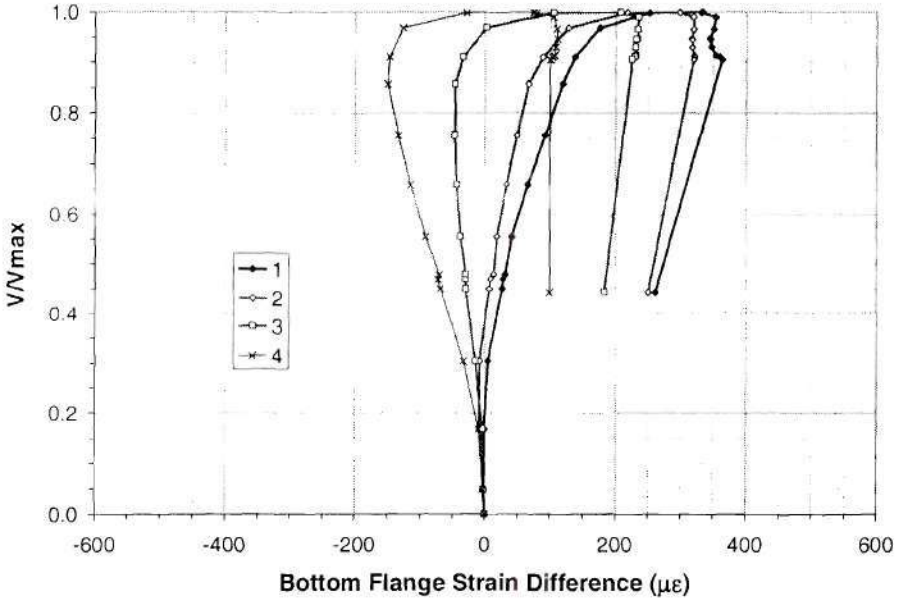

Figure 79 Bottom flange longitudinal membrane strain differences versus V/V_{max} in girder S1-S

CHAPTER V - COMPARISON WITH CALCULATED MEMBER STRENGTHS

This chapter evaluates the predictions by the five shear strength models discussed previously in Chapter II versus the experimental results for the four curved I-girders tested in this research. These models considered are:

- The current AASHTO LRFD (1998) shear strength formulae,
- A modified version of the AASHTO shear strength equations obtained by using the shear buckling coefficient developed by Lee et al. (1996),
- The shear strength model developed by Lee and Yoo (1998, 1999a and b),
- A modified version of the model proposed by Höglund (1971, 1995, 1996) and studied by Davies and Griffith (1999), and
- A modified form of the Cardiff shear strength model (Davies and Griffith 1999, Porter et al. 1975, Evans et al. 1978 and Evans 1983) combined with the use of Lee's shear buckling coefficient.

As discussed previously, the AASHTO, modified AASHTO and Lee and Yoo models are advantageous in that they do not require any direct consideration of contributions from the girder flanges (associated with anchorage of a tension field and/or with frame action). However, the modified AASHTO and Lee and Yoo models do include the effect of restraint from the flanges in the calculation of the web shear buckling strengths (via the use of the shear buckling coefficient proposed by Lee et al. (1996)). The model proposed by Höglund is also relatively simple to apply, but requires the calculation of a contribution from the flanges due to frame action. The Cardiff idealization is one of the more elaborate shear strength models within the literature. It also requires the direct calculation of a strength contribution from frame action of the flanges, as

well as the influence of the flange bending strength on the web postbuckling resistance. White et al. (2002a) found that the predictions by this model are slightly improved by using Lee's shear buckling coefficient in the calculation of the shear buckling strength. However, Höglund's model gave better predictions when utilized with an estimate of the shear buckling load based on simply-supported edge conditions. Therefore, Lee's shear buckling coefficient is utilized with the Cardiff model in the present study, but the shear buckling coefficient based on simply-supported boundary conditions at the edges of the web panel is utilized with Höglund's formulae.

The following section summarizes the five sets of shear strength equations considered in this study. Only brief discussions of the theoretical basis for the different equations are provided. The reader is referred to White et al. (2001) for more extensive discussion of the theoretical basis for the AASHTO (1998) and modified AASHTO equations, to White et al. (2001) and Lee and Yoo (1998, 1999a and b) for key concepts associated with Lee and Yoo's formulae, to (Höglund 1971, 1995, 1996) and (Davies and Griffith 1999) for discussion of the theoretical basis of Höglund's model, and to (Porter et al. 1975, Evans et al. 1978, Evans 1983 and Davies and Griffith 1999) for discussion of the background for the Cardiff model. Section 5.2 compares the underlying behavior and associated strengths predicted by these five models to the behavior and shear strengths measured within the four curved I-girders tested in this work.

5.1 STRENGTH EQUATIONS

The nominal maximum shear strength in all of the above models is based in part on a theoretical web shear buckling load. The next subsection summarizes the different theoretical shear buckling equations utilized in these models. This is followed by a subsection that outlines the formulae for the postbuckling strength contribution in each of the idealizations. Finally, the third

subsection addresses the calculation of the flange contribution to the shear strength in the Höglund and Cardiff theories. The nominal maximum shear strength is obtained in each of the models by summing the contributions.

5.1.1 Web Shear Buckling Strength

In general, the elastic shear buckling strength may be expressed as

$$V_{cr} = \frac{\pi^2 Ek}{12(1-\upsilon^2)\left(\frac{D}{t_w}\right)^2} Dt_w = \frac{0.90Ek}{\left(\frac{D}{t_w}\right)^2} Dt_w \tag{16}$$

based on an assumed Poisson ratio υ of 0.3 (Galambos and Ravindra 1978), and where k is the shear buckling coefficient. In AASHTO (1998), the elastic shear buckling strength is written indirectly as its ratio relative to the plastic shear capacity as

$$C = \frac{V_{cr}}{V_p} = \frac{1.52Ek}{\left(\frac{D}{t_w}\right)^2 F_{yw}} \qquad \text{for} \quad \frac{D}{t_w} > 1.38\sqrt{\frac{Ek}{F_{yw}}} \tag{17}$$

where

$$V_p = 0.58F_{yw}Dt_w \tag{18}$$

Equation (18) is a simplification of the expression

$$V_p = \frac{F_{yw}}{\sqrt{3}} Dt_w \tag{19}$$

where $F_{yw}/\sqrt{3}$ is the web shear yield strength based on the von Mises yield criterion. By multiplying Eq. (17) by Eq. (18), the effective AASHTO elastic shear buckling load is obtained as

$$V_{cr} = \frac{0.88Ek}{\left(\frac{D}{t_w}\right)^2} Dt_w \tag{20}$$

The different coefficients of 0.90 and 0.88 in Eqs. (16) and (20) are believed to be due to round-off in development of the AASHTO equations. Based on Eqs. (16) and (19), the ratio of the elastic shear buckling load to the web plastic shear strength is obtained as

$$C = \frac{V_{cr}}{V_p} = \frac{1.57Ek}{\left(\frac{D}{t_w}\right)^2 F_{yw}} \qquad \text{for} \qquad \frac{D}{t_w} > 1.38\sqrt{\frac{Ek}{F_{yw}}} \tag{21}$$

The reader should note that inelastic shear buckling equations are also provided in (AASHTO 1998) and within a number of the other references. These equations are not presented here since the theoretical web buckling for the four curved I girders tested in this work is elastic.

The web shear buckling coefficient is a key attribute of the different shear strength models. The shear buckling coefficient utilized in (AASHTO 1998) is

$$k_{AASHTO} = 5 + \frac{5}{\left(\frac{d_o}{D}\right)^2} \tag{22}$$

for $d_o/D \leq 3$. This is a simplification of the following approximate polynomial equations for the shear buckling coefficient (SSRC 1998):

$$k_{ss} = 4 + \frac{5.34}{\left(\frac{d_o}{D}\right)^2} \qquad \text{for } \frac{d_o}{D} < 1 \tag{23}$$

$$k_{ss} = 5.34 + \frac{4}{\left(\frac{d_o}{D}\right)^2} \qquad \text{for } \frac{d_o}{D} \geq 1 \tag{24}$$

All the above equations are based on the assumption of ideally simply-supported boundary conditions on all edges of the web panel. For a panel with fixed rotational restraint at its top and bottom and simply-supported conditions on its sides, the shear buckling coefficient may be written as (SSRC 1998)

$$k_{sf} = \frac{5.34}{\left(\frac{d_o}{D}\right)^2} + \frac{2.31}{\frac{d_o}{D}} - 3.44 + 8.39\frac{d_o}{D} \qquad \text{for } \frac{d_o}{D} < 1 \tag{25}$$

$$k_{sf} = 8.98 + \frac{5.61}{\left(\frac{d_o}{D}\right)^2} - \frac{1.99}{\left(\frac{d_o}{D}\right)^3} \qquad \text{for } \frac{d_o}{D} \geq 1 \tag{26}$$

These equations are also an approximate polynomial fit to analytical shear buckling solutions. Lee et al. (1996) studied the degree of restraint at the web-flange juncture for a wide range of representative I-girders using elastic finite element models. They found that for $(t_{ft} + t_{fb})/2t_w \geq 2$, where the symbols t_{ft} and t_{fb} denote the thicknesses of the top and bottom flanges, the shear buckling load can be predicted reasonably well by assuming a buckling coefficient nearly equal to that associated with fully-fixed boundary conditions at the web-flange juncture, i.e.,

$$k_{Lee} = k_{ss} + \frac{4}{5}(k_{sf} - k_{ss}) \qquad \text{for } \frac{(t_{fb} + t_{ft})}{2t_w} \geq 2 \tag{27}$$

and that for girders with thinner flanges, the shear buckling coefficient could be expressed as

$$k_{Lee} = k_{ss} + \frac{4}{5}(k_{sf} - k_{ss})\left[1 - \frac{2}{3}\left(2 - \frac{(t_{fb} + t_{ft})}{2t_w}\right)\right] \qquad \text{for } \frac{1}{2} \leq \frac{(t_{fb} + t_{ft})}{2t_w} < 2 \tag{28}$$

Bradford (1996) also studied the effect of restraint from the flanges on the web elastic shear buckling capacity, and developed charts for the shear buckling coefficient that give values close to those predicted by Eqs. (27) and (28). The correlation of these equations with elastic finite element linear buckling solutions has also been confirmed by White et al. (2001).

with respect to the longitudinal direction. The orientation of the tension field in Eq. (30) is based on Basler's initial assumption that the flanges do not provide any anchorage for the tension field stresses. The above attributes of Basler's model have been noted in previous research by Gaylord (1963), Fujii (1968) and Selberg (1973).

As a result of the above anomaly in Basler's (1961) model, Eq. (29) is based implicitly on the assumption that the flanges are sufficient to provide some anchorage to the tension field. Basler (1963) acknowledges this characteristic of his model, and illustrates that the flanges are actually not loaded to the extent that would be required by his theory within physical tests. Nevertheless, he argues that his theory still provides an acceptable characterization of I-girder shear strengths. Gaylord (1963) also points out that "The good correlation between predicted values and experimental results cannot be dismissed. For this reason, the author's analysis may be an acceptable prediction of the postbuckling behavior of thin-webbed girders for the practicable range of parameters in civil engineering practice."

Lee and Yoo (1998 and 1999a) also highlight the issue that the flange strains are generally not as large as would be implied by Basler's model, and that Basler's model and other shear strength models do not consider important plate bending effects that exist in web panels of practical bridge I girders. They suggest a simplified expression for the postbuckling contribution to the strength of

$$V_{PB(Lee)} = 0.40R_d(V_p - V_{cr}) \tag{31}$$

where R_d is a factor intended to account for the influence of plate bending due to geometric imperfections. This equation gives a contribution similar in magnitude to that obtained from Basler's formula, Eq. (29). However, as shown by White et al. (2001), it generally predicts a small anomalous increase in the postbuckling strength with increasing d_o/D. This characteristic

of Eq. (31) can be discerned by recognizing that the shear buckling coefficient k and the critical shear load V_{cr} generally decrease when the stiffener spacing is increased. Since V_p is not affected by the stiffener spacing, the result is that $V_{PB(Lee)}$ increases with increasing d_o. This behavior is of course not physical, but is an artifact of Lee and Yoo's simplification.

Lee and Yoo (1998, 1999a and b) conclude that the shear strength is in general influenced significantly by geometric imperfection effects. They specify the following formulae for the term R_d in Eq. (31) to account for these effects:

$$R_d = 0.8 \quad \text{for} \quad \frac{D}{t_w} \le 1.10\sqrt{\frac{Ek_{Lee}}{F_{yw}}} \tag{32}$$

$$R_d = 0.8 + 0.2\frac{\frac{D}{t_w} - 1.10\sqrt{\frac{Ek_{Lee}}{F_{yw}}}}{\sqrt{\frac{Ek_{Lee}}{F_{yw}}}} \quad \text{for} \quad 1.10\sqrt{\frac{Ek_{Lee}}{F_{yw}}} < \frac{D}{t_w} < 2.20\sqrt{\frac{Ek_{Lee}}{F_{yw}}} \tag{33}$$

and

$$R_d = 1.0 \quad \text{for} \quad \frac{D}{t_w} > 2.20\sqrt{\frac{Ek_{Lee}}{F_{yw}}} \tag{34}$$

The total shear strength is then expressed by Lee and Yoo as

$$V_n = R_d V_p(C + 0.4[1 - C]) = R_d V_p(0.6C + 0.4) \tag{35}$$

That is, the imperfection factor R_d is applied to both the shear buckling and postbuckling contributions. Unfortunately, this equation suggests that $V_n = 0.8V_p$ in the limit that C = 1 if the web is stocky enough such that Eq. (32) is satisfied. This is an incorrect limit that is not supported by physical test data (White et al. 2002a). In (Lee and Yoo 1999a), the authors state the above equations but in fact use $R_d = 1$ throughout in predicting the shear strengths of their experimen-

The models considered in this report utilize the following equations for calculation of the theoretical elastic shear buckling load V_{cr} and the ratio $C = V_{cr}/V_p$:

- AASHTO LRFD: Eqs. (17), (18), (20) and (22).
- Modified AASHTO: Eqs. (17), (18), (20), (27) and (28).
- Lee and Yoo: Eqs. (16), (18), (21), (27) and (28).
- Höglund: Eqs. (16), (19), (21), (23) and (24).
- Cardiff: Eqs. (16), (19), (21), (27) and (28).

5.1.2 Postbuckling Strength

The AASHTO (1998) and modified AASHTO models are based on Basler's (1961) tension field idealization for calculating the postbuckling strength. This idealization produces the formula

$$V_{PB(Basler)} = \frac{0.87(1-C)}{\sqrt{1+\left(\frac{d_o}{D}\right)^2}} \tag{29}$$

As discussed in White et al. (2001), although the flanges are assumed to provide zero anchorage to the theoretical tension field in the initial stages of Basler's derivation – such that the tension field extends only over a portion of the web – the final result expressed by the above equation is actually based on the development of a "complete" tension field. That is, the tension field contribution to the shear strength in Eq. (29) is based on uniform yielding throughout the web panel with a principal tension angle of

$$\Theta_{t(Basler)} = \frac{1}{2}\tan^{-1}\left(\frac{D}{d_o}\right) \tag{30}$$

tal tests. The above anomalous geometric imperfection effect is an artifact of the finite element solutions in (Lee and Yoo 1998). Lee and Yoo developed Eqs. (32) to (34) based on differences in their predicted FEA strengths for initial web out-of-flatness values of D/120,000 and D/120.

Höglund (1971, 1995, 1996) proposed formulae for the combined buckling and postbuckling contributions of the web based on his rotating stress-field theory. His strength model idealizes the web as a system of perpendicular bars in compression and tension. Höglund's most recent formulation is outlined and studied by Davies and Griffith (1999); the reader should note that this formulation is different from the Höglund model presented in (SSRC 1998). Davies and Griffith consider six different categories of I-girders in their paper. They show that in each of these categories Höglund's more recent model gives better predictions than another set of formulae that they propose.

The following slightly modified form of Höglund's model is utilized for the total (buckling plus postbuckling) contribution from the web to the shear strength in this work:

$$V_w = V_p \quad \text{for} \quad \frac{D}{t_w} \le \sqrt{\frac{Ek_{ss}}{F_{yw}}} \tag{36}$$

$$V_w = 0.8\sqrt{C_{ss}}V_p \quad \text{for} \quad \sqrt{\frac{Ek_{ss}}{F_{yw}}} < \frac{D}{t_w} < 1.23\sqrt{\frac{Ek_{ss}}{F_{yw}}} \tag{37}$$

$$V_w = \frac{1.37}{0.7 + \sqrt{\frac{1}{C_{ss}}}}V_p \quad \text{for} \quad \frac{D}{t_w} \ge 1.23\sqrt{\frac{Ek_{ss}}{F_{yw}}} \tag{38}$$

where V_w is the total web contribution to the shear strength, C_{ss} is the ratio of the elastic shear buckling load to web plastic shear capacity based on Eqs. (21), (23) and (24), and V_p is the web plastic shear capacity given by Eq. (19). These equations are applicable for both stiffened and unstiffened I-girders. The slight modification of Höglund's equations, other than writing them in

a format similar to that in (AASHTO 1998), is that the maximum web shear contribution is capped at V_p. Höglund proposes the use of Eq. (37) up to $V_w = 1.16V_p$. The above equations are applicable to steel I-girders with "rigid end posts." The SSRC Stability Design Guide (SSRC 1998) outlines the end-stiffener and end-panel requirements for this condition to be satisfied. Of 131 stiffened and unstiffened I-girder tests considered for statistical analysis in (White et al. 2002a), the largest unconservative difference between Eqs. (36) to (38) and the experimental strengths is 13 percent. In addition, it is interesting that Eqs. (36) to (38) give strength ratios V_{max}/V_n of 1.03, 1.02 and 1.32 (where V_{max} is the measured experimental shear capacity) for three tests conducted by Basler et al. (1960) in which the failure occurred within the girder end panels.

Although an expression is not provided for the isolated postbuckling contribution to the strength in Höglund's equations, this contribution can be written as

$$V_{PB(Höglund)} = V_w - V_{cr(ss)} \tag{39}$$

assuming elastic shear buckling (which is the case for the four curved I girders tested in this research), where $V_{cr(ss)}$ is based on Eqs. (16), (23) and (24).

Finally, for the Cardiff model, the web postbuckling strength is determined based on the tension field idealization originally posed by Porter et al. (1975). The tension field contribution in this model can expressed as

$$V_{PB(Cardiff)} = F_t^y t_w \sin^2(\Theta_{t(Cardiff)})\left[D\cot(\Theta_{t(Cardiff)}) - d_o + \frac{c_{b(Cardiff)}}{2} + \frac{c_{t(Cardiff)}}{2}\right] \tag{40}$$

where

$$F_t^y = -\frac{3}{2}\tau_{cr}\sin(2\Theta_{t(Cardiff)}) + \sqrt{F_{yw}^2 + \tau_{cr}^2\left[\left(\frac{3}{2}\sin(2\Theta_{t(Cardiff)})\right)^2 - 3\right]} \tag{41}$$

is the tensile principal stress within the tension field, τ_{cr} is the web critical shear stress V_{cr}/Dt_w, and $\Theta_{t(Cardiff)}$ is the inclination of the tension field with respect to the longitudinal direction of the girder. The angle $\Theta_{t(Cardiff)}$ must be determined in general by iteration, but it can be approximated as

$$\Theta_{t(Cardiff)approx} = \frac{2}{3}\tan^{-1}\left(\frac{D}{d_o}\right) \tag{42}$$

The "exact" $\Theta_{t(Cardiff)}$ is the one that maximizes the overall shear capacity. The variables $c_{b(Cardff)}$ and $c_{t(Cardff)}$ in Eq. (40) are the distances inward from the transverse stiffeners at which plastic hinges form in the top and bottom flanges due to frame action as shown in Fig. 80.

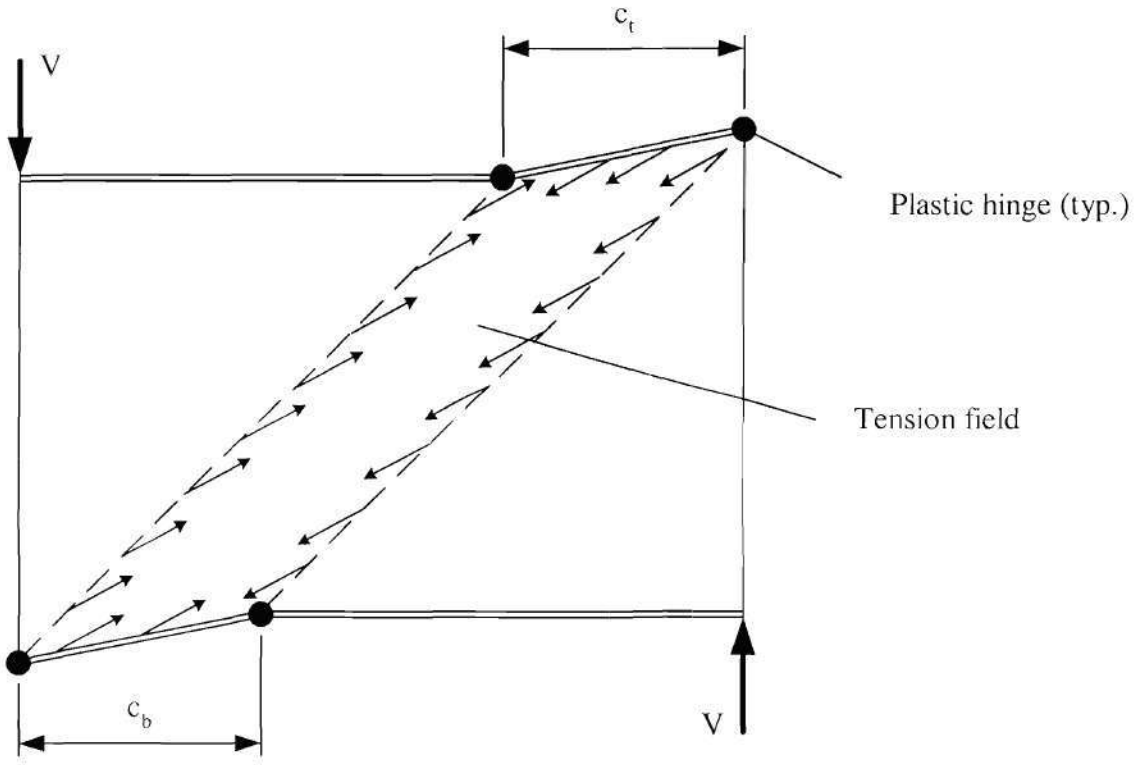

Figure 80 Assumed shear failure mechanism involving the development of flange plastic hinges

These distances may be calculated as

$$c_{(Cardiff)} = \max\left(d_o, \min\left(0, \frac{2}{\sin(\Theta_{t(Cardiff)})}\sqrt{\frac{m_{pf}}{F_t^y t_w}}\right)\right) \tag{43}$$

where

$$m_{pf} = \frac{F_{yf} b_f t_f^2}{4}\left[1 - \left(\frac{M}{M_n}\right)^2\right] \tag{44}$$

is the plastic moment resistance of the corresponding flange[1]. Subscripts "b" and "t" may be added to the applicable terms in these equations to denote the bottom and top flanges respectively.

Equation (44) is a modification from various Cardiff formulae for the flange plastic resistance proposed in (Porter et al. 1975, Evans et al. 1978, Evans 1983 and Davies and Griffith 1999). The bracketed term within Eq. (44) accounts conservatively for the reduction in the flange plastic bending capacity due to axial forces within the flanges from overall bending of the girder. This term comes specifically from the theoretical reduction in the plastic bending resistance of a rectangular cross-section due to axial force. The term M in this expression is the maximum total girder bending moment within the length of the web panel, and M_n is the nominal bending strength of the girder within the unsupported segment being considered. Höglund suggests a similar expression for the reduction in the flange plastic bending capacity (SSRC 1998), but he uses the flange moment $M_f = F_{yf} A_f h$ (assuming a doubly symmetric cross-section shape) instead of M_n. The use of M_n is more general in that it accommodates all types of I

1. The term $F_{yf} b_f t_f^2/4$ in Eq. (44) applies strictly only to a flange I-girder, i.e., an I-girder without cover plates, etc. For a girder that contains cover plates, this term may be replaced by the plastic moment resistance of the combined flange and cover plates acting together as a beam (assuming that slip is prevented between the flange and the cover plates).

shapes (including monosymmetric as well as composite I sections) as well as potential reductions in the flange strength associated with flange local and/or lateral buckling.

Equation (44) is a simplification from various proposals by Porter et al. (1975), Evans et al. (1979), Evans (1983), and Davies and Griffith (1999) for calculation of the flange plastic bending resistance of the flanges. One suggestion made in a number of the prior papers is to use the average flange stress between the flange plastic hinging locations in reducing the flange plastic bending capacity. Porter et al. (1975) and Evans et al. (1979) provide equations for the flange stress based on a free-body diagram of a portion of the girder, accounting for the load transfer mechanisms within the Cardiff model. These procedures generally require iteration in calculating the nominal design strength. Davies and Griffith (1999) suggest a simple linear equation in terms of M/M_f for the reduction in the flange plastic bending contribution to the shear strength in the Cardiff model. They are silent, however, about how M is to be calculated. If M is taken as the average moment within the web panels in girders S1 and S2 of this research, the result is zero reduction in the flange plastic bending strength.

The shear capacity predicted by the Cardiff equations is based on an assumed equilibrium stress field (i.e., tension field) in the girder, which satisfies the theoretical conditions for a lower-bound strength prediction provided that the material possesses sufficient ductility for the tension field to develop. This solution therefore possesses a certain degree of rigor. Nevertheless, it is still only an idealized model. For example, the effects of plate bending on the stress state in the web panels are neglected. Also, due to stability effects, it is possible in general to reach the maximum strength of a structure or a structural component prior to development of a plastic collapse mechanism.

5.1.3 Contribution of the Flanges to the Shear Strength

Höglund (1971, 1995, 1996), Porter et al. (1975) and Davies and Griffith (1999) all obtain reasonable predictions of the maximum shear capacity of I girders by combining their models for the total buckling plus postbuckling contribution of the web (e.g., Eqs. (36) to (38)) with a contribution from the frame action of the flanges. The contribution from frame action of the flanges can be written generally as

$$V_f = \frac{2m_{pft}}{c_t} + \frac{2m_{pfb}}{c_b} \tag{45}$$

where m_{pfb} and m_{pft} are the plastic bending resistances of the top and bottom flanges, which are calculated in the current study per Eq. (44), and c_t and c_b are the distances from the ends of the web panel to the intermediate flange plastic hinge locations within the panel (see Fig. 80). Höglund (1971, 1995, 1996) suggested a simple equation for calculation of the distances c_t and c_b that can be expressed as follows:

$$c = d_o\left(0.25 + 6.4\frac{m_{pfo}}{t_w D^2 F_{yw}}\right) \tag{46}$$

where m_{pfo} is the base flange (or flange plus cover plate) plastic resistance corresponding to $M = 0$, and subscripts t or b are added to the applicable flange terms to denote the top or bottom flange. Davies and Griffith (1999) use this equation in their evaluation of the Höglund model as well as in several other shear strength predictors. This equation is employed with Eq. (45) in the calculations per the Höglund model in this research. Conversely, for the calculations per the Cardiff model, Eqs. (43) and (45) are utilized to estimate the contribution from the flanges due to frame action.

It is interesting to note that the Eq. (45) and other equations such as Eq. (43) do not include the contribution from a composite bridge deck essentially acting as a large flange element. This contribution may be significant, as evidenced in (Vasseghi and Frank 1987).

5.2 SHEAR STRENGTH PREDICTIONS FOR THE TEST GIRDERS

The values of the various shear buckling coefficients for the four curved I-girders tested in this research are summarized in Table 8. One can observe that the variation in these calculated values for the girders with $d_o/D = 1.5$ is not as great as that for the girders with $d_o/D = 3$. The ratio k_{Lee}/k_{AASHTO} is 1.40 for $d_o/D = 1.5$ versus 1.58 for $d_o/D = 3$. In other words, the effect of accounting for the rotational restraint from the flanges at the top and bottom edges of the web panels is greater for the girders with wider stiffener spacing.

Table 8 Shear buckling coefficients

Girder	d_o/D	k_{AASHTO}	k_{ss}	k_{sf}	k_{Lee}
S1	3	5.56	5.78	9.53	8.78
S2	3	5.56	5.78	9.53	8.78
S1-S	1.5	7.22	7.12	10.88	10.13
S2-S	1.5	7.22	7.12	10.88	10.13

The various elastic shear buckling loads are summarized in Table 9. All of these strengths are calculated based on E = 200 GPa (29000 ksi)[2]. The primary reason for the differences in the

2. E = 200 GPa (29000 ksi) is utilized throughout all the calculations in this chapter.

significantly better predictor than the above tension field models for unstiffened girders with very slender webs (White et al. 2002a; Davies and Griffith 1999). The lack of a significant change in the postbuckling strength predicted by Höglund's model with wider stiffener spacing is related to this model's capabilities as they relate to unstiffened girders. Lee and Yoo's model predicts approximately a 10 percent smaller postbuckling strength contribution for the girders with $d_o/D = 1.5$ versus those with $d_o/D = 3$. As noted previously, this anomaly is due to the simplified nature of Eq. (31), which was developed as an approximate fit to full nonlinear finite element analysis solutions of isolated web panels (Lee and Yoo 1998).

- The postbuckling contribution predicted by the modified AASHTO model is smaller than that obtained per the AASHTO (1998) equations. This is due to the increased shear buckling resistance in the modified AASHTO model via the use of Lee's shear buckling coefficient.

Table 10 Postbuckling strength contributions

Girder	F_{yw} MPa (ksi)	AASHTO $V_{PB(Basler)}$ kN (kips)	Modified AASHTO $V_{PB(Basler)}$ kN (kips)	Lee and Yoo $V_{PB(Lee)}$ kN (kips)	Höglund $V_{PB(Höglund)}$ kN (kips)	Cardiff $V_{PB(Cardiff)}$ kN (kips)
S1	410 (59.4)	543 (122)	463 (104)	653 (147)	649 (146)	377 (85)
S2	411 (59.6)	534 (120)	463 (104)	662 (149)	638 (143)	377 (85)
S1-S	410 (59.4)	876 (197)	752 (169)	591 (133)	619 (139)	614 (138)
S2-S	411 (59.6)	872 (196)	756 (170)	607 (136)	613 (138)	619 (139)

Table 11 gives the values of Lee and Yoo's imperfection parameter, obtained from Eqs. (32) through (34) for the four curved test components. All of the test girders had web slenderness values D/t_w close to the point of transition between Eqs. (33) and (34).

Table 11 Values of Lee and Yoo's (1998, 1999a and b) imperfection parameter R

S1	S2	S1-S	S2-S
0.989	1.000	0.966	0.976

Table 12 compares the angle of inclination of the tension field predicted by the Basler (1961) and Cardiff (Porter et al. 1975) models, $\Theta_{t(Basler)}$ and $\Theta_{t(Cardiff)}$, to the range of the measured orientations of the maximum principal membrane tension at plastic gage locations in the instrumented panels of the test girders. The measured values are taken at the end of the post-peak loading. In the calculations for the Cardiff model, $\Theta_{t(Cardiff)}$ is calculated iteratively such that the corresponding strength V_n is maximized. One can observe that both $\Theta_{t(Basler)}$ and $\Theta_{t(Cardiff)}$ significantly underestimate the actual orientations of the maximum principal membrane tension direction in all of the girders. In addition, as noted previously, $\Theta_{p1(exp)}$ varies significantly within the web panels in girders S1 and S2. These results are indicative of the fact that the actual web maximum strength behavior is significantly more complex than that predicted by either the Basler or the Cardiff idealizations.

Table 12 Theoretical tension field angles versus the range of angles corresponding to the maximum (tensile) principal strain at rosette locations that experience yielding, measured values taken at the end of the post-peak loading

Girder	$\Theta_{t(Basler)}$ degrees	$\Theta_{t(Cardiff)}$ degrees	$\Theta_{p1(exp)}$ degrees
S1	9.2	11.3	19 to 48
S2	9.2	11.4	18 to 26
S1-S	16.8	19.5	30 to 35
S2-S	16.8	19.8	30 to 36

Table 13 gives the predicted locations of plastic hinge formation in the flanges due to frame action, and the corresponding contribution of the flanges to the shear capacity from the Höglund and Cardiff models. These predictions can be compared to the locations of the maximum plastic curvature within the flanges detailed in Figs. 34, 36, 38 and 40. For girders S1 and S2, the measured "hinge locations" within the flanges are significantly different than predicted by either of these idealized models. These hinge locations did not form symmetrically within the critical web panel in the experimental tests, and in fact, there were no sharp "folds" in the flange plates at the locations of maximum plastic curvature. The larger curvatures in the vicinity of the maximum plastic curvature locations were well distributed over a finite length along the flanges. The maximum flange plastic curvature locations marked on the top flange of Fig. 34 and on the bottom flange of Fig. 36 indicate that these flanges provided some anchorage to a tension band that formed over only a fraction of the panel lengths. Conversely, the behavior of girders S1-S and S2-S was similar to that predicted by both of the above models, but the locations of maximum plastic curvature in the flanges were somewhat further removed from the ends of the panels within the experimental tests than in the idealized models.

The calculated flange strength contributions V_f range from seven and eight percent of the total nominal strengths in girders S1 and S2 to 12 to 13 percent of the total computed strengths in girders S1-S and S2-S via the Höglund model (the total computed shear strengths are reported in Table 14). With the Cardiff model, the flange contributions are slightly less than 10 percent of the computed maximum strength in all of the girders.

V_{cr} values is due to the calculation of the shear buckling coefficient. However, there are some additional minor differences due to roundoff between Eqs. (16) and (20), (21) and (17), and (19) and (18). In fact the differences among the V_{cr} values for the modified AASHTO, Lee and Yoo and Cardiff models are entirely due to roundoff in the different equations. Similarly, the difference between the V_{cr} values calculated per AASHTO and per Höglund are due only to the simpler expression for the shear buckling coefficient in Eq. (22) compared to Eqs. (23) and (24). The theoretical shear buckling loads in the three former models are larger than those predicted by the two latter models by approximately the ratio of the shear buckling coefficients reported above.

Table 9 Elastic shear buckling loads

Girder	D/t_w	AASHTO V_{cr} kN (kips)	Modified AASHTO V_{cr} kN (kips)	Lee and Yoo V_{cr} kN (kips)	Höglund V_{cr} kN (kips)	Cardiff V_{cr} kN (kips)
S1	143	498 (112)	792 (178)	818 (184)	534 (120)	805 (181)
S2	146	463 (104)	729 (164)	752 (169)	494 (111)	743 (167)
S1-S	144	632 (142)	885 (199)	916 (206)	641 (144)	907 (204)
S2-S	148	583 (131)	818 (184)	845 (190)	587 (132)	836 (188)

It is interesting that in Girder S1, the only test that exhibited measured web shear-radial deflection curves that could be interpreted as indicative of behavior close to a theoretical bifurcation response (see Fig. 25), the slopes of the normalized load versus radial deflection curves changed significantly between the shear force levels of approximately 0.46 V_{max} = 550 kN (120 kips) and 0.56 V_{max} = 670 kN (150 kips). These load levels can be compared to the theoretical shear buckling loads ranging from 498 kN (112 kips) per the AASHTO calculations to 818 kN

(184 kips) per the Lee and Yoo formulae. However, it should be emphasized that even in Girder S1, the measured change in the web response in the vicinity of these load levels did not appear to have a significant influence on the development of the girder maximum shear capacity. For instance, the radial web deflection in Girders S1 and S2 was approximately the same at 95 percent of the shear capacity (see Figs. 25 and 26), although the measured response curves were somewhat nonlinear for girder S1 (see Fig. 25) and essentially linear for girder S2 (see Fig. 26) up to this load level. In all the girders with the exception of S1, there was no indication of the web shear passing a theoretical web shear buckling load within the test data. Based on this and other similar results from straight-girder tests, e.g., (Basler et al. 1960) and (Lee and Yoo 1999a), one can conclude that the theoretical buckling load V_{cr} is a simply a useful index for quantifying the web stability behavior; the web load-radial deflection response is often a continuous curve without any semblance of bifurcation behavior in both straight and curved I-girders. In straight I-girders, this is due to typical geometric imperfections and the stable nature of the post-buckling response. In horizontally-curved I-girders, it is due to the combination of these effects plus the horizontal curvature.

Table 10 shows the postbuckling strengths predicted by the different models. The following trends can be observed in these values:

- The AASHTO, modified AASHTO and Cardiff models all predict a significant increase in the postbuckling strength contribution by changing d_o/D from 3 to 1.5. However, the Höglund model predicts only a minor increase in this strength by adding the additional intermediate transverse stiffener to the girders. This is due to the fact that the Cardiff model and both of the AASHTO models are based on tension field theories. However, Höglund's model is based on his rotating stress field theory. Interestingly enough, Höglund's model is a

Table 13 Flange plastic hinge locations and shear strength contributions by flange frame action

Girder	Höglund c_t/d_o	Höglund c_b/d_o	Cardiff c_t/d_o	Cardiff c_b/d_o	Höglund V_f kN (kips)	Cardiff V_f kN (kips)
S1	0.284	0.284	0.245	0.246	88 (20)	101 (23)
S2	0.286	0.286	0.256	0.254	94 (21)	105 (24)
S1-S	0.284	0.284	0.283	0.283	165 (37)	149 (34)
S2-S	0.287	0.287	0.295	0.295	179 (40)	159 (36)

Table 14 summarizes the measured experimental and predicted shear capacities, and Table 15 gives the ratio of the measured shear strengths to the shear capacities predicted by each of the models. The following observations can be made based on these tables:

- The AASHTO model tends to underpredict the capacity of the girders with wide stiffener spacing. It slightly overestimates the strength of the girders with $d_o/D = 1.5$.
- The modified AASHTO model gives accurate predictions for the girders with wide stiffener spacing, but overpredicts the strengths of the girders with $d_o/D = 1.5$ by 10 and 17 percent. It should be noted that these predictions are well within the range of strength ratios for this model with respect to tests of stiffened straight I-girders (White et al. 2002a).
- The Lee and Yoo model significantly overestimates the shear strength of girders S1 and S2; however, these predictions are also within the scatter band of straight I-girder results for this model, see (White et al. 2002a). It gives reasonably accurate estimates of the shear strengths for girders S1-S and S2-S. Interestingly, this model predicts that the shear strength of girder S1-S would be only 20 kN (4 kips) higher than that of girder S1, and that the shear strength of girder S2-S would be only 10 kN (3 kips) higher for girder than that of girder S2. The

experimental tests indicate a much larger strength increase due to the addition of the intermediate transverse stiffeners than this.

- Höglund's model gives the best prediction of the results from the four curved I-girder shear tests conducted in this work. These predictions range from two percent conservative to six percent unconservative. This good correlation is believed to be related in part to the fact that: (1) the strength ratios for Höglund's model have a smaller dispersion than the other models (with the exception the Cardiff model) with respect to test results for stiffened straight I-girders, and (2) Höglund's model tends to predict the shear strength of straight I-girders conservatively on average (White et al. 2002a). Therefore, since a small reduction in the shear strength is expected for the curved I-girder tests relative to hypothetical equivalent straight I-girders, it is not surprising that the curved I-girder test results would be predicted well by Höglund's model.
- The Cardiff model gives reasonably accurate predictions of the strengths for girders S1 and S2, but overpredicts the strengths of tests S1-S and S2-S by 13 and 18 percent. Similar to the above discussions, these predictions are within the range of strength predictions by this model for straight I girders (White et al. 2002a). It should be noted that the modified Cardiff model considered in this report, including the use of Lee's shear buckling coefficient, gives the best correlation with the available experimental data of all the shear strength models evaluated by White et al. (2002a) based on a number of measures. One might note that this model's predictions are just slightly larger than those of the modified AASHTO model for each of the four test girders. The consistent overprediction of the maximum strengths by the Cardiff model is believed to be related to the effects of horizontal curvature.

Table 15 Ratio of measured experimental shear capacities to predicted strengths

Girder	AASHTO V_{max}/V_n	Modified AASHTO V_{max}/V_n	Lee and Yoo V_{max}/V_n	Höglund V_{max}/V_n	Cardiff V_{max}/V_n
S1	1.15	0.96	0.82	0.95	0.93
S2	1.16	0.97	0.82	0.94	0.94
S1-S	0.91	0.83	0.93	0.96	0.82
S2-S	0.97	0.90	0.99	1.02	0.87

- Each of the shear strength models predicts a small decrease in the strength of girder S2 relative to girder S1. This prediction is due to the slightly higher slenderness D/t_w in girder S2. It is not related to the smaller radius of curvature (R) in this girder, since none of the shear strength predictors account for horizontal curvature effects. Although one might expect a small decrease in the capacity of girder S2 relative to S1 due to its smaller R value, the 40 kN (10 kip) decrease in the shear strength from S1 to S2 is equally well explained by the straight-girder strength formulae.
- Although all of the strength models predict a similar decrease in the strength of girder S2-S relative to S1-S, the measured shear strength of girder S2-S was actually slightly larger than that for S1-S. This discrepancy may be due in part to unavoidable measurement error within the experimental tests (see Table 7 and Fig. 16). However, it might also be related to the larger inward web imperfections in girder S2-S compared to girder S1-S (see Table 5).

Table 14 Experimental and predicted shear capacities

Girder	Measured Test Capacity V_{max} kN (kips)	AASHTO V_n kN (kips)	Modified AASHTO V_n kN (kips)	Lee and Yoo V_n kN (kips)	Höglund V_n kN (kips)	Cardiff V_n kN (kips)
S1	1200 (270)	1040 (234)	1250 (281)	1460 (328)	1270 (286)	1290 (289)
S2	1160 (260)	1000 (224)	1190 (268)	1420 (318)	1220 (275)	1230 (276)
S1-S	1370 (307)	1510 (339)	1640 (369)	1480 (332)	1420 (320)	1670 (375)
S2-S	1410 (317)	1450 (327)	1570 (354)	1430 (321)	1380 (310)	1610 (363)

CHAPTER VI - SUMMARY AND CONCLUSIONS

6.1 SUMMARY

The objective of this study was to experimentally determine the maximum strengths and the associated behavior of four full-scale curved I-girders subjected to high-shear low-moment loading. Of particular interest was the influence of horizontal curvature on the maximum strength of members with:

- Web slenderness D/t_w approximately equal to the largest values permitted for Grade 345 steels by the AASHTO LRFD (1998) straight-girder specifications, and
- Panel aspect ratios of $d_o/D = 1.5$ and 3.0, which are larger than previously considered in experimental tests of curved I-girders with similar or larger D/t_w values.

Each girder was instrumented and then loaded beyond its maximum capacity to a level of vertical deflection from 2.2 to 3.4 times the deflection at its maximum shear strength. Records of load, reactions, radial and vertical deflections, and strains were obtained throughout all stages of the loading.

6.2 CONCLUSIONS

The data from these tests showed that:

- The load-vertical displacement response of all four test girders was only slightly nonlinear until just before the shear capacity was reached. A linear elastic idealization of the load-vertical deflection response appears reasonable up to at least 95 percent of the maximum shear capacity.

- The observed girder distortions were relatively minor at the peak load level in all the girders.
- The measured web maximum radial deflections were of a similar magnitude in all the girders at the peak load level (approximately four times the thickness of the web), irrespective of the panel aspect ratio d_o/D.
- The measured web strains were relatively minor for all load levels up until just before the maximum shear strength was reached. At the most highly strained rosette locations, the curves for the shear versus the maximum principal strain and the principal strain differences started to exhibit at plateau at load levels slightly above about 95 percent of the maximum load capacity. In all cases, the maximum shear strength appeared to be associated with yielding through the entire web along a diagonal tension band.
- In all the test girders, irrespective of the panel aspect ratio d_o/D, initial yielding was detected at the most highly strained web rosette locations (based on the von Mises yield criterion and elastic isotropic material response) at approximately 65 to 70 percent of the maximum shear capacity. However, yielding occurred only on one surface of the web plate at this load level. There was no dramatic change in the web response associated with this measured localized onset of yielding.
- The shear-radial displacement curves for the webs ranged from essentially linear load-deflection response up to the peak load level to a somewhat nonlinear pre-peak load-deflection behavior. Although the load-radial deflection curves generally showed some nonlinearity, the maximum measured radial displacement increased gradually from the onset of the loading in all of the tests. None of the tests exhibited an abrupt bifurcation in the measured load-radial displacement response as would be predicted based on analytical solutions of perfectly flat web panels. This behavior is consistent with observations

documented in the literature from prior straight I-girder experiments, e.g., Basler et al. (1960).

- The measured flange strains indicated that flange bending associated with either frame action or anchorage of a theoretical tension field was small until just prior to or at the development of the maximum shear strength. However, significant bending of the flanges due to frame action occurred in the post-peak range of the response. This behavior supports both of two assertions made in the prior literature that: (1) the flanges are not highly strained up to the peak load level, e.g., (Lee and Yoo 1998, 1999a) and (Basler 1963), and (2) the flanges can provide a significant contribution to the shear strength via the development of a plastic collapse mechanism involving frame action, e.g., (Porter et al. (1975).
- The maximum reduction in the shear strength at the end of the post-peak loading in all the tests was approximately 15 percent. That is, the girders were capable of maintaining their shear resistance at levels close to the maximum strength for significant deformations beyond the peak load level, thus providing for some additional safety against catastrophic failure.
- All of the test girders developed maximum shear strengths similar in magnitude to values predicted by straight I-girder shear strength formulae. This includes the development of postbuckling shear strength based on various theories for straight I-girder webs. Any variations in the shear strengths due to differences in radius of curvature were too small to attribute to any specific cause.
- The various straight I-girder theories had only limited success in predicting the detailed behavior patterns associated with the development of the maximum strengths. Nevertheless, the limited realism of the various shear strength models compared to detailed experimental measurements is not uncommon in prior studies of straight I-girders.

The four curved I-girder shear tests conducted in this research, combined with the finite element parametric studies in White et al. (2002a) as well as other prior research, supports the following conclusion: curved I-girders can be designed under maximum strength loading conditions based on straight I-girder shear capacity equations, including the consideration of postbuckling strength, at least up to the following limits:

- $d_o/D \leq 3$
- $D/t_w \leq 160$
- $L_b/R \leq 0.10$

The increase in the theoretical web shear buckling strength, shown analytically in prior research, and the decrease in the maximum shear capacity due to horizontal curvature appear to be small compared to the effects of various other factors that lead to variability in nominal strength predictions relative to experimental tests and refined finite element solutions. It should be noted that the nondimensional parameter L_b/R listed above is more related to flexural behavior than shear response. However, $L_b/R \leq 0.10$ is a simple limit that is proposed to restrict the application of straight I-girder shear strength equations to cases that have been tested, rather than requiring the engineer to check a more complex parameter such as $c = d_o^2/8Rt_w$ (see Eq. (11)). The $L_b/R \leq 0.10$ limit is appropriate due to the fact that $d_o = L_b$ while d_o/D, D/t_w and L_b/R are all close to or at the maximum permitted limits in girder S2.

6.3 RECOMMENDATIONS FOR FURTHER RESEARCH

A number of questions and issues still exist regarding the limit state behavior of curved I-girders under high shear loading. These include:

- In the four I-girders tested in this research, the bearing and intermediate transverse stiffeners were designed conservatively to ensure that the test strengths would not be governed by a stiffener failure. In addition, the authors had the benefit of performing refined full nonlinear finite element analyses of the shear tests prior to the girder fabrication, to gain some additional confidence that the stiffener sizes were adequate. Although these stiffeners had reasonable proportions relative to the overall girder geometries, specific minimum size requirements for transverse stiffeners in curved I-girder webs are still unknown. As discussed in Chapter II, recent research calls the prior work on stiffener requirements for development of postbuckling strength in curved web panels into question. Nevertheless, the prior research only considered panel aspect ratios d_o/D up to 1.0. A small focused research effort is needed to define minimum stiffener size requirements for development of postbuckling strength in curved I-girders designed within the previously stated limits. Given the expected minor effect of conservative stiffener proportioning rules on overall design economy, simple conservative rules should be sufficient. However, design of curved I-girders for postbuckling shear strength up to the suggested limits would be risky until the effect on the transverse stiffeners is better understood. To the knowledge of the authors, the experiments discussed in (Nakai et al. 1984a, 1984c, 1985b) are the only physical curved I-girder tests in which the effects of various stiffener proportions were investigated. Any new research on stiffener proportioning requirements should consider these tests.
- Although the flange proportions were varied to some extent, and the effect of these changes on the shear strength behavior were ascertained in the parametric studies conducted by White et al. (2001), further studies of the influence of flange size on the shear strength would be prudent. Of particular interest is the effect of lateral bending within narrow flanges, and

whether the shear strengths are still predicted adequately by straight I-girder shear strength equations over a full range of practical I-girder D/b_f ratios. Parametric finite element studies are currently underway to address this issue (White and Jung 2002).

- The influence of high shear on the flexural strength and high moment on the shear strength should be studied in greater detail. Cases with high shear and high moment have been analyzed in (White et al. 2001) and have been tested experimentally in recent research at the FHWA Turner Fairbank Laboratory. Also, White and Jung's research (2002) should provide some further information about high shear high moment behavior, with an emphasis toward high shear. The results of these experimental and analytical investigations should be combined and analyzed to confirm or refute the conclusions by White et al. (2001) that interactions between the bending and shear strengths are small and can be neglected.
- The shear strength of curved I-girders with a top flange load applied at a non-braced location should be studied. This type of loading was considered in White et al. (2001) in the assessment of flexural strength, but has not been studied for high-shear loadings. There is a possibility for some reduction in the strength under this type of loading condition.
- The issue of potential distortion induced fatigue in curved I girder web panels needs to be evaluated more carefully. As noted in Chapter II, the AASHTO *2002 Guide Specifications* do not utilize prior equations that have been developed to guard against this mode of failure, but restrict the web shear force to the shear buckling load under all loading conditions. If the shear strength provisions are liberalized for curved I-girder design, an alternate restriction on the web slenderness would be necessary. Logically, it would seem that curved web proportioning requirements related to distortion induced fatigue should reduce to the corresponding requirements for straight I girder webs as the radius of curvature becomes

large. Significant economies may be gained if prior rules such as those proposed by Daniels et al. (1980) can be liberalized.

- It is likely that the straight I-girder shear strength equations are applicable for horizontal curvatures greater than those considered in the above studies. Further studies could be conducted to probe these limits. Specifically, it is suggested the a small number of finite element analyses could be conducted of girders having $L_b/R > 0.10$, but with $c = d_o^2/8Rt_w = 6$. This value of c was the maximum limit considered in the parametric studies by White et al. (2001), with $L_b/R \leq 0.10$, and is slightly larger than the maximum value in the four experimental tests conducted in this research.
- The above research efforts should be extended to longitudinally stiffened I girders. It is likely that postbuckling shear resistance also can be utilized in the design of these types of members.

APPENDIX I. CALCULATION OF STRAIN-HARDENING STRAIN AND MODULUS

The values for the strain hardening modulus E_{st} and strain hardening strain e_{st} reported in Chapter III were calculated using the method labeled as E_{st2} and suggested as a standard in (ASCE 1971). This method first requires that the point at the apparent onset of strain hardening be identified, but (ASCE 1971) does not provide a precise definition for this point. Therefore, the data point associated with the definition of the yield point elongation per ASTM E8-00b (ASTM 2000) was used for this purpose. This point is established as the intersection between (1) a horizontal line drawn tangent to the curve at the last zero slope within the yield plateau region and (2) a line drawn tangent to the strain hardening portion of the stress-strain curve at the point of inflection at or after the onset of strain-hardening. For purposes of discussion, this point is referred to as (e_{ype}, f_{ype}). Given this point, the (ASCE 1971) suggested procedure requires that the points on the stress-strain curve corresponding to strains of $e_1 = e_{ype} + 0.003$ and $e_2 = e_{ype} + 0.01$ be identified. These points are referred to here as (e_1, f_1) and (e_2, f_2). In this research, the strain hardening modulus E_{st} is calculated as the slope of the line between the above two points, i.e.,

$$E_{st} = \frac{(f_2 - f_1)}{(e_2 - e_1)} = \frac{(f_2 - f_1)}{0.007} \tag{47}$$

The strain hardening strain e_{st} is defined by the intersection of the line through (e_1, f_1) and (e_2, f_2) with a horizontal line at the ordinate $f = f_{ype}$. This procedure is somewhat involved, and Alpsten (1972) suggests an alternate simpler procedure. However, the value of E_{st} determined in this manner exhibits the least scatter of experimental values, and it defines the average slope of

the part of the stress-strain curve into which most steel members are strain hardened (ASCE 1971). Although the procedure is involved, the method can be programmed if the point (e_{ype}, f_{ype}) is used as the definition of the onset of strain hardening.

Figures 81 and 82 show an enlarged view within the yield plateau and initial strain-hardening regions from the example stress-strain curves previously shown in Fig. 4, and illustrate the calculation of E_{st} and e_{st} as explained above.

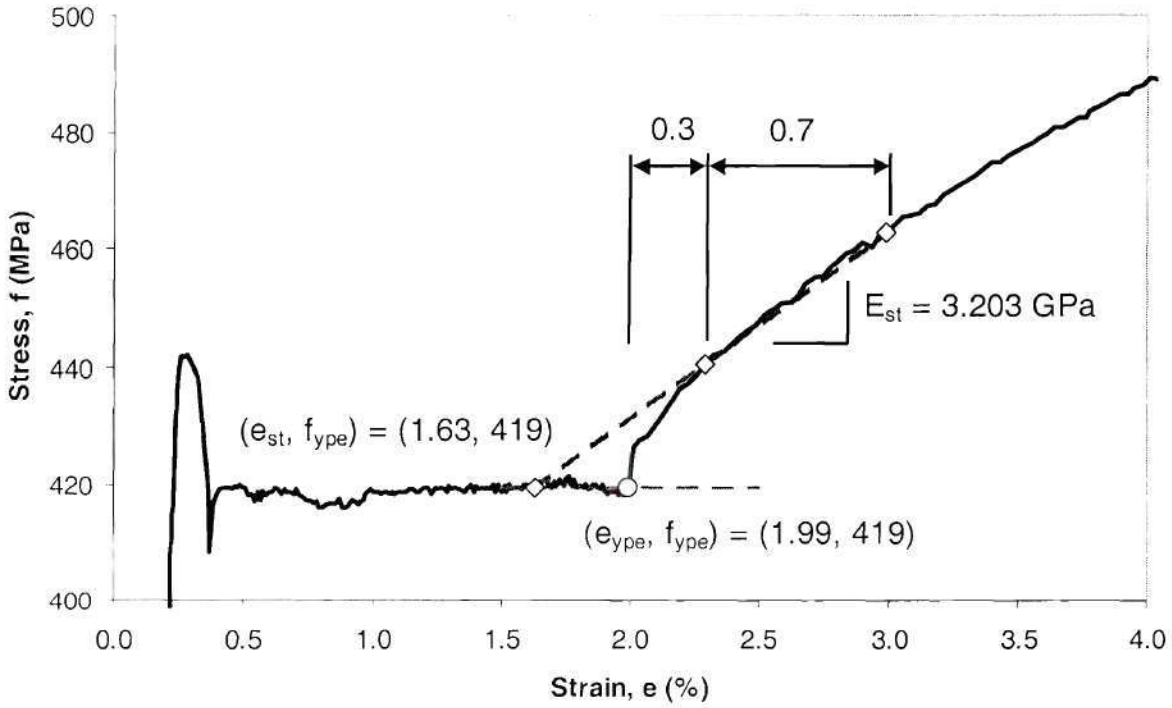

Figure 81 Enlarged view of a typical stress-strain curve for the web plates of Girders S2 and S2-S illustrating the calculation of e_{st} and E_{st}

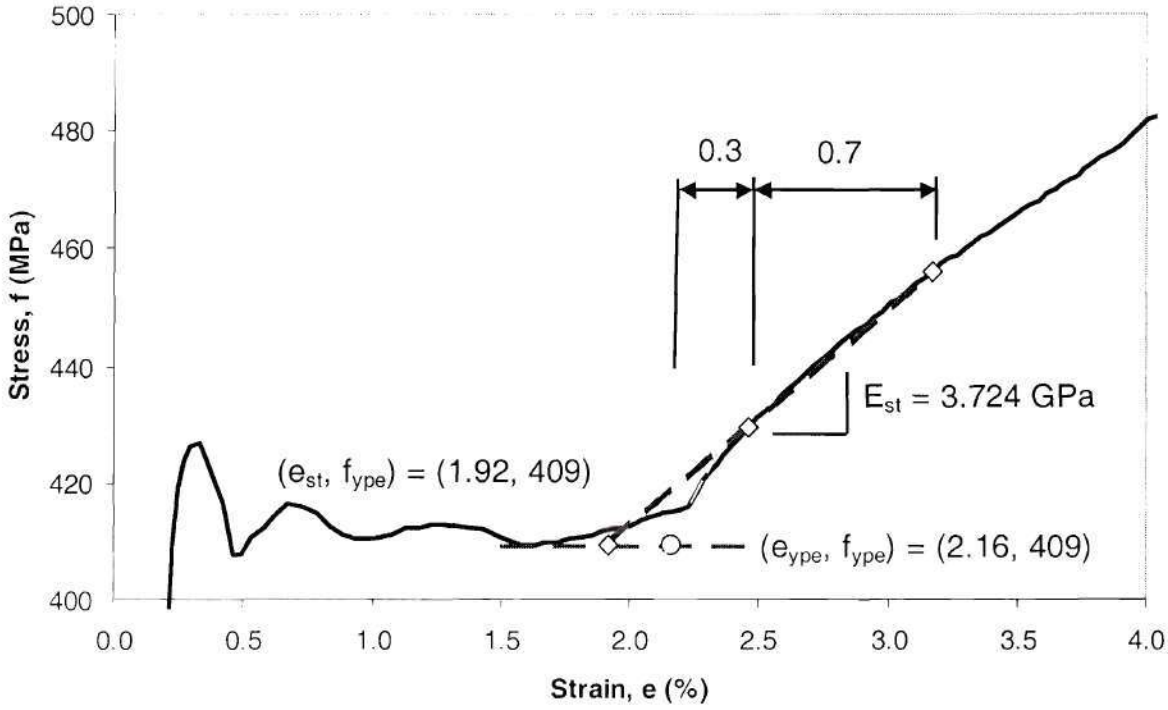

Figure 82 Enlarged view of a typical stress-strain curve for the flange plates of Girders S2 and S2-S illustrating the calculation of e_{st} and E_{st}

The calculation of e_{st} and E_{st} merits some further discussion. Adams et al. (1964) point out that e_{st} depends upon the distribution of inhomogeneities in the tension coupons as well as the amount of prestraining that has taken place in the coupon material before testing. Therefore, the value of this parameter can be highly variable. Adams et al. (1964), ASCE (1971), Alpsten (1972) and Galambos and Ravindra (1978) all indicate considerable scatter in values of the strain hardening modulus determined from tension coupon tests, even when the same method of measurement is employed. Also, ASCE (1971) indicates that the value of E_{st} is consistently somewhat higher in compression than in tension. Furthermore, Alpsten (1972) shows that there appears to be some relationship between the strain hardening properties and plate thickness, with

REFERENCES

AASHTO (1969). *Standard Specifications for Highway Bridges, 10th Edition*, American Association of State and Highway Transportation Officials, Washington D.C.

AASHTO (1993). *AASHTO Guide Specifications for Horizontally Curved Highway Bridges*, American Association of State and Highway Transportation Officials, Washington D.C.

AASHTO (1996), *Standard Specifications for Highway Bridges, 16th Edition*, American Association of State and Highway Transportation Officials, Washington D.C.

AASHTO (1998). *AASHTO LRFD Bridge Design Specifications 2nd Edition with 1999, 2000 and 2001 Interims*, American Association of State and Highway Transportation Officials, Washington D.C.

AASHTO (2002). *Guide Specifications for Horizontally Curved Highway Bridges*, American Association of State and Highway Transportation Officials, Washington D.C. (in press).

Abdel-Sayed, G. (1973). "Curved Webs Under Combined Shear and Normal Stresses," *Journal of the Structural Division*, ASCE, 99 (ST3), 511-525.

Adams, P.F., Lay, M.G. and Galambos, T.V. (1964). "Experiments on High Strength Steel Members," Fritz Engineering Laboratory Report No. 297.8, 71 pp.

AISC (1999). *Load and Resistance Factor Design Specification for Structural Steel Buildings*, American Institute of Steel Construction, Chicago, IL, 292 pp.

Alpsten, G.A. (1972). "State of the Art Report No. 1, Variation in Mechanical and Cross-Sectional Properties of Steel," Quality Control Criteria, Planning and Design of Tall Buildings, Criteria and Loading, Technical Committee No. 9, International Conference on Planning and Design of Tall Buildings, Lehigh Univ., Bethlehem, PA, August 21-26, ASCE-IABSE International Conference Preprints: Reports Vol. Ib-9, pp. 1-51.

ASCE (1968). "Design of Hybrid Steel Beams," *Journal of the Structural Division*, ASCE, 94(ST6), 1397-1426.

ASCE (1971). *Plastic Design in Steel, A Guide and Commentary*, ASCE Manuals and Reports on Engineering Practice - No. 41, ASCE-WRC, 2nd ed., 336 pp.

ASTM (1997). "Standard Test Method for Young's Modulus, Tangent Modulus, and Chord Modulus," ASTM E111-97, American Society for Testing and Materials.

E_{st} increasing and e_{st} decreasing with increasing plate thickness. In Table 6, these trends are exhibited in both E_{st} and e_{st} for the S1 and S1-S plates, but only in E_{st} for the S2 and S2-S plates, with no significant difference between e_{st} for the flanges and web of these girders.

Adams et al. (1964) found that they needed to resort to a special series of tension tests, in which the test was stopped and the specimen held at zero strain rate for a long period of time at and just after the onset of strain hardening, to determine consistent values for E_{st} in their research. Via their special test procedure, they were able to obtain values of E_{st}, defined as the tangent to the stress-strain curve at the onset of strain-hardening, to within about two percent in 28 of 30 tension coupons. The Adams et al. (1964) tests indicated that the drop in load obtained from static measurements within the strain-hardening region is similar to that within the yield plateau region, and that E_{st} is not sensitive to the time that the specimen is held prior to taking the static measurements. This provides some justification for the use of the "non-static" e_{st} and E_{st} values determined by the procedures selected in this work along with the measured static F_y values. That is, based on the discussion in Adams et al. (1964), the "non-static" E_{st} values such as those determined in this research appear to be representative of carefully measured "static" values of E_{st}.

ASTM (2000). "Standard Test Methods for Tension Testing of Metallic Materials," ASTM E8-00b, American Society for Testing and Materials.

AWS (2000). *Structural Welding Code–Steel*, AWS D1.1:2000, 17th ed., prepared by AWS Committee on Structural Welding, 450 pp.

AWS (1966). *Specifications for Welded Highway and Railroad Bridges*, American Welding Society.

Basler, K., Yen, B.T., Mueller, J.A., and Thurlimann, B. (1960). "Web Buckling Tests on Welded Plate Girders," WRC Bulletin No. 64, Welding Research Council, New York, NY, 63 pp.

Basler, K. and Thurlimann, B. (1961). "Strength of Plate Girders in Bending," *Journal of Structural Division*, ASCE, 87(ST6), 153-181.

Basler, K. (1961). "Strength of Plate Girders in Shear," *Journal of Structural Division*, ASCE, 87(ST7), 151-180.

Basler, K. (1963). "Discussion of K. Basler 'Strength of Plate Girders in Shear,'" *Transaction ASCE*, 128(II), 712-719.

Bradford, M.A. (1996). "Improved Shear Strength of Webs Designed in Accordance with the LRFD Specification," *Engineering Journal*, AISC, 33(3), 95-100.

Culver, C.G., Dym, C. and Brogan, D. (1972a). "*Instability of Horizontally Curved Members-Bending Behavior of Cylindrical Web Panels,*" Carnegie-Mellon University, Report to Pennsylvania Department of Transportation, January, 31 pp.

Culver, C.G., Dym, C. and Brogan, D. (1972b). "Bending Behavior of Cylindrical Web Panels," *Journal of the Structural Division*, ASCE, 98(ST 10), 2291-2308.

Culver, C.G., Mariani, N., Mozer, J. and Brogan, D. (1972c). "*Instability of Horizontally Curved Members-Shear Buckling of Cylindrical Web Panels,*" Carnegie-Mellon University, Report to Pennsylvania Department of Transportation, June.

Culver, C.G., Dym, C.L. and Uddin, T. (1973). "Web Slenderness Requirements for Curved Girders," *Journal of the Structural Division*, ASCE, 99(ST3), 417-430.

Daniels, J.H. and Herbein, W.C. (1980). "*Fatigue of Curved Steel Bridge Elements – Fatigue Tests of Curved Plate Girder Assemblies.*" Lehigh University, Bethlehem, PA, FHWA-RD-79-132 (1980), 91 pp.

Daniels, J.H., Fisher, J.W. and Yen, B.T. (1980). "Fatigue of Curved Steel Bridge Elements, Design Recommendations for Fatigue of Curved Plate Girder and Box Girder Bridges." Report No. FHWA-RD-79-138, Federal Highway Administration, Washington, D.C., 54 pp.

Davidson, J.S. (1996). "Nominal Bending and Shear Strength of Curved Steel I-Girder Bridge Systems," Ph.D. dissertation, Auburn University, Auburn, AL.

Davidson, J.S., Ballance, S.R. and Yoo, C.H. (1999a). "Analytical Model of Curved I-Girder Web Panels Subjected to Bending," *Journal of Bridge Engineering*, ASCE, 4(3), 204-212.

Davidson, J.S., Ballance, S.R and Yoo, C.H. (1999b). "Finite Displacement Behavior of Curved I-Girder Webs Subjected to Bending," *Journal of Bridge Engineering*, ASCE, 4(3), 213-220.

Davidson, J.S., Ballance, S.R. and Yoo, C.H. (2000). "Behavior of Curved I-Girder Webs Subjected to Combined Bending and Shear," *Journal of Bridge Engineering*, ASCE, 5(2), 165-170.

Davies, A.W. and Griffith, D.S.C. (1999). "Shear Strength of Steel Plate Girders," *Proceedings of the Institution of Civil Engineers, Structures and Buildings*, 134, May, 147-157.

Duchene, Y. and Maquoi, R. (1995). "Secondary Bending Stresses due to Out-of-Plane Displacements of Slender Web Panels Subject to Shear," *Stability of Steel Structures*, Budapest, Hungary, 267-274.

Evans, H.R. (1983). "Longitudinally and Transversely Reinforced Plate Girders," *Plated Structures – Stability and Strength*, R. Narayanan (ed.), Applied Science Publishers, New York, NY, 1-37.

Evans, H.R., Porter, D.M. and Rockey, K.C. (1978). "The Collapse Behaviour of Plate Girders Subjected to Shear and Bending," *IABSE Proceedings*, P-18/78, November, 1-20.

Fisher, J. W., Yen, B.T. and Frank, K.H. (1979). "Minimizing Fatigue and Fracture in Steel Bridges," *Structural Integrity Technology,* 1979 ASME Conference, New York, 155-161.

Frost, R.W. and Schilling, C.G. (1964). "Behavior of Hybrid Beams Subjected to Static Loads," *Journal of the Structural Division*, ASCE, 90(ST3), 55-88.

Fujii, T. (1968). "On an Improved Theory for Dr. Basler's Theory," IABSE 8th Congress, Final Report, New York.

Galambos, T.V., Frank, K. H. and McGogney, C.H. (1977). "Effect of Yielding on the Fatigue Strength of Steel Beams," *Public Roads,* 41(1), 10-17.

Galambos, T.V. and Ravindra, M.K. (1978). "Properties of Steel for Use in LRFD," *Journal of the Structural Division*, ASCE, 104(ST9), 1459-1468.

Gaylord, E.H. (1963). "Discussion of K. Basler 'Strength of Plate Girders in Shear,'" *Transaction ASCE, 128(II), 712-719.*

Hall, D.H. (2000). Personal communication.

Hall, D.H., Grubb, M.A. and Yoo, C.H. (1999). "Improved Design Specifications for Horizontally Curved Steel Girder Highway Bridges," *NCHRP Report 424*, NCHRP, Washington, D.C., 130 pp.

Hash, J.B. (2001). "Shear Capacity of Hybrid Steel Girders," M.S. Thesis, University of Nebraska, Lincoln, Nebraska, December, 407 pp.

Höglund, T. (1971). "Simply Supported Long Thin Plate I Girders Without Web Stiffeners Subjected to Distributed Transverse Load," *Proceedings of the Design of Plate and Box Girders for Ultimate Strength Colloquium*, IABSE, London, 85-97.

Höglund, T. (1995). "Strength of Steel and Aluminum Plate Girders - Shear Buckling and Overall Buckling of Plane and Trapezoidal Webs - Comparisons with Test," Department of Structural Engineering, Royal Institute of Technology, Stockholm, Technical Report 1995:4 – Steel Structures.

Höglund, T. (1996). "Shear Buckling Resistance of Steel and Aluminum Plate Girders," *Proceedings of the Bicentenary Conference on Thin-Walled Structures*, University of Strathclyde, 1-18.

Lee, S.C., Davidson, J.S. and Yoo, C.H. (1996). "Shear Buckling Coefficients of Plate Girder Web Panels," *Computers & Structures*, 59(5), 789-795.

Lee, S.C. and Yoo, C.H. (1998). "Strength of Plate Girder Web Panels Under Pure Shear," *Journal of Structural Engineering*, ASCE, 124(2), 184-194.

Lee, S.C. and Yoo, C.H. (1999a). "Experimental Study on Ultimate Shear Strength of Web Panels," *Journal of Structural Engineering*, ASCE, 125(8), 838-846.

Lee, S.C. and Yoo, C.H. (1999b). "Strength of Curved I-Girder Web Panels under Pure Shear," *Journal of Structural Engineering*, ASCE, 125(8), 847-853.

Lee, S.C., Yoo, C.H., and Yoon, D.Y. (2002). "Behavior of Intermediate Transverse Stiffeners Attached on Web Panels," *Journal of Structural Engineering*, ASCE, 128(3), 337-345.

Mariani, N, Mozer, J.D., Dym, C.L. and Culver, C.G. (1973). "Transverse Stiffener Requirements for Curved Webs," *Journal of Structural Division*, ASCE, 99(ST4), 757-771.

Mikami, I. and Furunishi, K. (1984). "Nonlinear Behavior of Cylindrical Web Panels," *Journal of Engineering Mechanics*, ASCE, 110(2), 239-251.

Montgomery, S.L. (1987). "Fatigue And Ultimate Strength of A Transversely Stiffened Plate Girder" M.S. thesis, University of Texas at Austin, Austin, TX, 1987.

Mozer, J. and Culver, C.G. (1970). "Horizontally Curved Highway Bridges: Stability of Curved Plate Girders," *Report No. P1*, Prepared for U.S. Department of Transportation, Federal Highway Administration, August, 95 pp.

Mozer, J., Ohlson, R. and Culver, C.G. (1971). "Horizontally Curved Highway Bridges: Stability of Curved Plate Girders," *Report No. P2*, Prepared for U.S. Department of Transportation, Federal Highway Administration, September, 121 pp.

Mozer, J., Cook, J. and Culver, C.G. (1973). "Horizontally Curved Highway Bridges: Stability of Curved Plate Girders," *Report No. P3*, Prepared for U.S. Department of Transportation, Federal Highway Administration, January, 111 pp.

Mueller, J.A. and Yen, B.T. (1968). "Girder Web Boundary Stresses and Fatigue," WRC Bulletin No. 127, January.

Nakai, H., Muramatsu, S., Yoshikawa, N., Kitada, T. and Ohminami, R. (1981). "A Survey for Web Plates of Horizontally Curved Girder Bridges," *Bridges and Found. Engineering*, Japan, 15, 38-45 (in Japanese).

Nakai, H., Kitada, R., Ohminami, R. and Fukumoto, K. (1984a). "Experimental Study on Shear Strength of Horizontally Curved Plate Girders," *Proceedings of the Japanese Society of Civil Engineers*, 350(I-2), October, 281-290 (in Japanese, and English translation by International Translation Center, Inc., Washington, D.C.).

Nakai, H., Kitada, T. and Ohminami, R. (1984b). "Experimental Study on Ultimate Strength of Web Panels in Horizontally Curved Girder Bridges Subjected to Bending, Shear, and their Combinations," *Proceeding, Annual Technical Session Meeting*, Structural Stability Research Council, San Francisco, CA, 91-102.

Nakai, H., Kitada, T., Ohminami, R. and Fukumoto, K. (1984c). "A Proposition for Designing Transverse Stiffeners of Horizontally Curved Girders in Ultimate State," *Memoirs of the Faculty of Engineering*, Osaka University, Japan, Vol. 25, December, 111-131.

Nakai, H., Kitada, T. and Ohminami, R. (1985a). "Experimental Study on Buckling and Ultimate Strength of Curved Girders Subjected to Combined Loads of Bending and Shear," *Proceedings of the Japanese Society of Civil Engineers*, 356(I-3), April, 445-454 (in Japanese, and English translation by International Translation Center, Inc., Washington, D.C.).

Nakai, H., Kitada, T. and Ohminami, R. (1985b). "A Proposition for Designing Intermediate Transverse Stiffeners in Web Plates of Horizontally Curved Girders," *Proceedings of the Japanese Society of Civil Engineers*, 362(I-4), October, 249-257 (in Japanese).

Nakai, H., Kitada, T., Ohminami, R. and Kawai, T. (1986). "A Study on Analysis and Design of Web Plates in Curved Bridges Subjected to Bending," *Proceedings of the Japanese Society of Civil Engineers*, 368(I-5), 235-244 (in Japanese).

Nakai, H. and Yoo, C.H. (1988). *Analysis and Design of Curved Steel Bridges*, McGraw-Hill, NY, 673 pp.

Nowak, A.S., Nassif, H. and Frank, K.H. (1993). "Fatigue Load Spectra for a Steel Girder Bridge," *Transportation Research Record* No. 1393, 154-161.

Okura, J., Yen, B.T. and Fisher, S.W. (1993), "Fatigue of Thin-Walled Plate Girders," *Structural Engineering International*, 1/93, 39-44.

Patterson, P.J., Corrado, J.A., Huang, J.S. and Yen, B.T. (1970). "Fatigue and Static Tests of Two Welded Plate Girders," *Welding Research Council Bulletin No. 155*, October.

Porter, D.M., Rockey, K.C. and Evans, H.R. (1975). "The Ultimate Load Behavior of Plate Girders Loaded in Shear," *The Structural Engineer*, 53(8), 313-325.

Ramadi, A., Aribert, J.M. and Raoul, J. (1995). "Secondary Bending Stresses due to Out-of-Plane Displacement of Slender Web Panels Subject to a Bending Moment," *Stability of Steel Structures*, Budapest, Hungary, 275-282.

Schilling, C.G. (1968). "Bending Behavior of Composite Hybrid Beams," *Journal of the Structural Division*, ASCE, 94(ST8), 1945-1964.

Selberg, A. (1973). "On the Shear Capacity of Girder Webs," University of Trondheim Report.

SSRC (1998). *Guide to Stability Design Criteria for Metal Structures 5th Edition*. Structural Stability Research Council, T.V. Galambos (ed.), McGraw-Hill, New York, 910 pp.

Vasseghi, A. and Frank, K.H. (1987). "Static Shear and Bending Strength of Composite Plate Girders," PMFSEL Report No. 87-4, University of Texas at Austin, Austin, TX, June.

Vincent, G.S. (1969). "Tentative Criteria for Load Factor Design of Steel Highway Bridges," Bulletin No. 15, American Iron and Steel Institute, New York, NY, March.

Wachowiak, J. (1967). "Die Berechnung gekrumutter Stege von dunnwandigen Tragern auf Grund der Schalen Theorie," *Dissertation*, Politechnika, Gdanska, Poland (in Polish).

White, D.W. and Aydemir, M.A. (2002). "Moment-Shear Interaction in HPS Hybrid Plate Girders," Final Report to American Iron and Steel Institute Transportation and Infrastructure Committee, in preparation.

White, D.W. and Jung, S-K. (2002). "Shear Strength of Horizontally Curved Steel I Girders – Finite Element Analysis Studies," Final Report to Federal Highway Administration, in preparation.

White, D.W., Zureick, A.H., Phoawanich, N. and Jung, S.-K. (2001). *Development of Unified Equations for Design of Curved and Straight Steel Bridge I Girders*, Final Report to American Iron and Steel Institute Transportation and Infrastructure Committee, Professional Services Industries, Inc., and Federal Highway Administration, School of Civil and Environmental Engineering, Georgia Institute of Technology, Atlanta, GA, October, 551 pp.

White, D.W., Zureick, A.H., and Barker, M.G. (2002a). "Shear Strength of Steel I Girders," *Journal of Structural Engineering*, ASCE, in review.

White, D.W., Barker, M.G., and Azzizinamini, A. (2002b). "Strength of Steel I Girders Subjected to High Moment and High Shear," *Journal of Structural Engineering*, ASCE, in review.

Yen, B.T. and Mueller, J.A. (1966). "Fatigue Tests of Large Size Welded Plate Girders," WRC Bulletin No. 118, November.

Zureick, A.H. (1998). "Horizontally Curved Steel I-Girders," Chapter 9, *Guide to Stability Design Criteria for Metal Structures 5th Edition*. Structural Stability Research Council, T.V. Galambos (ed.), McGraw-Hill, New York, pp. 365-382.